hiPSC generation and redifferentiation into induced myogenic cells
-
dependent on the cell type of origin?

Inaugural-Dissertation

to obtain the academic degree

Doctor rerum naturalium (Dr. rer. nat.)

submitted to the Department of Biology, Chemistry and Pharmacy

of Freie Universität Berlin

by

Eric Metzler

from Cologne, Germany

2019

This work was conducted from January 2015 to July 2019 under the supervision of Professor Simone Spuler at the Experimental and Clinical Research Center (a joint cooperation of the Charité Medical Faculty and the Max Delbrück Center for Molecular Medicine, Berlin, Germany). The experiments were conducted in the laboratories of Professor Simone Spuler and Dr. Sebastian Diecke (Stem Cell Core Facility, Berlin Institute of Health (BIH) / Max Delbrück Center for Molecular Medicine, Berlin, Germany).

1st reviewer: **Prof. Dr. Simone Spuler**
Institute for Chemistry and Biochemistry
Department of Biology, Chemistry and Pharmacy
Freie Universität Berlin

and

Department of Muscle Sciences and
University Outpatient Clinic for Muscle Disorders
Experimental and Clinical Research Center, Berlin

2nd reviewer: **Prof. Dr. Sigmar Stricker**
Institute for Chemistry and Biochemistry
Department of Biology, Chemistry and Pharmacy
Freie Universität Berlin

Date of defence: 18.12.2019

ACKNOWLEDGEMENTS

First of all, I would like to express my particular gratitude to Professor Simone Spuler for supervising my work, for her advice and extensive support and for giving me the opportunity to do my PhD in her laboratory at the Experimental and Clinical Research Center. I would also like to thank Professor Sigmar Stricker for reviewing my thesis.

I especially thank Dr. Sebastian Diecke for his extensive support and for teaching me the handling of induced pluripotent stem cells, while welcoming me to his laboratory in the stem cell core facility, where I spend many hours during the first two years of my PhD. I would also like to thank the current and former members of his team Norman Krüger, Polixeni Burazi, Sandra Wegener, Anna Iwanska and Narasimha Swamy Telugu for their great support and for making it a very enjoyable time during extensive hiPSC cell culture hours.

I thank Dr. Andreas Marg for introducing me to the muscle research field and for being always available for helpful discussions and for sharing his extensive knowledge in microscopy and experiment planning with me.

I especially thank Dr. Helena Escobar for her constant support, for being a thorough judge of my doings, for fruitful discussions and constructive criticism, for teaching me the handling and transplantation of mice and sharing the daily obstacles in hiPSC culture and office routine with late night supplies of Makrelenfilets.

I would like to thank Susanne Wissler for her support with all the administrative and organisational hurdles at any time.

I thank the people of the University Outpatient Clinic for Muscle Disorders and especially Dr. Ulrike Grieben for her support in organising the exchange between the clinics and the research facility. I also thank the donors that made this study possible.

I would like to thank Stephanie Meyer-Liesener and Stefanie Haafke for teaching me the handling of primary muscle cells and their continuing support throughout my whole PhD.

I thank Andrea Behm and Adrienne Rothe for their help with the irradiation and transplantation experiments and the histological preparations. I also thank Diana Pasemann and Anne Kathrin Kluge from the Charité Cyber Knife facility for their great support in conducting the irradiation experiments.

I thank Dr. Yumi Sunaga-Franze for her support in the analysis of the RNA-Sequencing data and Kirsten Richter for the introduction to library preparation.

I thank Dr. Stefanie Grunwald and Stefanie Haafke for sharing their genomics and transcriptomics knowledge and for bioinformatical advice.

I would like to thank Silvia Di Francescantonio for all the encouragement and lots of spontaneous beers, discussions and memories.

Thanks to Henning Langer for our frequent discussions about life and our quite diverging research projects during constant lunchtime routine.

I would like to especially thank Dr. Helena Escobar, Silvia Di Francescantonio, Henning Langer, Dr. Jakub Malcher, Cristina Pablo, Stefanie Müthel and the members of the Rock inhibitors (hiPSC-culture weekend support team) Dr. Helena Escobar, Dr. Angélica García, Dr. Ena Kolundzic and Michael Mücke for their friendship and the awesome time in and outside the lab that really made these years enjoyable and memorable.

I would like to thank Dr. Verena Schöwel for her encouragement and the nice atmosphere back to back in the office with a never-ending flow of gummy bears and chocolate cookies.

I would generally like to thank all of the members of the Spuler lab for the great daily atmosphere which made my PhD an enjoyable experience.

Finally, I would like to express my special gratitude to my family and friends for their continuous support and especially Maja for being a part of my life.

TABLE OF CONTENTS

SUMMARY

Muscular dystrophies (MDs) are a heterogeneous group of inherited myogenic disorders characterised by progressive muscle wasting and degeneration. Cell replacement therapies aiming to regenerate and restore the diseased muscles are considered as promising therapeutic strategies for patients affected by MDs. Muscle regeneration relies on satellite cells, the adult stem cells of the skeletal muscle. However, they exist only in low numbers and cannot be extensively cultured and manipulated ex vivo. On the other hand, human induced pluripotent stem cells (hiPSCs) are a keystone to unrestricted numbers of autologous cells, which are necessary for gene correction and repopulation of large muscles in many genetic disorders without evoking an immune response. hiPSCs have been generated from many different cell types and several protocols have been established to differentiate them into muscle cells or dedicated muscle stem cells. However, the biotechnological and therapeutic capabilities of these induced myogenic cells remain unclear. In addition, whether the epigenetic memory passed on to the hiPSCs from the somatic cell type they originated from has an influence on their myogenic differentiation capacity has not yet been examined.

Myoblasts and peripheral blood mononuclear cells (PBMCs) represent the most relevant cell types for the generation of autologous hiPSCs for the treatment of muscular disorders, as blood samples are easy to retrieve from donors and myoblasts can easily be extracted from muscle biopsy specimens that are regularly taken for diagnostic purposes from patients with suspected muscular dystrophies. Thus, we compared primary human myoblasts and human PBMCs, derived from the same donor (n=4), with regard to their ability to reprogramme into hiPSCs, their transcriptomic characteristics and their ability to differentiate into the myogenic lineage using a directed transgene-free differentiation protocol. In addition, we investigated the potential of the hiPSC-derived induced myogenic cells to contribute to myofibre regeneration in an immunocompromised mouse model.

We found considerable differences in the ability of primary myoblasts and PBMCs to reprogramme into hiPSCs with a higher efficiency for myogenic cells. RNA-Sequencing of myoblast- and PBMC-derived hiPSCs revealed 122 significantly differentially expressed transcripts that are involved in signalling pathways potentially influencing the differentiation capacities of pluripotent stem cells.

However, the in vitro differentiation experiments revealed no significant differences in the number of myogenic cells obtained after differentiation of myoblast- and PBMC-derived hiPSCs from the same donor. On the other hand, we found distinct differences between the donors, clearly showing an influence of the donor's genetic background on the ability of hiPSCs to differentiate into the myogenic lineage in vitro.

Finally, intramuscular transplantation of induced myogenic progenitor cells into immunocompromised mice resulted in human myofibre formation for both, myoblast- and PBMC-derived myogenic cells. However, the human muscle fibres remained small in diameter and the overall number of human myofibres remained low, which hampered a reliable quantitative comparison between the two cell types.

The results obtained in this study show no difference in the vitro myogenic differentiation efficiency of myoblast- and PBMC-derived hiPSCs. However, we show that, when readily available, myoblasts are a better cell source to generate autologous hiPSCs for patients with muscular dystrophies due to their significant higher reprogramming efficiency as compared to PBMCs.

This work highlights the existence of intrinsic differences between hiPSC lines and their impact on the differentiation capacity, some of which being related to the genetic background of the donor. A thorough understanding of the factors responsible for these differences will be of great value to improve the differentiation protocols for the myogenic lineage and to help select hiPSCs with the highest prospects of success for obtaining large numbers of myogenic cells with the potential for robust myofibre regeneration in vivo.

ZUSAMMENFASSUNG

Muskeldystrophien sind eine heterogene Gruppe von erblichen Muskelerkrankungen, die durch progressive Muskeldegeneration charakterisiert sind. Zellersatztherapien zielen darauf ab die geschädigten Muskelzellen zu ersetzten und den degenerierten Muskel zu regenerieren und gelten als vielversprechende therapeutische Strategie zur Behandlung von Patienten mit Muskeldystrophien. Die Regeneration von Muskelgewebe hängt von muskelspezifischen Stammzellen ab, den sogenannten Satellitenzellen. Satellitenzellen kommen jedoch nur in sehr geringer Anzahl vor und sind daher nicht in ausreichendem Maße für eine ex vivo Kultivierung und genetische Korrektur vorhanden. Humane induzierte pluripotente Stammzellen (hiPSCs) hingegen, stellen den Schlüssel zu einer uneingeschränkten Anzahl autologer Zellen dar, die zur genetischen Korrektur und zur Regeneration von großen Muskeln benötigt werden, ohne dass es dabei zu Immunabstoßungsreaktionen kommt. hiPSCs wurden bereits aus diversen Zelltypen generiert. Zudem wurden bereits diverse Protokolle zur Generierung von Muskelzellen oder auch Muskelstammzellen aus hiPSCs etabliert. Dennoch ist das biotechnologische und therapeutische Potential dieser aus hiPSCs induzierten Muskelzellen bisher unklar. Auch der Einfluss des somatischen Ursprungszelltyps der hiPSCs auf ihre Kapazität in Muskelzellen zu differenzieren ist nicht abschließend geklärt.

Myoblasten und periphere mononukleäre Blutzellen (PBMCs) stellen die beiden Zelltypen mit der größten Relevanz für die Generierung von autologen hiPSCs zur Behandlung von Muskeldystrophien dar. Blutproben sind leicht zu entnehmen und Myoblasten können aus Muskelbiopsie-Proben isolierten werden, die zu diagnostischen Zwecken von Patienten mit Verdacht auf Muskelerkrankungen entnommen werden. Daher wurden in dieser Arbeit humane Myoblasten und PBMCs vom selben Donor isoliert (n=4) und deren Kapazität zur Reprogrammierung in hiPSCs untersucht. Zudem wurden die generierten hiPSCs auf transkriptioneller Ebene verglichen und, unter Verwendung eines nicht-integrativen myogenen Differenzierungsprotokolls, ihre Kapazität zur in vitro Differenzierung in die myogene Linie bestimmt. Im Anschluss wurde das Potential dieser aus hiPSCs induzierten Muskelzellen zur Bildung von humanen Muskelfasern in einem immunsupprimierten Mausmodell analysiert.

Die Reprogrammierung in hiPSCs war mit Myoblasten deutlich effizienter als mit PBMCs. Der Vergleich der generierten hiPSCs auf transkriptioneller Ebene ergab 122 signifikant unterschiedlich exprimierte Transkripte zwischen den beiden Zelltypen. Diese Transkripte sind in Signalwege mit potentiellem Einfluss auf die Differenzierungskapazitäten dieser pluripotenten Stammzellen involviert.

Dennoch zeigten die in vitro Differenzierungsexperimente keine signifikanten Unterschiede in der Anzahl an generierten Muskelzellen zwischen den aus Myoblasten und PBMCs generierten

hiPSCs vom selben Donor. Die Differenzierungskapazität der hiPSCs aus verschiedenen Donoren unterschied sich allerdings stark voneinander, was den Einfluss des genetischen Hintergrunds auf die Differenzierungskapazität zeigt.

Die Transplantation von aus hiPSCs generierten induzierten Muskelvorläuferzellen zeigte in beiden Zelltypen das Potential zur Muskelfaserregeneration. Die regenerierten Muskelfasern waren jedoch klein und ihre Anzahl war gering. Daher war eine Quantifizierung der Unterschiede nach Transplantation zwischen den aus Myoblasten und den aus PBMCs generierten Muskelzellen nicht sicher möglich.

Die Versuche in dieser Studie zeigen keine Unterschiede in der Effizienz zur Muskeldifferenzierung zwischen den aus Myoblasten und den aus PBMCs generierten hiPSCs. Dennoch kommen wir zu dem Schluss, dass zur Generierung von hiPSCs, falls vorhanden, Myoblasten verwendet werden sollten, da mit diesen eine signifikant höhere Reprogrammierungseffizienz erreicht wurde.

Diese Arbeit stellt den Einfluss von Faktoren heraus, die für intrinsischen Unterschiede zwischen hiPSC Linien verantwortlich sind und deren Differenzierungspotential beeinflussen. Diese Unterschiede sind unter anderem auf den genetischen Hintergrund der Spender zurückzuführen. Ein besseres Verständnis dieser Faktoren könnte eine Optimierung der Muskeldifferenzierungsprotokolle und eine Selektion der hiPSCs ermöglichen, um eine ausreichende Menge an potenten induzierten Muskelzellen zu generieren.

LIST OF FIGURES

LIST OF TABLES

LIST OF ABBREVIATIONS

B_hiPSCs	Blood derived human induced pluripotent stem cells
B_iMCs	Blood derived induced myogenic cells
B_iMPCs	Blood derived induced myogenic progenitor cells
BMP	Bone morphogenetic protein, signalling pathway
c-Myc	Avian Myelocytomatosis Viral Oncogene Homolog
CD	Cluster of differentiation
CHIR	Glycogen synthase kinase 3 (GSK3) inhibitor
CK	Creatin Kinase
Ct	Cycle threshold
DAVID	Database for annotation, visualisation and integrated discovery
DETs	Differentially expressed transcripts
DICER	Endoribonuclease Dicer or helicase with RNase motif
DMSO	Dimethyl sulfoxide
EDTA	Ethylenediaminetetraacetic acid
ERBB3	Receptor tyrosine-protein kinase
ESC	Embryonic stem cells
FACS	Fluorescence activated cell sorting/system
FCS	Fetal calf serum
FGF	Fibroblast growth factor
GAPDH	Glyceraldehyde 3-phosphate dehydrogenase, housekeeping gene
GO	Gene ontology
HGF	Hepatocyte growth factor
HGNC	HUGO (Human Genome Organisation) Gene Nomenclature Committee
hiPSCs	Human induced pluripotent stem cells
HMFF	Human muscle fibre fragment
Hu18SRNA	Human 18S rRNAs, housekeeping gene
i.m.	Intramuscular
i.p.	Intraperitoneal
IGF	Insulin-like growth factor
iPSCs	Induced pluripotent stem cells

ITGA7	Integrin alpha 7, surface molecule
ITS	Insulin, Transferrin, Selenium
KLF4	Kruppel like factor 4
KOS	KLF4, OCT3/4, SOX2
KSR	Knockout™ Serum Replacement
LDN	BMP pathway inhibitor
M_hiPSCs	Myoblast derived human induced pluripotent stem cells
M_iMCs	Myoblast derived induced myogenic cells
M_iMPCs	Myoblast derived induced myogenic progenitor cells
MAGED4B	Melanoma-associated antigen D4B
MCAM	Melanoma cell adhesion molecule, surface molecule
MDs	Muscular Dystrophies
MEFs	Mouse embryonic feeder cells
MG	Matrigel
MRF4	Myogenic regulatory factor 4
MRFs	Muscle regulatory factors
MYH	Myosin Heavy Chain gene
MyHC	Myosin Heavy Chain protein
MYOD1	Myogenic differentiation 1
MYOG	Myogenin
n.s.	Not significant
NANOG	Homeobox protein NANOG
NCAM	Neural cell adhesion molecule, also known as CD56
NDUFS1	NADH-ubiquinone oxidoreductase
NMP	Neuromesodermal progenitor cells
NOG-M	Immunodeficient mice, NOD.Cg-Prkdc^{scid} Il2rg^{tm1Sug}/JigTac, Taconic Biosciences
OCT3/4	Octamer-binding transcription factor 3/4, also known as POU5F1
OSKM	OCT3/4, SOX2, KLF4, c-Myc, Yamanaka Factors
padj	p value adjusted
PAX7	Paired-box protein 7
PBMCs	Peripheral blood mononuclear cells
PCA	Principal component analysis

PECAM1	Platelet And Endothelial Cell Adhesion Molecule 1
PSC	Pluripotent stem cell
qRT-PCR	Quantitative real-time polymerase chain reaction
RIN	RNA integrity number
RT	Room temperature
SCNT	Somatic cell nuclear transfer
SeV	Sendai-virus
SMAD4	SMAD family member 4
SMARCA4	ATP-dependent chromatin remodeler SMARCA4
SMARCAD1	SWI/SNF-related matrix-associated actin-dependent regulator of chromatin subfamily A containing DEAD/H box 1
SNP	Single nucleotide polymorphism
SOX2	Sex determining region Y-box 2
TBST	Tris-buffered saline with Tween20
TBX6	T-box transcription factor 6
TGF beta	Transforming growth factor beta
TRA-1-60	Podocalyxin-Like Protein 1
TUJ1	Class III beta-tubulin
Wnt	Wingless Int-1, signalling pathway

1. INTRODUCTION

1.1 Adult skeletal muscle

Skeletal muscle comprises up to 40% of the human body mass. It allows voluntary movement and plays a key role in regulating metabolism and homeostasis in the organism. Skeletal muscle is one of the most dynamic and plastic tissues of the human body and its mass depends on the balance between muscle fibre synthesis and degradation. This balance is influenced by factors like age, activity, nutrition, injury or disease with a significant impact on life quality (Reviewed in Frontera and Ochala 2015).

Human skeletal muscle is composed of longitudinally aligned muscle fibres grouped in fascicles that are connected at their extremities to the tendons. The tendons themselves are connected to the bones. Each muscle is surrounded by a layer of connective tissue called epimysium. The fascicles are surrounded by the perimysium and each single muscle fibre is surrounded by the basal lamina (endomysium). A single muscle fibre is composed of multiple post-mitotic nuclei and consecutively assembled sarcomeres. Sarcomeres are the contractile unit of the skeletal muscle, containing thin and thick myosin and actin filaments. Interaction of these filaments together with ATP-dependent movement of the globular heads of myosin are responsible for muscle contractions triggered by $Ca2^{+}$ influx into the sarcoplasm induced by action potentials coming from the motor neurons (Reviewed by Frontera and Ochala 2015 and Kandel et al. 2013).

1.2 Embryonic skeletal muscle development

Skeletal muscles of the body originate from the somites, which are structures formed in the paraxial mesoderm during embryonic development. Exceptions like the muscles of the head and the neck are formed in the anterior part of the paraxial mesoderm, where no somites are formed. The paraxial mesoderm is an embryonic structure flanking the neural tube during embryonic axis elongation. It is subdivided in a committed anterior and an immature posterior part. The somites are formed in the committed anterior part of the paraxial mesoderm while the posterior part is composed of unsegmented structures forming the presomitic mesoderm (Figure 1.1). The specification of the paraxial mesoderm into different cell stages is largely based on Wnt- and fibroblast growth factor (FGF) signalling gradients (Ciruna & Rossant, 2001). Essential transcription factors for the segmented specification of the paraxial mesoderm like T, TBX6 and Msgn1 are targets of the Wnt/FGF signalling pathways. The specification of paraxial mesoderm begins with the exit of precursor cells from the progenitor zone entering the posterior presomitic mesoderm in which cells are marked by the expression of Msgn1 and TBX6 (Figure 1.1, A) (Chapman et al., 1996) (Reviewed by Chal and Pourquié 2017).

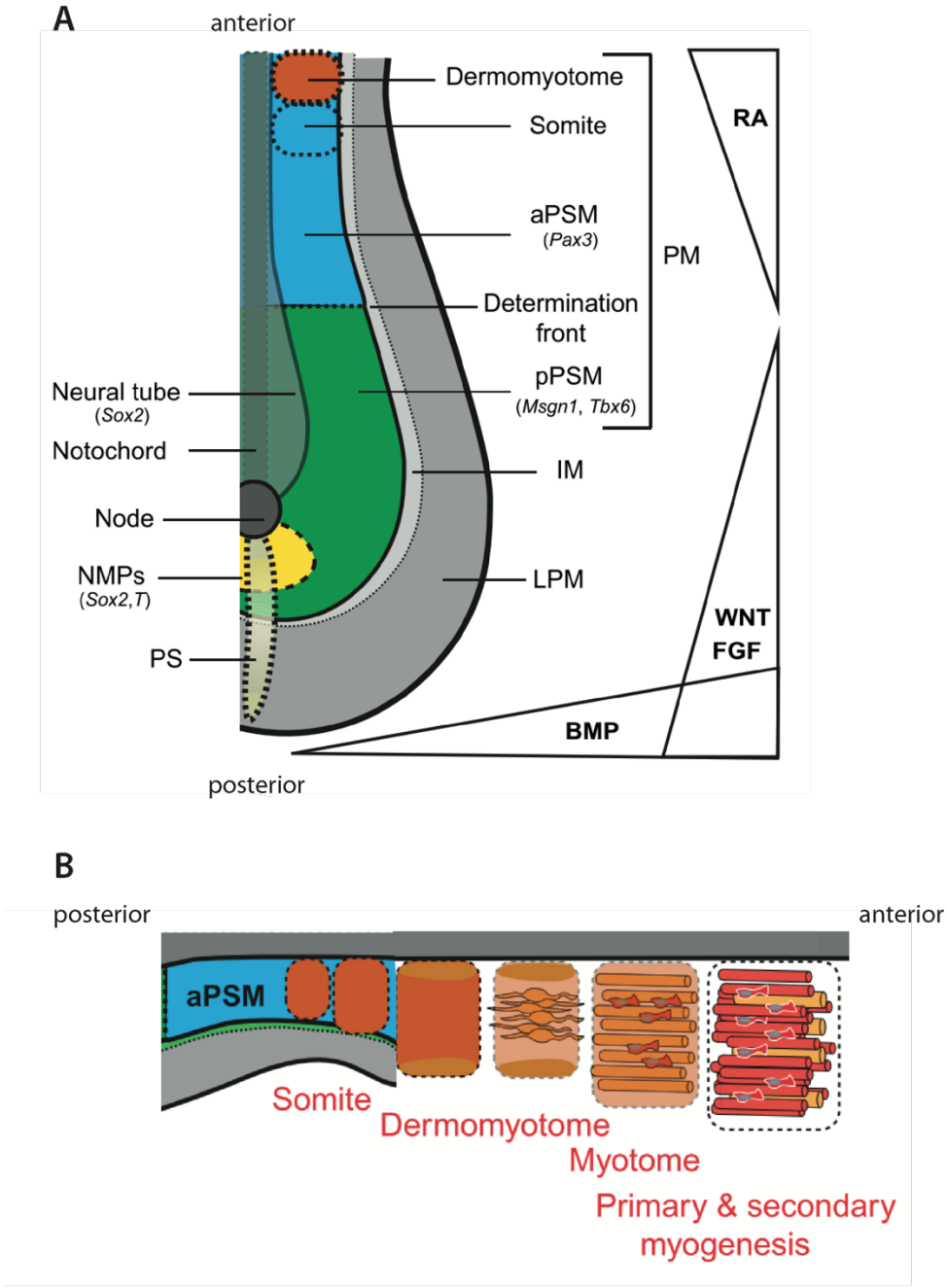

Figure 1.1: Myogenesis in the early developmental stages
Colours indicate different mesodermal developmental stages and are matched within A and B. (A) Spatial organisation of mesoderm development in the posterior part of an amniote embryo. Mesoderm forms by migration of cells from the primitive streak (PS). Progressively, mesoderm tissues are separated by lateral development forming paraxial mesoderm (PM), intermediate mesoderm (IM) and lateral plate mesoderm (LPM). The development is depending on gradients of signalling pathways like BMP, Wnt, FGF and Retinoic acid (RA). Paraxial mesoderm progenitors are located in the anterior part of the primitive streak (PS) that includes the neuromesodermal progenitors (NMPs). The determination front within the paraxial mesoderm defines a signalling threshold between Wnt/FGF and counteracting RA signalling, which drives the specification of posterior presomitic mesoderm (pPSM) and anterior presomitic mesoderm (aPSM). Adapted and modified from (Chal & Pourquié, 2017). (B) Somites are formed in the anterior part of the aPSM and develop into further specialised tissues like Dermomyotome and Myotome. Adapted and modified from (Pourquié, Al Tanoury, & Chal, 2018)

Bone morphogenetic protein (BMP) signalling also plays an essential role in the development of the paraxial mesoderm. BMP is expressed by lateral tissues like the lateral plate mesoderm (Figure 1.1) while its signalling is counteracted by BMP antagonists like Noggin in the axial structures of the embryo where the paraxial mesoderm is formed (Reviewed by Chal and Pourquié 2017; Reshef, Maroto, and Lassar 1998). Tonegawa et al. demonstrated, that a Noggin-producing bead, grafted into tissues giving rise to lateral plate mesoderm, converted cells towards a paraxial mesoderm fate (Tonegawa et al., 1997). This shows the plasticity of the developing tissues and indicates the importance of BMP inhibition to acquire and maintain paraxial mesoderm fate.

The development towards the somites is controlled by a molecular oscillator, the so called segmentation clock, that is periodically inducing somite production by pulses of Wnt, FGF and Notch signalling (Reviewed in Hubaud and Pourquié 2014). The determination front within the paraxial mesoderm defines a signalling threshold between Wnt/FGF and counteracting RA signalling, which drives the specification of posterior presomitic mesoderm (pPSM) and anterior presomitic mesoderm (aPSM). Behind the determination front, the Wnt/FGF signalling is counteracted by retinoic acid signalling (RA), necessary for somite formation (Figure 1.1) (Reviewed by Chal and Pourquié 2017).

The newly formed somites are segmented into the dermomyotome and the sclerotome. While the sclerotome gives rise to the axial skeleton and tendons, the dermomyotome is the origin of the skeletal muscle, brown fat and dermis of the back. In the newly formed dermomyotome, cells start to express the early myogenic factor PAX3 (Bober et al., 1994) and subsequentially also MYF5 and PAX7 (Gros et al., 2005; Relaix et al., 2005). Further development leads to the formation of the myotome between the dermomyotome and the sclerotome, containing the first postmitotic nuclei expressing myogenic genes like slow (Myh7) and embryonic (Myh3) myosin heavy chain, a-actins and Desmin (Babai et al., 1990; Lyons et al., 1990). The newly formed myocytes mature by elongation and more $PAX3^+$ cells migrate from the dermomyotome into the myotome and into the developing limb buds progressively organising into myofibres (Reviewed by Buckingham et al. 2003; Relaix et al. 2005). These early myofibres represent the basis upon which adult muscles will be built (Murphy & Kardon, 2011). They are controlled by a specific set of muscle regulatory factors (MRFs) including MYF5, MYOD1, MRF4 and Myogenin (Berkes & Tapscott, 2005). Myogenin is specifically responsible for the terminal differentiation of myoblasts into myocytes (Venuti et al., 1995).

Myogenesis can be divided into two phases. The primary or embryonic phase describes the formation of primary myofibres from PAX3 expressing dermomyotomal progenitor cells (Horst et al., 2006). During secondary myogenesis, $PAX3^+$ cells start to express PAX7 and fuse with each other or with the existing early myofibres (Figure 1.2). These myofibres start to express also the fast myosin heavy chain isoforms (Myh1, Myh2, Myh4) (Reviewed by Schiaffino and Reggiani 2011) and further mature to become highly organised skeletal muscle structures. A subset of the $PAX7^+$ cells will later form the pool of adult $PAX7^+$ muscle stem cells, known as satellite cells (Relaix et al., 2005; Lepper &

Fan, 2010). PAX7$^+$ nuclei constitute up to 30% of the sublaminal nuclei on myofibres in early postnatal murine muscles. This number declines to less than 5% in adult muscles (Allbrook, Han, & Hellmuth, 1971). Once the pool of satellite cells is established, the number of satellite cells remains stable even after multiple rounds of injuries and is only decreasing at a very old age (Shi & Garry, 2006; Sousa-Victor et al., 2014).

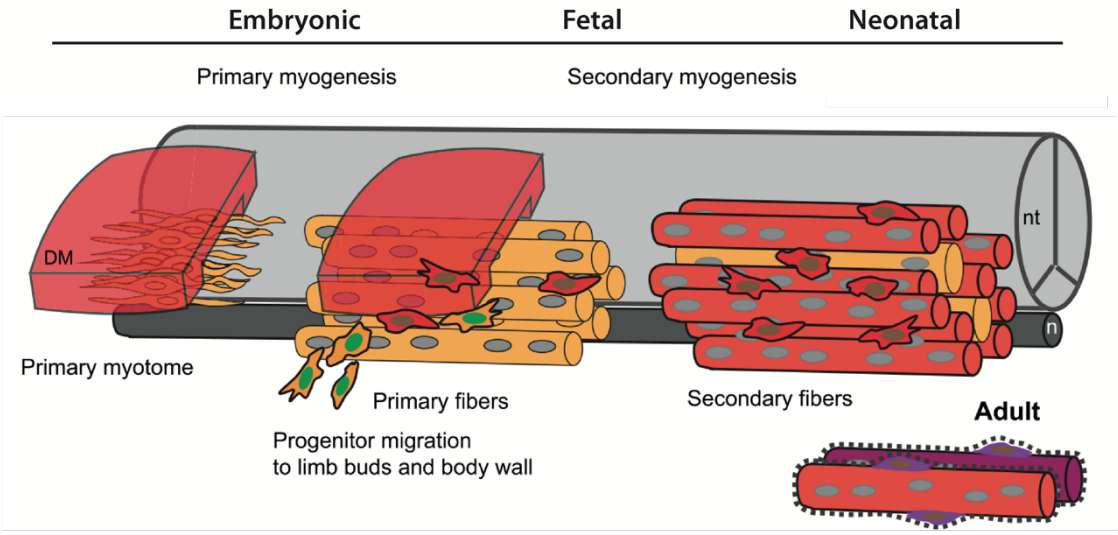

Somitic stem cells	Fetal stem cells	Myocytes	Satellite cells	Myofibers
PAX3	PAX7	MYOD1	PAX7	Fast MyHC
PAX7	MYF5	Myogenin	MYF5	IIa (Myh2)
	PAX3	Slow MyHC (MYH7)	PAX3	IIb (MyH4)
		Embryonic MyHC (MYH3)	VCAM1	IIx (Myh1)
		Perinatal MyHC (MYH8)	NCAM1	

Figure 1.2: Myogenesis from the embryo to the adult
Early myocytes in the early myotome are aligned along a posterior/anterior axis (left, mononuclear cells in yellow). In primary myogenesis PAX3$^+$ progenitor cells (mononuclear cells with yellow cytoplasm and green nucleus) contribute to the formation of primary myofibres (multinucleated, cylinder-shaped, yellow). During secondary myogenesis, PAX7$^+$ cells (mononuclear cells with red cytoplasm and brown nucleus) fuse to the existing primary myofibres to form secondary myofibres (multinucleated, cylinder-shaped, red). At the same time PAX7$^+$ satellite cells (mononuclear cells with purple cytoplasm and brown nucleus) migrate below the basal lamina (dotted line) where they are found in the adult muscle. Markers expressed during the specific stages are listed. Adapted and modified from (Chal & Pourquié, 2017).

Signalling molecules like hepatocyte growth factor (HGF), insulin-like growth factor (IGF), fibroblast growth factor (FGF) and Wnt signalling have all been shown to be important for the activation of satellite cells. Besides, IGF signalling together with Wnt signalling promote myogenesis and myoblasts fusion while FGF signalling promotes myoblasts proliferation and blocks differentiation (Chargé and Rudnicki 2004).

1.3 Adult skeletal muscle regeneration

Adult skeletal muscle possesses the regeneration capacity to initiate a synchronised biological response that leads to complete regeneration of injuries in healthy adults. This regenerative capacity is based on an inflammatory response and on the function of adult muscle satellite stem cells that in part recapitulate embryonic developmental stages controlled by sequential expression of essential myogenic transcription factors. In case of muscle damage like injury, trauma or also in case of muscular dystrophies, a defined sequential series of biological processes is activated, regardless of the type or severity of the injury (Schmidt et al., 2019).

1. Degenerative / Inflammatory phase: The initial phase takes place during the first days after the injury. It is characterised by necrosis of muscle fibres, followed by an invasion of immune cells and the removal of cellular debris. Neutrophils are the first immune cells to invade the site of injury, expressing high amounts of pro-inflammatory cytokines, chemokines and growth factors attracting other inflammatory cells such as monocytes and macrophages. (Reviewed in Laumonier and Menetrey 2016).
2. Regeneration phase: This phase starts a few days after injury. Pro inflammatory M1 macrophages remove debris and secrete cytokines that stimulate the proliferation and migration of satellite cells. Following activation, satellite cells proliferate and generate a population of myogenic progenitor cells (myoblasts) that can either differentiate to repair damaged fibres or self-renew to maintain the satellite stem cell pool. M1 macrophages turn into anti-inflammatory M2 macrophages which stimulate the fusion of myoblasts into multinucleated myotubes. There are also other cell types influencing this process, among them the Fibro-adipogenic-progenitor cells (FAPs) that can activate satellite cells and induce differentiation in activated myogenic progenitor cells (Reviewed in Laumonier & Menetrey, 2016; Qazi et al., 2019; Schmidt et al., 2019).
3. Remodelling / Maturation phase: The final phase involves the maturation of myotubes into functional, contractile myofibres, revascularisation and the establishment of neuromuscular junctions. The remodelling of the connective tissue extracellular matrix is an omnipresent process during regeneration, as it is needed to provide a scaffold for myofibre regeneration. However, tight regulation of connective tissue remodelling is essential for the degree of scar tissue formation (Reviewed in Laumonier and Menetrey 2016; Qazi et al. 2019).

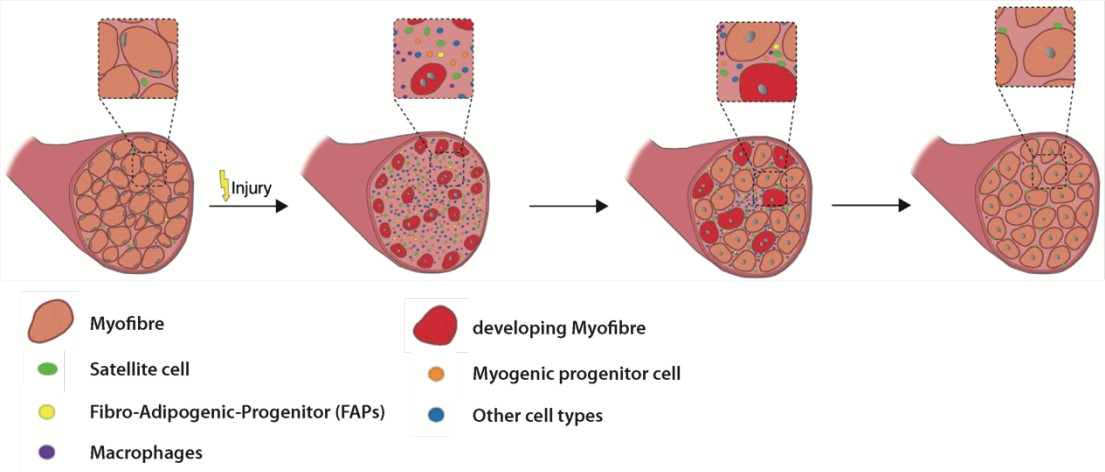

Figure 1.3: Schematic description of the muscle regenerative process
Following muscle injury, immune cells clear the site of injury and satellite cells activate and differentiate to form new myofibres. Myogenic progenitor cells fuse to myofibres so that the muscle structure is re-established. The newly regenerating myofibres are characterised by centrally located nuclei. During maturation the nuclei migrate to the periphery. Adapted and modified from (Schmidt et al., 2019).

1.3.1 Satellite cells

Satellite cells were first discovered by Alexander Mauro in 1961 as mononuclear cells with a high nucleus to cytoplasm ratio. These cells were named satellite cells because of their defined dispersed location described as "wedged" in between the basal lamina and the sarcolemma (Mauro, 1961). Mauro suggested that satellite cells may be "pertinent for the vexing problem of skeletal muscle regeneration". Indeed, up to the present day, studies have shown that progenitor cells become committed to myogenesis in embryonic development and maintain this commitment in the adult as satellite cells (Relaix et al., 2005; Lepper & Fan, 2010). Adult satellite cells mainly remain in a quiescent state in the muscle stem cell niche (Schultz, Gibson, & Champion, 1978). Following an injury to the skeletal muscle, satellite cells activate and re-enter the cell cycle. Satellite cells either divide symmetrically for self-renewal and maintenance of the satellite cell pool or enter asymmetric division to produce committed myoblasts that contribute to muscle fibre repair (Shinin et al., 2006; Kuang et al., 2007). Self-renewal and specific differentiation fulfil the defining criteria of a tissue specific adult stem cell. Satellite cells possess those two characteristics, and as suggested by Alexander Mauro, they indeed contribute to, and furthermore are mainly responsible, for the regenerative process of skeletal muscle as was first shown by Bischoff and Konigsberg (Bischoff, 1975; Konigsberg, Lipton, & Konigsberg, 1975) (Reviewed by Dumont et al. 2015 and Wosczyna and Rando 2018).

In adult skeletal muscle, quiescent and activated satellite cells are characterised by the expression of the paired box transcription factor PAX7 (Seale et al., 2000). Ablation of the PAX7 gene in mice has been shown to result in a reduced number of satellite cells in the skeletal muscle and the majority of mice die 2-3 weeks after birth (Seale et al., 2000; Oustanina, Hause, & Braun, 2004; Günther et al., 2013). Various studies have shown a complete lack of injury induced skeletal muscle

regeneration after depletion of PAX7$^+$ satellite cells (Lepper, Partridge, & Fan, 2011; Sambasivan et al., 2011; Günther et al., 2013; von Maltzahn et al., 2013). Interestingly, the induced depletion of PAX7 in young adult mice, which was sufficient to impair muscle regeneration throughout the rest of their lives, did not lead to myopathies or muscle degeneration (Fry et al., 2015).

The population of PAX7$^+$ satellite cells has been shown to be heterogeneous. A subset of satellite cells was shown to express higher levels of PAX7 and specifically segregate template DNA strands to the daughter cells that will become a stem cell in asymmetric cell divisions. Cells with high PAX7 expression showed a delayed initiation of the first mitosis compared to cells with low PAX7 expression, which points towards a mechanism in stem cell pool maintenance involving high PAX7 expressing cells (Rocheteau et al., 2012).

1.3.2 Myogenic regulatory factors

PAX7 and PAX3 induce the expression of genes involved in proliferation and commitment to the myogenic lineage but block further differentiation (Soleimani et al., 2012). MYOD1, MYF5 and MYOG are transcription factors downstream of PAX7 and PAX3 which promote myogenic differentiation (Hernández-Hernández et al., 2017). Upon an injury, quiescent PAX7$^+$ satellite cells activate, re-enter the cell cycle and start to express the transcription factor MYOD1 (Figure 1.4) (Zammit et al., 2004).

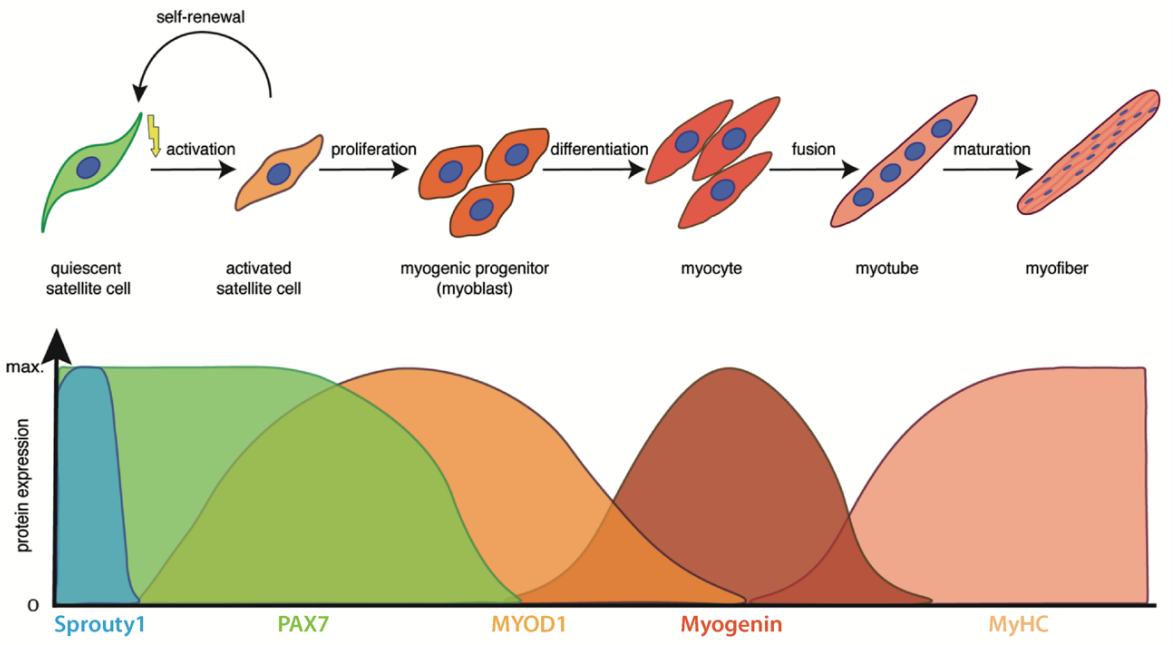

Figure 1.4: Myogenic differentiation states and marker expression during regeneration.
PAX7$^+$ quiescent satellite cells activate and start to express MYOD1. Myogenic progenitor cells differentiate into myocytes and fuse to becomemultinucleated myotubes and myofibres which is accompanied by the expression of late myogenic markers Myogenin and Myosin Heavy Chain (MyHC). Modified from (Schmidt et al., 2019)

A subpopulation of activated satellite cells re-enters quiescence and returns to the satellite cell niche (Olguín & Pisconti, 2012). Quiescent satellite cells maintain a mitotically inactive state, a process that is depending on Sprouty1 (Shea et al., 2010). PAX7 and MYOD1^{+} progenitor cells migrate towards the site of injury to fuse with the damaged muscle fibres. Upon further differentiation, upregulation of Myogenin happens simultaneously with the downregulation of MYOD1. The expression of myosin heavy chain marks the terminally differentiated multinucleated myotubes and myofibres. (Reviewed in Chen and Shan 2019 and Schmidt et al. 2019).

1.3.3 Regenerative potential of transplanted PAX7^{+} satellite cells

Murine PAX7^{+} satellite cells, isolated by mechanical and enzymatical disruption of the skeletal muscle followed by FACS purification using cell surface markers, have been shown to contribute to muscle fibre regeneration and repopulation of the stem cell niche (Montarras et al., 2005; Cerletti et al., 2008; Sacco et al., 2008).

Unfortunately, the surface marker profile used for the isolation of murine cells, was not simply adaptable to enrich human satellite cells. However, various studies have recently reported isolation protocols for human myogenic progenitor and satellite cells with engraftment potential in xenograft mouse models using large sets of surface markers like CD45^{-}/CD11b^{-}/GlyA^{-}/CD31^{-}/CD34^{-}/CD56^{int}/ITGA7^{hi} (Castiglioni et al., 2014), CD34^{-}/CD31^{-}/CD45^{-}/ITGB1^{+}/EGFR^{+} (Charville et al., 2015), MCAM/CD82 (Alexander et al., 2016) or Sytox^{-}/CD31^{-}/CD34^{-}/CD45^{-}/CXCR4^{+}/CD29^{+}/ CD56^{+} (Garcia et al., 2018). Importantly, in addition to the formation of human myofibres, the repopulation of the muscle stem cell niche was confirmed by the presence of human PAX7^{+} cells in the satellite cell position. Moreover, the engrafted human satellite cells robustly formed human myofibres after additional injury (Xiaoti Xu et al., 2015). Human myofibre regeneration and repopulation of the muscle stem cell niche with human PAX7^{+} cells was also shown by transplantation of whole human muscle fibre fragments (HMFFs). HMFFs were prepared and dissociated manually, without enzymatic digestion, leaving the basal lamina and the satellite cell niche intact, leading to a robust engraftment capacity and large numbers of PAX7^{+} cells derived from HMFFs in vitro (Marg et al., 2014).

These results are encouraging for the application of human satellite cells in clinical cell therapies. However, the availability of human satellite cells is often an issue due to their low abundance and dispersed location in the muscle stem cell niche. Therefore, autologous cell transplantations using satellite cells are complicated, as satellite cells will hardly become available in the very high numbers that would be necessary for gene correction and repopulation in many genetic disorders.

1.4 Inherited myogenic disorders

Muscular dystrophies (MDs) are a heterogeneous group of inherited muscle disorders that are characterised by progressive muscle wasting and degeneration. The clinical presentation includes a wide range of different disorders like Duchenne, Becker, Emery-Dreifuss, distal, myotonic, facioscapulohumeral, oculopharyngeal or the group of limb-girdle muscular dystrophies. They are characterised by the age of onset, mode of inheritance and the muscle groups initially affected. The main muscles affected are the limb muscles, axial and facial muscles and in specific forms respiratory, cardiac smooth and swallowing muscles (Emery, 2002; Mercuri & Muntoni, 2013). Muscular dystrophies may lead to severe pain, disability and eventually death by respiratory or cardiac insufficiency, depending on the muscle groups affected. The most severe and most common childhood form, Duchenne Muscular Dystrophy (DMD), has an incidence of 1:3500 male births and leads to wheelchair dependency before the age of 13 (Annexstad, Lund-Petersen, & Rasmussen, 2014). Currently, there is no definitive cure available for muscular dystrophies and treatments aim to delay progression and ease the discomfort of the patients (Mercuri & Muntoni, 2013).

1.4.1 Regeneration in disease conditions

Muscular dystrophies are caused by mutations in genes with a large functional diversity of the encoded proteins, ranging from the extracellular matrix to the plasma membrane to cytosolic enzymes or nuclear proteins (Kinter & Sinnreich, 2014). The pathophysiological mechanisms leading from the mutations to the development of the dystrophic features are still not completely understood. However, the lack of those proteins increases the probability of muscle damage during muscle contraction and homeostasis and the ensuing replacement of muscle fibres by adipose and connective tissue (Berardi et al., 2014; Kinter & Sinnreich, 2014; Negroni et al., 2015). Due to the continuous degeneration, an imbalance between muscle damage or degeneration and muscle repair mediated by the stem cells is thought to contribute to the disease pathology (Wallace & McNally, 2009). Unfortunately, in case of muscular dystrophies, satellite cells and the regenerated muscle fibres carry the genetic defect and are thus still diseased. This in turn leads to continuous cycles of damage and repair until the muscle stem cell pool is exhausted (Luz, Marques, & Santo Neto, 2002; Palmieri & Tremblay, 2010; Berardi et al., 2014).

1.4.2 Cell transplantations for muscular dystrophies

Cell replacement therapies represent a key element in the development of therapeutic approaches to muscular dystrophies. Various clinical trials are ongoing concerning different subtypes of muscular dystrophies. Trials concerning Duchenne muscular dystrophy, the most common form of muscular dystrophies, currently focus on cell and gene therapy approaches (Reviewed in Shimizu-Motohashi et al., 2019).

Despite the recent advancements in purification and transplantation of satellite cells into xenograft-compatible mouse models, they are still isolated in small numbers (Xiaoti Xu et al., 2015). Once satellite cells are activated they start to differentiated into myoblasts and rapidly downregulate the stem cell marker PAX7 while upregulating markers of differentiation (Reviewed by Briggs & Morgan, 2013). Thus, in vitro expanded myoblasts were used in clinical trials because they were available in sufficient numbers. A clinical study using myoblasts for the transplantation into patients with Duchenne muscular dystrophy showed 10% of donor-derived dystrophin but did not improve muscle strength (Mendell et al., 1995). Another clinical trial is currently ongoing using high-density injections of myoblasts with optimised procedures originating from primate studies (Skuk et al., 2006; Clinical Trial Number: NCT02196467).

Other cell types with myogenic potential have been described, like $CD133^+$ cells (Torrente et al., 2004), mesangioblasts (Minasi et al., 2002) and pericytes (Dellavalle et al., 2007). Human $CD133^+$ cells have been shown to repopulate the muscle stem cell niche position in xenografts (Meng et al., 2014). Although these cells were shown to be safe in clinical application (Torrente et al., 2007), their myogenic potential is reduced after prolonged culture reducing their applicability for therapy (Meng et al., 2014). Mesangioblasts seemed to hold great promise for therapeutic application due to their robust muscle regenerative capacity and ability to be cultured for prolonged time periods in vitro enabling gene correction (Minasi et al., 2002). Sampaolesi et al. could show very promising results in ameliorating muscle function in dystrophic dogs (Sampaolesi et al., 2006). Unfortunately, the same did not hold true for humans, even though Cossu et al. could verify the safety of the method (Cossu et al., 2015).

Besides primary cells with myogenic potential, pluripotent stem cells (PSCs) hold great promise for the development of cell therapies for muscular dystrophies due to their ability to differentiate into the myogenic lineage and at the same time the potential for unlimited numbers of autologous cells. Several protocols have been established for the differentiation of PSCs towards the myogenic lineage (Darabi et al., 2012; Tedesco et al., 2012; Shelton et al., 2014; Chal et al., 2015, 2016). PSCs are highly proliferative and can be cultured for long time periods in vitro, which facilitates the genetic correction of the disease-causing mutations. Indeed, in vitro CRISPR/Cas9 correction of many mutations within muscular dystrophy-causing genes like dystrophin (Reviewed by Min, Bassel-Duby, & Olson, 2018) or dysferlin and alpha-sarcoglycan (Turan et al., 2016) has been successfully shown. In addition, genetically corrected hiPSCs were differentiated into myogenic cells and have been engrafted into xenograft-compatible mouse models, showing the formation of human muscle fibres (Tedesco et al., 2012; Young et al., 2016; Hicks et al., 2018). These results hold great promise for any future therapeutic application of these cells, although major safety issues as the tumorigenic subpopulations in hiPSC-derived cells have to be detected and eliminated, as recently shown for hiPSC-derived cardiomyocytes (Ito et al., 2019).

1.5 Pluripotent stem cells

In 1957, C.H. Waddington published his well-known model of embryonic development, depicting the process of embryonic cell development as a ball rolling down a hill with many branch points giving multiple routes to reach the end point of terminal differentiation (Waddington, 1957). As early as 1962 the dogma of unidirectional development was challenged by the experiments of John Gurdon. He used somatic cell nuclear transfer (SCNT) and injected the nucleus from a differentiated intestinal epithelial cell into an enucleated oocyte (Gurdon, 1962), showing cellular reprogramming by cloning a frog. The cloning of the sheep Dolly by SCNT showed that mammalian adult somatic cells were capable of reverting back to a totipotent state and develop into a whole animal (Wilmut et al., 1997).

An important hint for the existence of factors that have the potential to alter cell fate in vitro, the so called reprogramming factors, came from the direct programming of mouse fibroblasts into myoblasts by ectopic overexpression of the myogenic differentiation factor 1 (MYOD1) (Davis, Weintraub, & Lassar, 1987). The establishment of culture techniques for embryonic stem cells (ESCs), isolated from early mice embryos, enabled the investigation of cells in vitro that were characterised by self-renewal and the potential to generate all cell types of the body (Evans & Kaufman, 1981; Martin, 1981). Later, fusion experiments of somatic cells to ESCs showed that the resulting hybrid cells have proper characteristics of ESCs (Tada et al., 2001; Cowan et al., 2005) suggesting that there are reprogramming factors that can be potentially controlled by scientist. Finally in 2006, the key factors for in vitro reprogramming of mouse somatic cells into pluripotent stem cells were discovered by the group of Shin'ya Yamanaka (Takahashi & Yamanaka, 2006). The newly reprogrammed cells were named induced pluripotent stem cells (iPSCs) and the adopted protocol for human cells was published one year later (Takahashi et al., 2007).

1.5.1 Generation of induced pluripotent stem cells (hiPSCs)

The establishment of induced pluripotent stem cells from adult somatic cells was a significant breakthrough and opened up new perspectives for the research of basic developmental biology as well as for new clinical applications. iPSCs could potentially replace ESCs, thus overcoming the ethical controversy regarding ESCs, which originate from the inner cell mass (ICM) of the embryo and whose retrieval thus results in the destruction of a human embryo.

The four so called "Yamanaka factors", that were sufficient for the reprogramming process, were OCT3/4, SOX2, KLF4 and c-Myc (OSKM) (Takahashi & Yamanaka, 2006; Takahashi et al., 2007). Shortly after Shin'ya Yamanaka´s group discovered the OSKM reprogramming cocktail, another group, led by James Thomson, also reported about the reprogramming of human somatic cells into hiPSCs by four transcription factors. They used OCT3/4 and SOX2 as well, but instead of using KLF4 and c-Myc, NANOG and LIN28 were used (Yu et al., 2007). Following studies showed that some but

not all protein family members of the OSKM cocktail alone or in combination can reprogramme mouse embryonic feeder cells into hiPSCs (Nakagawa et al., 2008). The same study showed that the reprogramming of mouse and human somatic cells is possible without c-Myc but results in a decreased reprogramming efficiency. Other studies showed that OCT3/4 can be replaced by E-cadherin (Redmer et al., 2011) or OCT3/4 and SOX2 can be replaced by GATA3 and ZFP521 (Montserrat et al., 2013). In addition, all OSKM factors can be replaced by their own downstream targets (Buganim et al., 2012). A number of small molecules was discovered that can compensate for one or more Yamanaka factors (Reviewed by Borgohain et al. 2019) or even completely replace the need of the initial OSKM cocktail for chemical reprogramming into iPSCs (Hou et al., 2013; Long et al., 2015; Ye et al., 2016). The complete replacement of transcription factor delivery was only achieved in mouse cells so far. Even though many discoveries have been made regarding the replacement of reprogramming factors, the initial OSKM Yamanaka cocktail is still the most commonly used mixture in research.

1.5.1.1 Delivery systems for the reprogramming factors

The first reprogramming experiments were performed using retroviruses as delivery systems for the OSKM transcription factors. Unfortunately, this technique harbours the risk of tumorgenicity due to the random genomic integration of the virus-delivered transgenes and the transactivation of neighbouring genes. The transgenes are not removed but stably integrated into the genome and the reactivation of the transgene c-Myc was shown to be responsible for increased tumorgenicity in iPSCs (Okita, Ichisaka, & Yamanaka, 2007). Additionally, the residual expression of OSKM factors affected the transcriptional programmes and epigenetic signatures of iPSCs (Sommer et al., 2012). Non-viral reprogramming via plasmids was shown as an alternative (Okita et al., 2008) but this technique still harbours the risk of random genomic integrations.

Thus, integration-free delivery systems were developed as first shown with the use of Sendai-viruses for the reprogramming of fibroblasts into integration free iPSCs (Fusaki et al., 2009). The advantage of Sendai-viruses is that they have a negative sense, single stranded RNA genome with a replication cycle without a DNA phase. In addition, the replication only occurs in the cytoplasm, resulting in non-integrating transcription factor delivery (Figure 1.5). Furthermore, Sendai-viruses have been shown to have a high transduction efficiency for a broad range of tissues (Bitzer et al., 2003) and a high and rapid expression rate of proteins within twenty-four hours of transduction (Hosoya et al., 2008). Sendai-viruses and associated proteins are lost within 10 to 20 passages in the newly generated iPSCs. To diminish the ability of self-replication and reduce the immunogenicity, next generation Sendai-viruses were developed with deletions of the structural virus genes F, HN and M (Nishimura et al., 2011). Furthermore, to be able to eliminate Sendai-viruses from the host cells, point mutations in the viral P and L genes were inserted to produce Sendai-viruses sensitive to a short temperature shift (Ban et al., 2011). In general, the production of Sendai-viruses is very expensive, but

the availability of a commercially available kit makes it still the most popular technique used for reprogramming.

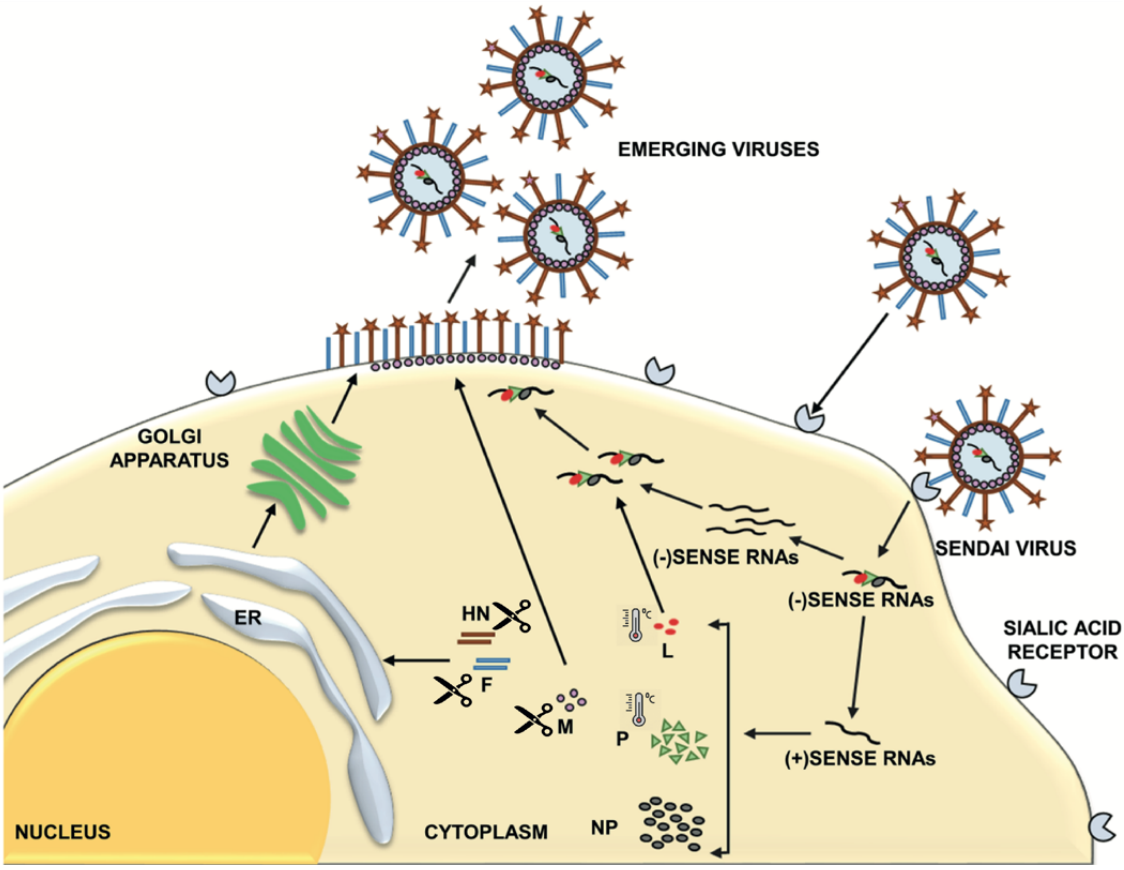

Figure 1.5: Life cycle of Sendai-viruses
The Sendai-virus is binding to the sialic acid receptor via the HN (haemagglutinin-neuraminidase) protein and releases its nucleocapsid into the host cell by F (Fusion) protein-mediated membrane fusion. Replication and transcription of the negative sense RNA takes place exclusively in the cytoplasm and does not require host nuclear components. L (Large) and P (Phospho) proteins comprise the RNA polymerase complex. Newly generated L, P and NP (Nucleoprotein) proteins bind to the negative sense RNA and form the nucleocapsid. The M (Matrix) protein migrates towards the cell membrane together with the HN and F proteins, after they have been processed through the endoplasmatic reticulum and Golgi apparatus. New virus particles are released when enough NP protein is available. The enhanced Sendai-viruses, used for biotechnological applications, are deleted of the structural virus genes F, HN and M, making them less immunogenic and self-replicating (marked by scissors). Additionally, point mutations in the L and P proteins were inserted to make the viruses temperature sensitive for enhanced removal from the host cells (marked by thermometer). Adapted and modified from (Borgohain et al., 2019).

Other promising delivery methods have been developed and successfully tested like the use of recombinant proteins, mRNAs, microRNAs or the reprogramming via the use of small molecules (Reviewed by Borgohain et al. 2019). The use of small molecules was so far only shown in mouse cells. The reprogramming via recombinant proteins is slow and inefficient but considered to be the safest methods among all. The mRNA approach is currently more and more improved to derive iPSCs efficiently and fast and to overcome hurdles like immunogenicity and the need of daily transfections.

1.5.1.2 Efficiency of somatic cell reprogramming

Reprogramming of somatic cells remains inefficient with only a small population of cells actually transforming into induced pluripotent stem cells. Reprogramming has been reported with an efficiency of 0.001 – 1% using different delivery methods for the reprogramming factors and different somatic cell types (Reviewed by Borgohain et al. 2019).

Two models exist for explaining of these low efficiency rates. The so-called elite model describes a heterogeneous population of somatic cells, with only a small population of progenitor or stem cells within this population that are able to reprogramme into iPSCs. However, studies explicitly using terminally differentiated cells like B lymphocytes and pancreatic beta cells showed reprogramming into iPSCs, arguing against this model (Hanna et al., 2008; Stadtfeld, Brennand, & Hochedlinger, 2008). The other so-called stochastic model presumes that reprogramming is induced in all cells which received the OSKM cocktail but only a few cells finish the reprogramming process until the end. The majority of the cells faces issues in the process of reprogramming, thus ending in the collapse of the whole process within these cells (Reviewd by Karagiannis et al., 2018).

The early phase of reprogramming is marked by dynamic remodelling of the chromatin status of the cells (Soufi, Donahue, & Zaret, 2012). Important steps in the early phase of the reprogramming are the deactivation of genes defining the somatic phenotype of the cells and the switch from oxidative phosphorylation to glycolysis (Panopoulos et al., 2012). Additionally, cells are going through an mesendodermal phase during the reprogramming process (Takahashi et al., 2014). The maturation of reprogrammed cells has been shown as the major roadblock to gaining fully reprogrammed iPSCs and that cells in the late phase of reprogramming slowly oscillate between complete and incomplete reprogramming stages (Tanabe et al., 2013). The same study showed that the mesendodermal state is trigger by high OCT3/4 and low SOX2 expression and that the proper amount of all OSKM transcription factors during all stages of the reprogramming process is crucial for its success. The late phase of reprogramming is marked by the activation of pluripotency genes and methylation events. Failing in completing any of these crucial events may result in abortion of the reprogramming process. In addition, DNA damage was shown to prevent the reprogramming process (Marión et al., 2009). So far, many reprogramming barriers have been identified like epigenetic roadblocks, signalling pathways, the ubiquitin proteasome system, genomic instability, certain microRNAs and transcription factors, etc. all of which a somatic cell has to overcome in order to attain a pluripotent state (Ebrahimi, 2015). These barriers might explain the low efficiency rate of reprogramming somatic cells into the pluripotent state.

1.5.1.3 Characterisation of induced pluripotent stem cells (iPSCs)

iPSCs have been characterised by their comparability to embryonic stem cells (ESCs) as established by the first iPSC studies (Takahashi & Yamanaka, 2006; Takahashi et al., 2007). Mouse iPSCs

are characterised by their morphology, their expression of pluripotent marker genes, the formation of all three germ layers in teratomas and the generation of chimeras after injection into blastocysts (Okita et al., 2007). Due to ethical reasons, chimera formation assays are not permitted for human iPSCs. Instead, the pluripotency of human iPSCs is assessed by the expression of pluripotency markers as OCT3/4, SOX2, NANOG and TRA-1-60 and by the formation of tissues of all three germ layers in teratomas formed after transplantation into immunodeficient animals (Karagiannis et al., 2018).

As the residual expression of the OSKM factors affects the transcriptional programmes of iPSCs (Sommer et al., 2012) and even increases tumorgenicity (Okita et al., 2007), it is necessary to assure the absence of any residual presence of the OSKM factors or of the delivery system used. Furthermore, as copy number variations, mutations or even chromosomal aberrations were detected in newly established iPSCs (Mayshar et al., 2010; Hussein et al., 2011), the evaluation of genomic integrity after the reprogramming process is of importance. As these genomic changes might also affect the cell morphology (Kilpinen et al., 2017), its thorough and continuous analyses is recommended.

1.5.2 Epigenetic memory

The epigenetic memory of a cell describes a pattern of epigenetic modifications like methylations or histone modifications that is originating from the cell type of origin of the cell. Such epigenetic modifications do not alter the genomic sequence of the DNA but are influencing gene expression and thus the properties of the cells including the capability to differentiate into certain tissues in case of PSCs.

hiPSCs have been described to be similar to ESCs regarding morphology, pluripotency marker expression and in vivo teratoma formation (Takahashi & Yamanaka, 2006; Takahashi et al., 2007; Yu et al., 2007). However, hiPSCs are derived from adult somatic cells by severe alteration of the epigenome and functionality of the cells, which may result in differences on the epigenetic and gene expression level for hiPSCs derived from different origins, donors or in comparison to ESCs. Epigenetic and gene expression differences can have a great impact on the characteristics and capabilities of the cells to differentiate into a specific lineage. Therefore, iPSCs have been investigated regarding their epigenetic signatures by methylation pattern, gene expression analysis and differentiation into different lineages compared to ESCs and among different hiPSCs.

1.5.2.1 Aberrant DNA methylations during the reprogramming process

Various studies described the DNA methylation changes that take place during the reprogramming process. Whole-genome DNA-methylation profiles of human iPSCs, ESCs and somatic cells of origin showed significant reprogramming variabilities including aberrant reprogramming of DNA methylation (Lister et al., 2011). Some of these genes were identified as aberrant DNA

modifications occurring during the reprogramming process. (Stadtfeld et al., 2010; Teichroeb, Betts, & Vaziri, 2011; Ruiz et al., 2012). These aberrant modifications can affect the pluripotent characteristics of the generated iPSCs, as cells with hypermethylation of the imprinted loci of the Dlk-Dio3 gene cluster were shown to contribute poorly to chimaeras and failed to develop entirely iPSC-derived animals (Stadtfeld et al., 2010). Furthermore, female hiPSCs have been shown to have defects in X-chromosome reactivation (Anguera et al., 2012) and Ruiz et al. identified nine aberrantly methylated genes using a set of 17 different hiPSCs, enabling the separation of hESCs and hiPSCs (Ruiz et al., 2012). Thus, a major difference between newly generated hiPSCs are the randomly occurring aberrant methylations, that may affect the transcriptomic profile and properties of the generated cells.

1.5.2.2 Influence of the somatic cell type of origin

Several studies showed, that the parental cell origin of the hiPSCs has an influence on the epigenetic profile of the newly generated mouse iPSCs (K. Kim et al., 2010; Polo et al., 2010). These studies found distinct methylation profiles for hiPSCs depending on their somatic cell type of origin. Furthermore, these newly generated hiPSCs still contained transcriptional profiles of genes involved in the lineage specification for their original cell type. The same epigenetic patterns were also found in human iPSCs depending on their cell type of origin (Kitai Kim et al., 2011; Lister et al., 2011; Ohi et al., 2011). Furthermore, several of these studies and others showed a differentiation preference of these iPSCs towards the tissue they were derived from. Polo et al. showed a distinct higher differentiation capacity towards the haematopoietic lineage for blood-derived iPSCs compared to fibroblast-derived iPSCs (Polo et al., 2010). Another study showed higher frequencies of keratinocyte-derived human iPSCs to differentiate back into keratinocytes compared to cord-blood-derived hiPSCs (Kitai Kim et al., 2011). The same effect was shown for cell types like retinal-pigmented epithelial cell (Q. Hu et al., 2010), insulin-producing pancreatic beta cells (Bar-Nur et al., 2011), endothelial cells (Phetfong et al., 2016; S. Hu et al., 2016), limbal epithelial stem cells (Sareen et al., 2014) and cardiomyocytes (Sanchez-Freire et al., 2014). Regarding skeletal muscle, there are two studies using mouse and equine mesangioblasts-derived hiPSCs, demonstrating higher myogenic differentiation capacities for mesangioblast-derived hiPSCs than fibroblast or chondrogenic mesenchymal stem cell-derived hiPSCs (Quattrocelli et al., 2011, 2016). Of note, there are also two studies reporting the opposite. In those studies no preferential differentiation was found, comparing the differentiation of blood- and fibroblast-derived hiPSCs into the haematopoietic lineage (Dorn et al., 2014; Kyttälä et al., 2016).

Interestingly, most of the studies mentioned above were conducted with iPSCs at passages below P20, which is considered to be low or early. Some studies reported that differences between the generated iPSCs diminished over continuous passaging (Polo et al., 2010; Nishino et al., 2011; Ohi et al., 2011; Sanchez-Freire et al., 2014; S. Hu et al., 2016). On the other hand, again the opposite was

reported where no diminution of epigenetic differences and preferential differentiation capacities even in high passages could be found (Kitai Kim et al., 2011; Sareen et al., 2014).

The studies, that reported preferential differentiation into the somatic cell type of origin mainly based their results on in vitro marker expression. On the other hand, in vivo assessment of hiPSC-derived cardiomyocyte function, using a small animal myocardial infarction model, indicated comparable therapeutic capabilities of cardiomyocytes that were differentiated from cardiomyocyte- and fibroblast-derived hiPSCs. (Sanchez-Freire et al., 2014).

1.5.2.3 Influence of the genetic background on hiPSCs

Another influencing factor for differences between hiPSCs, besides aberrant DNA methylations and the somatic cell type of origin, is the genetic background of the donor. Two large studies comparing 28 and 25 hiPSCs lines from different somatic origins across different donors identified the donor background as the major influencing factor for transcriptional variations between the cell lines (Kajiwara et al., 2012; Rouhani et al., 2014). Human iPSCs from different donors have been shown to maintain donor specific differences in methylation patterns in non-promoter regions and outside of CpG islands (Shao et al., 2013). Of note, Kajiwara et al. also reported differences due to the somatic origin of the cells but the interindividual differences have a greater effect on gene expression variation. Kyttälä et al. generated hiPSC lines from only four different donors from fibroblasts and blood cells. They compared gene expression, methylation pattern and differentiation potential towards the haematopoietic lineage and found differences mainly depending on the donor and not on the cell type of origin (Kyttälä et al., 2016).

Interestingly, Nishizawa et al. correlated gene expression, DNA methylation, and chromatin status of of 35 hiPSCs and 4 hESCs with their haematopoietic differentiation potential. They reported on a correlation between insulin-like growth factor 2 (IGF2) expression and haematopoietic commitment of the hiPSCs/ESCs, which is surprising, because IGF2 is not related to the haematopoietic lineage, but its expression turns on signalling-dependent chromatin accessibility at genes that are directly related to the haematopoietic lineage (Nishizawa et al., 2016). Another study reported recently the identification of CXCL4/PF4 as a predictive biomarker of cardiac differentiation potential of human induced pluripotent stem cells (Ohashi et al., 2019).

1.5.2.4 Other influences on the variability of hiPSCs

Other influencing factors have been described that may alter the transcriptome of hiPSCs. The donor age might be important as a study reported an increased risk of somatic mutations in hiPSCs with increasing donor age (Sardo et al., 2016). Additionally, it is a matter of debate whether an increased mutation rate in mitochondria of hiPSCs is related to the donor or to the process of reprogramming itself (Karagiannis et al., 2018).

In addition, different reprogramming methods have been shown to have an effect on transcriptomics and epigenomics of hiPSCs (Churko et al., 2017) and finally also lab-specific gene expression signatures for both iPSCs and ESCs were described (Newman & Cooper, 2010).

1.5.3 Application of human induced pluripotent stem cells

Pluripotent stem cells (PSCs) are able to differentiate into all three germ layers, thus harbouring the potential of autologous cell manufacturing of every tissue of the human body. This potential is promising for disease modelling and drug screening and for the development of therapeutic strategies, especially in combination with new tools like CRISPR/Cas9 gene editing.

1.5.3.1 hiPSCs for disease modelling

The possibility of patient specific disease modelling expanded tremendously since the development of hiPSCs and is now applied in many fields of diseases as a broad range of different tissues can be differentiated from hiPSCs. Promising advancements have been accomplished in the fields of disease modelling for neurological, metabolic/hepatic, immunological and cardiac disorders (Reviewed by Karagiannis et al. 2018). All of these disease modelling approaches aim to understand the disease phenotype of the different disorders and develop screening methods for drug testing. Despite the development of a broad range of model systems, a common limitation for all of them is the variance in maturity and functionality of the differentiated cell types. Thus, the focus of disease modelling shifted from 2D models to 3D model systems that can achieve a higher grade of cell maturity by self-organization and better recapitulation of the disease dynamics (Takebe et al., 2013; Sampaziotis et al., 2015; Centeno, Cimarosti, & Bithell, 2018). Recently, two groups reported on 3D culture systems with multilineage co-differentiation from hiPSCs to develop organised tissues aiming to resemble the in vivo tissue structures for cardiomyocytes and endothelial cells (Giacomelli et al., 2017) and for muscle models containing vascular endothelial cells, pericytes and motor neurons (Maffioletti et al., 2018).

An efficient screening platform for tissue analysis and disease modelling for biological and pharmacological applications is the recently developed organ-on-a-chip technique. A recent study showed the fabrication of a microfluidic approach with the differentiation of human iPSCs to functional cardiomyocytes and hepatocytes (Giobbe et al., 2015; Lind et al., 2017). In addition, another group reported on a microphysiological platform with functionally connected vascular, liver and cardiac microtissues derived from a single line of human iPSCs (Vunjak-Novakovic et al., 2013).

1.5.3.2 hiPSCs in cell therapy approaches

The potential to manufacture every tissue of the human body drives also the hope for clinical applications for cell therapies for diseases that have not been treatable to the present day.

Clinical phase I and II studies are testing the safety and benefit of PSC-derivatives in areas of unmet clinical needs like age-related macular degeneration, Parkinson disease, spinal cord injury, diabetes and myocardial infarction (Reviewed in Trounson & DeWitt, 2016).

The first clinical trial for human induced PSCs was conducted for age-related macular degeneration (AMD) (Mandai et al., 2017). Retinal pigment epithelial (RPE) cells were differentiated from autologous hiPSCs generated from fibroblasts and transplanted as sheets under the retina after extensive in vitro and in vivo testing. The transplanted sheets remained intact for one year after the transplantation but the best corrected visual acuity did not improve or worsen.

However, the potential of hiPSCs for effective cell therapies with unrestricted cell numbers and without immunogenic complications lead to intensive research in a diversity of disease areas aiming for clinical approval. Of note, the aim of recent clinical approaches switched from autologous to allogenic cells, due to the high costs and the long time period necessary to produce and test autologous hiPSCs. Thus, allogenic hiPSC banks are prepared from healthy donors that are homozygous for the human leukocyte antigene (HLA), expected to reduce the risk of immunogenicity (Azuma & Yamanaka, 2016). The feasibility of allogenic transplants was shown by transplantation of iPSC-derived cardiomyocytes into a myocardial infarction model of Macaca monkey resulting in improved cardiac contractile function (Shiba et al., 2016). Macaca monkeys were also used to engraft human iPSC-derived dopaminergic neurons into a Parkinson´s disease model (Kikuchi et al., 2017) with cells surviving and functioning as midbrain dopaminergic neurons without any tumorigenicity after two years.

1.6 Myogenic differentiation of pluripotent stem cells

The first evidence for the possibility of a guided induction of the myogenic lineage from other tissues was shown as early as 1987 by converting mouse embryonic fibroblasts into myoblasts by expression of a single cDNA coding for the myogenic gene MYOD1 (Davis et al., 1987). The same gene was later used for the first differentiation of mouse embryonic stem cells into the myogenic lineage in 1992 (Dekel et al., 1992).

Since then a large number of different studies reported the induction of myogenic cells from pluripotent stem cells. There are two main strategies to generate myogenic cells in vitro. One strategy, the direct reprogramming, uses exogenous expression of myogenic transcription factors. The other strategy is called directed differentiation and aims to recapitulate myogenesis in vitro by exposing the cells to specific signalling molecules as they would experience them throughout lineage progression in vivo.

1.6.1 Direct reprogramming using transcription factors

The direct reprogramming approach was shown to work not only for MYOD1 but also for other myogenic transcription factors. The early myogenic transcription factor PAX3 converted mouse ESCs into MyHC$^+$ fibres. Transplantation of these cells after PDGFαR$^+$ Flk1$^-$ purification resulted in Dystrophin$^+$ fibres in a mouse model (Darabi et al., 2008). The myogenic regulatory factor MYF5 was also shown to generate MyHC$^+$ cells in vitro when expressed in human and mouse ESCs (Iacovino et al., 2011). The first myogenic direct reprogramming protocol using induced PSCs was reported in 2010 by the expression of MYOD1 (Warren et al., 2010).

Many groups developed protocols for efficient induction of human myogenic cells by expression of MYOD1 in monolayer cultures without the need of sorting and robust expression of myosin heavy chain in vitro (Tedesco et al., 2012; Tanaka et al., 2013; Abujarour et al., 2014; Young et al., 2016). Due to its robustness, this method was used for disease modelling for muscular dystrophies like limb-girdle muscular dystrophy 2D (LGMD2D) (Tedesco et al., 2012), Miyoshi Myopathy (Tanaka et al., 2013) and Duchenne Muscular Dystrophy (Abujarour et al., 2014; Young et al., 2016) with successful engraftment after intramuscular (i.m.) transplantation into mouse models (Tedesco et al., 2012; Young et al., 2016).

The transcription factor PAX7 was also shown to induce the myogenic lineage in mouse and human PSCs with engraftment capacity, as shown by the presence of dystrophin$^+$ myofibres after transplantation into mdx mice (Darabi et al., 2011, 2012). PAX7 expression was also used to show in vitro generation of contracting, multinucleated muscle bundles (Rao et al., 2018), although this protocol is strictly depending on FACS purification.

However, these protocols depend on the exogenous expression of transcription factors, which is often connected to the alteration of the genome.

1.6.2 Transgene-free directed differentiation

The directed differentiation of pluripotent stem cells is based on the exposure to specific molecules that recapitulate in vivo myogenesis. Thus, the genome of the pluripotent stem cells is not altered, as it is often done for direct reprogramming approaches, which makes this method more suitable for preclinical and clinical tests.

1.6.2.1 Recapitulation of in vivo myogenesis in vitro

In 1994, Rohwedel et al. were the first to report on recapitulating in vitro myogenesis features by differentiation of mouse embryonic stem cells towards embryoid bodies. They detected myogenic marker expression in the chronological order of in vivo myogenesis inside of embryoid bodies (Rohwedel et al., 1994). The embryoid bodies technique, using spontaneous differentiation into the three germ layers, is known to be heterogeneous and difficult to control (Yamada et al., 1994).

Thus, researchers developed adherent monolayer cultures for transgene-based and transgene-free differentiation methods.

To develop a robust human in vivo differentiation protocol from PSCs, not only a controllable monolayer cell culture setting but also a thorough understanding of in vivo myogenesis is required (Introduction section 1.1). The first monolayer myogenic differentiation protocol for human ESCs was reported in 2005 using conditioned medium from C2C12 mouse myoblasts (Barberi et al., 2005). Two years later, the same group published a protocol for human iPSCs without conditioned medium but still using mesenchymal progenitor cells, FACS sorted from an undefined early progenitor population (Barberi et al., 2007).

Many studies have been conducted to define the early developmental stages that lead to the formation of myogenic tissues. The activation of the transcription factor T/Brachyury in the primitive streak is a major event leading to muscle differentiation. In vitro studies showed, using PSCs, that T-positive populations arise from signals involving Wnt, BMP, FGF, insulin and Activin/Nodal pathways (Reviewed by Murry & Keller, 2008). Several studies established the requirement of Wnt signalling for mesoderm induction (Lindsley et al., 2006; Nakanishi et al., 2009) while BMP signalling was shown to be important for haematopoietic and cardiogenic progenitor development, which arise from the lateral plate and extraembryonic mesoderm (Chadwick et al., 2003; Yang et al., 2008).

Following downstream muscle differentiation, presomitic mesoderm markers like Tbx6 and Msgn1 were shown to be expressed in pluripotent stem cells when activating Wnt signalling alone, or in combination with other factors like FGF (Gouti et al., 2014; Mendjan et al., 2014). Wnt activation is a common feature for all in vitro transgene-free myogenic differentiation protocols recently published (Borchin, Chen, & Barberi, 2013; Shelton et al., 2014; Chal et al., 2015, 2016; Caron et al., 2016; Choi et al., 2016; Swartz et al., 2016). While the first protocols used Wnt/FGF and insulin signalling, Chal et al. added BMP inhibition to block lateral plate mesoderm and enhance differentiation towards the paraxial mesoderm (Chal et al., 2015, 2016). The beneficial effect of BMP inhibition was confirmed by Xi et al. in a later study (Xi et al., 2017). Additionally, as signalling molecules like hepatocyte growth factor (HGF), insulin-like growth factor (IGF) and fibroblast growth factor (FGF) have all been shown to be involved in the regulation of myogenesis (Reviewed by Chargé and Rudnicki 2004), they were included in the differentiation protocol by Chal et al. (Figure 1.6).

However, other protocols have also been shown to produce myogenic cells like BMP4 signalling together with Wnt/FGF and insulin signalling (Swartz et al., 2016) or Notch inhibition after Wnt activation (Choi et al., 2016). A combination of multiple factors (Wnt, Dexamethasone, TGFbeta, EGF, insulin, HGF, PDGF, FGF, IGF1 and Oncostatin) has been reported as a commercially available kit (Caron et al., 2016).

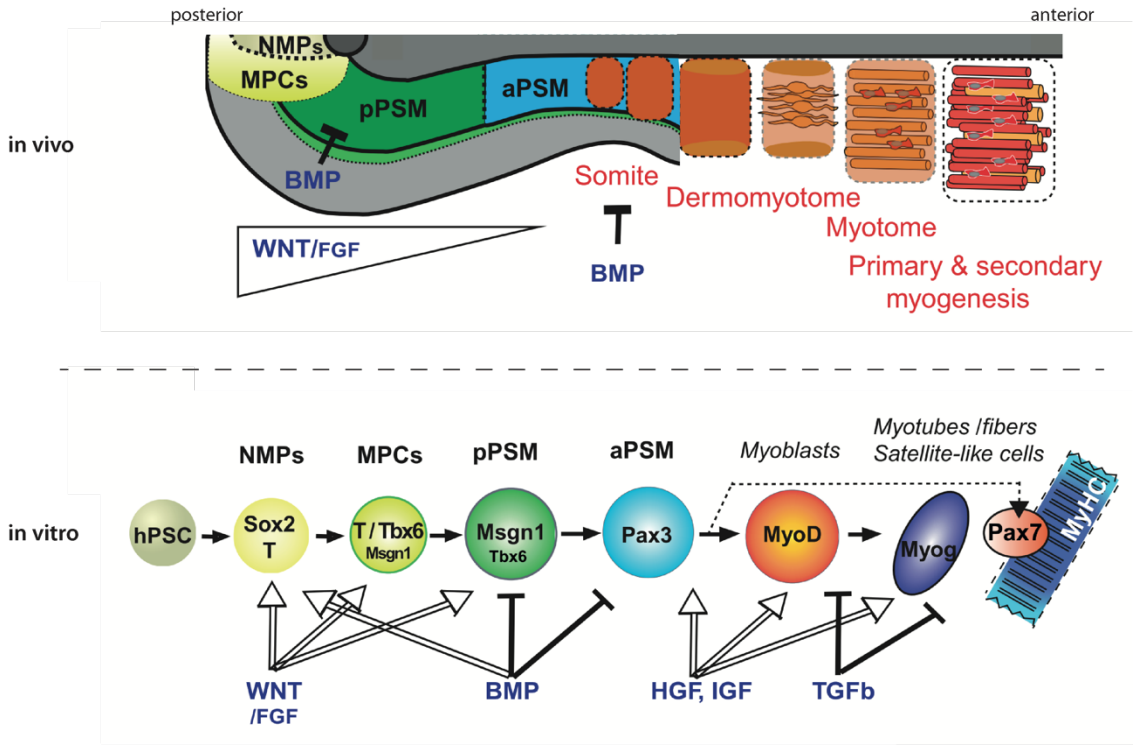

Figure 1.6: Myogenic differentiation protocol by Chal et al. – Adaptation from in vivo myogenesis
The signalling pathways that induce myogenesis in vivo (see Introduction section 1.1) were adopted to develop a protocol for in vitro myogenic differentiation. WNT/FGF signalling are used to induce Neuromesodermal progenitors (NMPs) from human pluripotent stem cells (hPSC) that further develop into mesodermal progenitor cells (MPCs). Posterior and anterior presomitic mesoderm fate (pPSM, aPSM) is promoted by BMP inhibition. HGF and IGF are added to further promote myogenesis while the inhibition of TGF beta signalling promotes terminal maturation of the myogenic progenitor cells. Adapted and modified from (Pourquié et al., 2018).

1.6.2.2 Properties of directed differentiated myogenic cells

Different kinetics were reported to reach terminal differentiated cells ranging from 26 days (Caron et al., 2016) to 50 days for maximal myosin heavy chain expression (Shelton et al., 2014; Chal et al., 2015, 2016) without the need for cell sorting as required for previous protocols (Borchin et al., 2013).

Important myogenic markers like PAX3, PAX7 and the myogenic regulatory factors (MRFs) MYOD1 and Myogenin as well as myosin heavy chain isoforms (embryonic, fetal, and perinatal/fast), were reported to be expressed in the specific early and late stages of all protocols (Borchin et al., 2013; Shelton et al., 2014; Chal et al., 2015, 2016; Caron et al., 2016; Swartz et al., 2016). Further maturation like the presence of striation in $MyHC^{+}$ fibres was shown (Chal et al., 2015, 2016; Choi et al., 2016; Swartz et al., 2016) and even functional maturation of the induced myogenic cells by spontaneous contractions (Shelton et al., 2014; Chal et al., 2015, 2016; Caron et al., 2016; Choi et al., 2016).

In general, the maturation state of the generated fibres by in vitro myogenic differentiation protocols seem to resemble the phenotype of perinatal primary myofibres (Chal & Pourquié, 2017) as it is also discussed for PSC-derived cardiomyocytes (Robertson, Tran, & George, 2013). Even PAX7-

induced myogenic cells only reached calcium and voltage properties, characteristic of immature myofibres (Skoglund et al., 2014).

Assessment of the in vivo engraftment properties of the transgene-free generated myogenic cells was performed by engrafting a purified mouse PAX7/GFP-positive progenitor population into the TA muscle of mdx mice. GFP-positive myofibres were found within the dystrophic muscle tissue (Chal et al., 2015). Also Choi et al. reported on successful transplantations with human Laminin$^+$ fibres and PAX7$^+$ donor-derived cells four weeks after transplantation into NOD mice (Choi et al., 2016). The transplantation experiments performed by Hicks et al. were the first to report successful engraftment of cell surface marker-purified myogenic cells that were differentiated with the protocol published by Shelton et al. The authors identified ERBB3 as a potent surface marker to increase the amount of myogenic cells and additionally reported on TGF beta inhibition to be beneficial for in vitro differentiation and in vivo formation of human Spectrin$^+$ and Dystrophin$^+$ fibres after transplantation into mdx-NSG mice (Hicks et al., 2018).

2. AIM OF THE STUDY

The main aim of this study was to investigate possible differences between human induced pluripotent stem cells (hiPSCs), either generated from primary myoblasts or generated from peripheral blood mononuclear cells (PBMCs) which are influencing their differentiation efficiency into the myogenic lineage. To answer this question, we aimed to:

1. assess the feasibility of generating hiPSCs from primary human myoblasts and PBMCs taken from 5 different donors and to establish fully characterised donor-matched myoblast-and PBMC-derived hiPSCs (M_hiPSCs, B_hiPSCs) from donors without any sign of neuromuscular disorders.
2. establish a directed transgene-free myogenic differentiation protocol for hiPSCs, that is applicable for the detection of possible differences between the hiPSCs.
3. compare the donor-matched M_hiPSCs and B_hiPSCs, that were generated from 3 gender- and age-matched donors, on transcriptome level and in their differentiation capacity in vitro into the myogenic lineage. Additionally, we aimed to compare the potential of the M_hiPSC- and B_hiPSC-derived induced myogenic cells to contribute to muscle fibre regeneration after transplantation into a xenograft-compatible mouse model.

The study was motivated by the unmet clinical need for a therapy for muscular dystrophies and the availability of human myoblast samples obtained for diagnostic purposes. Myoblasts and PBMCs are the most-likely used cell types of origin for a clinical application of hiPSCs regarding muscular dystrophies. hiPSCs represent the key to unrestricted cell numbers that are necessary to repopulate large muscles in disease conditions.

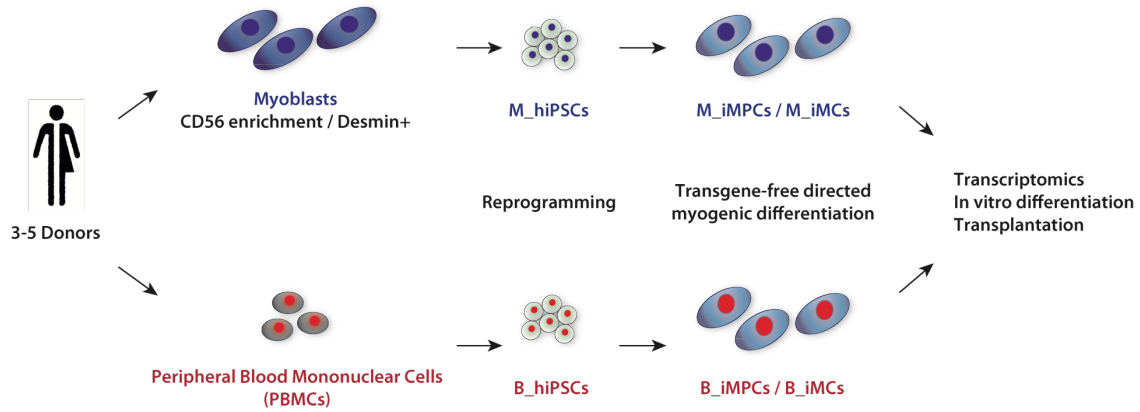

Figure 2.1: Study-design
M_hiPSCs: Myoblast-derived human induced pluripotent stem cells; B_hiPSCs PBMC-derived human induced pluripotent stem cells; M_iMPCs: Myoblast-derived induced myogenic progenitor cells; M_iMCs: Myoblast-derived induced myogenic cells; B_iMPCs: PBMC-derived induced myogenic progenitor cells; B_iMCs: PBMC-derived induced myogenic cells.

3. MATERIAL AND METHODS

3.1 Cell culture

3.1.1 Primary cell culture

3.1.1.1 Primary human cell sources

Human primary muscle biopsy specimen and full blood samples were obtained from patients visiting the University Outpatient Clinic for Muscle Disorders at the Experimental and Clinical Research Center (Berlin-Buch, Germany) with informed consent. Human muscle biopsy specimens were obtained via hip surgery from individuals for diagnostic purposes (ethical approval EA1/203/08, Charité). Table 3.1 shows the list of donors without neuromuscular disorders that were included in this study.

Table 3.1: List of donors

Donor	Gender/Age	Clinics
A	Female, 47	Myalgias, CK normal, Biopsy without signs of neuromuscular disorder
B	Female, 50	Myalgias, CK normal, Biopsy without signs of neuromuscular disorder
C	Male, 19	CK elevated (1900), Biopsy without signs of neuromuscular disorder
D	Female, 47	Myalgias, CK normal, Biopsy without signs of neuromuscular disorder
E	Male, 58	Myalgias, CK normal, Biopsy showed weak neurogenic atrophy

3.1.1.2 Isolation and purification of myogenic cells from human muscle biopsy specimen

The isolation and purification of myogenic cells from the muscle biopsy specimen was conducted as described in Philippi et al., 2012. In brief: after the biopsy was conducted, the muscle biopsy specimen was transferred and transported in Solution A, containing 30 mM HEPES, 130 mM NaCl, 3 mM KCl, 10 mM D-Glucose, 3.2 µM Phenol-red at pH 7.6. The muscle biopsy specimen was then transferred in sterile cell culture conditions to a 6 cm culture dish plate (TPP, Merck), washed 2 times with DPBS (Thermo Fisher Scientific) and was manually fragmented into medium sized pieces. The fragments were then digested in 254 U/ml Collagenase CLS II (Biochrom AG), 100 U/ml Dispase II (Roche) and 0.25% Trypsin/EDTA (Thermo Fisher Scientific) at 37 °C in a 15 ml tube for 45 min followed by centrifugation for 5 min at RT at 200 g in a 3-16K centrifuge (Sigma). The pelleted fragments were cultured in Skeletal muscle cell growth medium + supplement (ProVitro) in T25 cell culture flasks

(LabSolute) for 3 days. Outgrown muscle specimen-derived cells were detached with 0.25% Trypsin/EDTA for 5 min at 37 °C, centrifuged at 200 g for 5 min and seeded on 10 cm cell culture plates (Corning).

The cells were expanded and subsequently purified using the MACS® cell separation system with anti-CD56 antibody-coated magnetic beads (Miltenyi Biotech).

The cell preparations were then immunostained for Desmin$^+$ cells. If the purity was ≥ 99% Desmin$^+$ cells, they were frozen in FBS + 10% DMSO using the Mr. Frosty™ cell freezing container (Thermo Fisher Scientific) and stored in the gas phase of liquid nitrogen.

3.1.1.3 Standard cell culture of human primary myoblasts and terminal differentiation

Primary human myogenic cells were cultured for maintenance in skeletal muscle cell growth medium + supplement (ProVitro) on cell culture treated 10 cm plates (Corning). Cells were split every 2-4 days depending on the growth rate/confluency, which mainly depended on passage number and donor in order to prevent spontaneous fusion of myoblasts and to keep the cells in a proliferative state.

For passaging, cells were washed once with DPBS (Thermo Fisher Scientific) and then incubated with 0.25% Trypsin/EDTA (Thermo Fisher Scientific) at 37 °C for 5 min. Detached cells were collected in DMEM/F12 (1:1) medium (Thermo Fisher Scientific) to a dilution of 1:10 and centrifuged at 200 g for 5 min at RT. Pellet was resuspended in an appropriate volume of skeletal muscle cell growth medium + supplement and seeded at a density of 1-2*10^4 cells/cm^2 on 10 cm plates.

For terminal differentiation, primary myoblasts were seeded at a density of 2*10^4 cells/cm^2 and cultured to a confluence of 90%. Then medium was changed to OptiMEM (Thermo Fisher Scientific) and cells were terminally differentiated for 4 days with medium change every other day.

3.1.1.4 Isolation of peripheral blood mononuclear cells (PBMCs) from full blood samples

Patient-derived full blood samples in EDTA tubes were used for sterile isolation of peripheral blood mononuclear cells (PBMCs). EDTA tubes were kept at RT and were proceeded within two hours after blood withdrawal.

The full blood sample was transferred to a Vacutainer® CPT™ mononuclear cell preparation tube (BD) and inverted carefully 8-10 times. The CPT™ tube was centrifuged at RT for 20 min at 1850 g using a Labofuge 400R (Heraeus). After centrifugation, the CPT™ tube was inverted again carefully 3-4 times and the supernatant was transferred into a 50 ml tube filled with 40 ml of 2 mM DPBS/EDTA solution. The 50 ml tube was centrifuged for 10 min at RT at 500 g in the Labofuge 400R. The supernatant was discarded, and the resulting pellet resuspended in 4 ml 4 °C cold 2 mM DPBS/EDTA solution and transferred into a fresh 15 ml tube. At this stage the cells were counted and the 15 ml tube was subsequently centrifuged for 5 min at 4 °C at 500 g using the Labofuge 400R.

Pelleted cells were resuspended in FBS + 10% DMSO and frozen to a concentration of $1*10^6$ cells per ml per cryovial using the Mr. Frosty™ cell freezing container (Thermo Fisher Scientific) and stored in the gas phase of liquid nitrogen.

3.1.1.5 Standard cell culture of human peripheral blood mononuclear cells (PBMCs)

PBMCs were cultured in PBMC medium (StemPro™-34 SFM, StemPro™-34 Nutrient Supplement, L-Glutamine (2 mM), SCF (100 ng/ml), FLT-3 (100 ng/ml), IL-3 (20 ng/ml), IL-6 (20 ng/ml), Epo (2 U/ml)) in 24-,12- or 6-well cell culture plates (Corning). Medium was changed every other day by replacing 50% of the medium with fresh PBMC medium. 500 µl medium were taken from the well and centrifuged at 200 g for 10 min. The pellet was resuspended in fresh 500 µl PBMC medium and transferred back into the well. For passaging, the cells were divided into two wells.

3.1.2 Reprogramming

3.1.2.1 Reprogramming of human primary myoblasts into induced pluripotent stem cells

$Desmin^+$ cells, isolated and purified from muscle biopsy specimen (see 3.1.1.2), were used for the reprogramming procedure in order to generate induced pluripotent stem cells.

Primary myogenic cells were thawed and cultured in Skeletal muscle cell growth medium + supplement (ProVitro) for 5-6 days (two passages). After the second passaging procedure $5*10^4$ cells were collected in 1 ml Skeletal muscle cell growth medium + supplement, supplemented with 10 µg/ml Polybrene (Merck). Sendai-viruses from the CytoTune™-iPS 2.0 Sendai Reprogramming Kit (Thermo Fisher Scientific, Lot.: L2130018 and L2110088) were added according to the virus concentration recommended in the certificate of analysis of the according batch. The cell-virus suspension was gently resuspended using a 1 ml pipette and seeded in prepared Matrigel-coated 6-wells (see 3.1.3.1). Wells were incubated under normoxic conditions.

The following day, 1 ml of Skeletal muscle cell growth medium + supplement was added to the wells without aspirating the existing medium.

The next day the medium was aspirated and 2 ml of fresh Skeletal muscle cell growth medium + supplement, supplemented with Sodium Butyrate (200 µM) and Ascorbic acid (64 µg/µl) were added to the well. From now on the medium was changed every other day and the wells were monitored daily for up to 10 days for the appearance of hiPSC colonies.

After a maximum of 13 days, when hiPSC colonies showed well-defined borders and packed colony morphology without spontaneous differentiation, medium was changed to mTeSR™1 medium (Stem Cell Technologies). Additionally, cells were transferred to hypoxic conditions (5% O_2).

Colonies without spontaneous differentiation were picked after 16-26 days using a 10 µl pipette tip for fragmentation and a L226 IVF workstation picking hood (K-Systems) with an installed

microscope under laminar flow conditions. Colony pieces were transferred to prepared Matrigel-coated 24-wells with mTeSR™1 medium supplemented with 10 µM Rock inhibitor (Y-27632 2HCl, Biozol). Each colony is considered to be an hiPSC clone. Rock inhibitor was removed after attachment of the hiPSCs. hiPSC clones were furthermore expanded and stocked in BamBanker (Nippon Genetics) in the gas phase of liquid nitrogen before proceeding with the characterisation protocol.

3.1.2.2 Reprogramming of human PBMCs into induced pluripotent stem cells

The reprogramming of was performed as previously published by Churko et al., 2013.

Frozen peripheral blood mononuclear cells (PBMCs) were thawed in a 24-low adherence well (Greiner Bio-One) in 1 ml PBMC medium (StemPro™-34 SFM, StemPro™-34 Nutrient Supplement, L-Glutamine (2 mM), SCF (100 ng/ml), FLT-3 (100 ng/ml), IL-3 (20 ng/ml), IL-6 (20 ng/ml), Epo (2 U/ml), all Thermo Fisher Scientific). Every other day 50% of the medium was exchanged with fresh PBMC medium. 500 µl medium were taken from the well, centrifuged at 200 g for 10 min and the pellet was resuspended in fresh 500 µl PBMC medium. This procedure was continued for at least 6 days and monitored via microscopy until a significant increase in the cell number was detected.

$3*10^5$ PBMCs were seeded in a 24-low adherence well (Greiner Bio-One) in 500 µl PBMC medium + 10 µg/ml Polybrene (Merck) and infected with the CytoTune™-iPS 2.0 Sendai Reprogramming Kit (Thermo Fisher Scientific, Lot.: L2130018 and L2110088) according to the virus concentration recommended in the certificate of analysis of the according batch. The next day the cell/virus solution was washed to erase the virus by centrifugation at 200 g for 10 min and resuspension in 500 µl fresh PBMC medium + Sodium Butyrate (200 µM) + Ascorbic acid (64 µg/µl).

After two days the cells were centrifuged at 200 g for 10 min. The resuspended pellet was either transferred to a 6-well coated with Matrigel (3.1.3.1) or to a 6-well with CF-1 mouse embryonic feeder cells (MEFs) (Tebu-Bio). Cells were kept in 2 ml PBMC medium + Sodium Butyrate (200 µM) + Ascorbic acid (64 µg/µl).

The following day the cells were centrifuged again and medium was changed to basal PBMC medium (StemPro™-34 SFM, StemPro™-34 Nutrient Supplement, 2 mM L-Glutamine; all Thermo Fisher Scientific). Cells were kept in basal PBMC medium for 3-6 days with daily medium change until human induced pluripotent stem cell (hiPSC) colonies started to appear.

With small hiPSC colonies present, the medium was changed to 50/50 basal PBMC medium and chemically defined TeSR™-E7™ medium (Stem Cell Technologies) for 2 days and then changed to 100% TeSR™-E7™ medium for additional 3-4 days.

The handling of the generated PBMC-derived hiPSCs is conform with the handling of myoblast-derived hiPSCs. After a maximum of 13 days, when hiPSC colonies showed well-defined borders and packed colony morphology without spontaneous differentiation, medium was changed

to mTeSR™1 medium (Stem Cell Technologies). Additionally, cells were transferred to hypoxic conditions (5% O_2).

Colonies without spontaneous differentiation were picked after 16-26 days using a 10 µl pipette tip for fragmentation and a L226 IVF workstation picking hood (K-Systems) with an installed microscope under laminar flow conditions. Colony pieces were transferred to prepared Matrigel-coated 24-wells with mTeSR™1 medium supplemented with 10 µM Rock inhibitor (Y-27632 2HCl, Biozol). Each colony is considered to be an hiPSC clone. Rock inhibitor was removed after attachment of the hiPSCs. hiPSC clones were furthermore expanded and stocked in BamBanker (Nippon Genetics) in the gas phase of liquid nitrogen before proceeding with the characterisation protocol.

3.1.3 Human induced pluripotent stem cells

3.1.3.1 Matrigel-coating

For the standard cell culture of human induced pluripotent stem cells, Matrigel coating was used. Matrigel (Corning) was stored in aliquots at – 20 °C until use. For coating, aliquots were thawed at 4 °C for 1 h and resuspended in cold DMEM/F12 medium (1:1) (Thermo Fisher Scientific) to a concentration given in the manufacturers batch information.

3.1.3.2 Feeder-free culture / Passaging

Human induced pluripotent stem cells were cultured regularly on Matrigel-coated (Corning) Falcon™ 6-well cell culture plates (Corning) in mTeSR™1 medium (Stem Cell Technologies) under hypoxic conditions (5% O_2). Passaging for maintenance was done using the DPBS/EDTA detachment method (see 3.1.3.2.1). Every 3-4 days cells were split with a ratio of 1:5 and 1:10, depending on the overall confluency and size of the hiPSC colonies. Overall confluency should not exceed 70% and the hiPSC colonies did not exceed the size where considerable differences between the inner and outer part of the colonies were detectable. Experiments were started using the Accutase detachment method (see 3.1.3.2.2) for seeding a defined number of cells.

3.1.3.2.1 Passaging with DPBS/EDTA

To avoid cell stress due to enzymatic digestion and single cell state, the hiPSC colonies were passaged for maintenance using 0.5 mM DPBS/EDTA (0.5 M EDTA, Thermo Fisher Scientific).

After medium aspiration, human induced pluripotent stem cells were washed once with DPBS (Thermo Fisher Scientific) and then incubated with 0.5 mM 100 µl/cm^2 DPBS/EDTA for 4 - 6 min at 37 °C until the hiPSC colonies showed a considerable brighter appearance. DPBS/EDTA solution was aspirated before any cell detachment and 100 µl/cm^2 mTeSR™1 medium were added. Cells were detached using a scraper and resuspended until cell colony fragments were homogenous in size. Cell

colony fragments were then transferred into a fresh Matrigel-coated (see 3.1.3.1) 6-well, filled with 2 ml mTeSR™1 medium. For maintenance cells were split with a ratio of 1:5 and 1:10 every 3-4 days.

3.1.3.2.2 Passaging with Accutase / TrypLE™ Express

Passaging with StemPro Accutase (Thermo Fisher Scientific) or TrypLE™ Express (Thermo Fisher Scientific) was used to gain single cell solutions to start experiments with defined numbers of cells.

After medium aspiration, human induced pluripotent stem cells were washed once with DPBS (Thermo Fisher Scientific) and then incubated with 100 µl/cm^2 Accutase or TrypLE™ Express for 5 min at 37 °C until the hiPSC colonies detached from the surface in single cells and colony fragments. Cells were collected in 9 ml DMEM/F12 (1:1) medium (Thermo Fisher Scientific) in 15 ml Falcon™ tubes (Corning) and centrifuged for 5 min at 300 g. The pellet was resuspended in 2 ml mTeSR™1 medium supplemented with 10 µM Rock inhibitor (Y-27632 2HCl, Biozol). If needed, cells were counted using a Neubauer chamber and seeded in 2 ml mTeSR™1 medium supplemented with 10 µM Rock inhibitor. The following day Rock inhibitor was removed if the cell density was sufficient for cell survival and colony formation.

3.1.3.3 Morphological characterisation

Human induced pluripotent stem cells were monitored daily for cell density, colony size and the appearance of spontaneous differentiating colony parts, using a Leica DM IL Fluo Invers microscope (Leica Microsystems) equipped with 4x, 10x, 20x and 40x magnification objectives (HI PLAN 4x/0.10, HI PLAN I 10x/0.22 Ph1, HI PLAN I 20x/0.30Ph1, HI PLAN I 40x/0.50 Ph2).

For characterisation of the newly established human induced pluripotent stem cells brightfield pictures were taken with an inverted light microscope EVOS® FL Cell Imaging System (Thermo Fisher Scientific) with 4x, 10x, 20x or 40x magnification objectives (PL FL 4X LWD PH, 0.13NA/16.9WD, PL FL 10X LWD PH, 0.25NA/9.2WD, PL FL 20X LWD PH, 0.40NA/3.1WD, PL FL 40X LWD PH, 0.65NA/1.6WD). Only those hiPSC clones passed characterisation test parameters showing well-defined borders, packed colony morphology and no sign of spontaneous differentiation.

3.1.4 Transgene-free myogenic differentiation

The myogenic differentiation protocol for the differentiation of induced pluripotent stem cells (hiPSCs) into the myogenic lineage was performed as previously published by Chal et al., 2016.

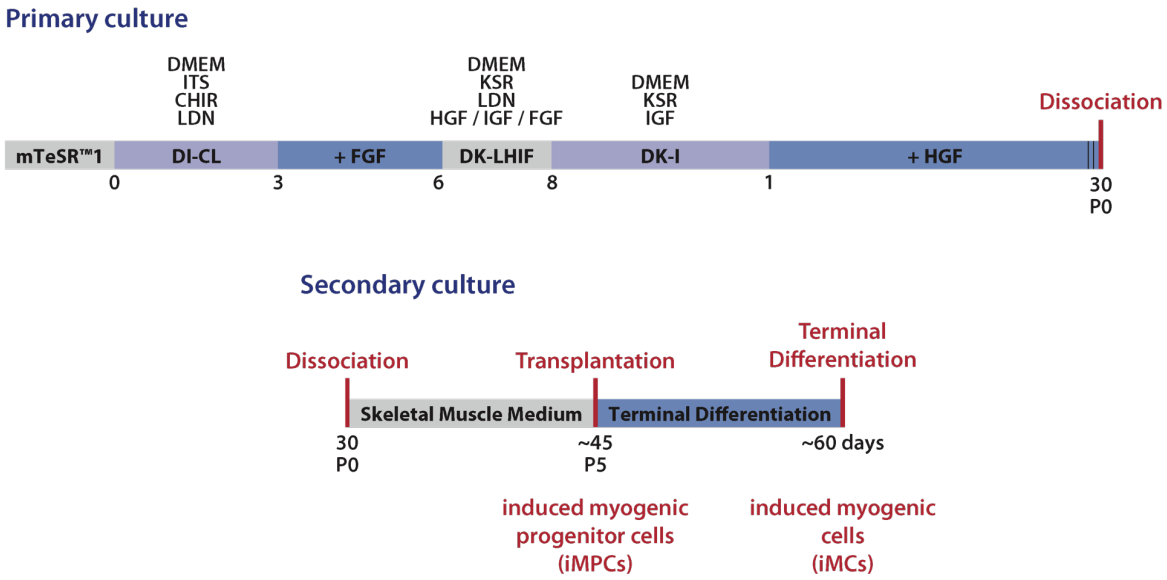

Figure 3.1: Schematic description of the myogenic differentiation protocol
Cells were cultured in mTeSR™1 medium. Differentiation protocol was started with changing the medium to DI-CL medium containing 3 µM CHIR and 0.5 µM LDN. Further differentiation steps included Knockout™ Serum Replacement and a series of growth factors including FGF, IGF and HGF. After 30 days, primary cell culture was dissociated and single cells were cultured in skeletal muscle medium. The experimental procedure of this work includes transplantation of the newly generated induced myogenic progenitor cells (iMPCs) around day 45 and the terminal in vitro differentiation into induced myogenic cells (iMCs) at around day 60 of the protocol.

3.1.4.1 Primary myogenic differentiation

hiPSCs were cultured on a regular basis in mTeSR™1 medium (Stem Cell Technologies) in hypoxic conditions (5% O_2) on Matrigel-coated 6-well plates (Corning). Cells were monitored daily and passaged with DPBS/EDTA as described in 3.1.3.2.1. The myogenic differentiation protocol was started only using healthy cells without any sign of spontaneous differentiation.

To start the differentiation protocol, hiPSCs were incubated for 2 h with fresh mTeSR™1 medium supplemented with 10 µM Rock inhibitor (Y-27632 2HCl, Biozol) to increase cell survival after single cell detachment. Cells were then washed with DPBS and detached for 5 min at 37 °C with TrypLE™ Express (Thermo Fisher Scientific). The detached cell suspension was resuspended in DMEM/F12 (1:1) medium (Thermo Fisher Scientific) with a dilution of 1:10 and centrifuged at 300 g for 5 min at RT. Pellet was resuspended in an appropriate volume of mTeSR™1 medium + Rock inhibitor and seeded in three different densities to freshly prepared Matrigel-coated 6-wells ($2.5*10^4$ cells/cm^2, $3.5*10^4$ cells/cm^2, $4.5*10^4$ cells/cm^2). For each density technical triplicates (3x 6-well) were seeded. Cells were transferred to normoxic conditions as required for the differentiation protocol. The next day cells were checked for cell survival and homogenous cell distribution within the well and medium was changed to mTeSR™1 medium without Rock inhibitor in the morning.

Cells were monitored constantly until cell morphology changed from a very spiky single cell morphology to a beginning normal iPSC colony morphology. Depending on the morphology,

myogenic differentiation was started either on the same day or early the next day. Myogenic differentiation was started by changing the medium to 420 µl/cm² DI-CL medium (DMEM, ITS, CHIR, LDN, see Table 3.2). This point in time was considered to be day 0 of the differentiation protocol. DI-CL medium was changed daily until day 3 by keeping the timeframe of 24 h in between the medium changes.

On day 3 medium was changed to DI-CL + FGF medium (DMEM, ITS, CHIR, LDN, FGF, see Table 3.2) and changed every 24 h for additional 3 days until day 6. Notably, from day 4 onwards, massive cell detachment occurred for low and high initial cell seeding densities and continued until day 8-9. Different cell density approaches were evaluated around day 10 and technical triplicates of the seeding density with the highest cell survival were kept, continuing the differentiation protocol until the end. Other densities were discarded.

At day 6 medium was changed to DK-LHIF (DMEM, KSR, LDN, HGF, IGF, FGF, see Table 3.2) and then changed again daily within a 24 h time frame for 2 days until medium was changed to DK-I medium (DMEM, KSR, IGF, see Table 3.2) on day 8. Daily medium change continued until day 12 when medium was changed to DK-I + HGF medium (DMEM, KSR, IGF, HGF, see Table 3.2). From this point in time onwards, medium was changed every other day until day 30.

3.1.4.2 Dissociation of primary differentiation cultures

After 30 days of myogenic differentiation, the initial monolayer culture developed into a very stable 3D structure composed of presumably many different cell types and extracellular matrix components. To obtain induced myogenic progenitor single cells, those very stable structured were decomposed using a harsh dissociation protocol.

Cell cultures were incubated with DK-I + HGF medium + 10 µM Rock inhibitor for 2 h followed by 10 min of DPBS. Cells were then incubated for 5 min with 160 µl/cm² TrypLE™ Express and manually dissociated by flushing the cell matrix harshly with a 1 ml pipette. After 8 - 10 min of incubation and manual dissociation, cells in suspension were collected in 20 ml of DMEM/F12 medium, supplemented with 20% FCS. The remaining cell matrix in the dish was again incubated with 160 µl/cm² TrypLE™ Express and the procedure was repeated once.

After two rounds of enzymatic incubation, cells were incubated with 160 µl/cm² 0.25% Trypsin/EDTA (Thermo Fisher Scientific) for 5 min at 37 °C. Subsequently, the remaining cell/matrix fragments within the dish were manually dissected using two 25 G needles and finally broken down using an FCS-immersed 1 ml pipette. The almost completely dissociated cell/matrix mix was again collected into the DMEM/F12/FCS tube.

The DMEM/FCS/cell solution was filtered through a 70 µm filter and centrifuged for 5 min at RT at 300 g. The resulting pellet was resuspended in Skeletal muscle cell growth medium (SkGM-2 BulletKit, Lonza) + 10 µM rock inhibitor. Cells were counted using a Neubauer chamber and either

stocked in BamBanker (Nippon Genetics) in the gas phase of liquid nitrogen or seeded at a density of $7*10^4$ cells/cm^2 in Matrigel-coated 6-well plates for maintenance or in 8-well ibiTreat Ibidi slides (Ibidi) for immunofluorescence staining.

3.1.4.3 Secondary differentiation culture: induced myogenic progenitor cells (iMPCs) + induced myogenic cells (iMCs)

Skeletal muscle cell growth medium was changed every other day and cells were cultured on Matrigel-coated 6-wells and passaged using TrypLE™ Express every 3-4 days.

At passage 5, cells were seeded at a density of $7*10^4$ cells/cm^2 on Matrigel-coated 8-well ibiTreat Ibidi slides (Ibidi) for immunofluorescence staining or Matrigel-coated 12-well plates for RNA pellet collection. Cells were kept in skeletal muscle cell growth medium for 4 additional days. Medium was then changed to terminal differentiation medium (see Table 3.2) which was changed every other day. After 10 days of terminal differentiation, cells were fixed with 3.7% Formaldehyde in DPBS and processed for immunofluorescence staining or pellets were taken for RNA isolation as described in 3.6.1.

Table 3.2: Medium composition for the myogenic differentiation protocol

Medium	Component	Company Cat. No.	Final concentration
DI-CL / DI-CL + FGF	DMEM/F12 (1:1)	Thermo Fisher Scientific 11320-033	
	Insulin-Transferrin-Selenium (ITS)	Thermo Fisher Scientific 41400-045	1%
	Non-essential amino acids (NEAA)	Thermo Fisher Scientific 11140-050	1%
	Penicillin-Streptomycin	Thermo Fisher Scientific 15140122	0.2%
	CHIR-99021	Sigma-Aldrich SML1046	3 µM
	LDN-193189	Miltenyi Biotech 130-106-540	0.5 µM
	Recombinant Human Fibroblast growth factor (FGF)	R&D Systems 233-FB	20 ng/ml

Medium	Component	Company Cat. No.	Final concentration
DK-LHIF	DMEM/F12 (1:1)	Thermo Fisher Scientific 11320-033	
	Knockout™ Serum Replacement (KSR)	Thermo Fisher Scientific 10828028	15%
	Non-essential amino acids (NEAA)	Thermo Fisher Scientific 11140-050	1%
	Penicillin-Streptomycin	Thermo Fisher Scientific 15140122	0.2%
	2-Mercaptoethanol	Thermo Fisher Scientific 21985023	0.1 mM
	LDN-193189	Miltenyi Biotech 130-106-540	0.5 µM
	Recombinant Human Hepatocyte growth factor (HGF)	R&D Systems 294-HG	10 ng/ml
	Recombinant Human Insulin-like growth factor (IGF)	R&D Systems 291-G1	2 ng/ml
	Recombinant Human Fibroblast growth factor (FGF)	R&D Systems 233-FB	20 ng/ml

Medium	Component	Company Cat. No.	Final concentration
DK-I / DK-I + HGF	DMEM/F12 (1:1)	Thermo Fisher Scientific 11320-033	
	Knockout™ Serum Replacement (KSR)	Thermo Fisher Scientific 10828028	15%
	Non-essential amino acids (NEAA)	Thermo Fisher Scientific 11140-050	1%
	Penicillin-Streptomycin	Thermo Fisher Scientific 15140122	0.2%
	2-Mercaptoethanol	Thermo Fisher Scientific 21985023	0. mM
	Recombinant Human Insulin-like growth factor (IGF)	R&D Systems 291-G1	2 ng/ml
	Recombinant Human Hepatocyte growth factor (HGF)	R&D Systems 294-HG	10 ng/ml

Medium	Component	Company Cat. No.	Final concentration
Terminal Differentiation medium	DMEM/F12 (1:1)	Thermo Fisher Scientific 11320-033	
	Insulin-Transferrin-Selenium (ITS)	Thermo Fisher Scientific 41400-045	1%
	Penicillin-Streptomycin	Thermo Fisher Scientific 15140122	0.2%
	L-Glutamin	Thermo Fisher Scientific 25030081	1%
	N2-Supplement	Thermo Fisher Scientific 17502048	1%

3.2 Immunofluorescence

3.2.1 Immunofluorescence staining in cultured cells (hiPSC characterisation)

Cultured hiPSCs were seeded in Matrigel-coated 8-well ibiTreat Ibidi slides (Ibidi) and cultured for at least 24 h until a sufficient attachment and density was reached. Cells were then washed with DPBS (Thermo Fisher Scientific) to remove cell debris. Cells were fixed with 200 µl/cm^2 fresh 3.7% Formaldehyde in DPBS for 10 min at RT. At this stage, fixed cells could be stored for up to 2 weeks in DPBS at 4 °C with weekly refixation.

For all stainings, except the TRA-1-60 staining, cells were permeabilised with 200 µl/cm^2 0.2% Triton X-100 in DPBS for 10 min at RT followed by 3 x 5 min washing steps with DPBS. Cells were blocked with 200 µl/cm^2 1% BSA in DPBS for 1 h at RT and subsequently incubated with 200 µl/cm^2 of the primary antibody diluted in 1% BSA in DPBS (for concentrations see 3.2.4) over night at 4 °C on a shaker.

The next day the primary antibody was removed and cells were washed 3 x for 5 min at RT on a shaker which was followed by an incubation period with the secondary antibody (for concentrations see 3.2.4) for 1 h at RT on a shaker. Cells were incubated with Hoechst (1:10000) for 5 min at RT before 3 x 5 min final washing steps. Cells were left in DPBS at 4 °C until examination.

3.2.2 Immunofluorescence staining in cultured cells (iMPCs + iMCs)

iMPCs and iMCs, differentiated from hiPSCs, were stained according to the protocol described in Chal et al. 2016.

$7*10^4$ cells/cm^2 were seeded on Matrigel-coated 8-well ibiTreat Ibidi slides (Ibidi) and cultured for at least 24 h until a sufficient attachment and density was reached. Then, cells were washed with DPBS (Thermo Fisher Scientific) to remove cell debris. Cells were then fixed with 200 µl/cm^2 fresh 3.7% Formaldehyde in DPBS for 10 min at RT. At this stage, fixed cells could be stored for up to 2 weeks in DPBS at 4 °C with weekly refixation.

Cells were permeabilised by incubating them for 3 x 3 min with 200 µl/cm^2 TBST buffer (0.1% Tween 20 in TBS) followed by a blocking period for 30 min at RT in blocking solution (0.1% Trition X-100 + 1% FBS in TBS). Primary antibody was diluted in blocking solution and incubated over night at 4 °C on a shaker (for concentrations see 3.2.4). The next day cells were washed 3 x 5 min at RT on a shaker with TBST. Secondary antibody was diluted in blocking solution and incubated again over night at 4 °C on a shaker (for concentrations see 3.2.4).

The day after that the secondary antibody was removed and cells were incubated with Hoechst (1:10000) for 5 min at RT before 3 x 5 min final washing steps with TBST. Cells were left in DPBS at 4 °C until examination.

3.2.3 Immunofluorescence staining on histological tissue-sections

Sections were thawed and dried from – 20 °C to RT for 45 min and then fixed for 5 min in – 20 °C cold acetone. Sections were dried again for 10 min at RT and then blocked with 5% BSA + 3% goat serum in DPBS (Thermo Fisher Scientific) for 1 h at RT in a humid chamber. Sections were washed once with DPBS and then incubated with the primary antibody in 1% BSA in DPBS for 2 h at RT in a humid chamber (for concentrations see 3.2.4). After primary antibody incubation, sections were washed 3 x 5 min with DPBS and then incubated with the secondary antibody in DPBS for 45 min at RT in a humid chamber (for concentrations see 3.2.4). Hoechst was incubated at a dilution of 1:5000 in DPBS for 5 min at RT and sections were washed finally 3 x 5 min at RT with DPBS. Sections were mounted on microscope slides using Aqua-Poly/Mount (Polysciences, Inc.) and were left to dry overnight at 4 °C.

3.2.4 Antibody list

Table 3.3: List of primary and secondary antibodies
For immunofluorescence staining for cultured cells (Cells) and tissue sections (Tissue).

Antibody	Host species	Company Cat. No.	Working dilution	2nd Antibody	Company Cat. No.	Dilution
OCT4	Rabbit polyclonal	Abcam ab19857	Cells: 1:1000	Alexa Fluor 568 donkey anti-rabbit	Thermo Fisher A10042	Cells: 1:1000
SOX2	Rabbit polyclonal	Abcam ab97959	Cells: 1:300	Alexa Fluor 568 donkey anti-rabbit	Thermo Fisher A10042	Cells: 1:1000

NANOG	Rabbit polyclonal	Abcam ab21624	Cells: 1:100	Alexa Fluor 568 donkey anti-rabbit	Thermo Fisher A10042	Cells: 1:1000
TRA-1-60	Mouse monoclonal	Abcam ab16288	Cells: 1:500	Alexa Fluor 488 goat anti-mouse	Thermo Fisher A11001	Cells: 1:1000
TBX6	Rabbit polyclonal	Abcam ab38883	Cells: 1:200	Alexa Fluor 488 goat anti-rabbit	Thermo Fisher A11008	Cells: 1:1000
Total MyHC	Mouse monoclonal	DSHB MF20	Cells: 1:300	Alexa Fluor 488 goat anti-mouse	Thermo Fisher A11001	Cells: 1:1000
Fast MyHC	Mouse monoclonal	Sigma-Aldrich M4276	Cells: 1:200	Alexa Fluor 568 goat anti-mouse	Thermo Fisher A11031	Cells: 1:1000
MyHC3	Rabbit polyclonal	Santa-Cruz sc-20641	Cells: 1:200	Alexa Fluor 568 donkey anti-rabbit	Thermo Fisher A10042	Cells: 1:1000
Desmin	Rabbit polyclonal	Abcam ab15200	Cells: 1:1000	Alexa Fluor 568 donkey anti-rabbit	Thermo Fisher A10042	Cells: 1:1000
PAX7	Mouse monoclonal	Santa-Cruz sc-81648	Cells: 1:200 Tissue: 1:100	Alexa Fluor 488 goat anti-mouse	Thermo Fisher A11001	Cells: 1:1000
				Alexa Fluor 647 donkey anti-mouse	Thermo Fisher A31571	Tissue: 1:500
MYOD1	Mouse monoclonal	Santa-Cruz sc-32758	Cells: 1:200	Alexa Fluor 488 goat anti-mouse	Thermo Fisher A11001	Cells: 1:1000
MYOG	Mouse monoclonal	Abcam ab1835	Cells: 1:800	Alexa Fluor 488 goat anti-mouse	Thermo Fisher A11001	Cells: 1:1000
MYOG	Rabbit polyclonal	Santa-Cruz sc-576	Cells: 1:800	Alexa Fluor 488 goat anti-rabbit	Thermo Fisher A11008	Cells: 1:1000
TUJ1	Mouse monoclonal	Sigma-Aldrich T8578	Cells: 1:1000	Alexa Fluor 568 goat anti-mouse	Thermo Fisher A11031	Cells: 1:1000
Human Lamin A/C	Rabbit monoclonal	Abcam ab108595	Tissue: 1:4000	Alexa Fluor 568 donkey anti-rabbit	Thermo Fisher A10042	Tissue: 1:500
				Alexa Fluor 568 goat anti-rabbit	Thermo Fisher A11036	Tissue: 1:500
Human Spectrin	Mouse monoclonal	Novocastra NCL-SPEC1	Tissue: 1:100	Alexa Fluor 647 goat anti-mouse	Thermo Fisher A21236	Tissue: 1:500

3.3 Image acquisition

3.3.1 Standard cell culture imaging

All cell types were routinely monitored via brightfield microscopy using a Leica DM IL Fluo Invers microscope (Leica Microsystems) equipped with 4x, 10x, 20x and 40x magnification objectives (HI PLAN 4x/0.10, HI PLAN I 10x/0.22 Ph1, HI PLAN I 20x/0.30Ph1, HI PLAN I 40x/0.50 Ph2).

Human induced pluripotent stem cells were checked daily for cell density, colony size and the appearance of spontaneous differentiation.

Primary human myogenic cells were checked daily for density and cell quality, depending mainly on passage number and donor, to assess usability for experiments and to prevent spontaneous fusion for standard maintenance cell culture.

Induced myogenic progenitor cells were also checked daily to monitor morphological changes occurring during the maturation process.

Brightfield pictures were taken with an inverted light microscope EVOS® FL Cell Imaging System (Thermo Fisher Scientific) with 4x, 10x, 20x or 40x magnification objectives (PL FL 4X LWD PH, 0.13NA/16.9WD, PL FL 10X LWD PH, 0.25NA/9.2WD, PL FL 20X LWD PH, 0.40NA/3.1WD, PL FL 40X LWD PH, 0.65NA/1.6WD).

3.3.2 Laser Scan Microscopy

Multi-colour, confocal immunofluorescence imaging was performed using the Laser Scan Microscope LSM 700 (Carl Zeiss) equipped with a 1-2-channel scanning module corresponding to laser class 3B (DIN EN 60825-1) (405 nm (5 mW), 488 nm (10 mW), 555 nm (10 mW), 639 nm (5 mW)). The LSM is attached to an Axio Observer Z1 inverted microscope (Carl Zeiss) equipped with 10x, 40x or 63x (oil) magnification objectives (N-Achroplan 10x/0.25 M27, Plan-Apochromat 40x/0.95 Korr M27, LCI Plan-Neofluar 63x/1.3 Imm Korr DIC M27). Images were acquired with the ZEN 2010 SP1 software (Carl Zeiss).

Appropriate control samples were used to adjust laser parameters to sample autofluorescence, secondary antibody fluorescence and spectral overlapping between different dyes. Same scan-settings were used for different samples that shared the same staining conditions.

3.3.3 Mosaic image acquisition

For mosaic image acquisition a Leica DMI 6000 B microscope was used equipped with a 10x magnification objective (HC PL FLUOTAR 10x 0.3 DRY), a DFC 350 FX R2 camera and a XY scanning stage (Leica Microsystems).

For mosaic image acquisition the "tile scan panel" of the LAS FL Software (Leica Microsystems) was used to mark start and end points of the scanning procedure via x- and y-values in a 2D coordinate system by manually moving the stage to the intended position. Automated image acquisition covered an area of 1 cm^2 per sample according to the complete size of an 8-well Ibidi slide well. About 150 single pictures were merged to one complete mosaic picture using the LAS FL Software and were then processed using the same software for suitable image presentation.

Appropriate control samples were used to adjust image acquisition parameters to sample autofluorescence and secondary antibody fluorescence. Same image acquisition-settings were used for different samples that shared the same staining conditions.

3.4 Teratoma formation assay (pluripotency assay)

Teratoma formation assay was performed by EPO – Experimental Pharmacology & Oncology Berlin-Buch GmbH (Campus Buch, Berlin, Germany). $2.5*10^6$ cells/cm^2, resuspended in 50 µl PBS + 50 µl Matrigel (Corning), were submitted to EPO and injected subcutaneously into both flanks of one immunodeficient NOG-M mice per cell line (NOD.Cg-Prkdc^{scid} Il2rg^{tm1Sug}/JigTac, Taconic Biosciences, Bomholtvej, Denmark). Tumour growth was documented by measuring 2 perpendicular diameters once a week. Animals were sacrificed when tumour size reached more than 1 cm^3, 8 weeks after transplantation or when the purpose of the experiment had been reached. Tumour samples were then processed to histopathological examination to evaluate the presence of tissues of all three germ layers.

3.5 DNA assays

3.5.1 gDNA isolation

Cultured human pluripotent stem cells were detached using the DPBS/EDTA detaching method (see 3.1.3.2.1) with cell colony fragments being collected in 1 ml DPBS after removal of DPBS/EDTA. Solution was transferred to an Eppendorf tube® and centrifuged for 5 min at RT at 500 g. Supernatant was removed and pellets were frozen to – 20°C until further processing.

Primary myoblasts were detached using the standard method (see 3.1.1.3). Pellet was resuspended in 1 ml DPBS and transferred to an Eppendorf tube®, centrifuged at RT for 5 min at 500 g and frozen to – 20 °C until further processing.

Genomic DNA isolation was performed using the FlexiGene® DNA isolation kit (Qiagen) according to the manufacturer's instructions.

3.5.2 SNP karyotyping

Single nucleotide polymorphism (SNP) karyotyping was performed and analysed by the Stem Cell Core Facility (Dr. Sebastian Diecke, Berlin Institute of Health (BIH) / Max Delbrück Center for Molecular Medicine, Berlin, Germany) in cooperation with the laboratory of Prof. Dr. Norbert Hübner (Max Delbrück Center for Molecular Medicine, Berlin, Germany).

15 µl isolated genomic DNA was submitted at 100 ng/µl to the Stem Cell Core Facility and processed for SNP karyotyping using the Illumina platform and the OMNI-EXPRESS-8v1.4 Chip (Illumina). Analysis was done using Karyostudio 1.4 (Illumina).

3.6 RNA assays

3.6.1 RNA isolation

Cultured cells were washed once with DPBS. Then, 350 µl of RP1 buffer (NucleoSpin® RNA/Protein isolation kit (Macherey-Nagel)) were added to each well and cells were detached using a scraper. Cell-lysis solution was then transferred to a 1.5 ml Eppendorf tube® and frozen immediately on dry ice and stored at – 80 °C until RNA isolation.

For RNA isolation, the NucleoSpin® RNA/Protein isolation kit (Macherey-Nagel) was used according to the manufacturer´s instructions. Elution volumes of 20-40 µl were used, depending on the size of the cell pellet. RNA concentration was determined using the NanoDrop™ One Microvolume UV-Vis Spectrophotometer (Thermo Fisher Scientific).

3.6.2 Reverse Transcription and qRT-PCR

400-1000 ng of isolated total RNA (see 3.6.1) were reverse transcribed using the QuantiTect Reverse Transcription Kit (Qiagen) according to the manufacturer´s instructions. cDNA samples were stored at – 20 °C.

Assuming that the used RNA amount corresponds to the cDNA amount after reverse transcription, resulting cDNA was diluted to 32 ng/5 µl and stored as stock solution. For testing all primers (either self-designed or from publication), different annealing temperatures were tested with standard curve assays using 32 ng, 8 ng, 2 ng and 0.5 ng cDNA input in order to define the amount of cDNA and annealing temperature needed for optimal primer efficiencies. Melting curve analysis and 2% agarose gels (100 V) of the resulting qRT-PCR products confirmed the absence of any unspecific products not corresponding to the expected product length. The primer sequences and corresponding optimal annealing temperatures are given in Table 3.4.

For PCR reaction, 10 µl KAPA SYBR® FAST qPCR Master Mix (2X) Universal (Sigma-Aldrich) were mixed with 1 µl 5 µM Primer mix (Forward + Reverse), 4 µl PCR grade water and 5 µl of the diluted

cDNA sample in the respective concentration to a final volume of 20 µl. For analysis the QuantStudio™ 6 Flex Real-Time PCR System (Thermo Fisher Scientific) together with MicroAmp® Optical 96-Well Reaction plates (Thermo Fisher Scientific) were used with three technical replicates per sample and per primer pair. For primer pairs with optimal annealing temperature at 60 °C, a two-step protocol with 40 cycles with denaturation at 95 °C and annealing at 60 °C was used. For primer pairs with optimal annealing temperatures different from 60 °C, a three-step protocol was used with 40 cycles with denaturation at 95 °C, annealing see Table 3.4, and elongation and acquisition at 72 °C. Two control samples were used, one being a qRT-PCR reaction per primer without cDNA but water and the other a qRT-PCR reaction per primer using a reverse transcription product without reverse transcription enzyme.

Ct values were normalised to the housekeeping gene GAPDH (ΔCt values) for each sample, each primer pair and each PCR plate. ΔΔCt values were calculated using the sample with the lowest expression as the relative expression value.

Table 3.4: Primer list for qRT-PCR

Gene		Primer	Annealing temperature
GAPDH	FWD	GAAGGTGAAGGTCGGAGTC	60 °C
	REV	GAAGATGGTGATGGGATTTC	
PAX7	FWD	TGGGCGACAAAGGGAA	60 °C
	REV	GGTAGTGGGTCCTCTCAAA	
MYOD1	FWD	GCGGAACTGCTACGAA	57 °C
	REV	AGATGCGCTCCACGAT	
Desmin	FWD	GGTACAAGTCGAAGGTGTCAG	60 °C
	REV	TCAATCTCGCAGGTGTAGGA	
MYOG	FWD	GCCAACCCAGGGGATCAT	60 °C
	REV	CCCGGCTTGGAAGACAATCT	
MYH2	FWD	GGAACGGGCTGACATTGCTG	60 °C
	REV	GTCATTCCATGGCATCAGGACA	
MYH3	FWD	GGAGCAGGACAGAAGATAT	55 °C
	REV	CCCAGATTGAAACAAAGCA	
MYH7	FWD	CTGTCCAAGTTCCGCAAGGT	60 °C
	REV	TCATTCAAGCCCTTCGTGCC	
PECAM1	FWD	TCGTGGTCAACATAACAGAACT	60 °C
	REV	TGAAGTTGGCTGGAGGTG	

3.6.3 Absence of Sendai-virus

To proof the absence of Sendai-virus particles, as part of the full characterisation of the newly generated human induced pluripotent stem cells, a PCR detection method on RNA/cDNA level was performed as described in Hildebrand et al. 2016.

Total RNA of human induced pluripotent stem cells was collected and isolated as described in 3.6.1. 1000 ng of isolated total RNA were reverse transcribed using the QuantiTect Reverse Transcription Kit (Qiagen) according to the manufacturer´s instructions and cDNA samples were stored at – 20 °C. Assuming that the RNA amount corresponds to the cDNA amount after reverse transcription, resulting cDNA was diluted to 20 ng/µl. For PCR reaction, 10 µl DreamTaq Green PCR Master Mix (2X) (Thermo Fisher Scientific) were mixed with 2 µl 10 µM Primer mix (Forward + Reverse) (Primer are listed in Table 3.5), 6 µl PCR grade water and 2 µl of the diluted cDNA sample to a final volume of 20 µl. For analysis the FlexCycler2 PCR machine (Analytik Jena) was used with the cycle programme: 95 °C for 5min, 35 cycles of 95 °C for 30 sec and 55 °C for 30 sec and 72 °C for 30 sec and finally 72 °C for 10 min. PCR products were analysed using a 2% agarose gel. As controls, two negative samples were used in one PCR reaction without enzyme and one PCR reaction without cDNA. As positive control RNA/cDNA isolated/transcribed from freshly Sendai-virus infected myoblasts was used.

Table 3.5: Primer list for Sendai-virus detection

Gene		Primer
SeV (total)	FWD	GGATCACTAGGTGATATCGAGC
	REV	ACCAGACAAGAGTTTAAGAGATATGTATC
SeV-Klf4	FWD	TTCCTGCATGCCAGAGGAGCCC
	REV	AATGTATCGAAGGTGCTCAA
SeV-c-Myc	FWD	TAACTGACTAGCAGGCTTGTCG
	REV	TCCACATACAGTCCTGGATGATGATG
SeV-KOS	FWD	ATGCACCGCTACGAGTGAGCGC
	REV	ACCTTGACAATCCTGATGTGG
Hu18SRNA	FWD	GTAACCCGTTGAACCCCATT
	REV	CCATCCAATCGGTAGTAGCG

3.6.4 Library preparation

RNA was isolated and stored at – 80 °C as described in 3.6.1. RNA quantity was assessed using the Qubit® 2.0 Fluorometer with the Qubit™ RNA HS Assay Kit (Thermo Fisher Scientific). The quality of the isolated RNA was furthermore analysed by the 4200 TapeStation System together with the high sensitivity RNA ScreenTape (Agilent). RIN values were above 7 for all samples.

Library preparation for total RNA-Sequencing was performed using the NEBNext Ultra II Directional RNA Library Prep Kit for Illumina® (New England Biolabs) together with the NEBNext rRNA Depletion Kit (Human/Mouse/Rat) (New England Biolabs). 250 ng total RNA were used per sample following the manufacturer´s instructions. NEBNext® Multiplex Oligos for Illumina® (New England Biolabs) were used for indexing with a final PCR enrichment of adapter ligated DNA of 10 cycles due to the 250 ng initial RNA. Purification of the final PCR reaction using Agencourt® AMPure XP PCR cleanup beads (Beckman Coulter Life Sciences) was performed twice to assure a clean end product without contaminating small fragments or adapters.

Library quality was checked with the 2100 Bioanalyzer together with the Bioanalyzer High Sensitivity DNA Analysis chips and reagents (Agilent). Library quantity was determined using the Qubit™ dsDNA HS assay kit (Agilent). Finally, samples were appropriately pooled with a final concentration of 10 mM per sample and delivered to the Genomics Platform (Dr. Sascha Sauer, Max Delbrück Center for Molecular Medicine, Berlin, Germany) to be sequenced with 2x76+16In (paired end, 76 cycles, 16 indices) using the HiSeq 4000 System (Illumina).

3.6.5 RNA-Sequencing and analysis

RNA-Sequencing and preliminary data processing was done by the Genomics Platform (Dr. Sascha Sauer, Max Delbrück Center for Molecular Medicine, Berlin, Germany) by Dr. Daniele Yumi Sunaga-Franze.

For each sample, the transcript quantification at isoform level was estimated by RSEM (bowtie2 default parameters, GRCh38) (Li & Dewey, 2011). DEseq2 paired designed and padj < 0.05 was used for the differential expression analysis between myoblasts vs. PBMC vs. M_hiPSCs vs. B_hiPSCs (Anders & Huber, 2010).

The differentially expressed isoforms were further annotated via Biomart R package (hsapiens_gene_ensembl). Pathway analysis and GO term enrichment analysis were performed using ConsensusPathDB (http://cpdb.molgen.mpg.de/). Further analysis was performed using the Database for Annotation, Visualisation and Integrated Discovery (DAVID) (https://david.ncifcrf.gov).

3.7 Transplantation studies

Mouse experiments were performed under the licence number G0035/14. Immunodeficient, xenograft compatible, female NOG-M mice (NOD.Cg-Prkdc^{scid} Il2rg^{tm1Sug}/JigTac, Taconic Biosciences, Bomholtvej, Denmark) were purchased at the age of 6-9 weeks ahead of each experiment. Animals were kept in a specific-pathogen-free (SPF) animal facility with controlled temperature and humidity at the Max Delbrück Center for Molecular Medicine, Berlin, Germany.

3.7.1 Focal irradiation of tibialis anterior muscles

Focal irradiation of female 6-9 weeks old NOG-M mice hind limb muscles (NOD.Cg-Prkdc^{scid} Il2rg^{tm1Sug}/JigTac, Taconic Biosciences, Bomholtvej, Denmark) was performed using an image-guided robotic system (CyberKnife Radiosurgery System, Accuracy Inc.) at the Charité CyberKnife facility (Virchow-Klinikum, Berlin, Germany) as previously described (Marg et al., 2014; Kufeld et al., 2017).

All mice were anaesthetised with ketamine-xylazine in PBS (9 mg/ml ketamine, 1.2 mg/ml xylazine) with an intra peritoneal (i.p.) dose of 160 µl/20g of body mass or by inhalation of 2% isoflurane using an Univentor 400 anaesthesia unit (Univentor) together with a flexible customised inhalation mask. For targeting the irradiation robot to the mouse hind limbs, an acrylic glass block with surface fiducial marks was constructed to which the mice hind limbs could reproducibly be attached, specifically targeting the hind limb and avoiding irradiation of other body parts. Digitally reconstructed radiographs (DDRs) were generated using a computer tomography (CT) scan with 0.75 mm slice thickness for radiation dose distribution, in order to reach the desired dose of 16 Gy in the three-dimensional target area of the limb. Treatment planning was based on the assumption that all legs and muscles of the selected mice were similar. The anaesthetised mice were placed in the customised acrylic gap and the treatment procedure could be conducted within an approximately time span of 5 min. Biafine lotion was applied on the irradiated area following the procedures.

3.7.2 Transplantation of induced myogenic progenitor cells (iMPCs) into tibialis anterior muscles of NOG-M mice

For transplantation, freshly differentiated induced myogenic progenitor cells (iMPCs) were detached using TrypLE™ Express (see 3.1.3.2.2) and resuspended in DPBS + 2% FCS. Cells were stored on ice until transplantation. Mice were anaesthetised by inhalation of 2% isoflurane using an Univentor 400 anaesthesia unit (Univentor) together with a flexible customised inhalation mask. When the anaesthesia was effective, a specific area of the right hind limb, below the knee, above the tibialis anterior muscle, was shaved and disinfected using isopropanol. $1*10^5$ cells in 11 µl injection volume were injected into the central part of the tibialis anterior muscle using a 25 µl model 702 RN SYR Hamilton® syringe (Hamilton) coupled with a custom-made 20 mm long 26 G small hub removable needle. Mice were monitored on a daily basis. In some mice, skin redness and hair loss in the irradiated areas was observed 14-20 days post irradiation. Bepanthen lotion (Bayer) was applied daily on the affected areas until the date of sacrifice.

3.7.3 Preparation of tibialis anterior muscles and histological sections

Mice were sacrificed 21 days after cell injection by cervical dislocation and tibialis anterior (TA) muscles were subsequently dissected. TA muscles were cut in two halves following a transversal plane. Each TA-half was separately mounted in gum tragacanth (12% Gum Tragacanth (Sigma-

Aldrich), a few granules of Crystal Thymol (Synopharm) and 4,6% glycerin in dH_2O) on cork disks with the cutting surface facing the top. The embedded muscles were then frozen in chilled isopentan for 15 sec and then immediately transferred to liquid nitrogen. For long-term storage muscles were transferred to – 80 °C.

Muscles were sectioned using a Leica CM3050S Cryostat (Leica Biosystems) preparing 10 µm thick sections that were stored at – 20 °C until further processing.

3.8 Statistics

Statistical analysis was performed using the GraphPad Prism 8 software (GraphPad). Differences were considered statistically significant for $p < 0.05$. Statistical tests performed for each specific experiment are indicated in the figure legends.

4. RESULTS

4.1 Reprogramming efficiencies of myoblasts and PBMCs into induced pluripotent stem cells (hiPSCs)

I reprogrammed myoblasts and peripheral blood mononuclear cells (PBMCs) from donors without any signs of neuromuscular disorders into hiPSCs. Myoblasts and PBMCs were reprogrammed from the same donor to assure a reasonable comparison of hiPSCs derived from different somatic cell types without donor related differences. Both cell types were reprogrammed using the same reprogramming protocol based on Sendai-virus delivery of the reprogramming factors OCT3/4, SOX2, KLF4 and c-MYC (Yamanaka factors, Takahashi et al. 2007). I selected 5 donors for this study without neuromuscular disorders. 3 donors were gender and age matched (female, 47-50 years of age) while two were selected for more heterogeneity within the study (male, 19 and 58 years of age) (see Table 3.1 (Material and Methods) and Table 4.1).

For reprogramming into hiPSCs, I enriched myoblasts for $CD56^+$ cells while the PBMCs were stimulated to proliferate. I infected both, myoblasts and PBMCs, with Sendai-viruses from the commercially available CytoTune™-iPS 2.0 Sendai Reprogramming Kit (Thermo Fisher Scientific) to deliver the reprogramming factors OCT3/4, SOX2, KLF4 and c-MYC. During the reprogramming process I treated the newly generated myoblast- and PBMC-derived hiPSCs equally using the same pluripotent stem cell medium and the same quality assurance procedures. For discrimination within the study, the newly generated muscle/myoblast-derived hiPSCs are referred to as M_hiPSCs and the blood/PBMC-derived hiPSCs as B_hiPSCs (Figure 4.1).

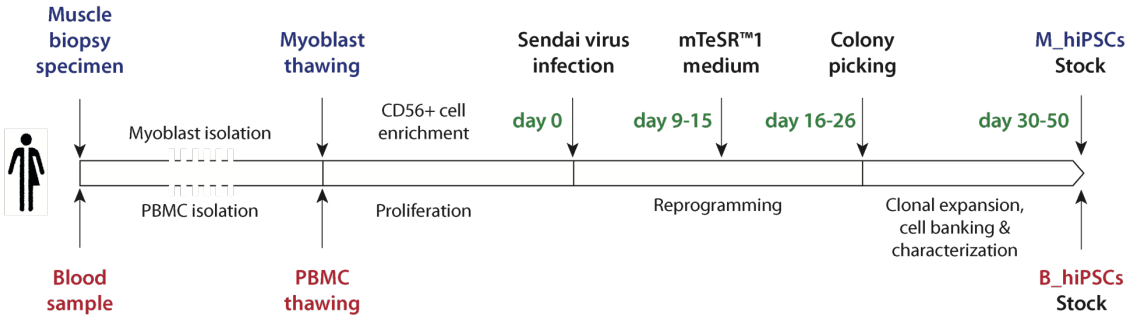

Figure 4.1: Schematic description of the reprogramming procedure
Muscle biopsy specimen and full blood samples were obtained from 5 healthy donors with informed consent. Myoblasts were enriched for $CD56^+$ cells and the purity of the population was confirmed by immunofluorescence staining for Desmin. PBMCs were stimulated for proliferation. Both, myoblasts and PBMCs, were infected with the commercially available CytoTune™-iPS 2.0 Sendai Reprogramming Kit (Thermo Fisher Scientific) to deliver the reprogramming factors OCT3/4, SOX2, KLF4 and c-MYC. When hiPSC colonies started to appear, the medium was changed to the pluripotent stem cell medium mTeSR™1 (Stem Cell Technologies). Both, myoblast- and PBMC-derived hiPSCs were treated equally with the same quality assurance procedures and stocked as M_hiPSCs (muscle/myoblast-derived hiPSCs) and B_hiPSCs (blood/PBMC-derived hiPSCs).

The reprogramming experiments resulted in a significantly higher efficiency when the hiPSCs were generated from myoblasts compared to when they were generated from PBMCs (Figure 4.2).

All reprogramming experiments using myoblast samples were successful, resulting in a maximum of 9 to 50 hiPSC colonies for all 5 donors A to E assessed on day 30 of the reprogramming protocol. Using PBMC samples, the reprogramming experiments resulted in a maximum of 2 to 15 hiPSC colonies from donors A, B, C and D (Table 4.1). I was not able to obtain any hiPSC colonies from PBMC samples of donor E, even after 5 independent reprogramming experiments. Considering the initial number of cells infected with Sendai-viruses the successful reprogramming experiments resulted in an efficiency ranging from 0.018% to 0.1% for myoblasts and 0.0007% to 0.005% for PBMCs, thus resulting in an average efficiency of 0.07% for myoblasts and 0.002% for PBMCs.

Regarding the PBMC samples of donor C, I was not able to obtain hiPSC colonies using Matrigel-coating, which I used for all other reprogramming experiments. Thus, for this 5th repetition of the reprogramming experiment with PBMCs from donor C, I used mouse embryonic feeder cells (MEFs) and was hence able to obtain 5 hiPSC colonies. I also repeated the reprogramming experiment for PBMCs from donor E using mouse embryonic feeder cells (MEFs) but still failed to obtain any hiPSC colonies.

As it was thus not possible to compare M_hiPSCs and B_hiPSCs I excluded donor E from further experiments. hiPSC colonies from donors A to D were further characterised.

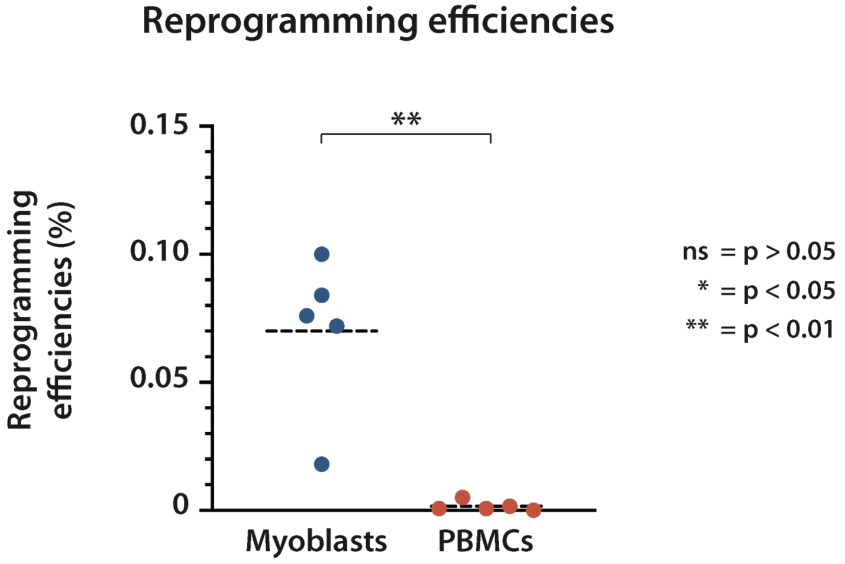

Figure 4.2: Quantification of the reprogramming efficiencies comparing myoblasts and PBMCs
The graph presents the reprogramming efficiencies in percent for myoblasts and PBMCs as they are given in Table 4.1. For statistical analysis the Students t-test ($p < 0.05$) was used. Dashed lines represent the mean.

Table 4.1: Reprogramming efficiencies for myoblasts and PBMCs
The table shows the numbers of appearing hiPSC colonies for myoblasts and PBMCs from donors A to E counted after 30 days after Sendai-virus infection. Efficiencies are given in percent calculated from the starting cell number, $5*10^4$ for myoblasts and $3*10^5$ for PBMCs. Average reprogramming efficiency for myoblasts is 0.07% and 0.002% for PBMCs. The second column shows the numbers of trials necessary to obtain any hiPSC colony. Cells were reprogrammed with the Sendai 2.0 Reprogramming Kit on Matrigel, if not mentioned otherwise. Mouse embryonic feeder cells (MEFs) were used as marked in the table.

		Number of appearing hiPSC colonies		**Number of reprogramming trials**	
Donor	Gender/Age	Myoblasts	PBMCs	Myoblasts	PBMCs
A	Female, 47	38 (0.076%)	15 (0.005%)	1	1
B	Female, 50	42 (0.084%)	2 (0.0007%)	1	1
C	Male, 19	50 (0.1%)	5 (0.0016%) (MEFs)	1	5
D	Female, 47	36 (0.072%)	2 (0.0007%)	1	1
E	Male, 58	9 (0.018%)	0 (0%) (MEFs)	1	5

4.2 Characterisation of the generated human induced pluripotent stem cells (hiPSCs)

The robust characterisation of newly generated human induced pluripotent stem cells is a critical step for a reliable comparison of their properties in the pluripotent state and of their differentiation capabilities. In order to conduct a statistically significant study I fully characterised 2 single colony-derived hiPSC clones per donor, that is 1 clone derived from myoblasts and the other clone derived from PBMCs. In total for the 4 donors, I characterised 8 hiPSC clones.

To ensure high cell quality standards of myoblast- and PBMC-derived hiPSCs (M_hiPSCs and B_hiPSCs), the full characterisation panel of the newly generated hiPSCs includes the assurance of the absence of the Sendai-viruses, used for the reprogramming procedure. Additionally, I examined the colony morphology of the hiPSCs and the stability of the karyotype via single nucleotide polymorphism analysis (SNP). I assured the expression of myoblast and pluripotency markers by immunofluorescence and finally, the teratoma formation assay was performed to verify the potential of each hiPSC clone to form all three germ layers.

4.2.1 Abundance of Sendai-viruses

The reprogramming procedure is based on the delivery of 4 transcription factors, OCT3/4, SOX2, KLF4 and c-MYC, known as Yamanaka factors, into human somatic cells (Takahashi et al., 2007). The reprogramming factors are transcription factors with the potential to change the cell´s fate as turning them into a pluripotent state (Takahashi & Yamanaka, 2006; Takahashi et al., 2007) and as the reactivation of c-Myc is associated with tumorigenicity (Okita et al., 2007). Thus, I assured that their ectopic expression via Sendia-viruses is stopped before the M_hiPSCs and B_hiPSCs were compared in any way.

In this work the commercially available CytoTune™-iPS 2.0 Sendai Reprogramming Kit (Thermo Fisher Scientific) was used for the reprogramming. Sendai-viruses replicate in the form of negative-sense single-stranded RNA in the cytoplasm of infected cells. They neither go through a DNA phase nor integrate into the host genome. Sendai-viruses remain in the cytoplasm of hiPSCs but due to their non-integrative properties are removed from the cells within 10-20 passages (Fusaki et al., 2009). Thus, I expanded the newly generated hiPSCs for at least 10 passages and then tested them for the absence of Sendai-virus RNA. The reprogramming kit is composed of 3 different Sendai-viruses for the delivery of specific amounts of the reprogramming factors. Using defined primers for each single virus, together with a primer pair for the detection of all 3 viruses, I verified the abundance of Sendai-virus-RNA to be below the detection limit of a cDNA-based PCR reaction (Figure 4.3). The absence of cDNA-bands for the specific expected band size in all of the samples verifies the absence of Sendai-virus RNA of all three Sendai-viruses included in the CytoTune™-iPS 2.0 Sendai Reprogramming Kit. A

positive control sample consisting of freshly Sendai-virus-infected myoblasts shows the expected band size. Human 18sRNA was used to verify the presence of cDNA in all samples.

All generated hiPSCs were negative for Sendai-viruses at passages 13-15. M_hiPSCs from donors B and D had to be subcloned by picking single colonies to reach a negative detection result. Although some hiPSC clones were Sendai-free in earlier passages, all clones were expanded to passages 13-15 for reasonable comparison of the hiPSC clones in their pluripotent state and in their capability to differentiate into the myogenic lineage.

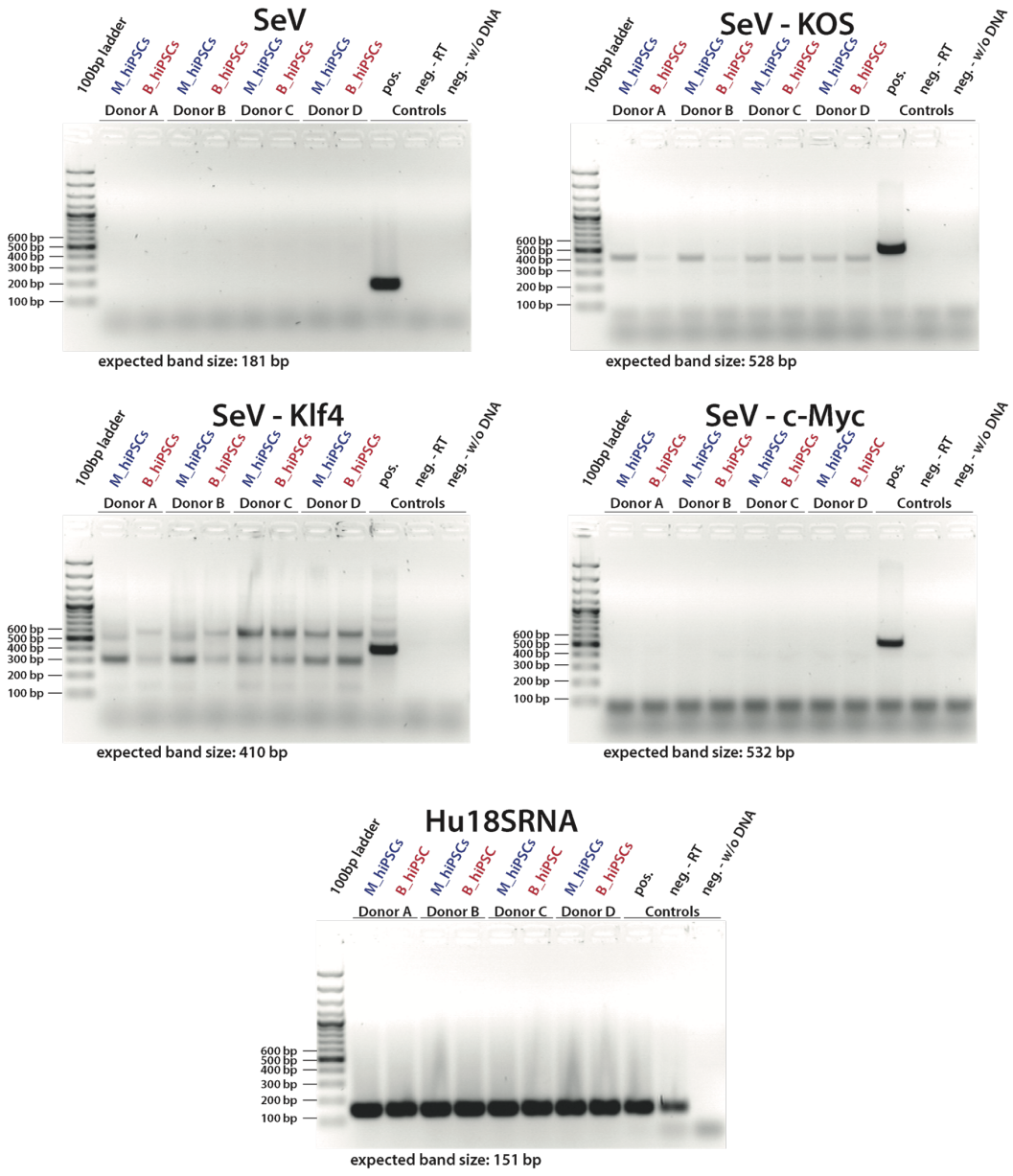

Figure 4.3: Absence of Sendai-viruses in hiPSC clones
RT-PCR for the abundance of Sendai-virus RNA for all 8 generated hiPSC clones in passages 13-15. SeV: total Sendai-virus; SeV-KOS: Sendai-virus for the expression of Klf4/OCT4/SOX2, SeV-Klf4 for the expression of Klf4, SeV-c-Myc for the expression of c-Myc. Human 18sRNA was used to verify the presence of cDNA in all samples. Two negative controls were used, a water only control and a RNA sample from one of the clones where no reverse transcriptase enzyme was added to the reaction for cDNA preparation. One positive control was used with RNA isolated from freshly Sendai-virus-infected myoblasts.

4.2.2 Morphological characteristics and karyotype

Severe genetic and chromosomal aberrations have been detected in newly generated human induced pluripotent stem cells (Mayshar et al., 2010; Hussein et al., 2011). I thus conducted karyotype analysis to ensure genomic integrity. For karyotyping the single nucleotide polymorphism (SNP) analysis was used which is based on the detection of millions of single-base sequence variations that are distributed throughout the genome (~1 SNP per 1 kb) (Butler, 2012). As severe genomic changes might also affect the cell morphology (Kilpinen et al., 2017), I additionally performed a thorough morphological analysis of the generated hiPSCs.

Appropriate morphological characteristics of hiPSCs as well-defined colony borders and packed colony morphology were documented (Figure 4.4, A). No signs of spontaneous differentiation were detected in the hiPSCs used in this work. However, a few dying cells in the centre of big colonies were not considered to be an exclusion criterium for this clone but were generally avoided by low hiPSC colony sizes in standard cell culture.

Karyotype analysis* of the generated hiPSC clones revealed no numerical chromosomal abnormalities for all 8 examined clones. Results show typical karyotypes with minor insertions (marked in green), deletions (marked in red) or loss of heterozygosity (marked in grey) (Figure 4.4, B). Microinsertions or deletions may be attributed to heterogeneity within donors and to the comparison to the reference standard human genome used in this assay.

For donor A it is important to note, that all aberrations, except the insertion on the X chromosome, can only be detected in the parental myoblast sample and are not present in the generated hiPSC clones. This might be due to a prolonged passaging of the myoblasts of donor A after the cells were used for reprogramming and before the cells were collected for karyotyping.

The donors B and C show aberrations only in the newly generated hiPSCs which indicates that genomic alterations might arise during the reprogramming process. Of note, none of the analysed samples show large deletions or insertions, verifying a widely normal karyotype for all samples.

The presence of a microinsertion on the X chromosome for donor A in all samples at the exact same position verifies the origin from the same donor for all three samples. This type of verification was also possible for donor C.

* SNP analysis was performed in cooperation with the Stem Cell Core Facility (Dr. Sebastian Diecke, Berlin Institute of Health (BIH) / Max Delbrück Center for Molecular Medicine, Berlin, Germany) in cooperation with the laboratory of Professor Norbert Hübner (Max Delbrück Center for Molecular Medicine, Berlin, Germany).

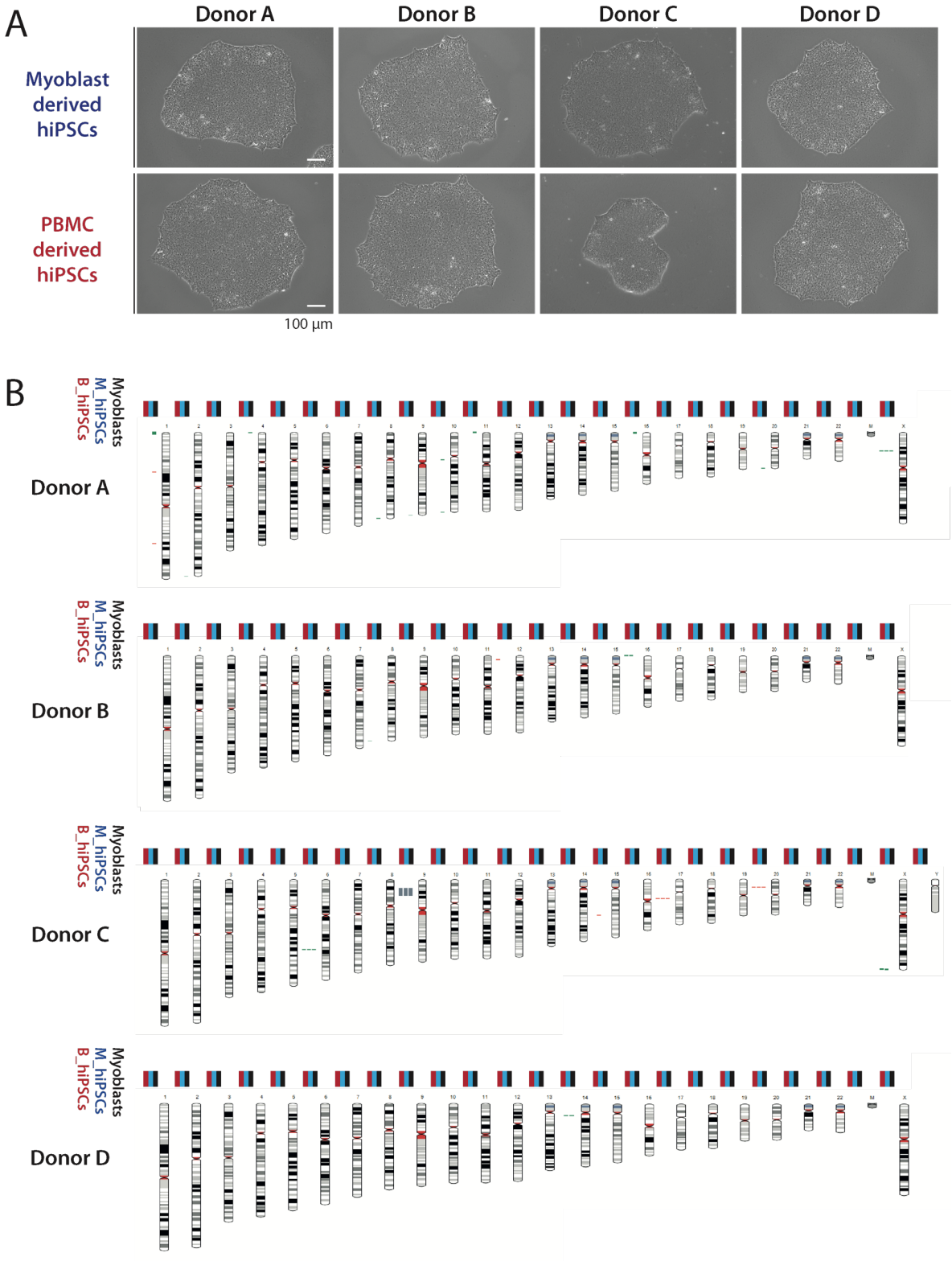

Figure 4.4: Morphological characterisation and virtual karyotype of generated hiPSC clones
(A) Representative brightfield pictures of all 8 generated, Sendai-free hiPSC clones after 13 to 15 passages in cell culture with well-defined colony borders, packed colony morphology and no sign of spontaneous differentiation. Scale bar: 100 µm **(B)** Virtual karyotypes of all generated hiPSC clones in passages 13-15 and donor myoblasts for each donor with widely normal karyotypes. Insertions (green), deletions (red) and loss of heterozygosity (grey) compared to the human reference genome are shown next to each chromosome for each individual sample. Legend shows myoblasts (black), M_hiPSCs (blue) and B_hiPSCs (red) for each donor).

4.2.3 Pluripotency marker expression

The expression of pluripotency markers like OCT3/4, SOX2, NANOG and TRA-1-60 is regularly used for the characterisation of pluripotency, as established by the group of Shin'ya Yamanaka in the introductory paper of hiPSCs (Takahashi et al., 2007). Of note, I excluded the marker SSEA4 in this study, a marker also commonly used for the characterisation of pluripotency, because it is also expressed by primary myoblasts and was therefore not suitable for the characterisation of the established hiPSC clones (data not shown). I included the stainings for the myogenic markers Desmin, MYOD1 and PAX7 as characterisation of the cells of origin and to verify the absence of these markers in the hiPSCs.

I detected the expression of the pluripotency markers OCT3/4, NANOG and SOX2 in the nucleus of all generated hiPSCs (Figure 4.5, Figure 4.6). In addition, I was able to detect the cell surface marker TRA-1-60 at the membrane of the hiPSCs. Simultaneously, I could not detect any signal of the myogenic markers Desmin, PAX7 or MYOD1 in the hiPSCs. The corresponding myoblasts, that were used for the generation of the myoblast-derived hiPSCs, did show the expression of all myogenic markers Desmin, PAX7 and MYOD1 and were negative for the pluripotency markers OCT3/4, SOX2, NANOG and TRA-1-60. M_hiPSCs and B_hiPSCs showed no difference in marker expression.

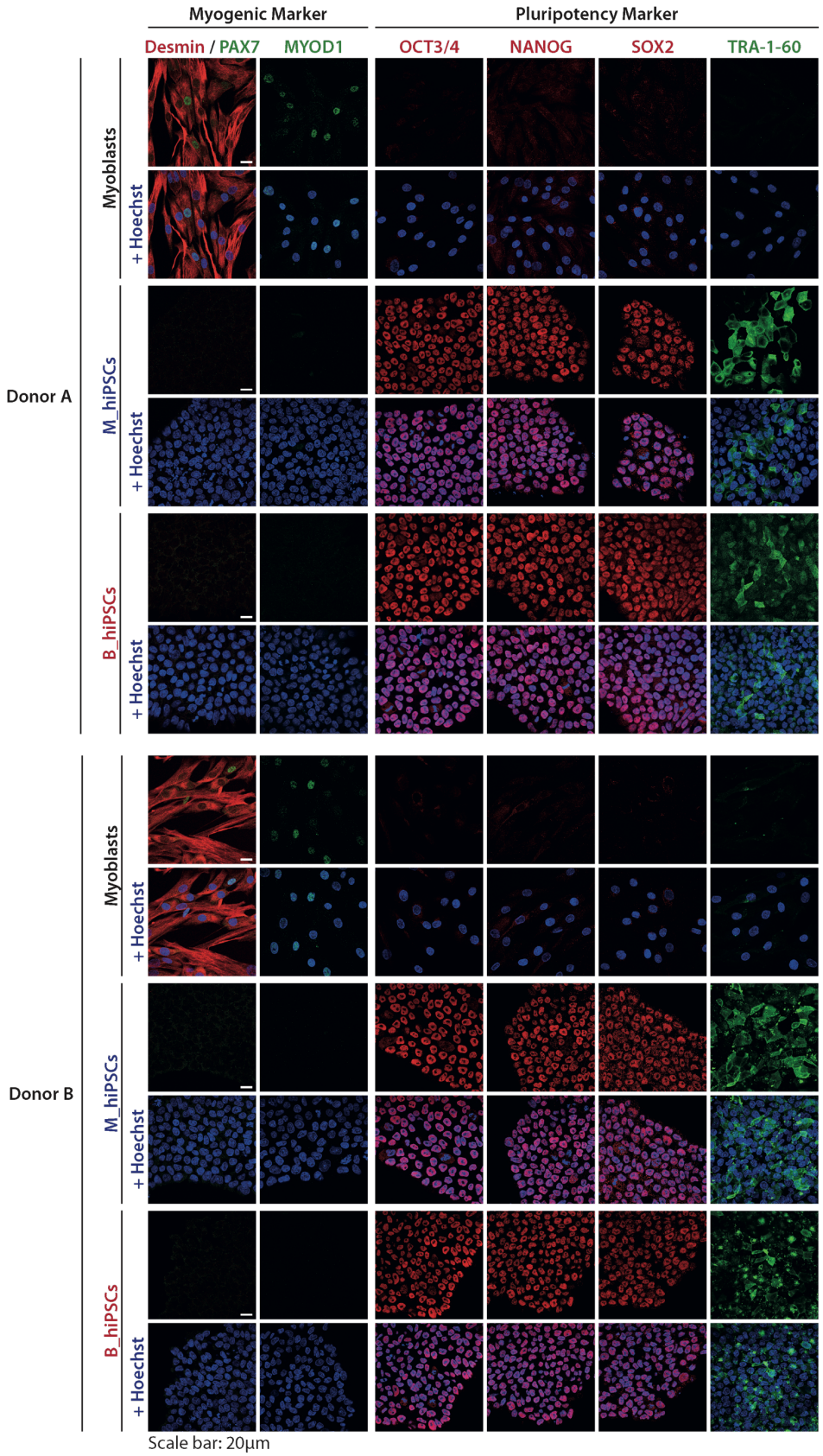

Figure 4.5: Myogenic and pluripotency marker expression in myoblasts, M_hiPSCs and B_hiPSCs for donors A and B

Representative images of immunofluorescence stainings for the myogenic markers Desmin, PAX7 and MYOD1 and the pluripotency markers OCT3/4, NANOG, SOX2 and TRA-1-60. Myoblast samples represent the samples of origin of the generated M_hiPSCs. Scale bar: 20 µm.

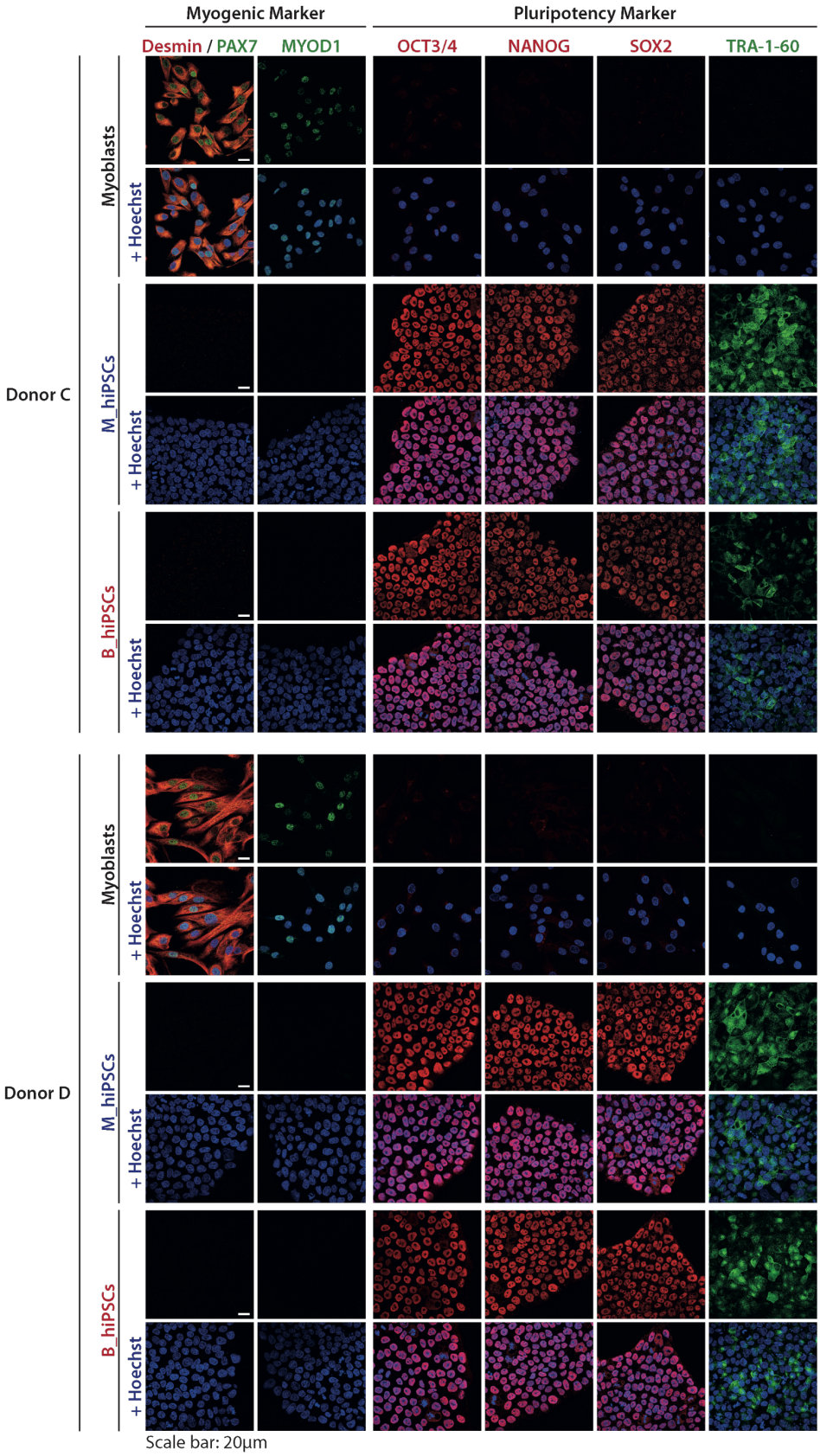

Figure 4.6: Myogenic and pluripotency marker expression in myoblasts, M_hiPSCs and B_hiPSCs for donors C and D

Representative images of immunofluorescence stainings for the myogenic markers Desmin, PAX7 and MYOD1 and the pluripotency markers OCT3/4, NANOG, SOX2 and TRA-1-60. Myoblast samples represent the samples of origin of the generated M_hiPSCs. Scale bar: 20 µm.

4.2.4 Pluripotent properties tested by teratoma formation assay

Teratoma formation is considered to be an index for the pluripotency of cells by the formation of all three germ layers and it is widely used to characterise human induced pluripotent stem cells as a functional test in addition to the in vitro verification of pluripotency marker expression (Evans & Kaufman, 1981; Hentze et al., 2009; Karagiannis et al., 2018).

The teratoma formation assay was performed for each clone by EPO – Experimental Pharmacology & Oncology Berlin-Buch GmbH (Campus Buch, Berlin, Germany). I prepared the cell suspensions and submitted them to EPO for transplantation of $2.5*10^6$ cells subcutaneously into both flanks of immunodeficient NOG-M mice (Taconic Biosciences, Bomholtvej, Denmark). The tumour growth was evaluated weekly and the animals were sacrificed when the tumour size reached more than 1 cm^3, 8 weeks after transplantation or when the purpose of the experiment had been reached.

The results of the teratoma formation assay showed tumour formation of all generated hiPSC clones with formation of tissues of all three germ layers as shown in the histopathological examination (Figure 4.7).

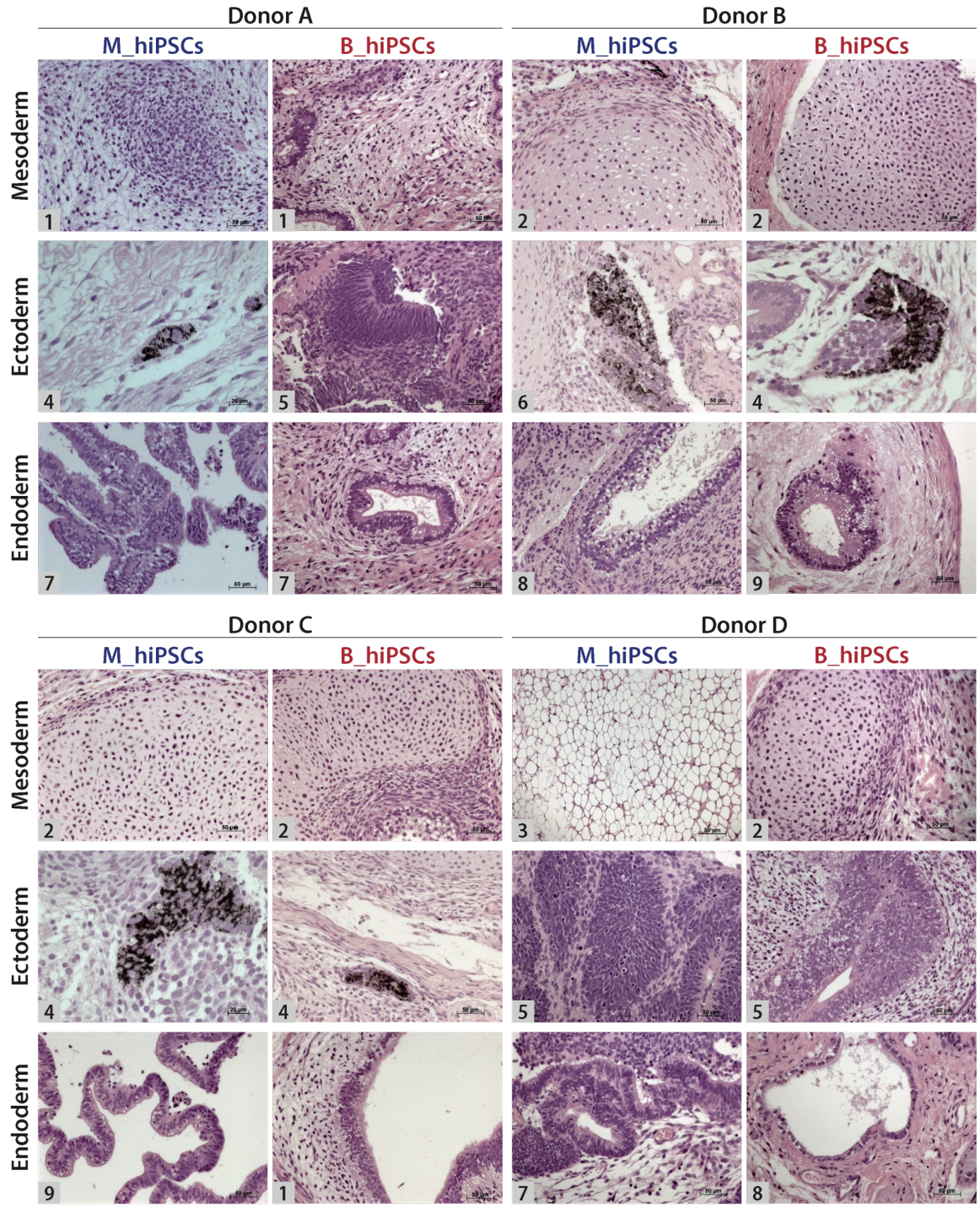

Figure 4.7: Histological analysis of teratomas formed after transplantation of hiPSCs into immunodeficient NOG-M mice

Mesoderm, ectoderm and endoderm formation within the teratomas are shown for each M_hiPSC and B_hiPSC cell clone from all donors. 2.5*10^6 cells, resuspended in 50 µl PBS + 50 µl Matrigel, were injected subcutaneously into both flanks of immunodeficient NOG-M mice. Animals were sacrificed when tumour size reached more than 1 cm^3 or 8 weeks after transplantation. Cell types mesoderm: 1: immature mesenchym, 2: chondroid tissue, 3: adipose tissue. Cell types ectoderm: 4: pigmented epithelial cells, 5: rosette formation, 6: columnar epithelial cells with vacuoles. Cell types endoderm: 7: isoprismatic epithelial cells, 8: cuboidal epithelial cells, 9: columnar epithelial cells, 10: endodermal cells. Scale bars: 20 µm or 50 µm, specified in the images.

4.3 RNA-Sequencing analysis comparing M_hiPSCs and B_hiPSCs

We* performed full RNA Sequencing on the newly generated hiPSCs and their corresponding samples of origin to investigate possible differences in the transcriptome profiles of M_hiPSCs and B_hiPSCs.

To gain reliable results, I prepared all samples in a comparable way using the same protocol to process all samples at the same point in time. First, I finished the full characterisation of all hiPSCs assuring full pluripotency, absence of Sendai-viruses and no fatal chromosomal aberrations (Results section 4.2). Then, I thawed the stocked hiPSCs all at the same time and cultured them for 2 passages (~ 1 week) to avoid any freezing artefacts in the maintenance culture of the hiPSCs. The hiPSCs were all used in passages 13-15. Primary myoblasts and PBMCs were cultured for 1 week as well. Cell pellets were collected with the same method. Accordingly, I performed RNA isolation and library preparation in one experiment on the same day. All libraries were prepared from samples with RNA integrity number (RIN) values above 7, assuring high RNA quality and the libraries were checked for the absence of interfering residual primers or adapter dimers. Finally, after barcoding, all 16 samples were pooled. I then delivered the samples to the Genomics Platform where they were analysed "paired end" in one experimental run on a HiSeq 4000 System (Illumina). DEseq2 with an adjusted p value $p < 0.05$ was used for the differential transcript expression analysis (Anders & Huber, 2010) performed by Dr. Daniele Yumi Sunaga-Franze in the Genomics Platform.

The principal component analysis (PCA) shows the clustering of all hiPSCs with a clear separation from their cell types of origin (Figure 4.8, A). Additionally, separated analysis comparing the cell types of origin with their respective hiPSCs, revealed a large difference of donor C to the other three donors. Especially in the comparison of PBMCs to B_hiPSCs, the large transcriptome differences between donor C and donors A, B and D did not allow a clear separation of all PBMCs vs. all B_hiPSC samples in the PCA plot (Figure 4.8, B & C). Donors A, B and D are all female, 47-50 years of age, whereas donor C is a 19-years-old male. To rule out the influence of age and gender for the comparison of M_hiPSCs and B_hiPSCs, we decided to exclude donor C and repeat the PCA with the samples of donors A, B and D, a dataset still suitable for statistical analysis.

* RNA sequencing was performed in cooperation with the Genomics Platform (Dr. Sascha Sauer, Max Delbrück Center for Molecular Medicine, Berlin, Germany)

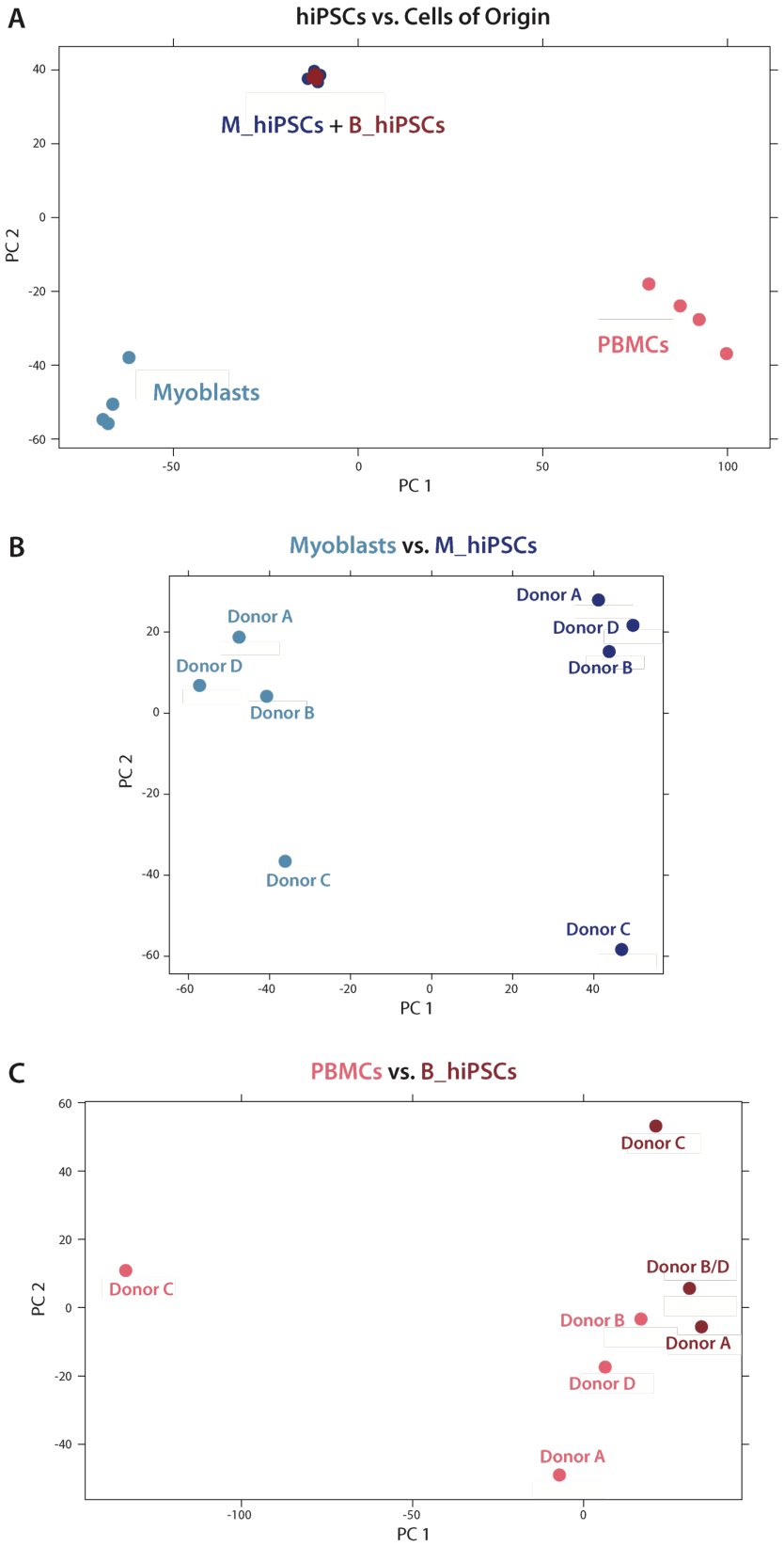

Figure 4.8: Principlal component analysis of full RNA-Sequencing comparing M_hiPSCs, B_hiPSCs, myoblasts and PBMCs of all 4 donors A, B, C and D.
Principlal component analysis (PCA) shows the distribution of the samples according to differentially expressed transcripts (DETs). M_hiPSCs (dark blue), myoblasts (light blue), B_hiPSCs (dark red), PBMCs (light red). **(A)** hiPSCs cluster together with large differences compared to their cell type of origin. **(B & C)** Donor C shows differential clustering compared to donors A, B and D.

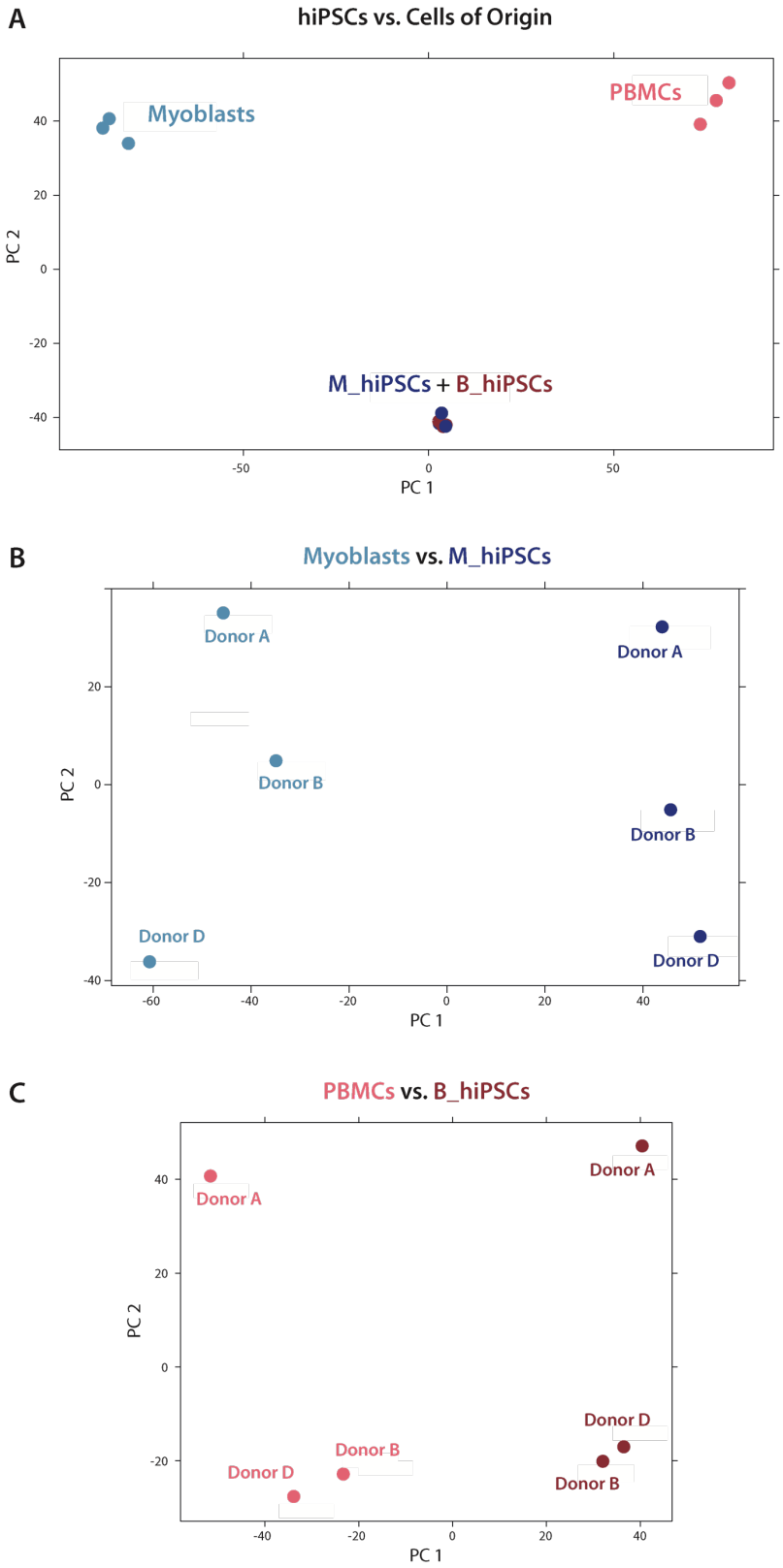

Figure 4.9: Principlal component analysis of full RNA-Sequencing comparing M_hiPSCs, B_hiPSCs, myoblasts and PBMCs of the 3 donors A, B and D.
Principlal component analysis (PCA) shows the distribution of the samples according to differentially expressed transcripts (DETs). M_hiPSCs (dark blue), myoblasts (light blue), B_hiPSCs (dark red), PBMCs (light red). Comparison of age and gender matched donors (female, 47-50 years of age; Donors A, B, D) **(A)** hiPSCs of different origins cluster together with large differences compared to their cell type of origin. **(B & C)** myoblasts separate from M_hiPSCs and PBMCs from B_hiPSCs. The different donors can be separated from each other as well.

The analysis, including donors A, B and D, confirmed the previously seen clustering of all hiPSC samples with clear differences to their cell types of origin (Figure 4.9, A). The exclusion of donor C reduced the influence of the donor variability and enabled the clear separation between myoblasts and M_hiPSCs and between PBMCs and B_hiPSCs (Figure 4.9, B & C). Of note, the samples of the same cell type still show large differences and the samples can be also separated by their donor. This shows, that the donor has a great influence on the transcriptional profile of the cells.

Next, we compared the M_hiPSCs to the B_hiPSCs in the principle component analysis. Interestingly, the PCA shows clustering of donor samples rather than clustering of myoblast- or blood-derived samples (Figure 4.10), showing that the donor influence on the transcriptomic identity of the cells is bigger than the cell type of origin. Nevertheless, differences between the cell types of origin can be detected, with small differences for donor A and similar differences for donors B and D. Finally, 122 transcripts were found to be significantly differentially expressed between M_hiPSCs and B_hiPSCs in all donors using a paired analysis with an adjusted p value $p < 0.05$ (Figure 4.11).

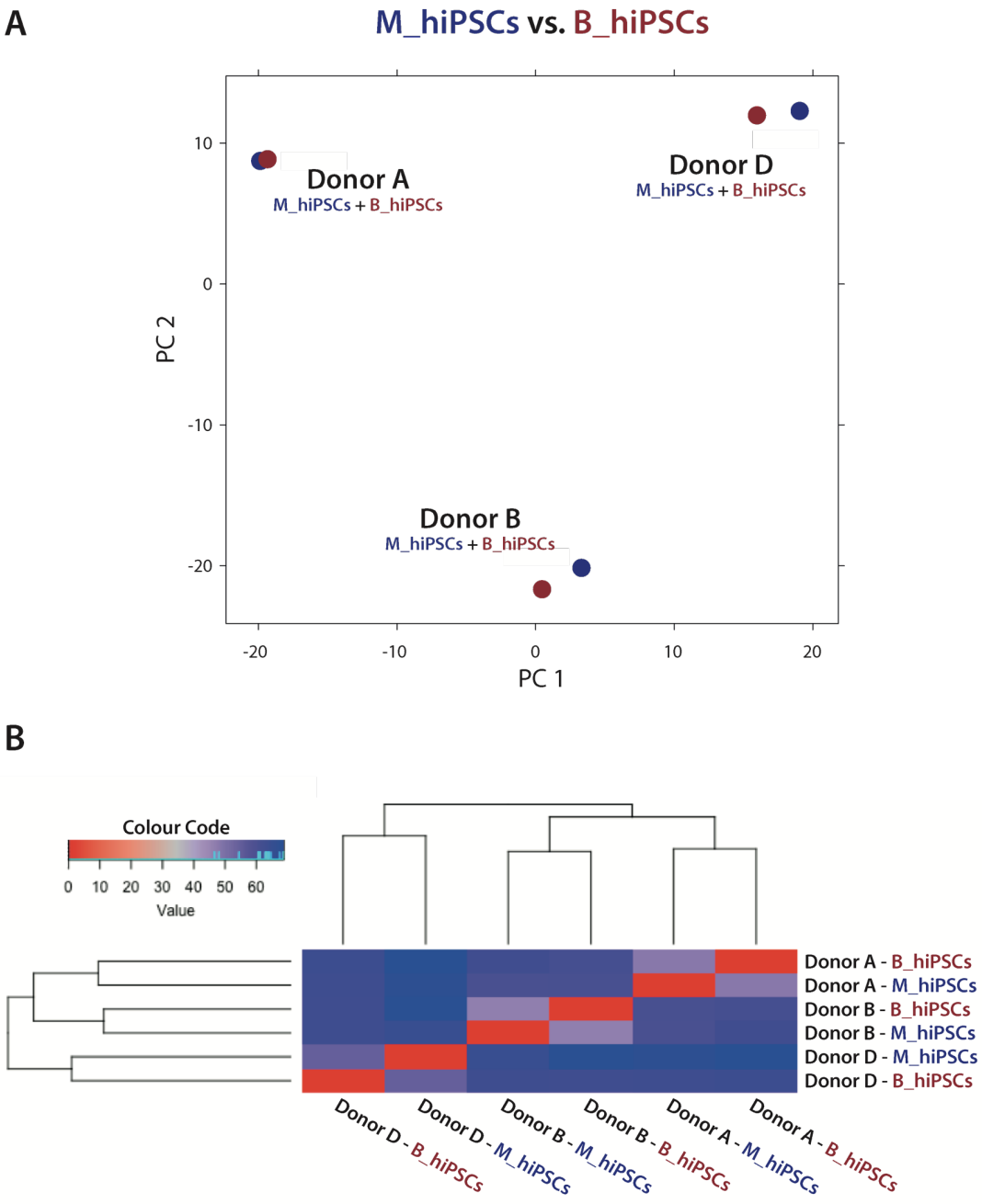

Figure 4.10: Principle component analysis of full RNA-Sequencing comparing M_hiPSCs and B_hiPSCs of 3 donors A, B and D.
Principle component analysis (PCA) shows the distribution of the samples according to differentially expressed transcripts (DETs). Comparison of age and gender matched donors (female, 47-50 years of age; Donors A, B, D). **(A)** PCA plot with M_hiPSCs (dark blue) and B_hiPSCs (dark red). Donor samples cluster together, rather than cell types of origin. Differences between the cell type of origin can be observed with small differences for donor A and similar differences for donors B and D. **(B)** Heat map shows relationship of the samples; donor samples are more related than cell types of origin.

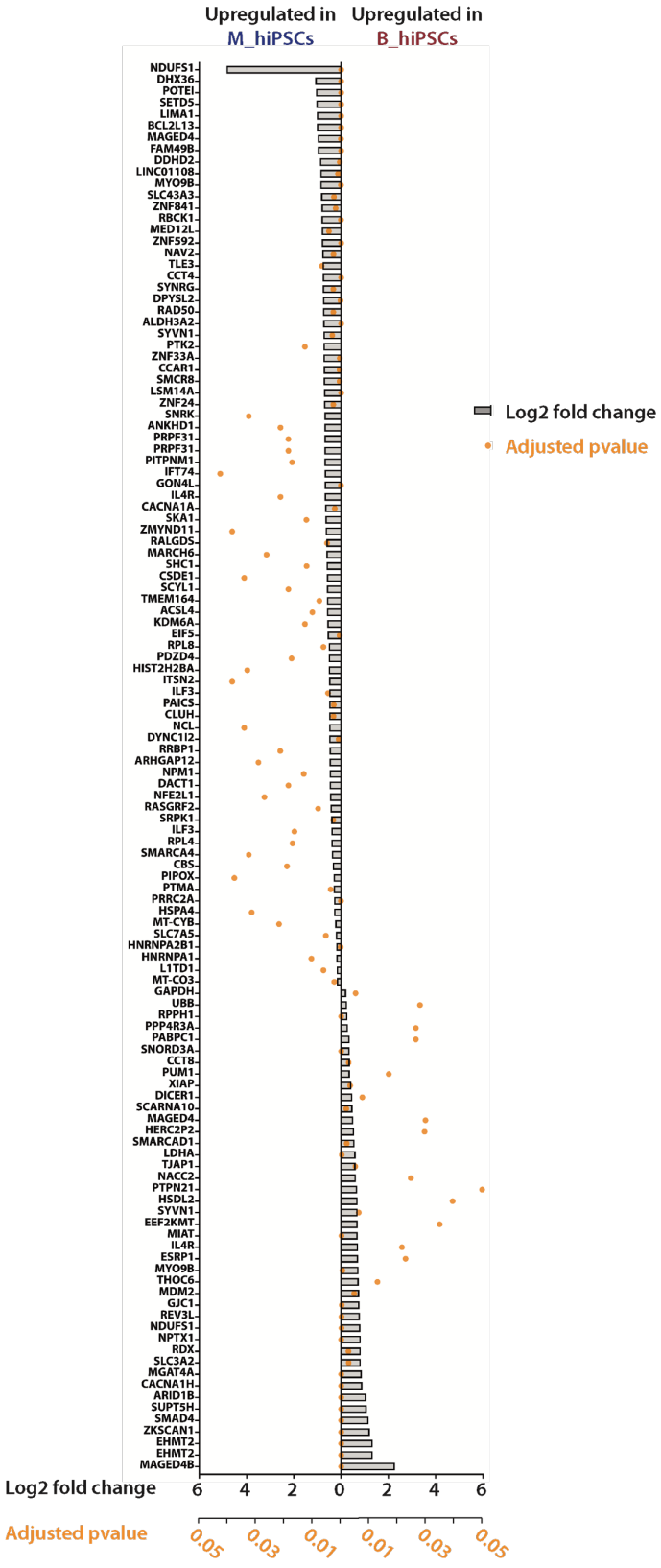

Figure 4.11: Differentially expressed transcripts of full RNA-Sequencing comparing M_hiPSCs and B_hiPSCs of 3 donors A, B and D.
Full RNA Sequencing comparing M_hiPSCs and B_hiPSCs of age and gender matched donors (female, 47-50 years of age; Donors A, B, D). 122 significantly differentially expressed transcripts (DETs) (padj <0.05) are ordered by log2 fold change for upregulated transcripts in M_hiPSCs and B_hiPSCs. For each transcript the adjusted p value is given (orange). List of the exact values is provided in the appendix together with the corresponding Ensemble transcript IDs (Appendix section 7.1). Double mentioning of HGNC symbols is due to different transcript variants for one gene.

The most differentially regulated transcript, highly expressed in B_hiPSCs, is MAGED4B (Melanoma-associated antigen D4B) (Figure 4.11), which is associated with oral squamous cell carcinoma and lymph node metastasis (Chong et al., 2012; Lim et al., 2014). The transcript variant of MAGED4B is not at all expressed in M_hiPSCs resulting in the large difference between M_hiPSCs and B_hiPSCs for this transcript (Supplement 7.1.2.). An important paralog to MAGED4B is MAGED4 of which 2 transcript variants in this dataset are significantly differentially expressed among the 122 transcripts, one high in M_hiPSCs and the other high in B_hiPSCs. NDUFS1 (NADH-ubiquinone oxidoreductase) is the most differentially expressed transcript highly expressed in M_hiPSCs and is known to be involved in mitochondrial respiratory electron transport (Elkholi et al., 2019). Interestingly, DICER, a gene known to impair the differentiation potential of ESCs (Kanellopoulou et al., 2005) is higher expressed in B_hiPSCs.

To investigate the 122 differentially expressed transcripts in more detail, I performed gene ontology (GO) term analysis using the database for annotation, visualisation and integrated discovery (DAVID). GO term analysis with a significance threshold of $p < 0.1$ indicated biological processes involved in viral processes, cell-cell adhesion, telomere maintenance and general regulation of transcription (Table 4.2). Additionally, signalling pathways were found that are known to be involved in a wide range of regulatory signalling mechanisms and more specific also in differentiation processes towards specific tissues like Wnt, FGF and TGF beta signalling. Of note, a transcript variant of SMAD4 (SMAD family member 4), an important signalling molecule in the transduction of TGF beta signalling (Lucarelli et al., 2018), is expressed in B_hiPSCs but not at all expressed in M_hiPSCs (Appendix section 7.1 & Figure 4.11). The GO term analysis also revealed a difference between M_hiPSCs and B_hiPSCs in the biological process of chromatin remodelling, based on the differential expression of SMARCA4, that is known as a regulator of differentiation and stemness (Güneş et al., 2019), and SMARCAD1, that was shown to be involved in the regulation of naïve pluripotency and cancer progression (Al Kubaisy et al., 2016; Xiao et al., 2017; Liu et al., 2019).

Table 4.2: DAVID GO term analysis – enriched biological processes for $p < 0.1$
The Count gives the number of genes found to be involved in the given pathway, percentage shows involved genes/total genes in the database for this pathway.

Biological process	GO term	Count (%)	P-value
Viral process	0016032	9 (8.3)	1.9E-4
Cell-cell adhesion	0098609	8 (7.4)	5.9E-4
Positive regulation of telomere maintenance	0032212	3 (2.8)	1.2E-2
Regulation of transcription from RNA polymerase I promoter	1901838	2 (1.9)	3.7E-2
Regulation of transcription from RNA polymerase II promoter	0000122	9 (8.3)	3.7E-2
Protein localisation to Cajal body	1904871	2 (1.9)	4.2E-2
DNA damage response	0006977	3 (6.5)	4.3E-2
Protein localisation to telomere	1904851	2 (1.9)	4.7E-2
Negative regulation of transcription	0045892	7 (6.5)	4.9E-2
Somite rostral/caudal axis specification	0032525	2 (1.9)	5.2E-2
Positive regulation of cellular protein catabolic process	1903364	2 (1.9)	5.7E-2

Positive regulation of telomere maintenance	0032206	2 (1.9)	5.7E-2
Amino acid transport	0015804	2 (1.9)	6.7E-2
Regulation of Rho protein signal transduction	0035023	3 (2.8)	6.9E-2
mRNA processing	0006397	4 (3.7)	7.0E-2
Fibroblast growth factor receptor signalling pathway	0008543	3 (2.8)	7.0E-2
Chromatin remodelling	0006338	3 (2.8)	7.6E-2
Telomerase RNA localisation to Cajal body	1904874	2 (1.9)	7.7E-2
DNA double-strand break processing	0000729	2 (1.9)	7.7E-2
Wnt signalling pathway	0016055	4 (3.7)	7.7 E-2
Positive regulation of GTPase activity	0043547	7 (6.5)	7.9E-2
Posttranscriptional regulation of gene expression	0010608	2 (1.9)	8.2E-2
Transforming growth factor beta receptor signalling pathway	0007179	3 (2.8)	8.6E-2
Negative regulation of apoptotic process	0043066	6 (5.6)	9.4E-2
Error-prone translesion synthesis	0042276	2 (1.9)	9.6E-2

4.4 Establishment and optimisation of the myogenic differentiation protocol

I established a directed transgene-free myogenic differentiation protocol for human induced pluripotent stem cells (hiPSCs) in the laboratory of Professor Simone Spuler. The protocol was developed in the laboratory of Olivier Pourquié and published in 2015, at the time this work was started (Chal et al., 2015, 2016). The differentiation is based on mesoderm induction by Wnt activation and blockade of lateral plate mesoderm differentiation by inhibition of BMP signalling followed by addition of a series of growth factors (Figure 3.1 & Figure 4.12, A). The authors reported on the possibility to dissociate the differentiation culture after 15 to 100 days to gain a single-cell myogenic progenitor population (Chal et al., 2016). The cell culture before dissociation is hereafter referred to as "primary culture", while the cell culture phase after dissociation is referred to as "secondary culture".

For the establishment of the protocol, an hiPSC clone was used, that was available in the laboratory of Professor Simone Spuler. This hiPSC line, hereafter referred to as donor 0, was kindly provided by the Jain Foundation. The hiPSC line was previously generated by the company Cellular Dynamics, from fibroblasts or blood cells of a healthy male donor. It was characterised by Cellular Dynamics for pluripotency marker expression and karyotype stability. Additionally, we confirmed the formation of all three germ layers in cooperation with EPO – Experimental Pharmacology & Oncology Berlin-Buch GmbH (data not shown).

As the myogenic differentiation protocol aims to recapitulate in vivo myogenesis, I selected an early developmental marker as a milestone to verify proper recapitulation of the described protocol. The posterior presomitic mesoderm marker TBX6 is an important marker for cells that acquire a mesodermal progenitor fate (Chalamalasetty et al., 2014) and is expressed in the in vitro differentiating cells (Chal et al., 2016). I detected robust nuclear TBX6 expression at day 4 of the differentiation protocol in the majority of the differentiating cells (Figure 4.12, B). Of note, not all cells are positive for TBX6 expression. Areas that are negative for TBX6 can be distinguished from the $TBX6^{+}$ areas by brightfield microscopy only. Areas positive for TBX6 are characterised by a high cell density while areas negative for TBX6 expression show low cell densities.

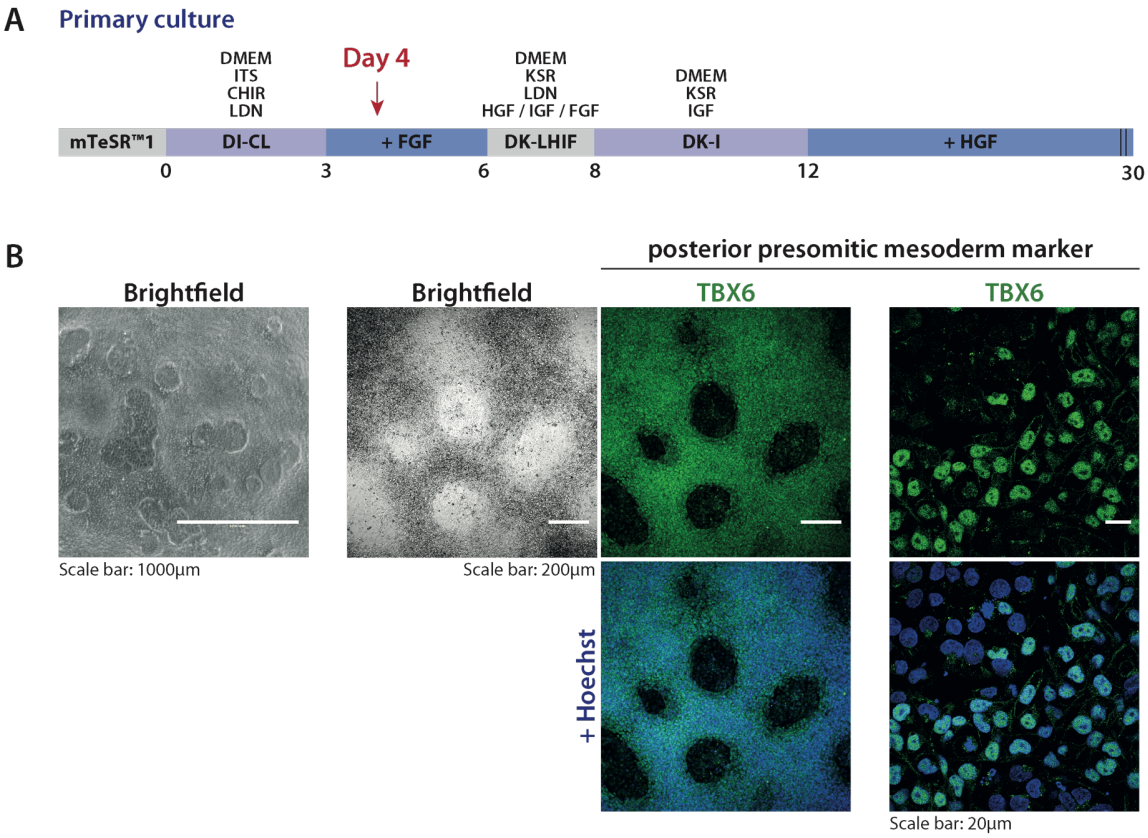

Figure 4.12: Expression of the posterior presomitic mesoderm marker TBX6 in primary differentiation cultures at day 4
(A) Timeline of the primary myogenic differentiation protocol starting at day 0. Day 4 of the differentiation is marked in red and shown in B. **(B)** Representative images of myogenic differentiation cultures at day 4 of the myogenic differentiation protocol. *(Left)* Brightfield picture, taken at day 4, shows morphologically different areas. (*Centre)* Immunofluorescence pictures show TBX6 expression present in large areas of the differentiating cultures which can be distinguished by morphological differences. *(Right)* TBX6 expression specifically in the nucleus. Nuclei were counterstained with Hoechst. Scale bar: 20, 200 and 1000 µm

After confirming posterior presomitic mesoderm induction by TBX6 expression, I proceeded to investigate the capacity to differentiate into myogenic cells. I thus analysed myogenic differentiation markers at day 30 of the protocol, as reported to be expressed in the protocol description (Chal et al., 2016).

The myogenic differentiation cultures at day 30 of the primary culture are characterised by a high density and a 3D multilayer appearance (Figure 4.13, B). Myosin heavy chain isoforms (MyHC) are markers expressed in late stages of the skeletal myogenic development and start to be expressed in vivo when myogenic progenitor cells mature to myofibres. Specifically, the fast MyHC isoforms are expressed during secondary myogenesis when $PAX7^{+}$ cells fuse with each other or with the existing early myofibres (Reviewed in Schiaffino & Reggiani, 2011 and Chal & Pourquié, 2017). In immunofluorescence stainings performed with day 30 cultures, I was able to detect large fields of fast MyHC positive fibres surrounded by areas not positive for fast MyHC (Figure 4.13, C). Additionally, I

could detect positive and negative areas for the muscle specific protein Desmin (Figure 4.13, C), which is located in the periphery of the z-discs of striated muscle (Kaufman & Foster, 1988; Paulin & Li, 2004).

In order to define the purity of the myogenic differentiation cultures, I investigated the presence of the class III beta tubulin (TUJ1) marker, in humans encoded by the gene TUBB3, that is constitutively expressed in neurons (Ferreira & Caceres, 1992; Latremoliere et al., 2018). I detected strong expression using an anti-TUJ1 antibody in the differentiating cultures at day 30 (Figure 4.13, C).

Due to the 3D multilayer appearance, single cell layer imaging was challenging, shown by the areas negative for nuclear Hoechst staining. Thus, and due to high background fluorescence, presumably caused by high amounts of extracellular matrix, single nuclear immunofluorescence in these cultures was not feasible.

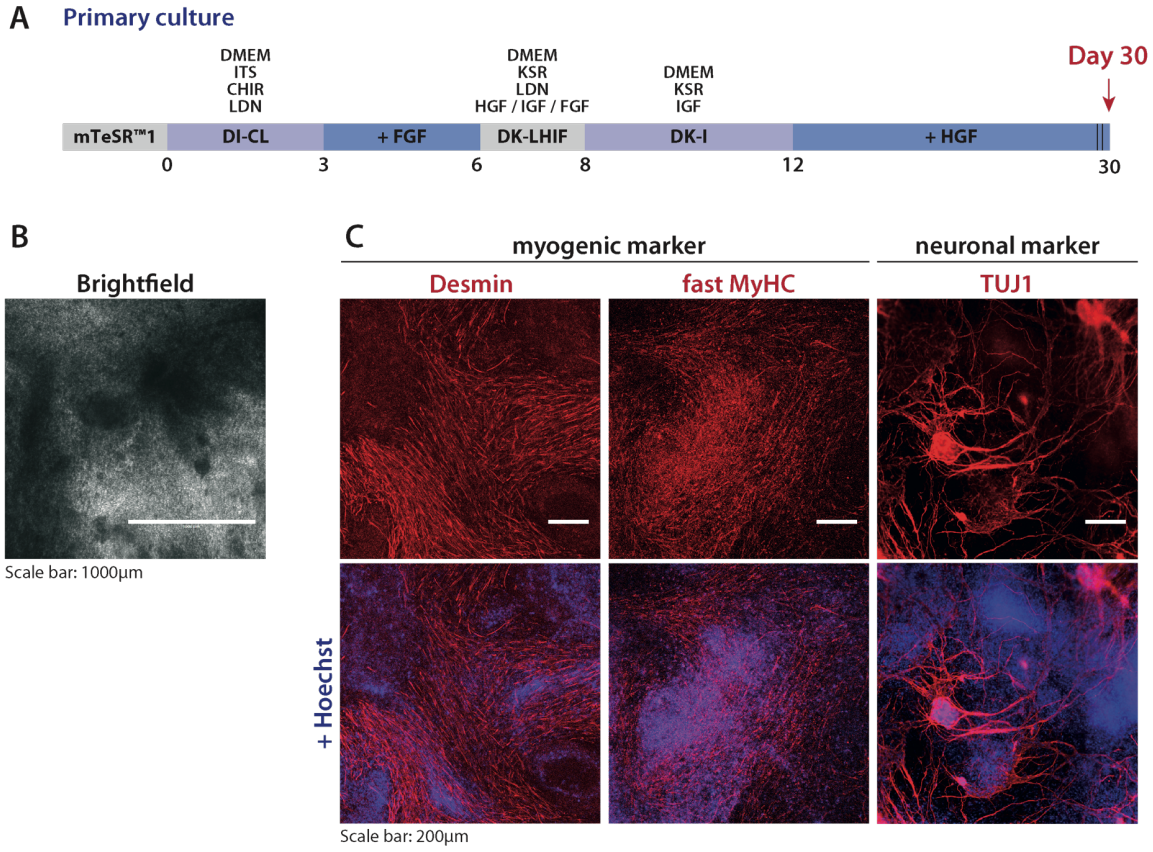

Figure 4.13: Expression of myogenic and neuronal markers in primary differentiation cultures at day 30
(A) Timeline of the primary myogenic differentiation protocol starting at day 0. Day 30 of the differentiation protocol is marked in red, and representative images of day 30 are shown in B. **(B)** Representative images of myogenic differentiation cultures at day 30 of the myogenic differentiation protocol. Brightfield picture shows extremely dense cultures with a 3D-structural multilayer appearance. Scale bar: 1000 µm **(C)** Areas positive and negative for myogenic markers Desmin and fast MyHC were detected in differentiating cultures at day 30. The neuronal marker class III beta tubulin (TUJ1) was also detected. Nuclei were counterstained with Hoechst. Scale bar: 200 µm

As the primary differentiation culture on day 30 revealed strong background staining, areas negative for myogenic cells and expression of the neuronal marker class III beta tubulin (TUJ1), I continued to investigate the secondary culture procedure for single myogenic progenitor cells obtained after dissociation of the primary culture.

The single cell myogenic progenitor population can be differentiated into cells expressing myogenic markers (Chal et al., 2016)(see Methods section 3.1.4.3). These terminally differentiated cells are hereafter referred to as induced myogenic cells (iMCs) (Figure 4.14, A).

After dissociation of the primary culture, single cells proliferated until nearly 100% of confluence was reached within 4 days. The cells arranged themselves in an aligned orientation but kept their single cell morphology. After terminal differentiation for additional 10 days, at day 44 counting from the start of the differentiation protocol, the cells were aligned and developed a prolonged morphology (Figure 4.14, B).

Immunofluorescence staining of the terminally differentiated iMCs revealed a high number of cells expressing the myogenic markers Desmin, fast MyHC and Myogenin (MYOG) (Figure 4.14, C). The background fluorescence was strongly reduced compared to the primary cultures. In addition, the cells were equally distributed within the cell culture wells without large areas free of myogenic markers. The nuclei were clearly distinguishable due to the monolayer culture. Notably, the detection of nuclear markers was possible, as shown for MYOG, an important late myogenic transcription factor responsible for the terminal differentiation of myoblasts into myocytes (Venuti et al., 1995). However, there were still cells not positive for the myogenic markers Desmin, fast MyHC or MYOG. Importantly, the staining for the neuronal marker beta III tubulin (TUJ1) only revealed background fluorescence signals, but no signs of neuronal cells as compared to the primary culture (Figure 4.13, C & Figure 4.14, C).

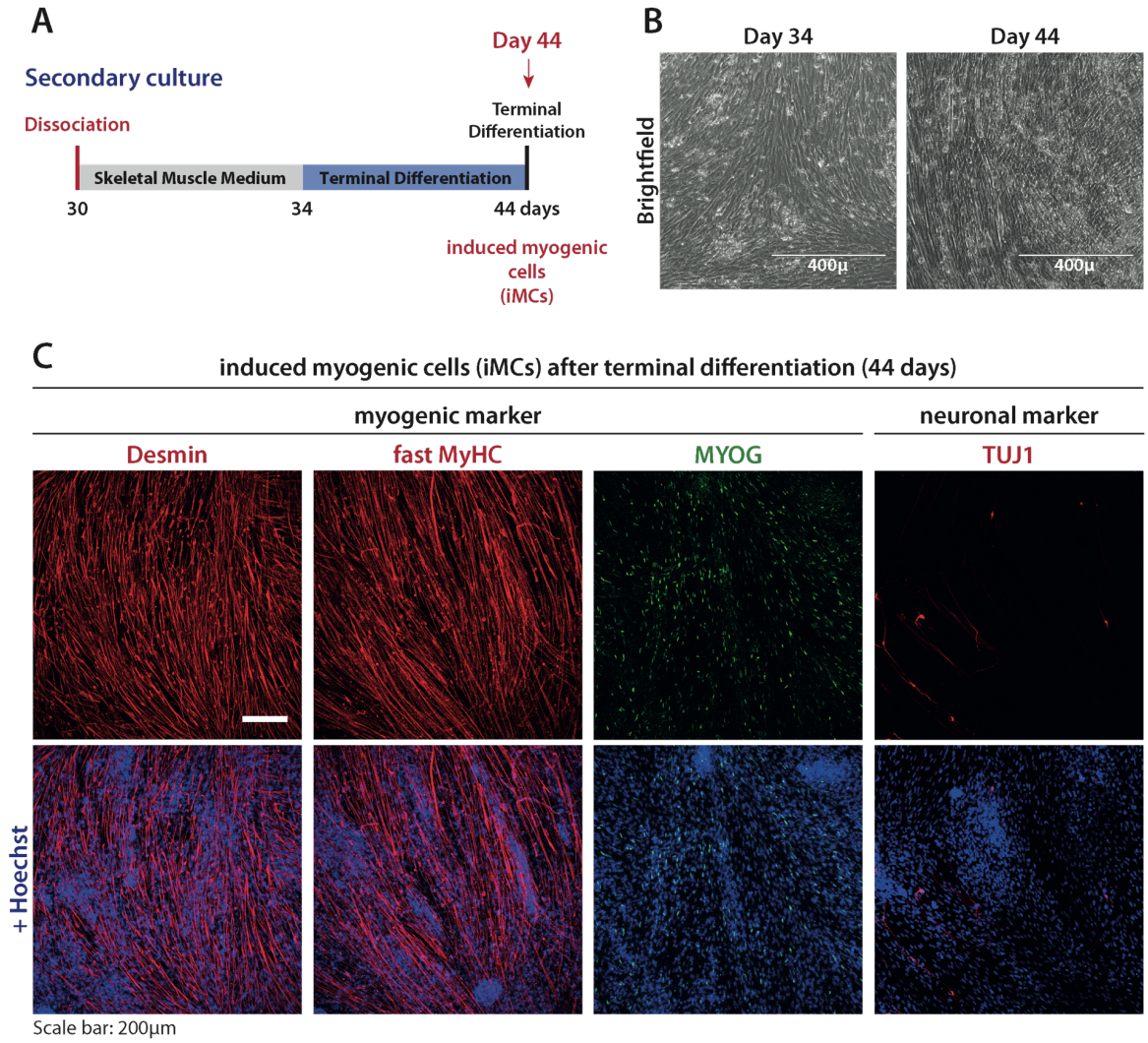

Figure 4.14: Expression of myogenic and neuronal markers after dissociation in secondary differentiation cultures at day 44
(A) Timeline of the secondary myogenic differentiation protocol starting at day 30 with the dissociation of the primary differentiation culture. Cells were kept for 4 days in skeletal muscle medium and were then terminally differentiated for 10 additional days into induced myogenic cells (iMCs) **(B)** Representative brightfield images of confluent cell culture differentiation at days 34 and 44 with aligned cell orientation. Scale bar: 400 µm **(C)** Representative immunofluorescence images of myogenic differentiation cultures at day 44 of the secondary differentiation protocol. Myogenic cytoplasmatic markers Desmin, fast MyHC as well as the myogenic nuclear marker MYOG are shown. In addition, the neuronal marker class III beta tubulin (TUJ1) was stained for. Nuclei were counterstained with Hoechst. Scale bar: 200 µm

I proceeded with additional tests to optimise the efficiency of the myogenic differentiation protocol to obtain high quality iMCs with the secondary culture protocol.

A prolonged time in culture of the dissociated single cells after dissociation led to a more mature status of the iMCs after terminal differentiation. In contrast to the protocol described in Chal et al. 2016, I kept the dissociated single cells from day 30 for 5 more passages in culture instead of starting the terminal differentiation right after dissociation (Figure 4.15, A). 5 more passages increased the total myogenic differentiation protocol to 60 days, instead of the initial 44 days. The iMCs of the 60-day protocol appear as multinucleated cells with nuclei located in very close proximity to the others (Figure 4.15, B). Multinucleation with "pearl chain" like nuclei alignment is described for primary myogenic cells (Capers, 1960; Blau & Webster, 1981; Yin, Price, & Rudnicki, 2013) and I confirmed this observation in primary human myotubes (Figure 4.16). In contrast, I could not detect "pearl chains" with nuclei in close proximity in iMCs of the 44-days protocol, although some fast MyHC$^+$ cells were detected with more than one nucleus (Figure 4.15, B).

Human primary multinucleated myotubes show a gain in size, compared to the mononucleated precursor myoblasts (Figure 4.16). I could detect larger fast MyHC$^+$ structures in the 60-days protocol compared to the fast MyHC$^+$ structures in the 44-days protocol (Figure 4.15, B).

Additionally, I could detect multinucleated fast MyHC$^+$ cells with "pearl chains" negative for MYOG for the 60-days protocol (Figure 4.15, B), which I could also detect for the primary human fused myotubes (Figure 4.16). MYOG is an important myogenic regulatory factor that is essential for fusion and which is downregulated in mature muscle fibres (Hernández-Hernández et al., 2017; Ganassi et al., 2018). Nuclei of the 44-days protocol inside of the fast MyHC$^+$ cells are not in very close proximity to each other and are positive for MYOG (Figure 4.15, B).

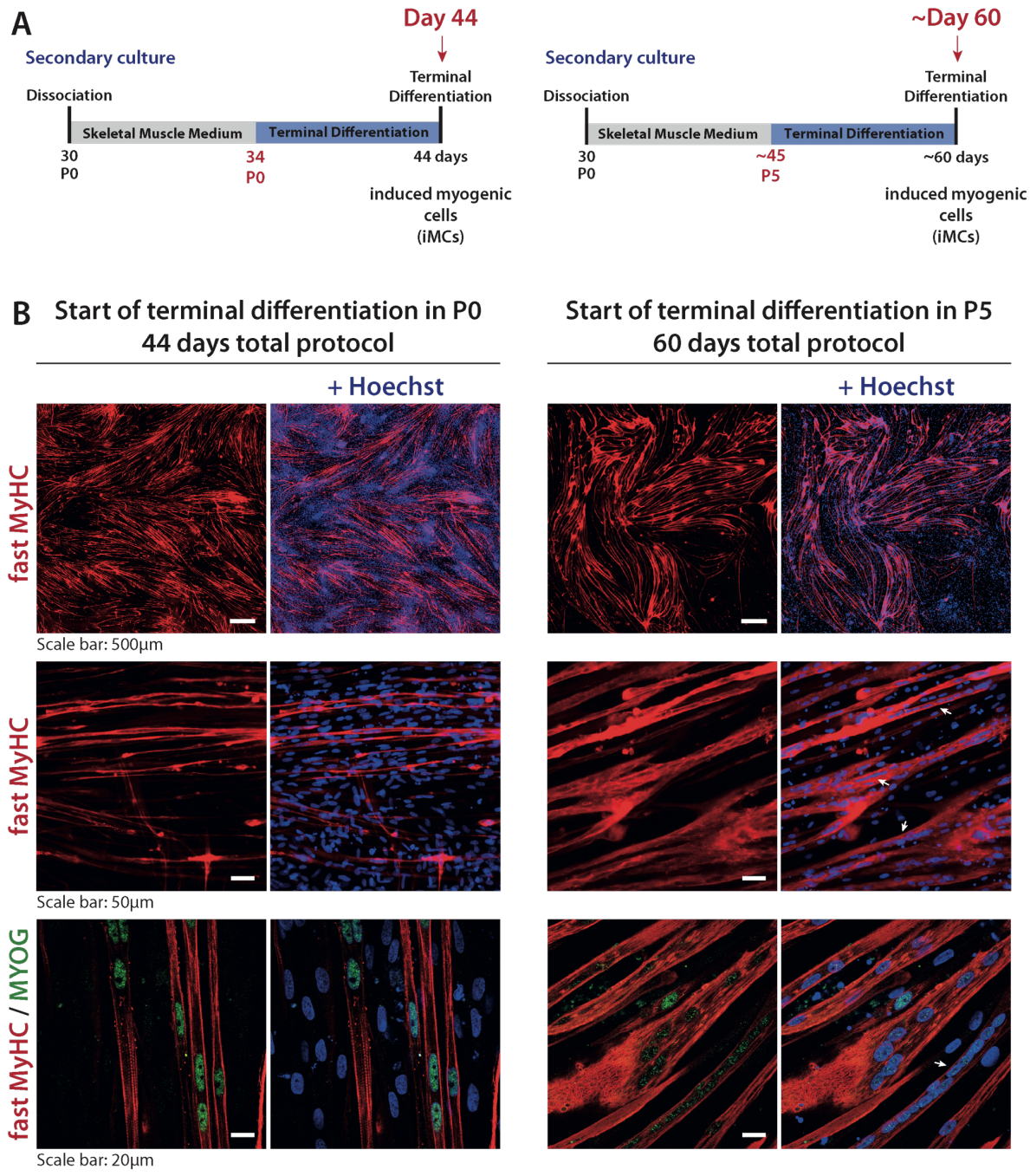

Figure 4.15: Comparison of iMCs after the 44-days and 60-days myogenic differentiation protocol
(A) Timeline of the secondary myogenic differentiation protocol starting at day 30 with the dissociation of the primary differentiation culture. (Left) 44-days myogenic differentiation protocol with dissociated single cells in skeletal muscle medium for 4 days before the start of terminal differentiation. (Right) 60-days myogenic differentiation protocol with dissociated single cells cultured for 5 passages (~15 days) before the start of the terminal differentiation. **(B)** Representative immunofluorescence images of myogenic differentiation cultures stained for the cytoplasmatic myogenic marker fast MyHC in three different magnifications. Highest magnification shows a co-staining with the nuclear myogenic marker MYOG. Nuclei were counterstained with Hoechst. White arrows mark the multinucleated fast MyHC$^+$ cells with "pearl chain" like nuclei alignments. (Left) 44-days myogenic differentiation protocol (Right) 60-days myogenic differentiation protocol. Scale bars: 20, 50 and 500 µm

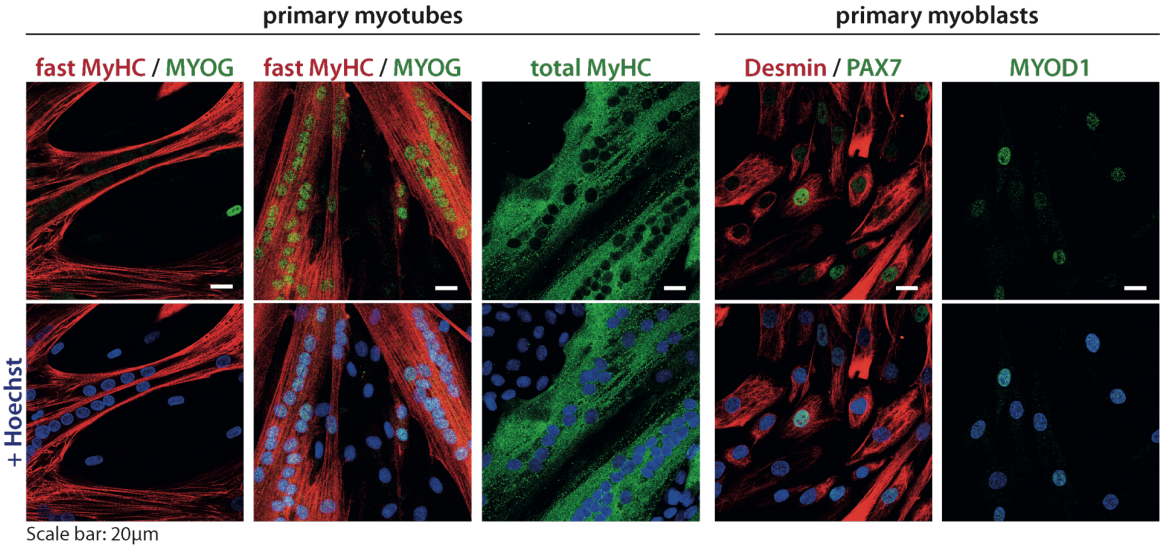

Figure 4.16: Expression of myogenic markers in human primary myotubes and myoblasts
Representative immunofluorescence images of primary human myotubes (left) and myoblasts (right). Myoblasts were obtained from human muscle biopsy specimens. Myotubes resulted from terminal differentiation of myoblasts for 4 days in OptiMEM medium. Myotubes were stained for fast MyHC, MYOG and total MyHC. Fast MyHC/MYOG co-staining shows multinucleated cells with nuclei positive or negative for MYOG and single nuclei outside of the fast MyHC positive cells that are positive for MYOG. Myoblasts were stained for Desmin, MYOD1 and the early myogenic marker PAX7. Nuclei were counterstained with Hoechst. Scale bar: 20 µm

As the iMCs resulting from the 60-days protocol hold more similarities to human primary myotubes than the 44-days protocol, I decided to use the 60-days protocol for further studies.

Further investigation of the properties of the iMCs after 60-days of the myogenic differentiation protocol revealed the presence of the early myogenic transcription factor PAX7 and the essential myogenic transcription factor MYOD1 in the culture (Figure 4.17, B, right panel). Both, PAX7 and MYOD1 are expressed by human primary myoblasts (Figure 4.16). Notably, the $PAX7^{+}$ nuclei of the iMCs are located outside of the multinucleated tube-like structures (Figure 4.17, B, right panel).

As the iMC cultures contain a large number of terminally differentiated cells, I investigated the myogenic progenitor cells before starting the terminal differentiation procedure. Those cells are hereafter referred to as induced myogenic progenitor cells (iMPCs) (Figure 4.17, A). Notably, iMPCs are positive for Desmin and the early myogenic transcription factor PAX7 while they are negative for fast MyHC, MYOG and MYOD1. Staining for total MyHC, including the early and late developmental MyHC isoforms, revealed some positive cells that were only single nucleated (Figure 4.17, B, left panel).

As the analysis revealed mature characteristics for iMCs and progenitor characteristic for iMPCs, I decided to use iMCs for in vitro myogenic differentiation experiments and iMPCs for the assessment of in vivo engraftment capabilities.

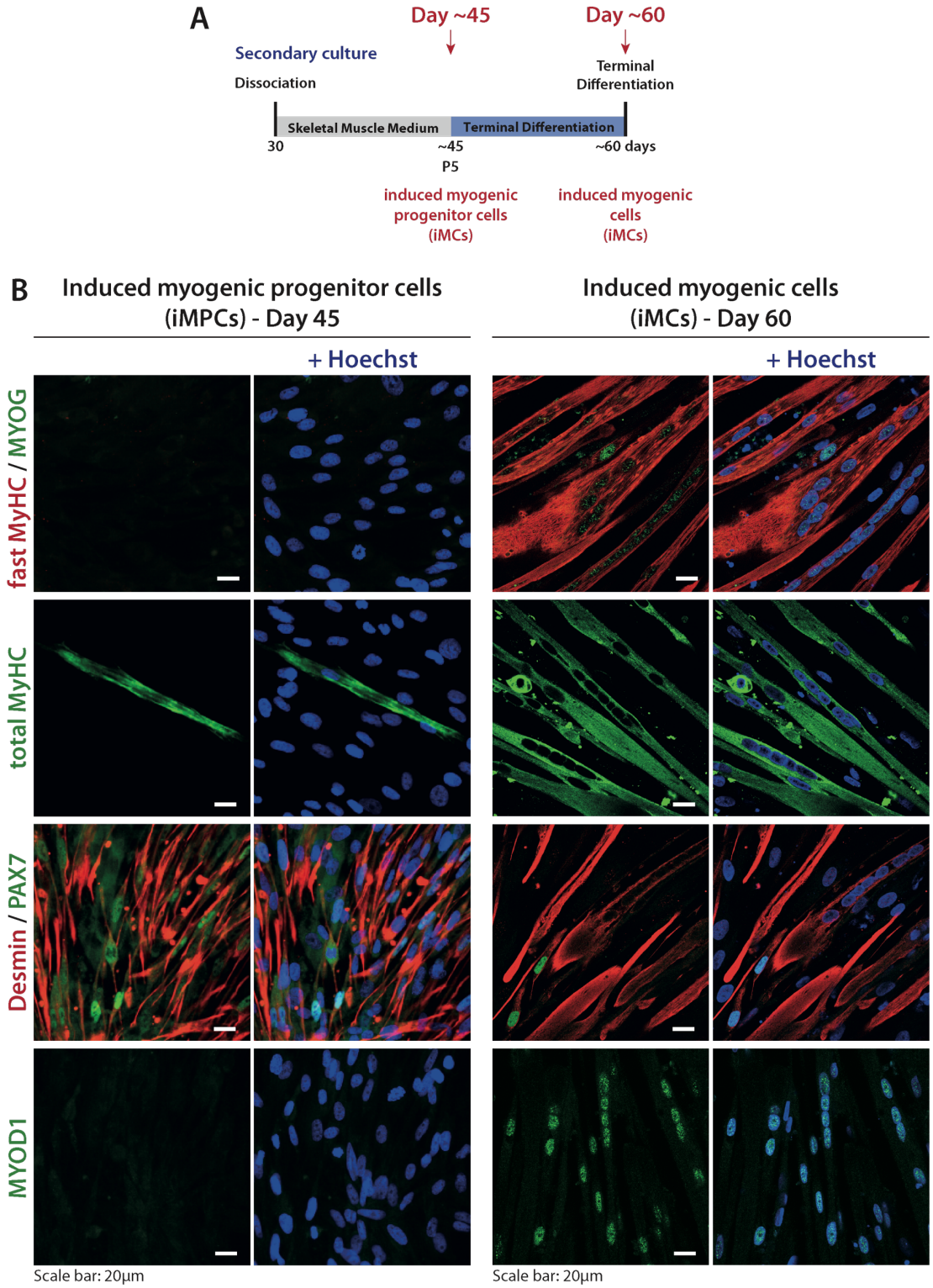

Figure 4.17: Expression of myogenic markers in iMPCs and iMCs using a 60-days myogenic differentiation protocol
(A) Timeline of the secondary myogenic differentiation protocol starting at day 30 with the dissociation of the primary differentiation culture. On day 44, cells arrived at the state of induced myogenic progenitor cells (iMPCs). On day 60, cells arrived at the state of terminally differentiated induced myogenic cells (iMCs). **(B)** Representative immunofluorescence images of myogenic differentiation cultures stained for the myogenic markers fast MyHC, MYOG, total MyHC, Desmin, PAX7 and MYOD1. Nuclei were counterstained with Hoechst. (Left) Induced myogenic progenitor cells (iMPCs) stained at day 44 positive for the markers Desmin and PAX7 (Right) Induced myogenic cells (iMCs) stained at day 60 of the myogenic differentiation protocol positive for all displayed myogenic markers. Scale bar: 20 µm

4.5 In vitro myogenic differentiation comparing M_hiPSCs and B_hiPSCs

To analyse the myogenic differentiation capacity of M_hiPSCs and B_hiPSCs, I performed the previously described and optimised myogenic differentiation protocol (Chal et al. 2015, 2016, Results section 4.1) with the M_hiPSCs and B_hiPSCs from the age and gender matched donors A, B and D.

Based on the optimisation experiments with donor 0 hiPSCs, each hiPSC clone was seeded in different densities to exclude differences due to the handling of the experimenter. Technical triplicates were seeded for each condition (3 independent 6-wells for each hiPSC clone and density). The triplicates of the cell density with the highest cell survival after 10 days were processed for terminal analysis. The primary differentiation protocol was followed for 30 days. After dissociation, the single cell myogenic progenitor cells (iMPCs) were cultured for 5 passages before their terminal differentiation for 10 days. The induced myogenic progenitor cells (iMCs) were analysed for myogenic marker expression after approximately 60-days of differentiation (Figure 4.18).

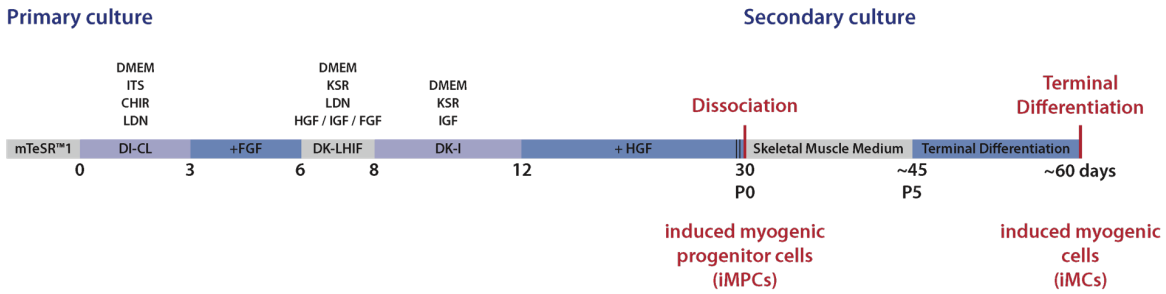

Figure 4.18: Schematic description of the transgene-free myogenic differentiation protocol
Cells were cultured in mTeSR™1 medium. The differentiation protocol was started by changing the medium to DI-CL medium containing 3 µM CHIR and 0.5 µM LDN. Further differentiation steps included Knockout™ Serum Replacement and a series of growth factors including FGF, IGF and HGF. After 30 days, primary cell culture was dissociated, and single cell induced myogenic progenitor cells (iMPCs) were cultured in skeletal muscle medium. Cells were kept in culture for 5 passages and then terminally differentiated for 10 days to obtain induced myogenic cells (iMCs).

After dissociation of the primary culture, I monitored the cell proliferation of the induced myogenic progenitor cells (iMPCs) for 5 passages in triplicates for each hiPSC clone, starting with a cell number of $1*10^6$ cells.

All iMPC cell lines showed a comparable proliferation rate, except for the B_iMPCs from donor B, which show a distinctly higher proliferation rate compared to all others (Figure 4.19). The proliferation curve of this cell line exhibits big error bars due to differences in the proliferation rates within its triplicates. However, the average maximum cell number after 5 passages of this line (~$1.1*10^7$ cells) is three times higher than the next highest maximum cell number of B_iMPCs from donor D (~$3.5*10^6$ cells). The myoblast-derived counterpart to the high proliferative cell line, M_iMPCs from donor B, showed an average proliferation rate with a maximum cell number of ~$3*10^6$ cells, thus being comparable to donor D derived M_hiPSCs and B_hiPSCs with maximum cell numbers of ~$3.5*10^6$ cells. Donor A derived M_iMPCs and B_iMPCs showed no proliferation (both maximum of 1 - $1.5*10^6$ cells).

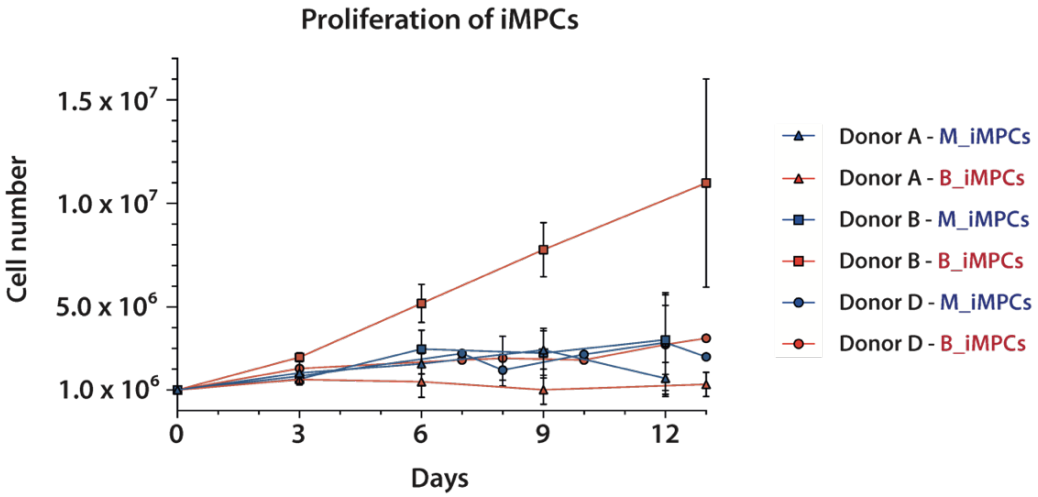

Figure 4.19: Proliferation curve of induced myogenic progenitor cells (iMPCs) after dissociation on day 30
The very dense cultures of the primary differentiation were dissociated on day 30 of the differentiation protocol. Derived single cells were cultured on Matrigel in skeletal muscle medium and passaged every 3-4 days. Cell number was determined using Neubauer chambers. Each line represents the mean of three replicates (differentiation in independent wells) with error bars showing the mean.

I analysed the myogenic marker expression after the terminal differentiation by qualitative immunofluorescence and quantitative qRT-PCR.

The myogenic differentiation of M_hiPSCs and B_hiPSCs into induced myogenic cells (iMCs) for all 3 donors showed no significant difference ($p < 0.05$) in the expression of the myogenic markers Desmin, PAX7, MYOD1, MYOG and the three myosin isoforms MYH2, MYH3 and MYH7 as shown by the quantification analysis (Figure 4.20). Furthermore, I observed large differences between the myogenic marker expression between the different donors A, B and D, as presented by the immunofluorescence and also by the quantification analysis (Figure 4.20 & Figure 4.21 & Figure 4.22). Donor D shows higher expression of all analysed myogenic genes than donors A and B, while donor A shows the lowest expression of all donors.

The comparison of M_iMCs and B_iMCs for donor B shows a trend towards a higher expression of myogenic marker genes in M_iMCs compared to B_iMCs. No such trend can be observed for donors A and D (Figure 4.20 & Figure 4.21 & Figure 4.22). However, the separated analysis for each donor is not suitable for quantification, as experimental restraints prevented the isolation of RNA from all triplicate samples of the myogenic differentiation experiments. Notably, for some markers a variation within the technical replicates for each differentiation was detected as shown for the expression of PAX7 in M_iMCs derived from donor D (Figure 4.20).

The results furthermore verify the absence of other terminally differentiated cell types like neuronal or endothelial cells, as shown by the absence of the neuronal tissues marker class III beta tubulin (TUJ1) (Figure 4.21 & Figure 4.22) and the endothelial PECAM1 marker (platelet endothelial cell adhesion molecule-1) (Figure 4.20). However, the low abundance of myogenic markers in iMC cultures of donors A and B suggests the presence of other cell types.

The qualitative assessment of the differentiation results by immunofluorescence illustrates the differences of the myogenic marker expression between the different iMCs and confirms the results found in the quantification on RNA level. Furthermore, it allows the detection of key characteristics of myogenic cells like the co - expression of MYOG and MyHC as shown for all three donors (Figure 4.22). Multinucleation was shown for donors D and B but the characteristic mature "pearl chain"-like nuclei structures were only observed in donor D iMCs. Donor A did not show any sign of multinucleation, which is possibly related to the low overall abundance of terminally differentiated myogenic cells. This might also be the reason why I did not find any $PAX7^+$ cells in donor A and B derived iMCs.

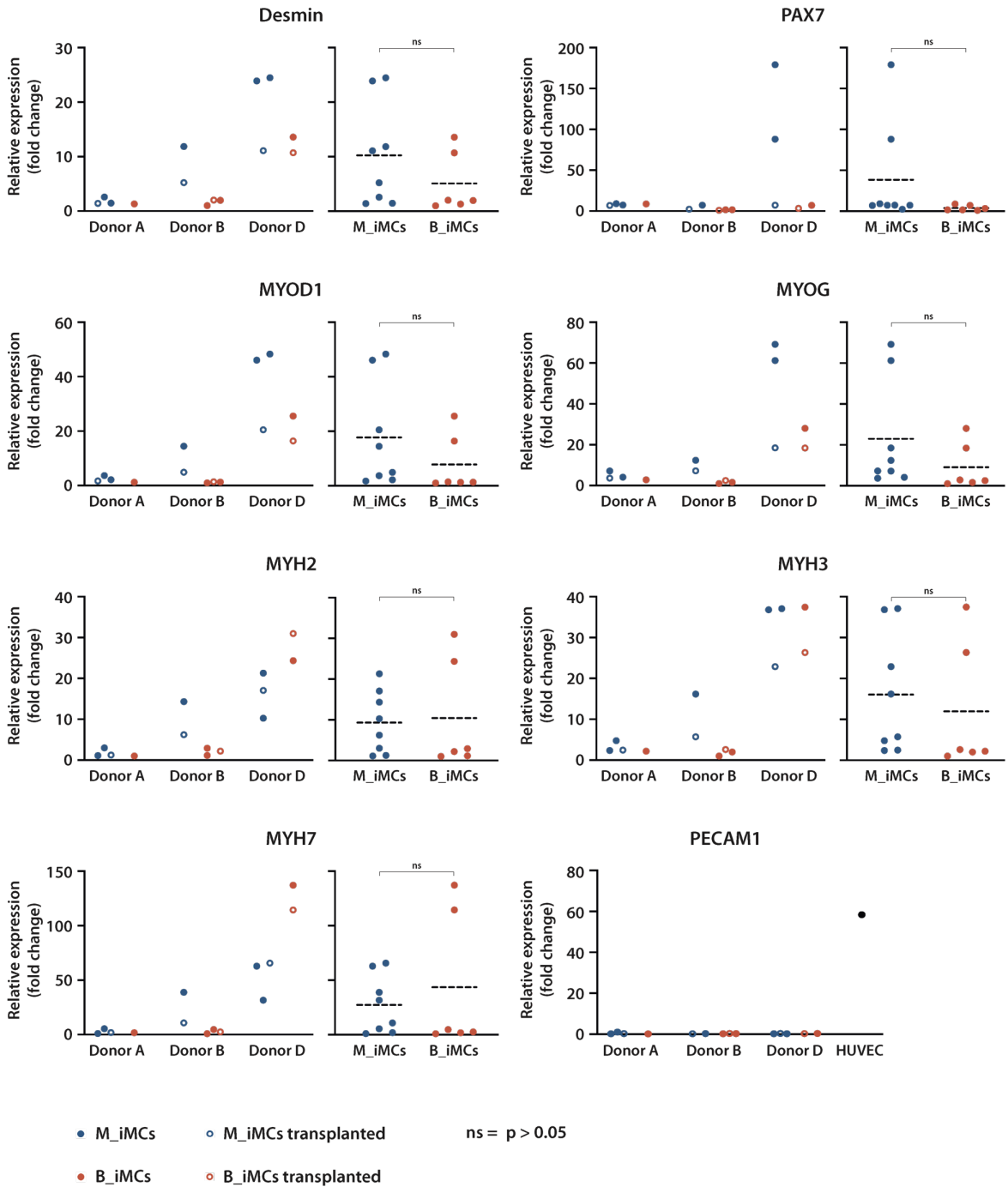

Figure 4.20: qRT-PCR quantification of myogenic markers in iMCs differentiated from M_iMCs and B_iMCs of donors A, B and D

qRT-PCR results of terminally differentiated induced myogenic cells (iMCs) differentiated from M_hiPSCs and B_hiPSCs of donors A, B and D after ~60 days of the differentiation protocol. Myogenic genes Desmin, PAX7, MYOD1, MYOG, MYH2, MYH3 and MYH7 were analysed and as a control the endothelial marker PECAM1. qRT-PCRs were performed using SYBR® Green and all primers were validated for specificity. ΔΔCt values are shown as fold change relative to the sample with the lowest expression value. All iMC samples exceeded Cts of 30 for PECAM1. Results are given separately for each donor (left for each gene) and combined for M_iMCs and B_iMCs (right for each gene). Each dot represents a technical replicate (differentiation in an independent well). Although all cell culture experiments were performed with 3 replicates, it was not possible to isolate RNA from all replicates. Statistical analysis was performed on the comparison of M_iMCs and B_iMCs using Students t-test ($p < 0.05$). Dashed lines represent the mean. For each technical replicate, the well/sample that was used for transplantation is shown as an empty circle.

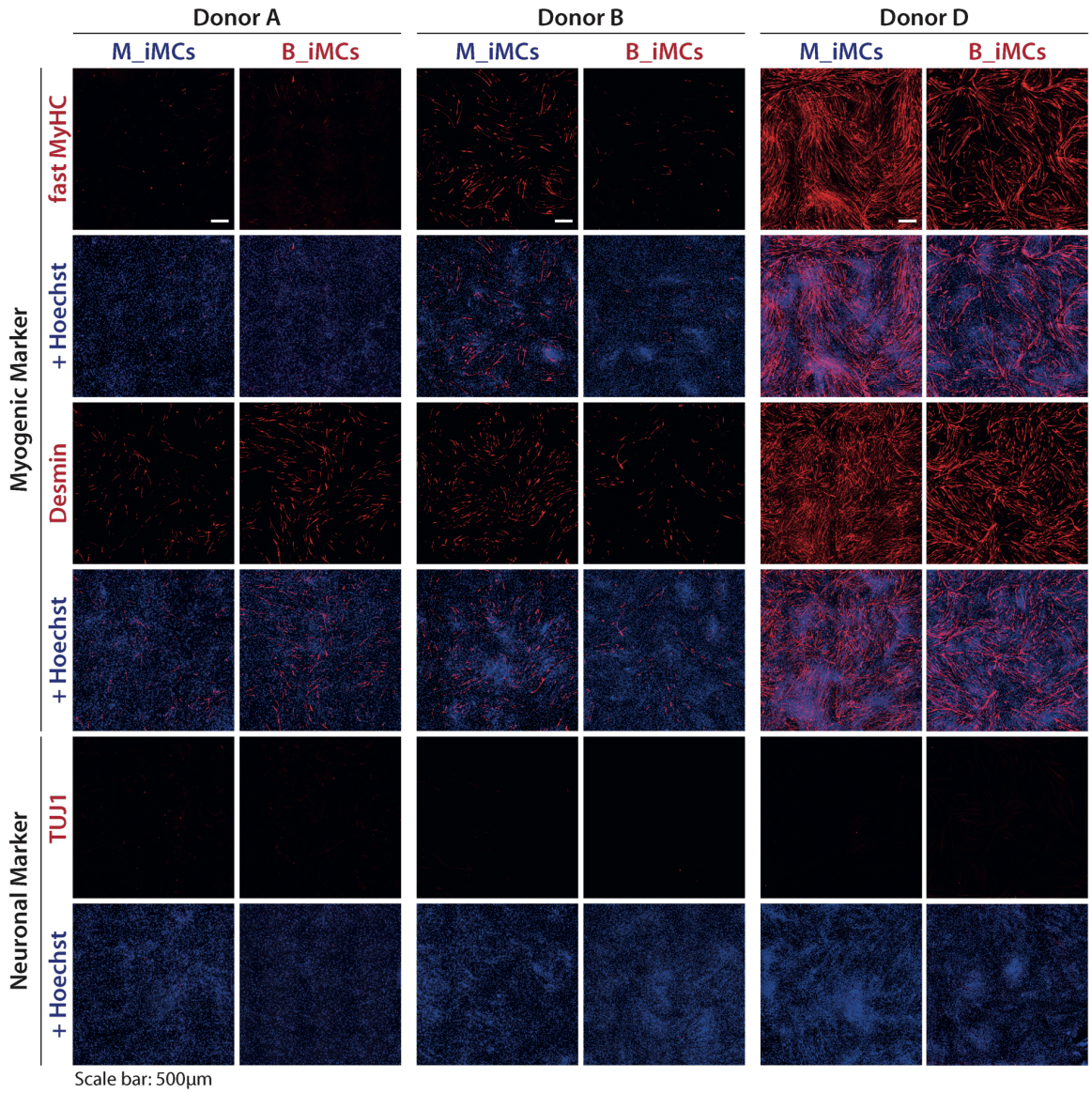

Figure 4.21: Mosaic immunofluorescence imaging of iMCs differentiated from M_hiPSCs and B_hiPSCs of donors A, B and D

Immunofluorescence imaging of terminally differentiated induced myogenic cells (iMCs) differentiated from M_hiPSCs and B_hiPSCs of donors A, B and D after ~60 days of the differentiation protocol. Stainings are shown for myogenic markers fast MyHC and Desmin and for the neuronal marker class III beta tubulin (TUJ1). Nuclei were counterstained with Hoechst. Mosaic images were acquired with a Leica DMI 6000 B microscope with a XY scanning stage and merged with the LAS FL software. Scale bar: 500 µm.

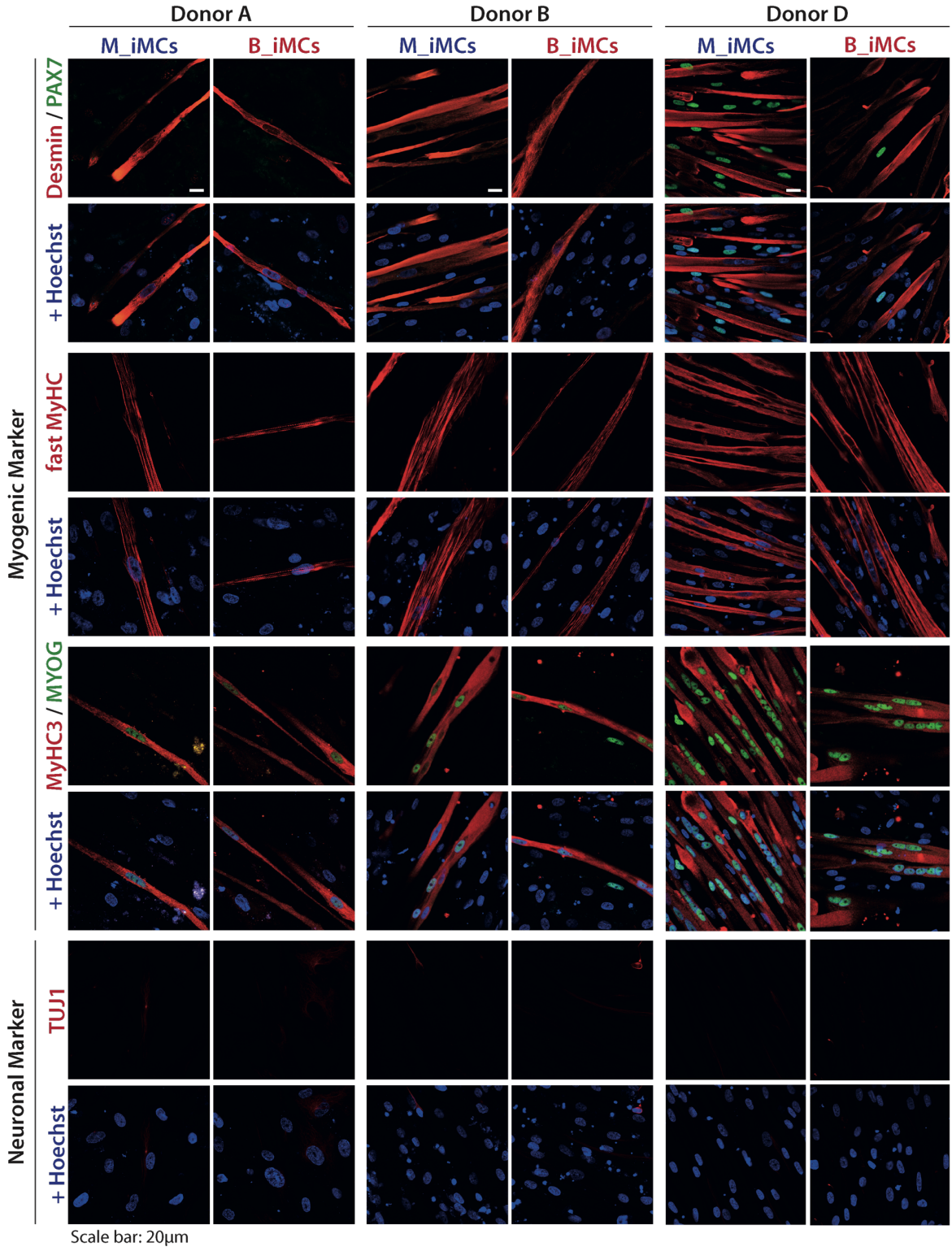

Figure 4.22: High resolution immunofluorescence imaging of iMCs derived from M_hiPSCs and B_hiPSCs of donors A, B and D

Immunofluorescence imaging of terminally differentiated induced myogenic cells (iMCs) differentiated from M_hiPSCs and B_hiPSCs of donors A, B and D after ~60 days of the differentiation protocol. Stainings are shown for myogenic markers Desmin, PAX7, fast MyHC, MyHC3 and MYOG and as a control the neuronal marker class III beta tubulin (TUJ1). Nuclei were counterstained with Hoechst. High resolution confocal images were acquired with a Laser Scan Microscope LSM 700 attached to an Axio Oberserver Z1 inverted light microscope. Images were processed with ZEN 2010 SP1 software. Scale bar: 20 µm.

4.6 Comparing the engraftment potential of M_iMPCs and B_iMPCS

To define the functional properties of the newly generated induced myogenic cells, I injected induced myogenic progenitor cells (iMPCs), positive for PAX7 and negative for the late myogenic differentiation marker MyHC (see Results section 4.4), into immunodeficient, xenograft compatible NOG-M mice.

The injected cells resulted from the exact same in vitro experiments described in the results section 4.4 and were injected freshly without prior freezing. Both, in vitro and in vivo experiments, were performed parallelly. The dissociated single cells from day 30 of the myogenic differentiation protocol were cultured for 5 passages and used for transplantation of $1*10^5$ cells (Figure 4.23, A). Simultaneously, the cells were seeded for the terminal in vitro differentiation. As the in vitro expression of myogenic markers was not yet determined when the cells were injected, one well of each triplicate was randomly chosen for transplantation (injected wells are marked in Figure 4.20 as circles).

The cells were injected into the irradiated tibialis anterior muscle (TA) of 6-9 weeks old xenograft-compatible NOG-M mice. Focal 16 Gray irradiation of the mice hind limbs was performed using an image guided robotic system at the Charité CyberKnife facility two days before the transplantation to impede the regeneration capacity of the mouse muscle by damaging the mouse satellite cells. The TA muscles were harvested after 21 days after transplantation, cryopreserved and processed for immunohistological analysis (Figure 4.23, B).

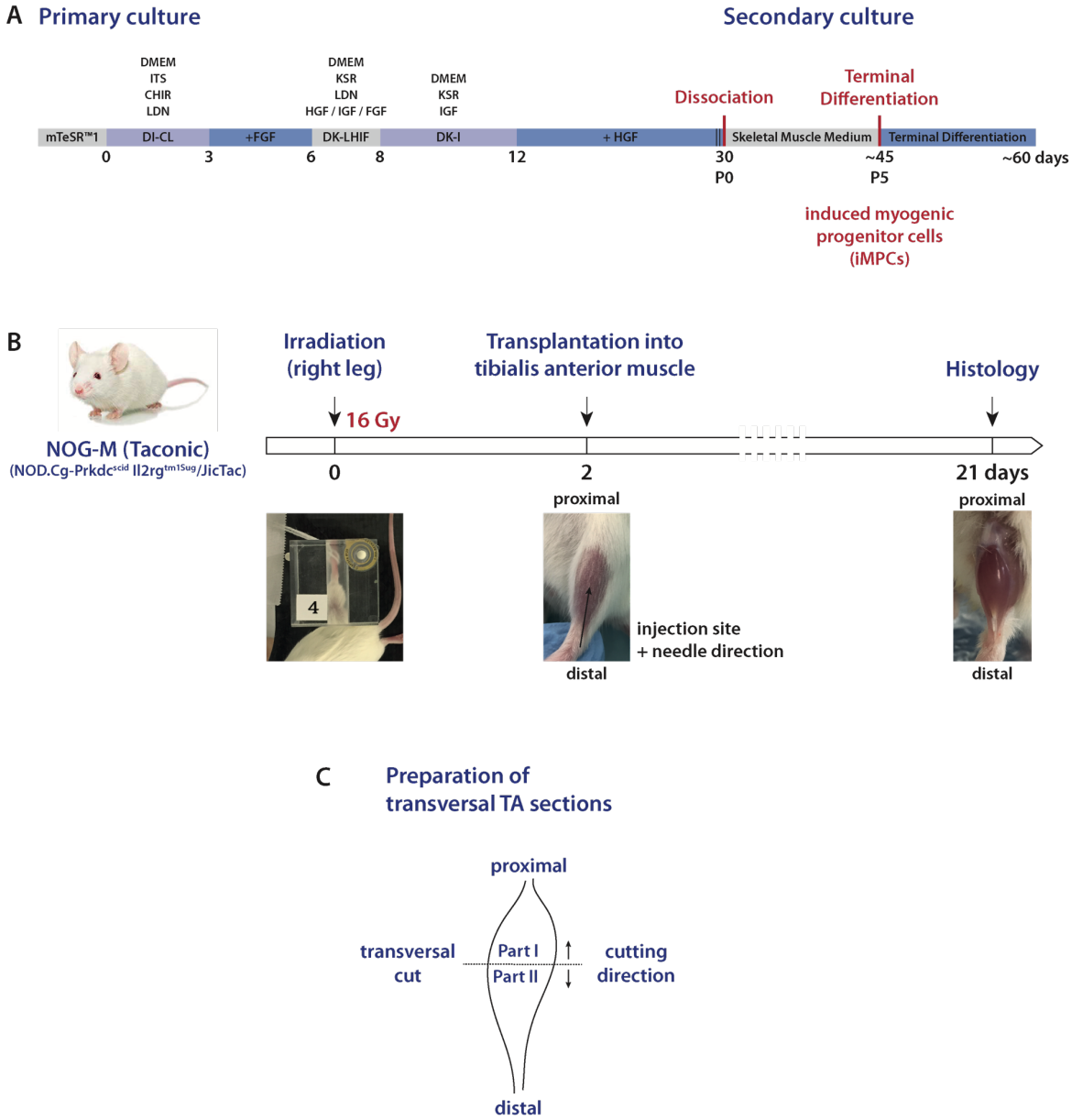

Figure 4.23: Schematic description of the transplantation experiments
(A) Induced myogenic progenitor cells (iMPCs) were taken from the exact same myogenic in vitro differentiation experiments. After dissociation on day 30, cells were cultured for 5 passages before transplantation. **(B)** Focal 16 Gray irradiation of female 6-9 weeks old xenograft compatible NOG-M mice hind limb muscles (NOD.Cg-Prkdc^{scid} Il2rg^{tm1Sug}/JigTac) was performed using an image-guided robotic system at the Charité CyberKnife facility. Two days after irradiation, freshly differentiated iMPCs were injected into the central part of the tibialis anterior (TA) muscle using a Hamilton® syringe. 21 days after transplantation mice were sacrificed and muscles harvested. **(C)** Schematic TA muscle shows the division of the muscle in two halves (part I / part II) following a transversal plane. Cryosections were prepared from each half, starting from the middle of the muscle towards the tendons.

The M_iMPCs and B_iMPCs, derived from donors A, B and D, showed a comparable number of human myofibres in transversal sections stained with a human-specific anti-Spectrin antibody (Figure 4.24, Table 4.3, Figure 4.25). The human myofibres, resulting from the transplantations of iMPCs, were counted for each section with fibre size diameters >10 µm (Table 4.3). The quantification of the human Spectrin$^+$ myofibres found for donors A, B and D revealed no significant differences between M_iMPCs and B_iMPCs for $p > 0.05$. No significance was reached for neither the separated comparison of M_iMPCs and B_iMPCs per donor nor for the combined comparison of M_iMPCs and B_iMPCs of all donors (Figure 4.25).

The representative images in Figure 4.24 show the appearance of human Spectrin$^+$ myofibres with a variety of fibre size diameters from 10 µm to 30 µm and an average of 5 human myofibres per cryosection (maximum/mouse) (Figure 4.25 & Table 4.3). The human myofibres are mainly solitary fibres surrounded by mouse muscle fibres. The myofibre formation remains poor compared to control grafts of human primary myoblasts. Transplantation of control primary myoblasts resulted in groups of human myofibres with a maximum fibre diameter of up to 60 µm, comparable to the size of the surrounding mouse muscle fibres. Quantification of control myoblast engraftment experiments resulted in an average of 20-30 human myofibres per cryosection (maximum/mouse) (data not published, assessed by Dr. Andreas Marg, laboratory of Professor Simone Spuler).

As an additional control, human primary fibroblasts were injected, which resulted in the absence of human muscle fibre formation and all human nuclei were located in the interstitium between the mouse muscle fibres (Figure 4.24). Notably, for the transplantations of iMPCs, I found the human nuclei mostly located in the interstitium between the muscle fibres, whereas most of the human nuclei from the primary myoblast transplantations are located inside the human fibres.

For each iMPC sample (donors A, B and D), I engrafted 4 mice. Successful engraftment was verified by the detection of human nuclei (human-specific Lamin A/C antibody) in cryosections from grafted muscles. The maximum number of human nuclei found in one section varies between the mice and donors. The average number of cells found for M_iMPCs and B_iMPCs was comparable within each donor. However, I found large differences between the donors, with the highest number of human nuclei found for donor D derived iMPCs and the lowest number found for donor A derived iMPCs (Table 4.3).

In addition to the human myofibre count, I investigated the presence of PAX7$^+$ human cells/nuclei within the graft, as PAX7 is the proper stem cell marker of the skeletal muscle (Relaix & Zammit, 2012). No PAX7$^+$ nuclei were found for all donors with 500 to 700 human nuclei analysed in three sections per condition. Control stainings of non-irradiated mouse muscle sections showed PAX7$^+$ nuclei in the satellite cell position (Figure 4.26).

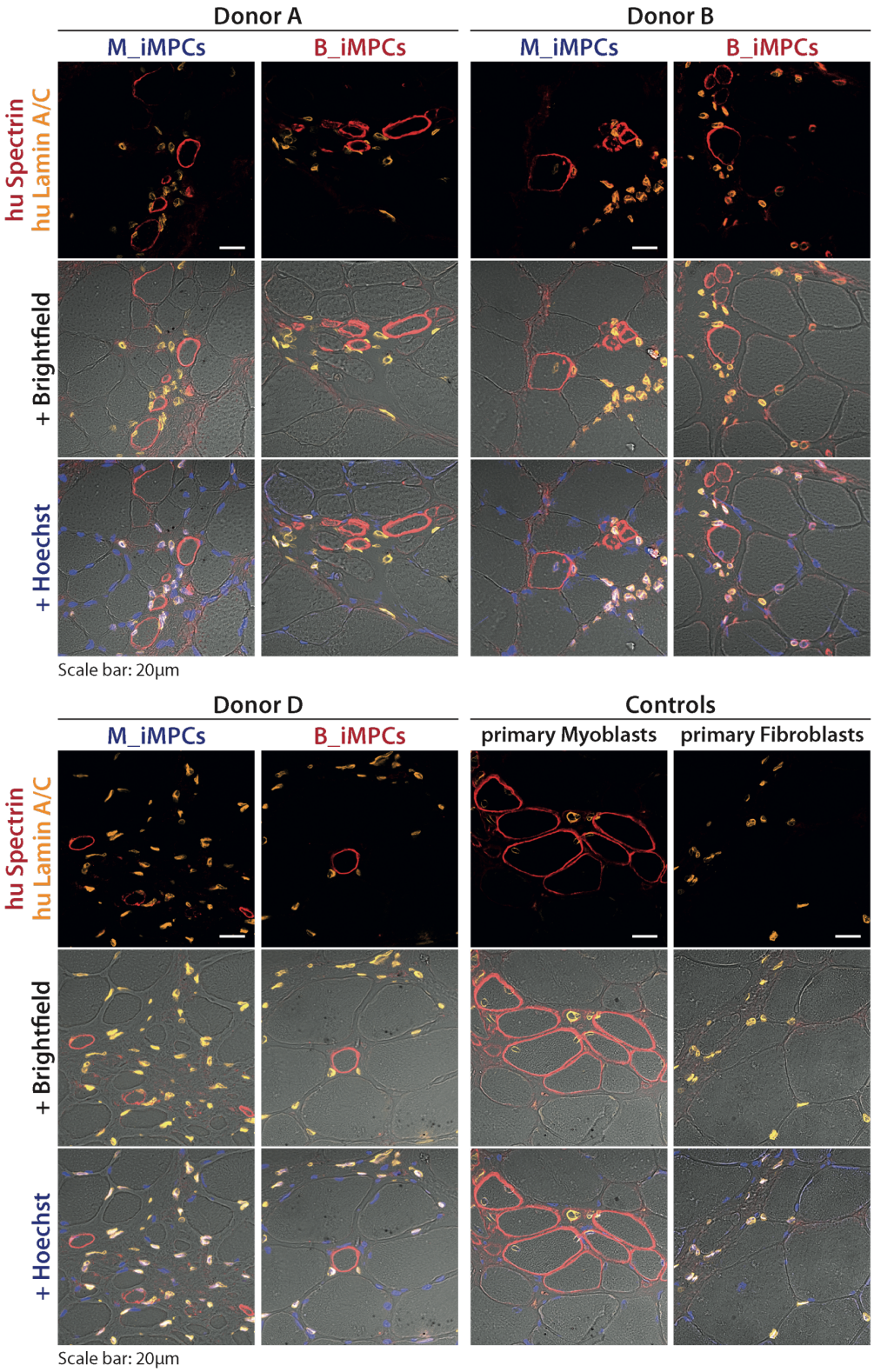

Figure 4.24: Immunohistological analysis of the transplantation experiments of M_iMPCs and B_iMPCs from donors A, B and D
Representative images of transversal tibialis anterior muscle sections of NOG-M mice. Muscles were irradiated with 16 Gray, two days later engrafted with induced myogenic progenitor cells (iMPCs) from donors A, B and D and harvested 21 days after transplantation. Sections are stained for human Spectrin (red), to visualise human muscle fibres, stained for human Lamin A/C to visualise human nuclei and counterstained with Hoechst to show mouse and human nuclei. As controls, primary myoblasts and primary fibroblasts, isolated from human muscle biopsy specimen, were injected. Scale bar: 20 µm.

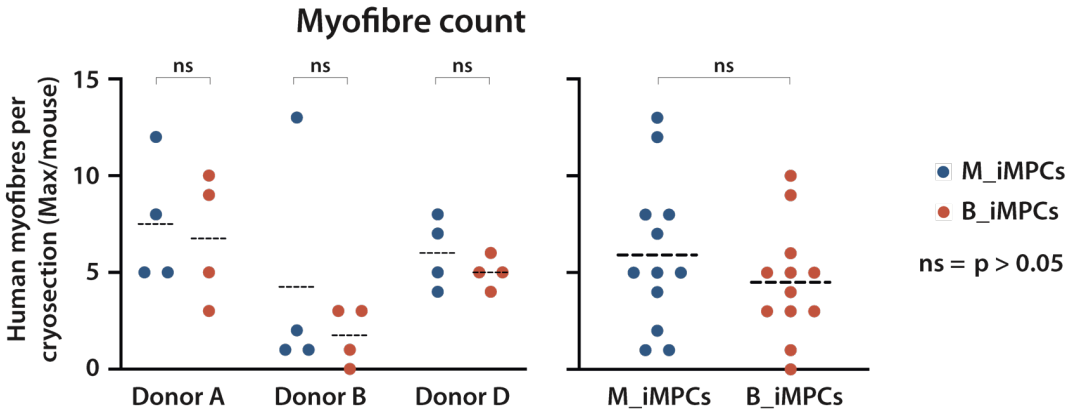

Figure 4.25: Quantification of human muscle fibres found for the transplantation of M_iMPCs and B_iMPCs from donors A, B and D
Human myofibre count per mouse was taken from Table 4.3. **(Left)** Visualisation was done by blotting the maximum number of human myofibres found in one cryosection for each donor A, B and D, separated by the origin of cell type (M_iMPCs blue, B_iMPCs red). Statistical analysis was done using the 2way ANOVA. **(Right)** Combined datasets of all three donors separated for M_iMPCs and B_iMPCs. Statistical analysis was done using the Students t test. Dashed lines represent the mean.

Table 4.3: List of transplantation results
The list gives the numbers of successful transplantations (amount of engrafted mice), the maximum number of human nuclei found for one section within 4 mice (given are the numbers for the mouse with the lowest maximum and the highest maximum) and the maximum number of human fibres found in one section for each of the analysed mice.

Cells		Successful transplantations (human nuclei found)	Maximum number of human nuclei /mouse / cryosection	Human muscle fibres per cryosection (Max/mouse)			
				1	2	3	4
Donor A	M_iMPCs	4/4	52 – 280	5	8	12	5
	B_iMPCs	4/4	17 – 233	10	9	5	3
Donor B	M_iMPCs	4/4	119 – 282	1	13	2	1
	B_iMPCs	4/4	113 – 471	0	3	1	3
Donor D	M_iMPCs	4/4	323 – 715	4	5	8	7
	B_iMPCs	4/4	320 – 393	5	5	6	4

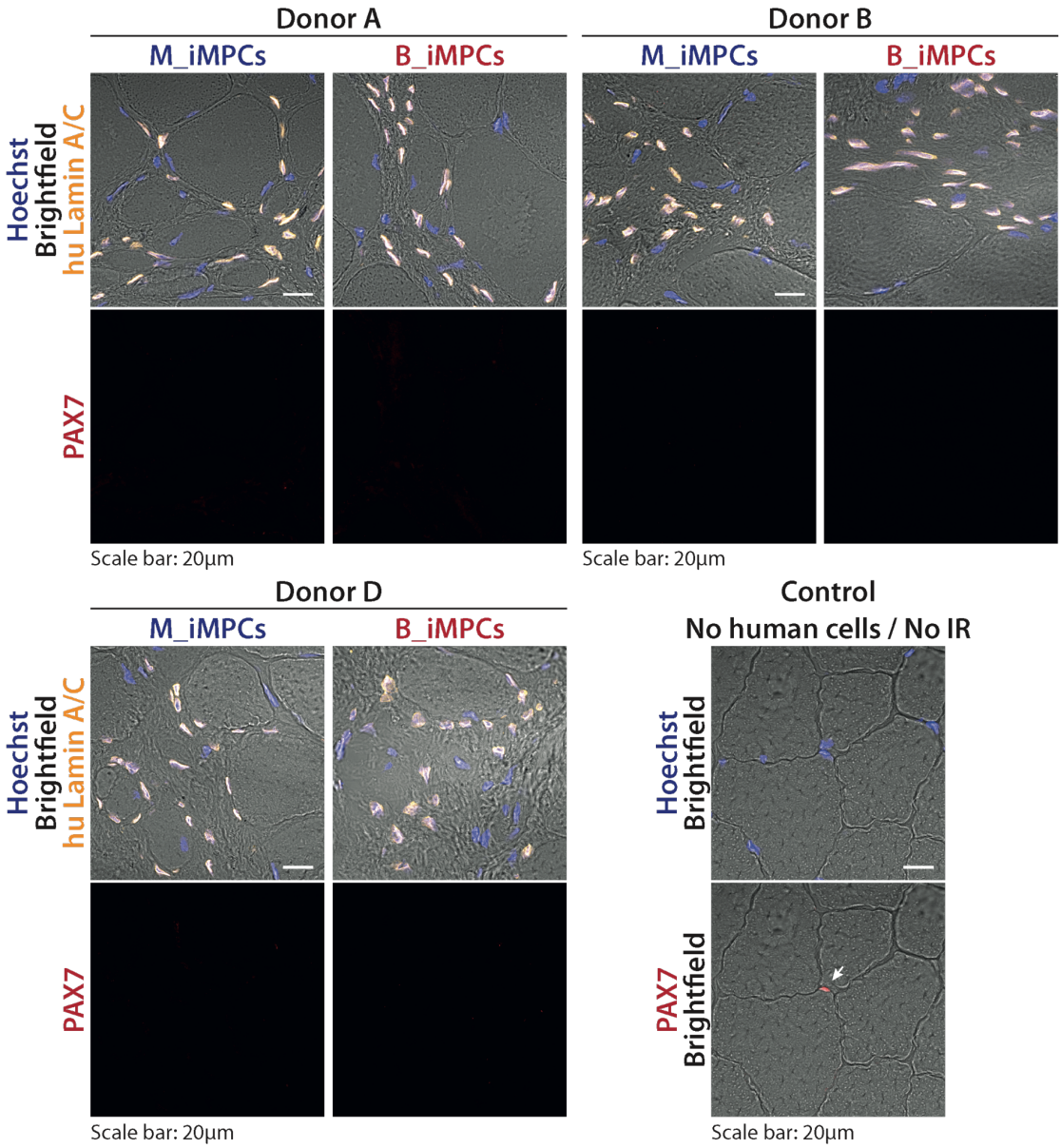

Figure 4.26: Immunofluorescence staining for PAX7⁺ nuclei in cryosections of TA mouse muscles engrafted with M_iMPCs and B_iMPCs from donors A, B and D
Representative images of transversal tibialis anterior muscle sections of NOG-M mice. Muscles were irradiated with 16 Gray, two days later engrafted with induced myogenic progenitor cells (iMPCs) from donors A, B and D and harvested after 21 days after transplantation. As control non-irradiated mouse muscle sections were prepared. Sections were freshly stained after preparation. Human PAX7 (red): visualisation of mouse and human muscle stem cells; human Lamin A/C: visualisation of human nuclei; Hoechst: visualisation of mouse and human nuclei. White arrow shows a PAX7 positive cell in the satellite cell position. Scale bar: 20 µm.

4.7 Comparing donors regardless of the cell type or origin for in vitro and in vivo experiments

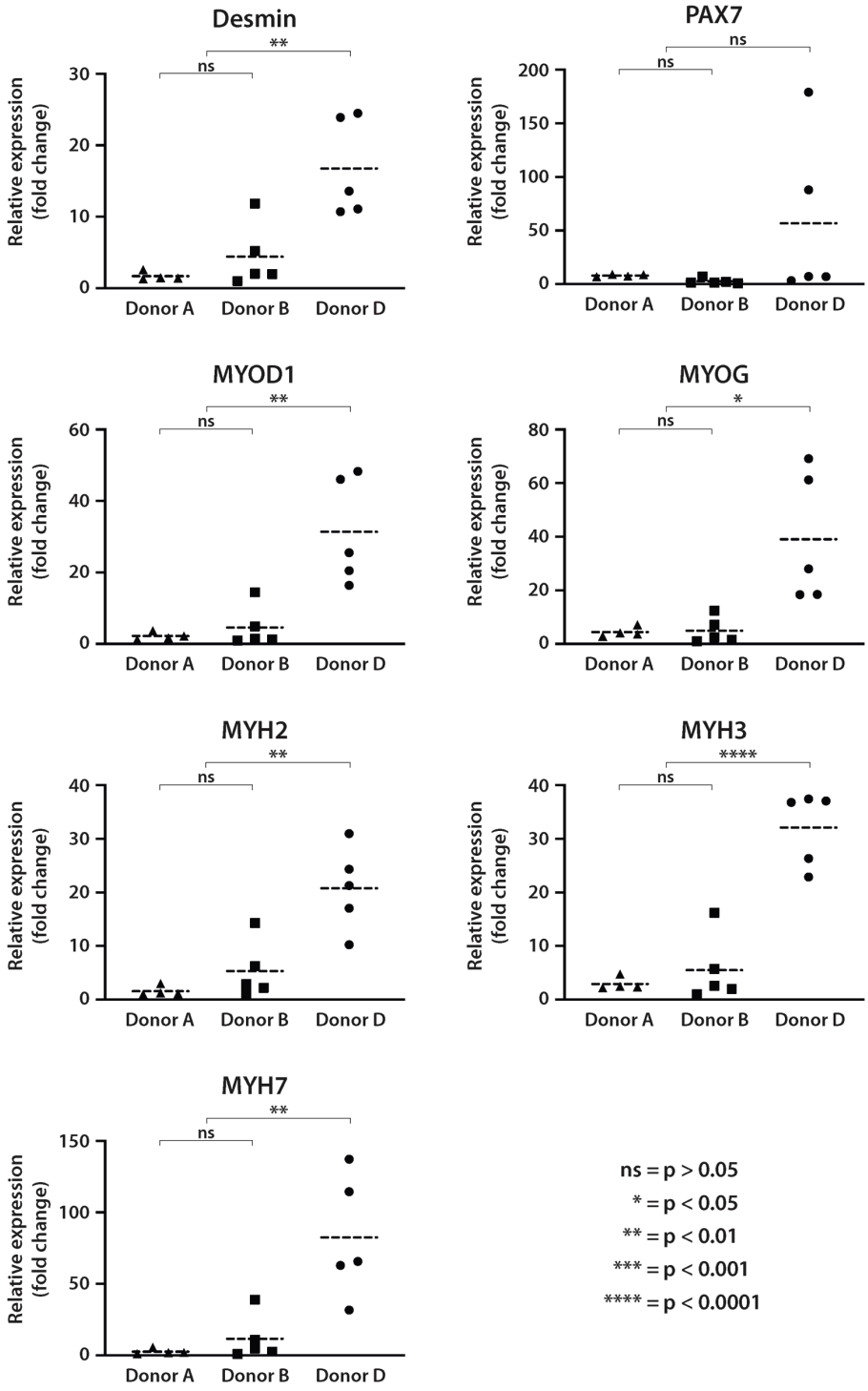

Figure 4.27: qRT-PCR quantification of myogenic marker expression in iMCs comparing donors A, B and D
Graphs present the same data as shown in Figure 4.20 without separation of M_iMCs and B_iMCs. qRT-PCR are shown for terminally differentiated induced myogenic cells (iMCs) differentiated from M_hiPSCs and B_hiPSCs of donors A, B and D after ~60 days of the differentiation protocol. Myogenic genes Desmin, PAX7, MYOD1, MYOG, MYH2, MYH3 and MYH7 were analysed. qRT-PCRs were performed using SYBR® Green and all primers were validated for specificity. ΔΔCt values are shown as fold change relative to the sample with the lowest expression value. Each dot represents a technical replicate (differentiation in an independent well). For statistical analysis one-way ANOVA ($p < 0.05$) was used. Dashed lines represent the mean.

The experiments shown in this work, comparing the myogenic differentiation of M_hiPSCs and B_hiPSCs, showed no significant difference for the cell type of origin for in vitro and in vivo experiments (Results sections 4.5 and 4.6).

However, the in vitro experiments showed differences between the donors in the capacity of their hiPSCs to differentiate into the myogenic lineage. To present this differences, I reanalysed the data shown in the results sections 4.5 and 4.6 by only comparing the donors, without considering the cell types of origin.

The in vitro myogenic marker expression of donor D iMCs is significantly higher compared to donors A and B (Figure 4.27). Significance ($p < 0.05$) was reached for all genes except PAX7. The myogenic marker expression of donors A and B iMCs are not significantly different. Both share the same significance values when compared to donor D.

While the in vitro experiments revealed a difference in marker expression between the iMCs of donors A and B compared to the iMCs of donor D, the in vivo engraftment experiments did show no such differences as there are no significant differences in the number of human muscle fibres found for each donor after transplantation of iMPCs into immunocompromised mice (Figure 4.28).

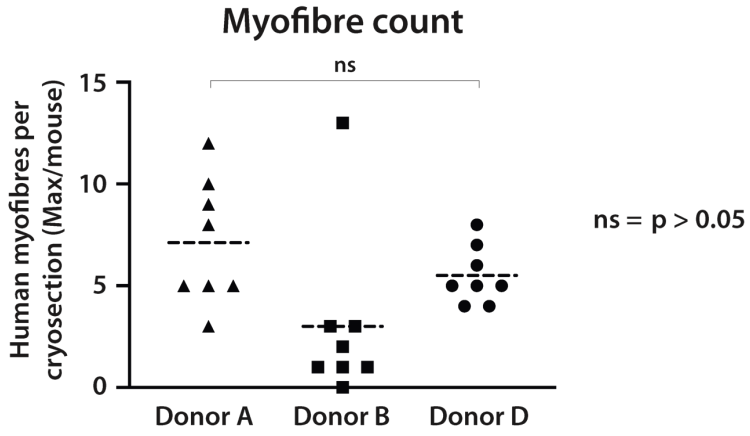

Figure 4.28: Number of human myofibres found after transplantation of iMPCs comparing donors A, B and D
Graph presents the same data as shown in Figure 4.25 without separation of M_iMPCs and B_iMPCs. Human fibre count per mouse was taken from Table 4.3 and visualised by blotting the maximum number of human fibres found in one cryosection for each donor A, B and D. Statistical analysis was done using one-way ANOVA. Dashed lines represent the mean.

5. DISCUSSION

The establishment of induced pluripotent stem cells (iPSCs) opened up the possibility of patient-specific disease modelling and greatly expanded the field of autologous stem cell therapies. Cell replacement therapies are a keystone in the research aiming to develop treatments for Muscular dystrophies (MDs). MDs are a heterogeneous group of myogenic disorders characterised by progressive muscle wasting and degeneration (Emery, 2002). Mutations causing Muscular Dystrophies, are leading to an imbalance between muscle damage and muscle repair, as the newly regenerated fibres are impaired as well due to the mutations (Berardi et al., 2014; Kinter & Sinnreich, 2014). Satellite cells are the proper stem cells of the skeletal muscle (Relaix & Zammit, 2012) and are therefore considered to be the gold standard for cell therapeutic applications. Unfortunately, primary human satellite cells will hardly become available in large numbers due to their low abundance and dispersed location within their natural stem cell niche. Thus, autologous hiPSCs differentiated into myogenic stem and progenitor cells represent the key to unrestricted cell numbers necessary for gene correction and repopulation of large muscles for therapeutic purposes.

It is of great importance to define the nature of iPSCs to develop efficient biotechnological and therapeutic application methods. iPSCs have been described to be similar to embryonic stem cells regarding morphology, pluripotency marker expression and in vivo teratoma formation (Takahashi & Yamanaka, 2006; Takahashi et al., 2007; Yu et al., 2007), while on the other hand epigenetic and transcriptomic differences have been described for hiPSCs from different sources. Various studies have shown that hiPSCs retain an epigenetic signature originating from the somatic cell type they were derived from (K. Kim et al., 2010; Polo et al., 2010; Kitai Kim et al., 2011; Lister et al., 2011; Ohi et al., 2011). Additional studies reported that this epigenetic signature is influencing the potential of the hiPSCs to differentiate into specific lineages, with preference for the lineage they originate from (Q. Hu et al., 2010; Bar-Nur et al., 2011; Kitai Kim et al., 2011; Sanchez-Freire et al., 2014; Sareen et al., 2014; S. Hu et al., 2016). In contrast, there are also reports showing no preferential differentiation of hiPSCs into their cell type of origin (Dorn et al., 2014; Kyttälä et al., 2016).

So far, no study investigated the influence of the epigenetic memory for human myoblast-derived hiPSCs and its influence on their myogenic differentiation capacity. In this study, I compared the myogenic differentiation capacity of myoblast- and PBMC-derived hiPSCs, which is of clinical importance as primary myoblasts and PBMCs represent the most relevant cell types for the generation of autologous hiPSCs for applications in the field of muscle disorders. Blood samples are easy to retrieve from donors and myoblasts can easily be extracted from muscle biopsy specimens that are regularly taken for diagnostic purposes from patients with suspected muscular dystrophies. As the genetic donor background was also described to influence the transcriptional identity of hiPSCs (Rouhani et al., 2014), myoblast- and PBMC samples were obtained from the same donor and age- and

gender-matched donors were selected for this study. The method to generate hiPSCs as well as the myogenic differentiation protocol were chosen to avoid the integration of transgenes into the hosts genome.

5.1 Generation of hiPSCs suitable for the analysis in this work

The aim of this work was to generate hiPSCs that are suitable for the detection of possible differences between the myoblast- and PBMC-derived hiPSCs. By using thorough characterisation methods and minimising the effects of the reprogramming method on the genome, I established a workflow that is also providing a basis for the future generation of hiPSCs that need to be suitable for clinical applications.

To deliver the reprogramming factors to the somatic cells, I chose non-integrating Sendai-viruses, instead of classical integrative delivery methods like lentiviruses. Classical integrative methods are associated with random genomic integrations and with associated tumorgenicity (Okita et al., 2007). In addition, they alter the transcriptional and epigenetic signatures of the iPSCs due to residual expression of the reprogramming factors (Sommer et al., 2012). The results of this work show the absence of Sendai-virus particles for all generated hiPSCs after 13-15 passages (Figure 4.3), confirming the suitability of this method to generate hiPSCs without exogenous transcription factor expression that would have interfered with the sensitive analysis comparing M_hiPSCs and B_hiPSCs. Of note, the removal of Sendai-viruses by temperature sensitivity (Ban et al., 2011) did not prove to be sufficient for all hiPSC clones and two clones had to be subcloned to retrieve hiPSCs without Sendai-virus particles. For this reason, subcloning should be considered in future experiments to reduce time and effort in the generation of Sendai-free hiPSCs. Sendai-viruses are still the most common delivery system for reprogramming, as they are efficient and relatively safe due to its multiple modifications leading to reduced immunogenicity and to a reduced production of infectious virus particles (Nishimura et al., 2011). However, the necessity to assure the absence of Sendai-virus particles is a drawback in biotechnological and clinical application that is currently addressed by the development of yet relatively inefficient mRNA, protein or small molecule-based reprogramming methods (Borgohain et al., 2019).

However, hiPSCs are known to acquire genomic alterations as they proliferate and differentiate (Peterson & Loring, 2014) and severe genetic and chromosomal aberrations have been detected in newly generated hiPSCs (Mayshar et al., 2010; Hussein et al., 2011). As those would severely compromise the intended analysis of this work, I assured a widely normal karyotype for all hiPSC samples using single nucleotide polymorphism analysis (SNP) (Figure 4.4). This analysis is crucial, as genomic alterations could influence the characteristics of the generated hiPSCs and hence likely their differentiation capacities. The analysis via SNPs would also be recommendable for clinical-

grade hiPSCs as duplications and deletions can be detected on a more detailed level as it is possible with classic cytogenetic karyotyping methods (Ben-David & Benvenisty, 2012).

The further analysis of the newly generated hiPSCs in this work followed stringent criteria to confirm the pluripotent characteristics of hiPSCs as described for ESCs (Takahashi et al., 2007; Wernig et al., 2007). Thus, morphology (Figure 4.4), pluripotency marker expression (Figure 4.5 & Figure 4.6) and the formation of all three germ layers after in vivo transplantation into immunocompromised mice (Figure 4.7) was confirmed. Pluripotency marker expression in hiPSCs was examined by the expression of OCT3/4, SOX2, NANOG and TRA-1-60. Those markers are sufficient to verify a PSC phenotype. In addition, I confirmed the absence of myogenic markers in the generated hiPSCs.

The teratoma formation assay was used in this study as it is still the gold standard for a functional characterisation of PSCs to form all three germ layers. As the test involves the use of animals, it may be replaced by the PluriTest, which is based on microarray data comparing the transcriptome profile of the newly generated iPSCs to a large database of pluripotent stem cells (Müller et al., 2011). It was shown recently, that only in vivo teratoma formation in combination with gene expression profiling of the teratoma tissue by TeratoScore provides the information on malignancy necessary for pre-clinical safety assessment (Allison et al., 2018). Therefore, the method used for functional pluripotency testing should consider the area of application of the generated hiPSCs.

5.1.1 Higher reprogramming efficiencies for myoblasts compared to PBMCs

Efficiencies, observed in this study, are ranging from 0.07% (average of 0.018% to 0.1%) for myoblasts and 0.002% (average of 0.0007% to 0.005%) for PBMCs (Table 4.1). The reprogramming efficiencies using PBMCs are significantly lower than the ones using myoblasts (Figure 4.2). This is in accordance with previous studies reporting efficiencies for PBMCs of 0.005% (Trokovic et al., 2014) or 0.011% (Tan et al., 2014) and up to 0.75% for skeletal myoblasts (Trokovic et al., 2013). However, this study provides to the best of my knowledge the first direct comparison of the generation of hiPSCs from myoblasts and PBMCs.

The differences in the reprogramming efficiencies between myoblasts and PBMCs may be explained by the stochastic reprogramming model. It describes, that reprogramming is induced in all cells that received the OSKM cocktail but only a few cells finish the procedure completely due to internal failures of the cells that lead to a premature abortion of the reprogramming process (Ebrahimi, 2015; Karagiannis et al., 2018). The fact that PBMCs are suspension cells and therefore have to implement severe morphological changes to become adherent hiPSCs, might increase the probability of failures which may result in less cells finishing the reprogramming process successfully, compared to already adherent myoblasts. Interestingly, fibroblasts reprogrammed with the same method in the same study were reported with an efficiency comparable to myoblasts, supporting this

hypothesis (Trokovic et al., 2013). Among many other factors, DNA damage has been reported to be a major reprogramming barrier to reach a pluripotent state (Marión et al., 2009). As PBMCs originate from haematopoietic stem cells in the bone marrow, and go through multiple maturation stages, the probability of accumulating DNA damage might be higher compared to myoblasts that differentiate directly from muscle stem cells that reside in a quiescent state in the satellite cell niche and have likely undergone less cell divisions. This may be another factor resulting in different reprogramming efficiencies using PBMCs and myoblasts and may be addressed in further studies. Nevertheless, a widely normal karyotype was shown for both, M_hiPSCs and B_hiPSCs (Figure 4.4), excluding large aberrations in the generated cells.

In addition, I was unable to obtain PBMC-derived hiPSCs from donor E and faced severe issues obtaining them from donor C, resulting in 5 trials in total for that donor and in the end the usage of mouse embryonic feeder cells as an alternative to Matrigel, which were used in the initial studies obtaining induced pluripotent stem cells (Takahashi & Yamanaka, 2006; Takahashi et al., 2007). In contrast, I successfully obtained a sufficient number of myoblast-derived hiPSCs from all donors in the first trial (Table 4.1). Thus, it might be recommended to use myoblasts, instead of PBMCs for the generation of hiPSCs in future studies to reduce time and effort in the generation of patient-specific hiPSCs.

5.2 Myogenic differentiation protocol – establishment and validation

I decided to establish the myogenic differentiation protocol by Chal et al., due to its recapitulation of in vivo myogenesis by the exposure to signalling molecules present in the embryonic development. Thus, this protocol differs from other methods that use overexpression of transcription factors that have been stably integrated into the host genome (Darabi et al., 2012; Tedesco et al., 2012; Abujarour et al., 2014). The alteration of the host genome would possibly alter the transcriptome and the differentiation into the myogenic lineage and therefore needed to be avoided in this work. In addition, the overexpression of myogenic transcription factors is forcing the cells into the myogenic lineage and presumably cover the intrinsic differences that may be present in the hiPSCs due to epigenetic and genetic differences. Besides, myogenic differentiation using non-integrating methods represents the appropriate approach of the generation of induced myogenic cells for future clinical applications.

5.2.1 Cell heterogeneity during differentiation

The experiments in this work did show heterogeneity in the myogenic differentiation results. Firstly, heterogeneity was observed for the differentiation from different hiPSCs with differences in the number of myogenic cells after terminal differentiation into induced myogenic cells (iMCs). The differences between the hiPSCs are discussed in 5.4 and 5.5. Secondly, a method-related

heterogeneity was observed for the myogenic differentiation protocol itself. Specifically, heterogeneity was observed for the induction of the mesodermal progenitor cell fate, for the purity of the cell population after primary culture and for the purity of the induced myogenic cells (iMPCs/iMCs).

The posterior presomitic mesoderm marker TBX6 was detected in large areas but not in all cells of the early differentiation culture (Figure 4.12). The fact that not all cells are positive for TBX6 is in accordance with the observations by Chal et al. This heterogeneous response of a cell population to differentiation signals may be attributed to physical differences of the Matrigel-matrix, which the cells are cultured on, as physical properties, including stiffness, surface pattern and geometry of the extracellular matrix have been recognised as crucial factors in regulating the differentiation of stem cells (Han, Bai, & Liu, 2014). Additionally, another study showed, that cells positive for the early transcription factor T, are preferentially located at the periphery of ESC colonies, concluding that geometrical confinement is influencing asymmetric gene expression resulting in heterogeneous cell populations (Blin et al., 2018). It will be of great interest to reveal the basic mechanisms of how to control whole cell populations in response to differentiation signals, as this is an important step for purity and thus reliability as well as biosafety of PSCs.

Interestingly, the presence of $TBX6^+$ cells is coupled to morphological differences dividing the cultures in $TBX6^+$ and $TBX6^-$ areas that can be recognised by light microscopy (Figure 4.12). Thus, morphological assessment of the differentiation cultures could be used for early screening for the efficiency of the mesodermal progenitor induction. Quantification of these differences between the hiPSC clones in this study was not performed but will be interesting for further investigation as one could possibly correlate early mesodermal fate induction and myogenic marker expression at the end of the protocol.

Heterogeneity of the differentiation protocol is also shown by the presence of different terminally differentiated cell types in the primary culture. The cells were found to be positive for the neuronal marker TUJ1 besides the presence of terminally differentiated myogenic cells (Figure 4.13). Interestingly, although the differentiation protocol is developed for the myogenic lineage, including sequential addition of growth factors promoting myogenesis, the protocol also leads to a subpopulation of cells which differentiate into terminally differentiated neuronal cells. As TBX6 is a marker for mesodermal progenitor cells (Chalamalasetty et al., 2014) but neuronal cells arise from ectodermal fate (Plouhinec et al., 2017) it could be assumed that the $TBX6^-$ cells are the origin of the neuronal cells. Thus, it would be highly interesting to investigate the marker expression in the $TBX6^-$ cell population. A promising candidate would be SOX2, as the development of $SOX2^+$ spinal cord progenitor cells and $TBX6^+$ mesodermal progenitor cells is tightly regulated by Wnt signalling and both cell types originate from neuromesodermal progenitor cells (NMPs) (Gouti et al., 2014, 2017).

As described by Chal et al., 2016, I confirmed the absence of the majority of terminally differentiated cells in the single cell population after dissociation of the primary culture (Figure 4.17). However, the heterogeneity of this progenitor cell population (iMPCs) is also shown by the expression of PAX7 in only a subpopulation of cells and the presence of cells that are negative for myogenic markers in the iMPC and iMC cell populations, even for hiPSCs, yielding a high amount of myogenic cells (Figure 4.17 & Figure 4.21 & Figure 4.22). The heterogeneity in the maturation status of the cells is correlated with the different efficiencies of the hiPSCs to differentiate into the myogenic lineage and is discussed in 5.2.2.

Due to the described heterogeneity of the differentiation protocol and due to the differences in the myogenic differentiation efficiencies of the hiPSCs, the purification of the myogenic progenitor population, as recently described by Hicks et al., 2018, would be a highly interesting approach to develop this protocol for applicability in disease modelling and future clinical perspectives. Optimisation of the protocol for each single hiPSC clone would also be an option but is time consuming while purification methods can also compensate for differences occurring from experiment to experiment. The purification would also be necessary to reduce the risk of tumour formation, as residual stem cells in the hiPSC-derived cell population bear the risk of tumour formation (Okano et al., 2013).

5.2.2 Maturation of the generated myogenic cells

The induced myogenic cells (iMCs), generated in this work, developed characteristics similar to human primary myogenic cells. I confirmed the expression of the essential myogenic markers PAX7, MYOD1, MYOG, Desmin and MyHC with the co - expression of the markers MyHC and MYOG and the characteristic multinucleation in matured myogenic cells with “pearl chain”-like nuclear structures inside of enlarged $MyHC^+$ cells (Figure 4.17 & Figure 4.21 & Figure 4.22). Although Desmin is not only expressed in skeletal but also in cardiac and smooth muscle (Paulin & Li, 2004) and developmental $PAX7^+$ progenitor cells are also known to give rise to brown fat cells (Lepper & Fan, 2010), the combination of all myogenic markers is sufficient to confirm the skeletal muscle phenotype of the generated cells. Although there is variation in the capacity to differentiate into the myogenic lineage, the myogenic identity of the iMCs was confirmed for all hiPSCs (Figure 4.17 & Figure 4.21 & Figure 4.22).

Multinucleation with “Pearl chain” like nuclear alignment was only found in iMCs from donors 0 and D, which is likely due to the high abundance of fast $MyHC^+$ cells in these differentiations, as fusion among myogenic cells can only happen if other myogenic cells are in close proximity. Thus, iMCs from donors A and B do not show this feature as the abundance of fast $MyHC^+$ cells is low. As discussed before, a purification for cells with myogenic properties would most likely be the key to optimise the differentiation results for all hiPSCs. Of note, the increased maturity of iMCs by prolonged

culture of the induced myogenic progenitor cells (iMPCs) (Figure 4.15) is not described in the original protocol (Chal et al., 2016) and also not in another study using this myogenic differentiation protocol (Hicks et al., 2018). However, as the degree of maturation, meaning the degree of multinucleation and size of $MyHC^+$ cells, differs from experiment to experiment and the 44-days protocol (differentiation starting in P0) was only investigated for donor 0, further experiments are required to establish a well-defined protocol for enhanced maturity.

Another feature of in vitro maturated myogenic cells is contraction, which is described for mouse and human myogenic cells, generated with the protocol by Chal et al. 2015, 2016. It is described to be observable in cultures from day 30 onwards. However, I could not detect any contractions in the cells generated in this work, even in cultures of donor 0 that were kept for 80 days (data not shown). It might be possible that the development of contracting myofibres requires an even higher maturation status than the one achieved in this work, which could be addressed in further experiments by purification of the myogenic cell population. In addition, further assessment of the maturation status of the generated iMCs may also include the analysis of sarcomere formation by electron microscopy or the formation of acetylcholine receptors that can be monitored by α-bungarotoxin (BTX), as shown in other studies (Demestre et al., 2015; Choi et al., 2016; Hicks et al., 2018; Rao et al., 2018).

The iMCs, generated in this work, resemble some characteristics of early state myofibres as they express the embryonic myosin heavy chain isoform 3 (MYH3) (Figure 4.20), which is downregulated after birth and only present in specialised muscles in the adult (Schiaffino et al., 2015). The identity as an early developmental state is furthermore supported by the prolonged and thin morphological appearance, especially regarding iMCs generated with the 44-days protocol (Figure 4.14, B & Figure 4.15 & Figure 4.22). Induced myofibres, generated from hiPSCs, are indeed thought to resemble the phenotype of perinatal primary myofibres (Chal & Pourquié, 2017). An early developmental state of hiPSC-derived cells is also discussed for other cell types like cardiomyocytes (Robertson et al., 2013). On the other hand, in this work I observed further maturation of the iMCs into multinucleated myofibres with enlarged $MyHC^+$ cell bodies. The expression of fast MyHC isoforms and myosin heavy chain isoform 7 (MYH7) that are expressed in fetal and adult muscles (Schiaffino et al., 2015), furthermore show the maturated phenotype of some of the iMCs. The co - expression of embryonic, fetal and adult myosin heavy chain isoforms in the iMC-culture furthermore shows the heterogeneity of the developing cell population.

Notably, induced myogenic progenitor cells (iMPCs) do not express fast MyHC but Desmin and PAX7 (Figure 4.17). Thus, they rather resemble myogenic progenitor cells, as Desmin and PAX7 are expressed in early myogenesis in cells that are about to fuse with existing myofibres (Chal & Pourquié, 2017). Desmin is expressed in the myotome together with early myosin heavy chain isoforms (Babai et al., 1990; Lyons et al., 1990) but staining of the total MyHC revealed only a rare

abundance of positive cells in this work (Figure 4.17). However, the specific assessment of early myosin heavy chain isoforms and the expression of the early myogenic transcription factor PAX3 would be interesting to further define the characteristics of these iMPCs.

As the analysis of the hiPSC-derived myogenic cells in this work revealed progenitor characteristic for iMPCs and mature characteristics for iMCs, I decided to use iMPCs for the assessment of the in vivo engraftment capabilities and iMCs to compare the in vitro myogenic differentiation capacities of the different hiPSCs that were generated in this work.

5.3 Evaluation of the in vivo potential of induced myogenic progenitor cells (iMPCs)

The transplantation experiments in this work showed, for the first time, the in vivo regenerative capacities of human induced myogenic cells generated with the protocol published by the group of Olivier Pourquié (Chal et al., 2016). However, that group reported on a successful transplantation of a PAX7-GFP-purified mouse cell population into mdx mice (Chal et al., 2015) but did not show this with non-genetically altered and non-purified human cells. Other groups reported on successful transplantations of human iPSC-derived myogenic cells using direct reprogramming methods by overexpression of the transcription factor PAX7 (Darabi et al., 2012) or MYOD1 (Tedesco et al., 2012; Young et al., 2016) or by engrafting cells generated by other directed transgene-free differentiation protocols (Choi et al., 2016; Hicks et al., 2018).

I could show human muscle fibre formation after transplantation of iMPCs into the muscle of immunocompromised mice for all iMPCs generated in this work (Figure 4.24 & Figure 4.25). However, the potential of in vivo myofibre regeneration of the iMPC populations is lower compared to human primary myoblasts, shown by the low number of human myofibres after transplantation of iMPCs compared to human primary myoblast transplantations. In addition, human nuclei are mostly located outside human myofibres in the interstitium in between the myofibres for iMPC transplantations whereas in grafts of human primary myoblasts human nuclei are mostly located inside the myofibres (Figure 4.24). The low number of human myofibres after transplantation of iMPCs may be attributed to a heterogeneous iMPC cell population, as shown by cells that are not positive for myogenic markers in the iMPC and also in the iMC populations in vitro (Figure 4.17 & Figure 4.21 & Figure 4.22). This heterogeneity could be addressed by purification of the iMPC population to enrich for cells with myogenic potential, as shown in other studies that enriched for the surface markers $HNK^-/NCAM^+$ (Choi et al., 2016) and $HNK^-/ERBB3^+/NGFR^+$ (Hicks et al., 2018) prior to transplantation, both showing higher numbers of regenerated human myofibres compared to the present study.

The host environment and injury model might greatly influence donor cell engraftment. The experiments performed in this work were based on previous successful engraftment studies with

human primary myoblasts (Marg et al., under review) to compare the regenerative potential of iMPCs and primary myoblasts. The recipient mouse muscles were devoid of endogenous satellite cells due to the pre-irradiation, which has been described to be required for donor cell engraftment and colonisation of the stem cell niche (Boldrin et al., 2012). The mouse model used in this work is not dystrophic and therefore the only areas of the muscle where regeneration occurred were those injured by the needle used for the transplantation. Therefore, as observed for the transplantation of human muscle fibre fragments (HMFFs) (Marg et al., 2014) and primary myoblast single cell suspensions (Marg et al., under review), the donor cells appeared to engraft and give rise to myofibers only in those injured areas of the recipient muscles where they are recruited to regenerate the damaged tissue. The transplantation studies performed by Choi et al. and Hicks et al. used cardiotoxin injections in combination with irradiation. Models using cardiotoxin injections induce a higher degree of muscle damage and thus might result in larger fields of engraftment and possibly more human regenerated myofibres in the artificial mouse environment. Choi et al. injected 1-3*10^6 while Hicks et al. injected 5-10*10^6 previously purified cells in contrast to 1*10^5 non-purified cells used in the present study, a number based on the previously established number of injected cells for primary human cell transplantations (Marg et al., under review). Finally, Hicks et al. reported on the addition of a TGF beta inhibitor in vivo to reach sufficient engraftment results, although this would be a major obstacle for patient application. In summary, the studies by Hicks et al. and Choi et al. used at least 10 times higher numbers of cells in a highly regenerative muscle environment, due to a mdx-NSG dystrophic mouse model (Hicks et al., 2018) and cardiotoxin injections (Choi et al., 2016; Hicks et al., 2018), with the transplantation of previously purified cells resulting in higher human myofibre formation than shown in this work. Therefore, in order to develop useful induced myogenic cells for biotechnological and clinical applications a purification of the myogenic progenitor population generated by the protocol by Chal et al. is necessary to aim for the same regenerative efficiency as when using primary myoblasts as in the described engraftment setting by Marg et al..

Interestingly, I did not detect any difference in the formation of human myofibres for iMPCs generated from different hiPSCs, although large differences were detected in vitro with regard to the number of myogenic cells after terminal differentiation. This might be related to the low overall myofibre regeneration in iMPC grafts, as a low efficiency prevents the detection of differences. However, I detected a variability in the amount of total human nuclei in the grafts between the different iMPCs (Table 4.3). This might be explained by different in vivo survival rates or different in vivo proliferation rates of the iMPCs and may be addressed in further experiments. On the other hand, the in vitro proliferation analysis of the iMPC populations showed no differences that would explain the different amounts of total human nuclei in the grafts (Figure 4.19).

An explanation for the absence of differences in the number of human myofibres between the engrafted iMPCs might be related to the presence of the muscle stem cell factor PAX7, that was

detected to be low in all iMCs that have been engrafted as iMPCs (Figure 4.20). As I injected freshly generated iMPCs, I selected one replicate for each iMPC for transplantation before the results of the in vitro terminal differentiation into iMCs were available. The influence of PAX7 expression on the in vivo capabilities of the different iMPCs to generate muscle would be interesting to address in further experiments by analysing the iMPC populations. However, a recent study showed that commonly used in vitro markers for ESC-derived dopamine neuron progenitors correlated poorly with dopaminergic maturation in vivo (Kirkeby et al., 2017). Thus, the authors correlated backwards from successful engraftment experiments and identified new in vitro markers, which in turn represents a promising approach for all PSC-derived therapeutic developments.

5.4 Differential gene expression between M_hiPSCs and B_hiPSCs does not significantly influence their myogenic differentiation capacity

The differentiation experiments in this work show no significant difference between M_hiPSCs and B_hiPSCs in their ability to differentiate into the myogenic lineage as shown by myogenic marker expression after terminal differentiation into iMCs (Results section 4.3). These results are interesting, as transcriptomic analysis revealed 122 significantly differentially expressed transcripts (DETs) between M_hiPSCs and B_hiPSCs, especially as some of these DETs are involved in chromatin remodelling and in signalling pathways that regulate differentiation and pluripotency of iPSCs (Results section 4.3).

The absence of any great influence of the differentially regulated genes on the myogenic differentiation capacity might be explained by the specific direct targeting of the differentially regulated signalling pathways by the myogenic differentiation protocol used in this work. Wnt/FGF and TGF beta signalling are specifically targeted by the protocol by Chal et al. to drive differentiation into the mesodermal and further on into the myogenic lineage specification. Thus, the intrinsic differences between the M_hiPSCs and B_hiPSCs in the activity of these pathways may be covered and no preferential differentiation into the somatic cell type of origin is detectable as they were described before in various studies for other cell types (Q. Hu et al., 2010; Bar-Nur et al., 2011; Quattrocelli et al., 2011, 2016; Sanchez-Freire et al., 2014; Sareen et al., 2014; Phetfong et al., 2016; S. Hu et al., 2016). Interestingly, early studies, using retinal-pigmented epithelial cells (Q. Hu et al., 2010) and insulin-producing pancreatic beta cells (Bar-Nur et al., 2011) used spontaneous differentiation from embryoid bodies in vitro or teratoma formation in vivo to determine the differentiation capacities of the generated hiPSCs into different cell types. Thus, it would be interesting to see whether spontaneous differentiation would reflect the intrinsic differences of M_hiPSCs and B_hiPSCs and influence the differentiation capacities. However, the usage of directed differentiation protocols is required, as the application of hiPSC-derived myogenic cells in biotechnological and clinical

applications necessitates purity and high numbers of cells that cannot be obtained with spontaneous differentiation approaches.

In line with the results shown in this work is a study investigating different hiPSCs to differentiate them into the haematopoietic lineage reporting no difference for the somatic cell type of origin for the differentiation into the haematopoietic lineage (Dorn et al., 2014). The authors used a directed differentiation protocol, but no further investigation of the transcriptome was performed in this study. Some other studies showed differences in the differentiation capacities only in low hiPSC-passage numbers (Sanchez-Freire et al., 2014; S. Hu et al., 2016). However, most of the studies that reported on preferential differentiation into the somatic cell type of origin performed their experiments with iPSCs below passage number 20, thus comparable to the present study and to the study of Dorn et al..

The results for the in vivo engraftment after iMPC transplantation into immunocompromised mice show myofibre formation for both cell types M_iMPCs and B_iMPCs (Figure 4.24). These results are considered to be a qualitative assessment of the potential to form myofibres, as the interpretation of the quantitative assessment is difficult due to the low size and low abundance of human myofibres throughout all iMPC samples and especially in comparison to transplantations of human primary myoblasts. As discussed before, a low efficiency may impede the detection of significant differences. Thus, the results confirm the potential for M_iMPCs and B_iMPCs to form human myofibres but the quantification remains inconclusive and could be addressed in further experiments using an optimised cell population with an adopted transplantation procedure as discussed in 5.3.

The experiments in this work showed a large variation between the donors to produce myogenic cells after terminal differentiation in vitro, which might influence the determination of the significance values analysing M_iMCs and B_iMCs combined for all donors (Figure 4.20). However, the analysis of each donor separately only shows a trend for donor B with slightly higher expression of myogenic markers in M_hiPSCs. Still, for the biotechnological and clinical application the genetic background of the donor rather than the cell type of origin has been shown to be crucial to derive myogenic cells from hiPSCs.

5.5 Donor background is pivotal for the myogenic capacity of hiPSCs

The transcriptomic analysis and the in vitro myogenic differentiation experiments of this work revealed that the genetic background of the donor is crucial and is of greater importance than the somatic cell type of origin for the potential of hiPSCs to differentiate into the myogenic lineage using the directed transgene-free differentiation protocol by Chal et al. In vitro differentiation of hiPSCs derived from donor D showed significantly higher numbers of myogenic cells after terminal differentiation into iMCs compared to donors A and B (Figure 4.27). In addition, the transcriptome

analysis of M_hiPSCs and B_hiPSCs showed that M_hiPSCs and B_hiPSCs group in the principal component analysis due to their donor rather than due to the somatic cell type of origin (Figure 4.10).

The influence of the donor-based differences being superior to the somatic cell type of origin was shown before in large sample sets comparing the transcriptome (Rouhani et al., 2014) and the differentiation into the hepatic lineage (Kajiwara et al., 2012). In addition, the present study shows that the effect of the donor background on the myogenic differentiation is still more important than the somatic cell type of origin even for an age- and gender-matched sample set, which is similar to the findings in a study comparing gender-matched donors in the haematopoietic lineage differentiation (Kyttälä et al., 2016).

In a biotechnological and clinical view, these findings point out that it might be beneficial to use HLA-matched rather than autologous cells for clinical applications, as this approach would enable the selection for hiPSCs with a high differentiation efficiency according to the donor. However, HLA-matched cell therapy recipients need immunosuppression. Thus, autologous transplants are advantageous over HLA-matched cells and differentiation protocols may be optimised by purification steps and optimisation of the differentiation protocol itself, depending on the intrinsic differences between the donors and the hiPSC lines. In this context, it would be highly interesting to define factors that are responsible for the differences in the myogenic differentiation efficiency between the different hiPSCs, as was shown for the correlation between IGF2 and the haematopoietic lineage (Nishizawa et al., 2016) or for CXCL4/PF4 for cardiac differentiation (Ohashi et al., 2019).

The fact that no significant difference was found between the donors for the formation of human myofibres after transplantation (Figure 4.28) is, like discussed before, probably related to the overall low efficiency of the transplantation experiments using iMPCs or due to the absence of a correlation between in vitro marker expression and successful in vivo engraftment and maturation (Kirkeby et al., 2017).

5.6 Summary and future prospects

Regarding the somatic cell type of origin, the experiments of this work do not show a significant difference between M_hiPSCs and B_hiPSCs concerning their ability to differentiate into the myogenic lineage using the directed differentiation protocol by Chal et al. However, the experiments show a higher reprogramming efficiency for myoblasts compared to PBMCs, suggesting that myoblasts are the more convenient cell type to produce patient-specific hiPSCs and induced myogenic cells, whenever a muscle biopsy is available which is generally the case for patients with muscle diseases. However, as this work shows differences between M_hiPSCs and B_hiPSCs on the transcriptome level that may generally influence their differentiation capacity, future experiments are required to investigate the impact on differentiations into other somatic cell types.

The directed transgene-free myogenic differentiation protocol, established in this work, shows large differences between the hiPSCs in their ability to produce myogenic cells after terminal differentiation. These differences are rather related to the genetic background of the donor than to the somatic cell type of origin, which has a great impact on the applicability in biotechnological or future clinical applications. The low differentiation efficiency for some donors illustrates the need for optimisation of the protocol as autologous transplants are advantageous over HLA-matched cells. However, it would be highly interesting to screen for markers that define the potential of hiPSCs to differentiate into the myogenic lineage using a large sample set.

As the engraftment experiments showed a low number of human myofibre formation for all iMPC populations used in this work, an optimisation of the engraftment capabilities of the injected induced myogenic cells is required. This could be achieved by the development of purification strategies to enrich for subpopulations responsible for the regenerative potential seen in this work. Alternatively, optimisation of the myogenic differentiation protocol for each hiPSC clone could enhance the number of cells with myogenic potential in the iMPC and iMC populations. However, optimisation for each hiPSC clone is time consuming and costly and thus hardly applicable for large scale biotechnological applications, while purification would also enable to compensate for differences originating from experiment to experiment.

In sum this work establishes that myoblast- and PBMC-derived hiPSCs do not differ in their myogenic differentiation efficiency using the transgene-free differentiation protocol by Chal et al. Nevertheless, differences in differentiation efficiencies related to the genetic background of the donor were detected and a thorough understanding of the factors responsible for these intrinsic differences will be of great value for the improvement of strategies for hiPSC-based cell replacement therapies for patients with muscular dystrophies.

6. CONTRIBUTIONS

The experiments in this work have been performed by me with some exceptions which are mentioned in the main text and are summarised here.

The teratoma formation assays were performed by EPO – Experimental Pharmacology & Oncology Berlin-Buch GmbH (Campus Buch, Berlin, Germany).

The single nucleotide polymorphism (SNP) karyotyping was performed by the Stem Cell Core Facility (Dr. Sebastian Diecke, Berlin Institute of Health (BIH) / Max Delbrück Center for Molecular Medicine, Berlin, Germany) in cooperation with the laboratory of Professor Norbert Hübner (Max Delbrück Center for Molecular Medicine, Berlin, Germany).

Full RNA-Sequencing and preliminary data processing was done by the Genomics Platform (Dr. Sascha Sauer, Max Delbrück Center for Molecular Medicine, Berlin, Germany) by Dr. Daniele Yumi Sunaga-Franze. Subsequent analysis was performed by me in close cooperation.

All transplantation experiments were performed in cooperation with Dr. Helena Escobar. The transplantations of human primary myoblasts and fibroblasts was performed together with Janine Kieshauer.

7. APPENDIX

7.1 RNA Sequencing – Differentially expressed transcripts (padj <0.05) comparing M_hiPSCs and B_hiPSCs of donors A, B and D

7.1.1 Ensemble transcript ID, HGNC Symbol, log2 fold change, padj

Table 7.1: log2 fold change and adjusted p values for upregulated transcripts in M_hiPSCs
Ordered by adjusted p value.

Upregulated in M_hiPSCs			
Ensemble Transcript ID	**HGNC – Symbol**	**log2 fold change**	**padj**
ENST00000233190	NDUFS1	-4,8486556	6,08E-198
ENST00000308361	DHX36	-1,089601	9,17E-08
ENST00000406341	SETD5	-1,045105	4,37E-07
ENST00000552491	LIMA1	-1,0242457	5,06E-07
ENST00000544079	CCT4	-0,7676492	6,22E-07
ENST00000579855	ALDH3A2	-0,7499826	1,66E-06
ENST00000355028	BCL2L13	-1,0117225	3,18E-06
ENST00000451531	POTEI	-1,0604026	8,96E-06
ENST00000299927	ZNF592	-0,8127723	2,00E-05
ENST00000519110	FAM49B	-0,9749457	2,00E-05
ENST00000544216	LSM14A	-0,7205	2,33E-05
ENST00000595641	MYO9B	-0,8726497	5,71E-05
ENST00000368331	GON4L	-0,6915033	7,82E-05
ENST00000498483	MAGED4	-0,980808	8,02E-05
ENST00000415942	RBCK1	-0,8221944	8,10E-05
ENST00000454306	PRRC2A	-0,2988192	9,55E-05
ENST00000356674	HNRNPA2B1	-0,205101	0,0001526
ENST00000523027	DPYSL2	-0,7668708	0,00028447
ENST00000520272	DDHD2	-0,8971242	0,00052901
ENST00000432900	ZNF33A	-0,737948	0,00054806
ENST00000392715	EIF5	-0,5641769	0,00058625
ENST00000406438	SMCR8	-0,7309717	0,00058625
ENST00000540210	CCAR1	-0,7326078	0,00063019
ENST00000409197	DYNC1I2	-0,4950308	0,00090139
ENST00000427276	LINC01108	-0,8740108	0,0010598
ENST00000389534	ZNF841	-0,826881	0,00193671
ENST00000360228	CACNA1A	-0,6698784	0,00229664
ENST00000362079	MT-CO3	-0,1748153	0,00242886
ENST00000395123	SLC43A3	-0,8456619	0,00250235

ENST00000399688	PAICS	-0,5008534	0,00262418
ENST00000435359	CLUH	-0,4984719	0,00270613
ENST00000533917	NAV2	-0,7932316	0,00270613
ENST00000261332	ZNF24	-0,7197753	0,00277964
ENST00000533482	RAD50	-0,7638051	0,00277964
ENST00000373825	SRPK1	-0,4156346	0,00281142
ENST00000618402	SYNRG	-0,7673068	0,00281142
ENST00000377190	SYVN1	-0,7457486	0,00313638
ENST00000341369	PTMA	-0,3082294	0,00369732
ENST00000273432	MED12L	-0,8175973	0,00431305
ENST00000590261	ILF3	-0,5016096	0,0046242
ENST00000372062	RALGDS	-0,6224395	0,00497359
ENST00000261622	SLC7A5	-0,2125485	0,00542998
ENST00000498273	L1TD1	-0,1862811	0,0062669
ENST00000529163	RPL8	-0,5148064	0,0062669
ENST00000558939	TLE3	-0,7824408	0,00688104
ENST00000372068	TMEM164	-0,5931578	0,00769565
ENST00000265080	RASGRF2	-0,4503368	0,008171
ENST00000340800	ACSL4	-0,5851568	0,01016267
ENST00000547566	HNRNPA1	-0,1977284	0,01051409
ENST00000368450	SHC1	-0,6107508	0,01221482
ENST00000285116	SKA1	-0,6611484	0,01230407
ENST00000433797	KDM6A	-0,5741544	0,01275732
ENST00000395218	PTK2	-0,7400039	0,01275732
ENST00000523339	NPM1	-0,4815147	0,01324027
ENST00000589998	ILF3	-0,4114465	0,0165272
ENST00000569438	RPL4	-0,4041304	0,01717171
ENST00000436757	PITPNM1	-0,7011312	0,01736062
ENST00000164640	PDZD4	-0,5146733	0,01753426
ENST00000395153	DACT1	-0,4801109	0,01862135
ENST00000420247	SCYL1	-0,5960006	0,01862135
ENST00000321030	PRPF31	-0,7024542	0,01862135
ENST00000613693	PRPF31	-0,7024542	0,01862135
ENST00000359624	CBS	-0,3416276	0,01913512
ENST00000543915	IL4R	-0,6908494	0,02145286
ENST00000433049	ANKHD1	-0,7029904	0,02145286
ENST00000246043	RRBP1	-0,4858267	0,02151424
ENST00000361789	MT-CYB	-0,2422498	0,02195811
ENST00000503788	06. Mär	-0,620155	0,02629611
ENST00000361665	NFE2L1	-0,4684157	0,02709229
ENST00000344936	ARHGAP12	-0,4832542	0,02925368
ENST00000617074	HSPA4	-0,2900354	0,03157124

ENST00000444061	SMARCA4	-0,3872303	0,03260298
ENST00000429705	SNRK	-0,7045272	0,03260298
ENST00000412169	HIST2H2BA	-0,5134496	0,03308414
ENST00000356936	NCL	-0,4967241	0,03422475
ENST00000534699	CSDE1	-0,6030272	0,03422475
ENST00000323372	PIPOX	-0,3190238	0,03765783
ENST00000406921	ITSN2	-0,5039694	0,03842538
ENST00000381607	ZMYND11	-0,6495202	0,03842538
ENST00000380062	IFT74	-0,6959944	0,04271784

Table 7.2: log2 fold change and adjusted p values for upregulated transcripts in B_hiPSCs
Ordered by adjusted p value.

Upregulated in B_hiPSCs

Ensemble Transcript ID	HGNC – Symbol	log2 fold change	padj
ENST00000497164	MAGED4B	2,28723116	6,58E-33
ENST00000620510	ZKSCAN1	1,22284455	1,84E-12
ENST00000458593	EHMT2	1,34082373	1,99E-11
ENST00000629838	EHMT2	1,34082373	1,99E-11
ENST00000306773	NPTX1	0,83630429	9,92E-11
ENST00000398417	SMAD4	1,16385448	1,31E-08
ENST00000625876	SNORD3A	0,3630356	1,62E-08
ENST00000636254	ARID1B	1,0681919	1,67E-07
ENST00000598725	SUPT5H	1,09194797	3,18E-06
ENST00000516869	RPPH1	0,27629344	7,73E-06
ENST00000638323	CACNA1H	0,90903807	1,09E-05
ENST00000264968	MGAT4A	0,88256876	2,00E-05
ENST00000635748	NDUFS1	0,82638807	7,38E-05
ENST00000613780	MIAT	0,71622661	9,55E-05
ENST00000368805	REV3L	0,8032639	0,00012417
ENST00000396222	LDHA	0,61564316	0,0001526
ENST00000590758	GJC1	0,78222749	0,00020093
ENST00000594824	MYO9B	0,7371891	0,00046313
ENST00000459255	SCARNA10	0,48779108	0,00176432
ENST00000359052	SMARCAD1	0,56474194	0,00195698
ENST00000532461	RDX	0,83640897	0,00250235
ENST00000470450	CCT8	0,37859549	0,00262418
ENST00000457660	SLC3A2	0,83798044	0,00263978
ENST00000434753	XIAP	0,43889224	0,00313638
ENST00000311420	MDM2	0,77426548	0,00460107
ENST00000436109	TJAP1	0,62347244	0,00497359
ENST00000229239	GAPDH	0,22577687	0,00508255

ENST00000294256	SYVN1	0,70483128	0,00616884
ENST00000343455	DICER1	0,47690217	0,00748962
ENST00000574549	THOC6	0,75036753	0,01275732
ENST00000373747	PUM1	0,38024334	0,01679533
ENST00000170630	IL4R	0,72368749	0,02145286
ENST00000523347	ESRP1	0,73473094	0,02268555
ENST00000277554	NACC2	0,63025881	0,02457685
ENST00000318607	PABPC1	0,36147896	0,02629611
ENST00000554684	PPP4R3A	0,29635003	0,02629611
ENST00000302182	UBB	0,25235926	0,02779825
ENST00000619021	HERC2P2	0,55832599	0,0293621
ENST00000599522	MAGED4	0,52125336	0,02969376
ENST00000427587	EEF2KMT	0,71042449	0,03467647
ENST00000398803	HSDL2	0,69888829	0,03929552
ENST00000556564	PTPN21	0,67803277	0,0497367

7.1.2 Reads for each donor

Table 7.3: Expression values (reads) for each donor for upregulated transcripts in M_hiPSCs
Separated by M_hiPSCs and B_hiPSCs. Ordered by adjusted p value.

Upregulated in M_hiPSCs

		M_hiPSCs			B_hiPSCs		
Ensemble Transcript ID	**HGNC – Symbol**	**Donor A**	**Donor B**	**Donor D**	**Donor A**	**Donor B**	**Donor D**
ENST00000233190	NDUFS1	1300,36455	1126,01412	1271,7855	2,91105123	2,67347975	4,23308245
ENST00000308361	DHX36	47,8864404	74,8992952	278,825456	0	0	0
ENST00000406341	SETD5	395,475948	186,827455	0	4,85175206	2,67347975	0
ENST00000552491	LIMA1	66,8758909	100,146249	174,9772	0	0	0
ENST00000544079	CCT4	605,185531	600,877492	625,934698	328,94879	365,375566	300,548854
ENST00000579855	ALDH3A2	362,450816	562,165497	765,347426	225,121295	286,062333	407,434186
ENST00000355028	BCL2L13	235,304061	244,053883	217,654565	80,5390842	101,59223	70,904131
ENST00000451531	POTEI	157,695002	260,885186	146,525622	26,1994611	82,8778722	35,9812008
ENST00000299927	ZNF592	298,05181	229,747276	438,154288	148,463613	110,50383	224,35337
ENST00000519110	FAM49B	188,243249	145,590765	273,135141	76,6576825	50,7961152	89,9530021
ENST00000544216	LSM14A	902,411713	1101,60874	1577,63995	606,469007	650,546739	694,225522
ENST00000595641	MYO9B	464,828723	306,329702	459,492971	154,285715	148,823706	244,460511
ENST00000368331	GON4L	355,84579	639,589487	566,186385	175,633425	373,396005	358,753738
ENST00000498483	MAGED4	102,377907	154,847981	270,289983	34,9326148	20,4966781	53,9718012
ENST00000415942	RBCK1	43,758299	128,759463	119,496624	0	0	0
ENST00000454306	PRRC2A	3438,7418	3175,22518	6240,85345	2919,78439	2470,29529	4996,09556

ENST00000356674	HNRNPA2B1	10191,5555	10249,4215	11054,8603	8886,46907	8907,14336	9473,63852
ENST00000523027	DPYSL2	72,6552889	47,1276464	142,257886	0	0	0
ENST00000520272	DDHD2	146,136206	267,617707	177,822357	58,2210247	68,6193136	74,0789429
ENST00000432900	ZNF33A	54,4914667	74,8992952	120,919203	0	0	0
ENST00000392715	EIF5	1072,49114	1024,18474	1553,45611	826,738551	568,560027	968,31761
ENST00000406438	SMCR8	766,183047	1133,58821	1280,32097	546,307282	599,750624	503,736812
ENST00000540210	CCAR1	70,1784041	132,967288	221,922302	1,94070082	0	0
ENST00000409197	DYNC1I2	736,460428	678,301483	571,876701	493,90836	477,661715	393,676668
ENST00000427276	LINC01108	73,4809172	218,80693	627,357276	36,8733156	94,4629511	142,866533
ENST00000389534	ZNF841	167,602541	122,026942	247,528721	57,2506743	55,2519148	104,768791
ENST00000360228	CACNA1A	106,506049	98,4631184	36,9870503	0	0	0
ENST00000362079	MT-CO3	20614,287	32639,2614	29002,1152	18591,9139	28337,103	25658,8293
ENST00000395123	SLC43A3	217,140238	130,442593	217,654565	99,9460924	28,5171173	62,4379661
ENST00000399688	PAICS	733,157915	596,669666	721,247481	461,886796	444,688798	484,68794
ENST00000435359	CLUH	1136,89015	1247,1995	1519,31422	890,781678	721,839532	1060,38715
ENST00000533917	NAV2	232,001548	195,243107	176,399778	85,3908362	87,3336718	89,9530021
ENST00000261332	ZNF24	765,357418	764,141124	527,776756	335,741242	326,164529	393,676668
ENST00000533482	RAD50	293,09804	249,944839	459,492971	172,722373	85,551352	226,469911
ENST00000373825	SRPK1	991,579568	1103,29187	1295,96934	692,830194	886,704117	911,170997
ENST00000618402	SYNRG	875,16598	440,138555	854,969894	507,493265	122,088909	468,813881
ENST00000377190	SYVN1	245,2116	230,588841	305,854454	100,916443	134,565147	146,041345
ENST00000341369	PTMA	1866,74555	1883,42273	1785,33647	1470,08087	1471,30502	1496,39465
ENST00000273432	MED12L	142,833693	198,609367	243,260985	22,3180595	76,6397528	86,7781902
ENST00000590261	ILF3	1011,39465	583,204625	894,802102	598,706204	445,579958	621,204849
ENST00000372062	RALGDS	151,089976	27,7716488	48,3676812	0	0	0
ENST00000261622	SLC7A5	13668,2762	12207,7436	12419,1134	12342,8572	10437,2649	10246,1761
ENST00000498273	L1TD1	6889,04239	7698,63767	9369,10436	6172,39897	6668,54965	8151,85853
ENST00000529163	RPL8	1019,65093	984,631184	1210,61461	600,646905	798,479285	749,255594
ENST00000558939	TLE3	365,753329	221,331625	241,838406	164,95957	114,068469	57,1466131
ENST00000372068	TMEM164	346,763879	306,329702	551,960597	220,269543	205,857941	294,19923
ENST00000265080	RASGRF2	534,181499	745,626692	936,056889	379,407011	572,124666	611,680414
ENST00000340800	ACSL4	31,3738748	58,909558	116,651466	0	0	0
ENST00000547566	HNRNPA1	7528,90431	7299,73581	6747,29152	6389,75746	6567,84858	5814,13874
ENST00000368450	SHC1	0	363,55613	32,7193137	0	11,5850789	3,17481184
ENST00000285116	SKA1	189,068877	311,379092	315,812506	102,857144	192,490542	149,216156
ENST00000433797	KDM6A	553,996578	627,807576	597,48312	389,110515	311,014811	407,434186
ENST00000395218	PTK2	407,034744	225,539451	251,796458	127,115904	141,694427	111,118414
ENST00000523339	NPM1	731,506659	901,316238	983,001991	430,835583	707,580974	680,468004
ENST00000589998	ILF3	988,277055	928,246322	569,031543	688,948792	659,458338	460,347716
ENST00000569438	RPL4	2063,24508	2420,34127	1759,73005	1620,48519	1515,86302	1444,53939

ENST00000436757	PITPNM1	288,969899	260,885186	375,560819	98,0053916	144,367906	221,178558
ENST00000164640	PDZD4	728,204146	901,316238	1136,64051	590,943401	581,036265	630,729285
ENST00000395153	DACT1	671,235794	776,764601	688,528167	474,501351	594,403664	405,317645
ENST00000420247	SCYL1	368,230214	357,665174	505,015495	213,477091	179,123143	361,928549
ENST00000321030	PRPF31	177,510081	212,074409	257,486773	75,6873321	89,1159916	154,507509
ENST00000613693	PRPF31	177,510081	212,074409	257,486773	75,6873321	89,1159916	154,507509
ENST00000359624	CBS	1321,00525	1204,27968	1007,18583	1019,83828	993,643307	740,789429
ENST00000543915	IL4R	232,001548	187,669021	241,838406	139,730459	88,2248317	99,4774376
ENST00000433049	ANKHD1	298,877438	308,854397	382,673713	92,1832891	162,191105	231,761264
ENST00000246043	RRBP1	834,710194	547,85889	894,802102	506,522915	350,225847	722,798828
ENST00000361789	MT-CYB	8248,02655	10023,0405	12271,1652	7525,06744	7888,54758	10184,7964
ENST00000503788	06. Mär	581,242311	527,661327	453,802656	444,420489	238,830858	232,819535
ENST00000361665	NFE2L1	712,517208	911,415019	799,489318	574,447444	545,389869	550,300718
ENST00000344936	ARHGAP12	336,856339	607,610013	479,409075	213,477091	403,695442	357,695467
ENST00000617074	HSPA4	1355,68164	1509,76782	1826,59125	1147,92454	1232,47416	1406,44164
ENST00000444061	SMARCA4	1522,45855	1434,02696	1478,05943	990,72777	1208,41285	1121,76685
ENST00000429705	SNRK	185,766364	167,471458	189,202988	57,2506743	82,8778722	96,3026257
ENST00000412169	HIST2H2BA	34,6763879	84,9980766	61,1708909	0	0	0
ENST00000356936	NCL	762,054905	727,112259	790,953845	423,072779	487,464474	634,962367
ENST00000534699	CSDE1	359,148303	479,692115	741,163585	264,905662	296,756252	320,655996
ENST00000323372	PIPOX	1002,31274	1114,23221	1140,90824	805,390842	906,309635	863,54882
ENST00000406921	ITSN2	75,957802	25,2469534	81,0869949	0	0	0
ENST00000381607	ZMYND11	248,514113	175,887109	203,428777	142,641511	98,0275908	88,8947314
ENST00000380062	IFT74	103,203535	146,43233	169,286884	21,3477091	73,0751131	48,6804482

Table 7.4: Expression values (reads) for each donor for upregulated transcripts in B_hiPSCs
Separated by M_hiPSCs and B_hiPSCs. Ordered by adjusted p value.

Upregulated in B_hiPSCs

		M_hiPSCs			**B_hiPSCs**		
Ensemble Transcript ID	**HGNC – Symbol**	**Donor A**	**Donor B**	**Donor D**	**Donor A**	**Donor B**	**Donor D**
ENST00000497164	MAGED4B	0	0	0	218,328843	245,068977	312,189831
ENST00000620510	ZKSCAN1	188,243249	355,140478	278,825456	742,318065	851,94888	775,712359
ENST00000458593	EHMT2	0	0	0	216,388142	145,259066	100,535708
ENST00000629838	EHMT2	0	0	0	216,388142	145,259066	100,535708
ENST00000306773	NPTX1	403,73223	824,733812	422,505921	821,886799	1701,22428	682,584545
ENST00000398417	SMAD4	0	0,84156511	4,26773657	249,380056	90,8983115	204,246228
ENST00000625876	SNORD3A	13541,9551	16251,4639	19120,8824	18728,7333	20656,1957	23528,5305
ENST00000636254	ARID1B	0	0	0	132,938006	101,59223	117,468038

ENST00000598725	SUPT5H	53,6658384	197,767802	227,612617	474,501351	703,125174	629,671014
ENST00000516869	RPPH1	41657,075	50376,0878	63661,8265	51114,1783	63631,4915	73692,6741
ENST00000638323	CACNA1H	0	0	0	61,1320759	179,123143	77,2537547
ENST00000264968	MGAT4A	0	0	0	102,857144	73,9662731	117,468038
ENST00000635748	NDUFS1	0,82562828	4,20782557	5,69031543	1283,77359	1154,94325	1088,96046
ENST00000613780	MIAT	615,918699	523,453501	322,925401	977,142865	865,316279	751,372135
ENST00000368805	REV3L	0	0	0	15,5256066	97,1364309	208,479311
ENST00000396222	LDHA	527,576473	869,336764	817,982843	1020,80863	1420,50891	1104,83452
ENST00000590758	GJC1	0	0	0	88,3018875	89,1159916	84,661649
ENST00000594824	MYO9B	213,012097	196,926237	150,793359	459,946095	372,504845	246,577053
ENST00000459255	SCARNA10	471,43375	416,574732	584,679911	657,897579	649,655579	815,926642
ENST00000359052	SMARCAD1	293,09804	376,179606	463,760708	474,501351	641,63514	639,19545
ENST00000532461	RDX	107,331677	176,728674	38,4096292	255,202158	393,001523	192,605251
ENST00000470450	CCT8	1791,61337	1508,08469	1882,07183	2459,83829	2138,7838	2212,84385
ENST00000457660	SLC3A2	72,6552889	29,454779	9,95805201	207,654988	146,150226	59,2631543
ENST00000434753	XIAP	533,355871	774,239906	780,995793	716,118604	1179,00457	1016,99806
ENST00000311420	MDM2	14,8613091	19,3559976	11,3806309	58,2210247	97,1364309	98,419167
ENST00000436109	TJAP1	0	0	0	109,649597	46,3403157	62,4379661
ENST00000229239	GAPDH	4262,71883	3515,21748	3499,54399	4947,81675	4255,2886	4017,19524
ENST00000294256	SYVN1	118,890473	126,234767	115,228887	229,002697	225,463459	247,635323
ENST00000343455	DICER1	1618,23143	1099,08404	1203,50171	1928,08627	1857,17727	1812,81756
ENST00000574549	THOC6	86,6909697	39,5535604	83,9321526	234,8248	71,2927933	216,945476
ENST00000373747	PUM1	914,796138	1142,00386	928,943994	1318,70621	1359,91003	1269,92473
ENST00000170630	IL4R	64,3990061	100,987814	95,3127835	201,832886	176,449663	223,295099
ENST00000523347	ESRP1	47,8864404	27,7716488	34,1418926	142,641511	78,4220726	89,9530021
ENST00000277554	NACC2	595,277992	248,261709	307,277033	1031,48249	622,029622	402,142833
ENST00000318607	PABPC1	2652,74367	2102,22966	1761,15263	3771,75205	2354,4445	2474,23669
ENST00000554684	PPP4R3A	1115,42381	987,997445	1014,29873	1372,07548	1218,21561	1275,21609
ENST00000302182	UBB	3108,49049	2586,97116	2567,75484	3882,372	3178,76742	2863,68028
ENST00000619021	HERC2P2	700,958412	764,141124	772,46032	839,353106	1600,52321	1259,34203
ENST00000599522	MAGED4	0	0	0	50,4582214	83,7690321	49,7387188
ENST00000427587	EEF2KMT	62,7477495	23,5638232	85,3547315	146,522912	111,39499	204,246228
ENST00000398803	HSDL2	22,2919636	69,0083394	52,6354177	112,560648	143,476747	175,672922
ENST00000556564	PTPN21	112,285446	95,9384231	278,825456	339,622644	264,674495	387,327044

8. BIBLIOGRAPHY

Abujarour, R., Bennett, M., Valamehr, B., Lee, T. T., Robinson, M., Robbins, D., Le, T., Lai, K., & Flynn, P. (2014). Myogenic Differentiation of Muscular Dystrophy- Specific Induced Pluripotent Stem Cells for Use in Drug Discovery. *Stem Cells Translational Medicine*, *3*(2), 149–160. doi: 10.5966/sctm.2013-0095

Al Kubaisy, E., Arafat, K., De Wever, O., Hassan, A. H., & Attoub, S. (2016). SMARCAD1 knockdown uncovers its role in breast cancer cell migration, invasion, and metastasis. *Expert Opinion on Therapeutic Targets*, *20*(9), 1035–1043. doi: 10.1080/14728222.2016.1195059

Alexander, M. S., Rozkalne, A., Colletta, A., Spinazzola, J. M., Johnson, S., Rahimov, F., Meng, H., Lawlor, M. W., … Gussoni, E. (2016). CD82 Is a Marker for Prospective Isolation of Human Muscle Satellite Cells and Is Linked to Muscular Dystrophies. *Cell Stem Cell*, *19*(6), 800–807. doi: 10.1016/j.stem.2016.08.006

Allbrook, D. B., Han, M. F., & Hellmuth, A. E. (1971). Population of Muscle Satellite Cells in Relation to Age and Mitotic Activity. *Pathology*, *3*(3), 233–243. doi: 10.3109/00313027109073739

Allison, T. F., Andrews, P. W., Avior, Y., Barbaric, I., Benvenisty, N., Bock, C., Brehm, J., Brüstle, O., … Yamanaka, S. (2018). Assessment of established techniques to determine developmental and malignant potential of human pluripotent stem cells. *Nature Communications*, *9*(1925), 1–15. doi: 10.1038/s41467-018-04011-3

Anders, S., & Huber, W. (2010). Differential expression analysis for sequence count data. *Genome Biology*, *98*(26), 14973–14978. doi: 10.1073/pnas.261574498

Anguera, M. C., Sadreyev, R., Zhang, Z., Szanto, A., Payer, B., Sheridan, S. D., Kwok, S., Haggarty, S. J., … Lee, J. T. (2012). Molecular signatures of human induced pluripotent stem cells highlight sex differences and cancer genes. *Cell Stem Cell*, *11*(1), 75–90. doi: 10.1016/j.stem.2012.03.008

Annexstad, E. J., Lund-Petersen, I., & Rasmussen, M. (2014). Duchenne muscular dystrophy. *Tidsskrift for Den Norske Lægeforening*, *134*(14), 1361–1364. doi: 10.4045/tidsskr.13.0836

Azuma, K., & Yamanaka, S. (2016). Recent policies that support clinical application of induced pluripotent stem cell-based regenerative therapies. *Regenerative Therapy*, *4*, 36–47. doi: 10.1016/j.reth.2016.01.009

Babai, F., Musevi-Aghdam, J., Schurch, W., Royal, A., & Gabbiani, G. (1990). Coexpression of α-sarcomeric actin, α-smooth muscle actin and desmin during myogenesis in rat and mouse embryos I. Skeletal muscle. *Differentiation*, *44*(2), 132–142. doi: 10.1111/j.1432-0436.1990.tb00546.x

Ban, H., Nishishita, N., Fusaki, N., Tabata, T., Saeki, K., Shikamura, M., Takada, N., Inoue, M., … Nishikawa, S.-I. (2011). Efficient generation of transgene-free human induced pluripotent stem cells (iPSCs) by temperature-sensitive Sendai virus vectors. *Proceedings of the National Academy of Sciences of the United States of America*, *108*(34), 14234–14239. doi: 10.1073/pnas.1103509108

Bar-Nur, O., Russ, H. A., Efrat, S., & Benvenisty, N. (2011). Epigenetic Memory and Preferential Lineage-Specific Differentiation in Induced Pluripotent Stem Cells Derived from Human Pancreatic Islet Beta Cells. *Stem Cell*, *9*(6), 17–23. doi: 10.1016/j.stem.2011.06.007

Barberi, T., Bradbury, M., Dincer, Z., Panagiotakos, G., Socci, N. D., & Studer, L. (2007). Derivation of engraftable skeletal myoblasts from human embryonic stem cells. *Nature Medicine*, *13*(5), 642–648. doi: 10.1038/nm1533

Barberi, T., Willis, L. M., Socci, N. D., & Studer, L. (2005). Derivation of multipotent mesenchymal precursors from human embryonic stem cells. *PLoS Medicine*, *2*(6), 0554–0560. doi: 10.1371/journal.pmed.0020161

Ben-David, U., & Benvenisty, N. (2012). Analyzing the genomic integrity of stem cells. *StemBook*, 1–11. doi: 10.3824/stembook.1.150.1

Berardi, E., Annibali, D., Cassano, M., Crippa, S., & Sampaolesi, M. (2014). Molecular and cell-based therapies for muscle degenerations: A road under construction. *Frontiers in Physiology*, Vol. 5, pp. 1–13. doi: 10.3389/fphys.2014.00119

Berkes, C. A., & Tapscott, S. J. (2005). MyoD and the transcriptional control of myogenesis. *Seminars in Cell and Developmental Biology*, *16*(4–5), 585–595. doi: 10.1016/j.semcdb.2005.07.006

Bischoff, R. (1975). Regeneration of single skeletal muscle fibers in vitro. *The Anatomical Record*, *182*, 215–235. doi: 10.1002/ar.1091820207

Bitzer, M., Armeanu, S., Lauer, U. M., & Neubert, W. J. (2003). Sendai virus vectors as an emerging negative-strand RNA viral vector system. *Journal of Gene Medicine*, *5*(7), 543–553. doi: 10.1002/jgm.426

Blau, H. M., & Webster, C. (1981). Isolation and characterization of human muscle cells. *Proceedings of the National Academy of Sciences of the United States of America*, *78*(9), 5623–5627. doi: 10.1073/pnas.78.9.5623

Blin, G., Wisniewski, D., Picart, C., Thery, M., Puceat, M., & Lowell, S. (2018). Geometrical confinement controls the asymmetric patterning of brachyury in cultures of pluripotent cells. *Development*, *145*(18), 1–15. doi: 10.1242/dev.166025

Bober, E., Franz, T., Arnold, H. H., Gruss, P., & Tremblay, P. (1994). Pax-3 is required for the development of limb muscles: a possible role for the migration of dermomyotomal muscle progenitor cells. *Development*, *120*, 603–612. Retrieved from http://www.ncbi.nlm.nih.gov/pubmed/8162858

Boldrin, L., Neal, A., Zammit, P. S., Muntoni, F., & Morgan, J. E. (2012). Donor satellite cell engraftment is significantly augmented when the host niche is preserved and endogenous satellite cells are incapacitated. *Stem Cells*, *30*(9), 1971–1984. doi: 10.1002/stem.1158

Borchin, B., Chen, J., & Barberi, T. (2013). Derivation and FACS-mediated purification of PAX3+/PAX7+ skeletal muscle precursors from human pluripotent stem cells. *Stem Cell Reports*, *1*(6), 620–631. doi: 10.1016/j.stemcr.2013.10.007

Borgohain, M. P., Haridhasapavalan, K. K., Dey, C., Adhikari, P., & Thummer, R. P. (2019). An Insight into DNA-free Reprogramming Approaches to Generate Integration-free Induced Pluripotent Stem Cells for Prospective Biomedical Applications. *Stem Cell Reviews and Reports*, *15*(2), 286–313. doi: 10.1007/s12015-018-9861-6

Briggs, D., & Morgan, J. E. (2013). Recent progress in satellite cell/myoblast engraftment - Relevance for

therapy. *FEBS Journal*, *280*(17), 4281–4293. doi: 10.1111/febs.12273

Buckingham, M., Bajard, L., Chang, T., Daubas, P., Hadchouel, J., Meilhac, S., Montarras, D., Rocancourt, D., & Relaix, F. (2003). The formation of skeletal muscle: from somite to limb. *Journal of Anatomy*, *202*(1), 59–68. doi: 10.1046/j.1469-7580.2003.00139.x

Buganim, Y., Faddah, D. A., Cheng, A. W., Itskovich, E., Markoulaki, S., Ganz, K., Klemm, S. L., Van Oudenaarden, A., & Jaenisch, R. (2012). Single-cell expression analyses during cellular reprogramming reveal an early stochastic and a late hierarchic phase. *Cell*, *150*(6), 1209–1222. doi: 10.1016/j.cell.2012.08.023

Butler, J. M. (2012). Single Nucleotide Polymorphisms and Applications. In *Advanced Topics in Forensic DNA Typing: Methodology* (pp. 347–369). doi: 10.1016/b978-0-12-374513-2.00012-9

Capers, C. R. (1960). Multinucleation of Skeletal Muscle in vitro. *The Journal of Biophysical and Biochemical Cytology*, *7*(3), 559–565. doi: 10.1083/jcb.7.3.559

Caron, L., Kher, D., Lee, K. L., McKernan, R., Dumevska, B., Hidalgo, A., Li, J., Yang, H., … Schmidt, U. (2016). A Human Pluripotent Stem Cell Model of Facioscapulohumeral Muscular Dystrophy-Affected Skeletal Muscles. *Stem Cells Translational Medicine*, *5*(9), 1145–1161. doi: 10.5966/sctm.2015-0224

Castiglioni, A., Hettmer, S., Lynes, M. D., Rao, T. N., Tchessalova, D., Sinha, I., Lee, B. T., Tseng, Y.-H. H., & Wagers, A. J. (2014). Isolation of progenitors that exhibit myogenic/osteogenic bipotency in vitro by fluorescence-activated cell sorting from human fetal muscle. *Stem Cell Reports*, *2*(1), 92–106. doi: 10.1016/j.stemcr.2013.12.006

Centeno, E. G. Z., Cimarosti, H., & Bithell, A. (2018). 2D versus 3D human induced pluripotent stem cell-derived cultures for neurodegenerative disease modelling. *Molecular Neurodegeneration*, *13*(1), 1–15. doi: 10.1186/s13024-018-0258-4

Cerletti, M., Jurga, S., Witczak, C. A., Hirshman, M. F., Shadrach, J. L., Goodyear, L. J., & Wagers, A. J. (2008). Highly Efficient, Functional Engraftment of Skeletal Muscle Stem Cells in Dystrophic Muscles. *Cell*, *134*(1), 37–47. doi: 10.1016/j.cell.2008.05.049

Chadwick, K., Wang, L., Li, L., Menendez, P., Murdoch, B., Rouleau, A., & Bhatia, M. (2003). Cytokines and BMP-4 promote hematopoietic differentiation of human embryonic stem cells. *Blood*, *102*(3), 906–915. doi: 10.1182/blood-2003-03-0832

Chal, J., Oginuma, M., Al Tanoury, Z., Gobert, B., Sumara, O., Hick, A., Bousson, F., Zidouni, Y., … Pourquie, O. (2015). Differentiation of pluripotent stem cells to muscle fiber to model Duchenne muscular dystrophy. *Nature Biotechnology*, *33*(9), 962–969. doi: 10.1038/nbt.3297

Chal, J., & Pourquié, O. (2017). Making muscle: skeletal myogenesis in vivo and in vitro. *Development*, *144*(12), 2104–2122. doi: 10.1242/dev.151035

Chal, J., Tanoury, Z. Al, Hestin, M., Gobert, B., Aivio, S., Hick, A., Cherrier, T., Nesmith, A. P., … Pourquié, O. (2016). Generation of human muscle fibers and satellite-like cells from human pluripotent stem cells in vitro. *Nature Protocols*, *11*(10), 1833–1850. doi: 10.1038/nbt.3297

Chalamalasetty, R. B., Garriock, R. J., Dunty, W. C., Kennedy, M. W., Jailwala, P., Si, H., & Yamaguchi, T. P. (2014).

Mesogenin 1 is a master regulator of paraxial presomitic mesoderm differentiation. *Development*, *141*(22), 4285–4297. doi: 10.1242/dev.110908

Chapman, D. L., Agulnik, I., Hancock, S., Silver, L. M., & Papaioannou, V. E. (1996). Tbx6, a mouse T-box gene implicated in paraxial mesoderm formation at gastrulation. *Developmental Biology*, *180*(2), 534–542. doi: 10.1006/dbio.1996.0326

Chargé, S. B. P., & Rudnicki, M. A. (2004). Cellular and Molecular Regulation of Muscle Regeneration. *Physiological Reviews*, *84*(1), 209–238. doi: 10.1152/physrev.00019.2003

Charville, G. W., Cheung, T. H., Yoo, B., Santos, P. J., Lee, G. K., Shrager, J. B., & Rando, T. A. (2015). Ex Vivo Expansion and In Vivo Self-Renewal of Human Muscle Stem Cells. *Stem Cell Reports*, *5*, 1–12. doi: 10.1016/j.stemcr.2015.08.004

Chen, B., & Shan, T. (2019). The role of satellite and other functional cell types in muscle repair and regeneration. *Journal of Muscle Research and Cell Motility*, Vol. 40, pp. 1–8. doi: 10.1007/s10974-019-09511-3

Choi, I. Y., Lim, H., Estrellas, K., Mula, J., Cohen, T. V., Zhang, Y., Donnelly, C. J., Richard, J.-P., … Lee, G. (2016). Concordant but Varied Phenotypes among Duchenne Muscular Dystrophy Patient-Specific Myoblasts Derived using a Human iPSC-Based Model. *Cell Reports*, *15*(10), 1–12. doi: 10.1016/j.celrep.2016.05.016

Chong, C. E., Lim, K. P., Gan, C. P., Marsh, C. A., Zain, R. B., Abraham, M. T., Prime, S. S., Teo, S. H., … Cheong, S. C. (2012). Over-expression of MAGED4B increases cell migration and growth in oral squamous cell carcinoma and is associated with poor disease outcome. *Cancer Letters*, *321*(1), 18–26. doi: 10.1016/j.canlet.2012.03.025

Churko, J. M., Burridge, P. W., & Wu, J. C. (2013). Generation of Human iPSCs from Human Peripheral Blood Mononuclear Cells Using Non-integrative Sendai Virus in Chemically Defined Conditions. *Methods in Molecular Biology*, *1036*, 81–88. doi: 10.1007/978-1-62703-511-8_7

Churko, J. M., Lee, J., Ameen, M., Gu, M., Venkatasubramanian, M., Diecke, S., Sallam, K., Im, H., … Wu, J. C. (2017). Transcriptomic and epigenomic differences in human induced pluripotent stem cells generated from six reprogramming methods. *Nature Biomedical Engineering*, *1*(10), 826–837. doi: 10.1038/s41551-017-0141-6

Ciruna, B., & Rossant, J. (2001). FGF Signaling Regulates Mesoderm Cell Fate Specification and Morphogenetic Movement at the Primitive Streak. *Developmental Cell*, *1*, 37–49. doi: 10.1016/S1534-5807(01)00017-X

Cossu, G., Previtali, S. C., Napolitano, S., Cicalese, M. P., Tedesco, F. S., Nicastro, F., Noviello, M., Roostalu, U., … Ciceri, F. (2015). Intra-arterial transplantation of HLA-matched donor mesoangioblasts in Duchenne muscular dystrophy. *EMBO Molecular Medicine*, *7*(12), 1513–1528. doi: 10.15252/emmm.201607129

Cowan, C. A., Atienza, J., Melton, D. A., & Kevin Eggan. (2005). Nuclear Reprogramming of Somatic Cells After Fusion with Human Embryonic Stem Cells. *Science*, *309*, 1369–1372. doi: 10.1126/science.1113399

Darabi, R., Arpke, R. W., Irion, S., Dimos, J. T., Grskovic, M., Kyba, M., & Perlingeiro, R. C. R. (2012). Human ES- and iPS-Derived Myogenic Progenitors Restore DYSTROPHIN and Improve Contractility upon Transplantation in Dystrophic Mice. *Cell Stem Cell*, *10*(5), 610–619. doi: 10.1016/j.stem.2012.02.015

Darabi, R., Gehlbach, K., Bachoo, R. M., Kamath, S., Osawa, M., Kamm, K. E., Kyba, M., & Perlingeiro, R. C. R. (2008). Functional skeletal muscle regeneration from differentiating embryonic stem cells. *Nature Medicine*, *14*(2), 134–143. doi: 10.1038/nm1705

Darabi, R., Santos, F. N. C., Filareto, A., Pan, W., Koene, R., Rudnicki, M. A., Kyba, M., & Perlingeiro, R. C. R. (2011). Assessment of the myogenic stem cell compartment following transplantation of Pax3/Pax7-induced embryonic stem cell-derived progenitors. *Stem Cells*, *29*(5), 777–790. doi: 10.1002/stem.625

Davis, R. L., Weintraub, H., & Lassar, A. B. (1987). Expression of a single transfected cDNA converts fibroblasts to myoblasts. *Cell*, *51*(6), 987–1000. doi: 10.1016/0092-8674(87)90585-X

Dekel, I., Magal, Y., Pearson-White, S., Emerson, C. P., & Shani, M. (1992). Conditional Conversion of ES Cells to Skeletal Muscle by an Exogenous MyoD1 Gene. *The New Biologist*, Vol. 4, pp. 217–224.

Dellavalle, A., Sampaolesi, M., Tonlorenzi, R., Tagliafico, E., Sacchetti, B., Perani, L., Innocenzi, A., Galvez, B. G., … Cossu, G. (2007). Pericytes of human skeletal muscle are myogenic precursors distinct from satellite cells. *Nature Cell Biology*, *9*(3), 255–267. doi: http://dx.doi.org/10.1038/ncb1542

Demestre, M., Orth, M., Föhr, K. J., Achberger, K., Ludolph, A. C., Liebau, S., & Boeckers, T. M. (2015). Formation and characterisation of neuromuscular junctions between hiPSC derived motoneurons and myotubes. *Stem Cell Research*, *15*(2), 328–336. doi: 10.1016/j.scr.2015.07.005

Dorn, I., Klich, K., Arauzo-Bravo, M. J., Radstaak, M., Santourlidis, S., Ghanjati, F., Radke, T. F., Psathaki, O. E., … Zaehres, H. (2014). Erythroid differentiation of human induced pluripotent stem cells is independent of donor cell type of origin. *Haematologica*, *100*(1), 32–41. doi: 10.3324/haematol.2014.108068

Dumont, N. a., Wang, Y. X. Y. X., & Rudnicki, M. A. (2015). Intrinsic and extrinsic mechanisms regulating satellite cell function. *Development*, *142*(9), 1572–1581. doi: 10.1242/dev.114223

Ebrahimi, B. (2015). Reprogramming barriers and enhancers: Strategies to enhance the efficiency and kinetics of induced pluripotency. *Cell Regeneration*, *4*(10), 1–12. doi: 10.1186/s13619-015-0024-9

Elkholi, R., Abraham-Enachescu, I., Trotta, A. P., Rubio-Patiño, C., Mohammed, J. N., Luna-Vargas, M. P. A., Gelles, J. D., Kaminetsky, J. R., … Chipuk, J. E. (2019). MDM2 Integrates Cellular Respiration and Apoptotic Signaling through NDUFS1 and the Mitochondrial Network. *Molecular Cell*, *74*(3), 452–465. doi: 10.1016/j.molcel.2019.02.012

Emery, A. E. H. (2002). The muscular dystrophies. *The Lancet*, *3*, 407–430. doi: 10.1016/S0140-6736(02)07815-7

Evans, M. J., & Kaufman, M. H. (1981). Establishment in culture of pluripotential cells from mouse embryos. *Nature*, *292*, 154–156. doi: 10.1038/292154a0

Ferreira, A., & Caceres, A. (1992). Expression of the Class III β-tubulin isotype in developing neurons in culture. *Journal of Neuroscience Research*, *32*(4), 516–529. doi: 10.1002/jnr.490320407

Frontera, W. R., & Ochala, J. (2015). Skeletal Muscle: A Brief Review of Structure and Function. *Calcified Tissue International*, *45*(2), 183–195. doi: 10.1007/s00223-014-9915-y

Fry, C. S., Lee, J. D., Mula, J., Kirby, T. J., Jackson, J. R., Liu, F., Yang, L., Mendias, C. L., … Peterson, C. A. (2015). Inducible depletion of satellite cells in adult, sedentary mice impairs muscle regenerative capacity but does not contribute to sarcopenia. *Nature Medicine*, *21*(1), 1–7. doi: 10.1038/NM.3710

Fusaki, N., Ban, H., Nishiyama, A., Saeki, K., & Hasegawa, M. (2009). Efficient induction of transgene-free human pluripotent stem cells using a vector based on Sendai virus, an RNA virus that does not integrate into the host genome. *Proceedings of the Japan Academy. Series B, Physical and Biological Sciences*, *85*(8), 348–362. doi: 10.2183/pjab.85.348

Ganassi, M., Badodi, S., Ortuste Quiroga, H. P., Zammit, P. S., Hinits, Y., & Hughes, S. M. (2018). Myogenin promotes myocyte fusion to balance fibre number and size. *Nature Communications*, *9*, 1–17. doi: 10.1038/s41467-018-06583-6

Garcia, S. M., Tamaki, S., Lee, S., Wong, A., Jose, A., Dreux, J., Kouklis, G., Sbitany, H., … Pomerantz, J. H. (2018). High-Yield Purification, Preservation, and Serial Transplantation of Human Satellite Cells. *Stem Cell Reports*, *10*(3), 1160–1174. doi: 10.1016/j.stemcr.2018.01.022

Giacomelli, E., Bellin, M., Sala, L., van Meer, B. J., Tertoolen, L. G. J., Orlova, V. V., & Mummery, C. L. (2017). Three-dimensional cardiac microtissues composed of cardiomyocytes and endothelial cells co-differentiated from human pluripotent stem cells. *Development*, *144*(6), 1008–1017. doi: 10.1242/dev.143438

Giobbe, G. G., Michielin, F., Luni, C., Giulitti, S., Martewicz, S., Dupont, S., Floreani, A., & Elvassore, N. (2015). Functional differentiation of human pluripotent stem cells on a chip. *Nature Methods*, *12*(7), 637–640. doi: 10.1038/nmeth.3411

Gouti, M., Delile, J., Stamataki, D., Wymeersch, F. J., Huang, Y., Kleinjung, J., Wilson, V., & Briscoe, J. (2017). A Gene Regulatory Network Balances Neural and Mesoderm Specification during Vertebrate Trunk Development. *Developmental Cell*, *41*(3), 243-261.e7. doi: 10.1016/j.devcel.2017.04.002

Gouti, M., Tsakiridis, A., Wymeersch, F. J., Huang, Y., Kleinjung, J., Wilson, V., & Briscoe, J. (2014). In Vitro Generation of Neuromesodermal Progenitors Reveals Distinct Roles for Wnt Signalling in the Specification of Spinal Cord and Paraxial Mesoderm Identity. *PLoS Biology*, *12*(8), e1001937. doi: 10.1371/journal.pbio.1001937

Gros, J., Manceau, M., Thomé, V., & Marcelle, C. (2005). A common somitic origin for embryonic muscle progenitors and satellite cells. *Nature*, *435*, 954–958. doi: 10.1038/nature03572

Güneş, C., Paszkowski-Rogacz, M., Rahmig, S., Khattak, S., Camgöz, A., Wermke, M., Dahl, A., Bornhäuser, M., … Buchholz, F. (2019). Comparative RNAi Screens in Isogenic Human Stem Cells Reveal SMARCA4 as a Differential Regulator. *Stem Cell Reports*, *12*(5), 1084–1098. doi: 10.1016/j.stemcr.2019.03.012

Günther, S., Kim, J., Kostin, S., Lepper, C., Fan, C. M., & Braun, T. (2013). Myf5-Positive Satellite Cells Contribute to Pax7-Dependent Long-Term Maintenance of Adult Muscle Stem Cells. *Cell Stem Cell*, *13*(5), 590–601. doi: 10.1016/j.stem.2013.07.016

Gurdon, J. B. (1962). The developmental capacity of nuclei taken from intestinal epithelium cells of feeding tadpoles. *Journal of Embryology and Experimental Morphology*, *10*(4), 622–640. Retrieved from http://www.ncbi.nlm.nih.gov/pubmed/13951335

Han, Y., Bai, T., & Liu, W. (2014). Controlled heterogeneous stem cell differentiation on a shape memory hydrogel surface. *Scientific Reports*, *4*, 1–7. doi: 10.1038/srep05815

Hanna, J., Markoulaki, S., Schorderet, P., Carey, B. W., Beard, C., Wernig, M., Creyghton, M. P. P., Steine, E. J., … Jaenisch, R. (2008). Direct Reprogramming of Terminally Differentiated Mature B Lymphocytes to Pluripotency. *Cell*, *133*(2), 250–264. doi: 10.1016/j.cell.2008.03.028

Hentze, H., Soong, P. L., Wang, S. T., Phillips, B. W., Putti, T. C., & Dunn, N. R. (2009). Teratoma formation by human embryonic stem cells: Evaluation of essential parameters for future safety studies. *Stem Cell Research*, *2*(3), 198–210. doi: 10.1016/j.scr.2009.02.002

Hernández-Hernández, J. M., García-González, E. G., Brun, C. E., & Rudnicki, M. A. (2017). The myogenic regulatory factors, determinants of muscle development, cell identity and regeneration. *Seminars in Cell and Developmental Biology*, *72*, 10–18. doi: 10.1016/j.semcdb.2017.11.010

Hicks, M. R., Hiserodt, J., Paras, K., Fujiwara, W., Eskin, A., Jan, M., Xi, H., Young, C. S., … Pyle, A. D. (2018). ERBB3 and NGFR mark a distinct skeletal muscle progenitor cell in human development and hPSCs. *Nature Cell Biology*, *20*(1), 46–57. doi: 10.1038/s41556-017-0010-2

Hildebrand, L., Rossbach, B., Kühnen, P., Gossen, M., Kurtz, A., Reinke, P., Seemann, P., & Stachelscheid, H. (2016). Generation of integration free induced pluripotent stem cells from fibrodysplasia ossificans progressiva (FOP) patients from urine samples. *Stem Cell Research*, *16*(1), 54–58. doi: 10.1016/j.scr.2015.11.017

Horst, D., Ustanina, S., Sergi, C., Mikuz, G., Juergens, H., Braun, T., & Vorobyov, E. (2006). Comparative expression analysis of Pax3 and Pax7 during mouse myogenesis. *International Journal of Developmental Biology*, *50*(1), 47–54. doi: 10.1387/ijdb.052111dh

Hosoya, N., Miura, T., Kawana-Tachikawa, A., Koibuchi, T., Shioda, T., Odawara, T., Nakamura, T., Kitamura, Y., … Iwamoto, A. (2008). Comparison Between Sendai Virus and Adenovirus Vectors to Transduce HIV-1 Genes Into Human Dendritic Cells. *Journal of Medical Virology*, *8*, 373–382. doi: 10.1002/jmv

Hou, P., Li, Y., Zhang, X., Liu, C., Guan, J., Li, H., Zhao, T., Ye, J., … Deng, H. (2013). Pluripotent Stem Cells Induced from Mouse Somatic Cells by Small-Molecule Compounds. *Science*, *341*, 651–654. doi: 10.1126/science.1239278

Hu, Q., Friedrich, A. M., Johnson, L. V., & Clegg, D. O. (2010). Memory in induced pluripotent stem cells: Reprogrammed human retinal-pigmented epithelial cells show tendency for spontaneous redifferentiation. *Stem Cells*, *28*(11), 1981–1991. doi: 10.1002/stem.531

Hu, S., Zhao, M., Jahanbani, F., Shao, N., Lee, W. H., Chen, H., Snyder, M. P., & Wu, J. C. (2016). Effects of cellular origin on differentiation of human induced pluripotent stem cell–derived endothelial cells. *JCI Insight*, *1*(8), 1–12. doi: 10.1172/jci.insight.85558

Hubaud, A., & Pourquié, O. (2014). Signalling dynamics in vertebrate segmentation. *Nature Reviews*

Molecular Cell Biology, *15*(11), 709–721. doi: 10.1038/nrm3891

Hussein, S. M., Batada, N. N., Vuoristo, S., Ching, R. W., Autio, R., Narvä¨, E., Ng, S., Sourour, M., … Otonkoski, T. (2011). Copy number variation and selection during reprogramming to pluripotency. *Nature*, *471*(7336), 58–62. doi: 10.1038/nature09871

Iacovino, M., Bosnakovski, D., Fey, H., Rux, D., Bajwa, G., Mahen, E., Mitanoska, A., Xu, Z., & Kyba, M. (2011). Inducible cassette exchange: a rapid and efficient system enabling conditional gene expression in embryonic stem and primary cells. *Stem Cells*, *29*(10), 1580–1588. Retrieved from http://www.ncbi.nlm.nih.gov/pubmed/22039605

Ito, E., Miyagawa, S., Takeda, M., Kawamura, A., Harada, A., Iseoka, H., Yajima, S., Sougawa, N., … Sawa, Y. (2019). Tumorigenicity assay essential for facilitating safety studies of hiPSC-derived cardiomyocytes for clinical application. *Scientific Reports*, *9*(1), 1–10. doi: 10.1038/s41598-018-38325-5

Kajiwara, M., Aoi, T., Okita, K., Takahashi, R., Inoue, H., Takayama, N., Endo, H., Eto, K., … Yamanaka, S. (2012). Donor-dependent variations in hepatic differentiation from human-induced pluripotent stem cells. *Proceedings of the National Academy of Sciences of the United States of America*, *109*(31), 12538–12543. doi: 10.1073/pnas.1209979109

Kandel, E. R., Schwartz, J. H., Jessell, T. M., Siegelbaum, S. A., & Hudspeth, A. J. (2013). *Principles of neural science* (5th ed.). McGraw Hill (ISBN 978-0-07-139011-8).

Kanellopoulou, C., Muljo, S. A., Kung, A. L., Ganesan, S., Drapkin, R., Jenuwein, T., Livingston, D. M., & Rajewsky, K. (2005). Dicer-deficient mouse embryonic stem cells are defective in differentiation and centromeric silencing. *Genes and Development*, *19*(4), 489–501. doi: 10.1101/gad.1248505

Karagiannis, P., Takahashi, K., Saito, M., Yoshida, Y., Okita, K., Watanabe, A., Inoue, H., Yamashita, J. K., … Osafune, K. (2018). Induced Pluripotent Stem Cells and Their Use in Human Models of Disease and Development. *Physiological Reviews*, *99*(1), 79–114. doi: 10.1152/physrev.00039.2017

Kaufman, S. J., & Foster, R. F. (1988). Replicating myoblasts express a muscle-specific phenotype. *Proceedings of the National Academy of Sciences*, *85*(24), 9606–9610. doi: 10.1073/pnas.85.24.9606

Kikuchi, T., Morizane, A., Doi, D., Magotani, H., Onoe, H., Hayashi, T., Mizuma, H., Takara, S., … Takahashi, J. (2017). Human iPS cell-derived dopaminergic neurons function in a primate Parkinson's disease model. *Nature*, *548*(7669), 592–596. doi: 10.1038/nature23664

Kilpinen, H., Goncalves, A., Leha, A., Afzal, V., Alasoo, K., Ashford, S., Bala, S., Bensaddek, D., … Gaffney, D. J. (2017). Common genetic variation drives molecular heterogeneity in human iPSCs. *Nature*, *546*(7658), 370–375. doi: 10.1038/nature22403

Kim, K., Doi, A., Wen, B., K.Ng, Zhao, R., Cahan, P., Kim, J., Aryee, M. J., … Daley, G. Q. (2010). Epigenetic memory in induced pluripotent stem cells. *Nature*, *467*(7313), 285–290. doi: 10.1038/nature09342

Kim, Kitai, Zhao, R., Doi, A., Ng, K., Unternaehrer, J., Hongguang, H., Loh, Y., Aryee, M. J., … Daley, G. Q. (2011). Donor cell type can influence the epigenome and differentiation potential of human induced pluripotent stem cells Kitai. *Nature Biotechnology*, *29*(12), 1117–1119. doi: 10.1038/nbt.2052.Donor

Kinter, J., & Sinnreich, M. (2014). Molecular targets to treat muscular dystrophies. *Swiss Medical Weekly*, *144*,

1–16. doi: 10.4414/smw.2014.13916

Kirkeby, A., Nolbrant, S., Tiklova, K., Heuer, A., Kee, N., Cardoso, T., Ottosson, D. R., Lelos, M. J., … Parmar, M. (2017). Predictive Markers Guide Differentiation to Improve Graft Outcome in Clinical Translation of hESC-Based Therapy for Parkinson's Disease. *Cell Stem Cell*, *20*(1), 135–148. doi: 10.1016/j.stem.2016.09.004

Konigsberg, U. R., Lipton, B. H., & Konigsberg, I. R. (1975). The regenerative response of single mature muscle fibers isolated in vitro. *Developmental Biology*, *45*, 260–275. doi: 10.1016/0012-1606(75)90065-2

Kuang, S., Kuroda, K., Grand, F. Le, Rudnicki, M. A. M., Le Grand, F., Rudnicki, M. A. M., Grand, F. Le, & Rudnicki, M. A. M. (2007). Asymmetric self-renewal and commitment of satellite stem cells in muscle. *Cell*, *129*(5), 999–1010. doi: 10.1016/j.cell.2007.03.044.Asymmetric

Kufeld, M., Escobar, H., Marg, A., Pasemann, D., Budach, V., & Spuler, S. (2017). Localized irradiation of mouse legs using an image-guided robotic linear accelerator. *Annals of Translational Medicine*, *5*(7), 1–4. doi: 10.21037/atm.2017.03.23

Kyttälä, A., Moraghebi, R., Valensisi, C., Kettunen, J., Andrus, C., Pasumarthy, K. K., Nakanishi, M., Nishimura, K., … Trokovic, R. (2016). Genetic Variability Overrides the Impact of Parental Cell Type and Determines iPSC Differentiation Potential. *Stem Cell Reports*, *6*(2), 200–212. doi: 10.1016/j.stemcr.2015.12.009

Latremoliere, A., Cheng, L., DeLisle, M., Wu, C., Chew, S., Hutchinson, E. B., Sheridan, A., Alexandre, C., … Engle, E. C. (2018). Neuronal-Specific TUBB3 Is Not Required for Normal Neuronal Function but Is Essential for Timely Axon Regeneration. *Cell Reports*, *24*(7), 1865–1879. doi: 10.1016/j.celrep.2018.07.029

Laumonier, T., & Menetrey, J. (2016). Muscle injuries and strategies for improving their repair. *Journal of Experimental Orthopaedics*, *3*(15), 1–9. doi: 10.1186/s40634-016-0051-7

Lepper, C., & Fan, C. M. (2010). Inducible lineage tracing of Pax7-descendant cells reveals embryonic origin of adult satellite cells. *Genesis*, *48*(7), 424–436. doi: 10.1002/dvg.20630

Lepper, C., Partridge, T. a, & Fan, C.-M. (2011). An absolute requirement for Pax7-positive satellite cells in acute injury-induced skeletal muscle regeneration. *Development (Cambridge, England)*, *138*(17), 3639–3646. doi: 10.1242/dev.067595

Li, B., & Dewey, C. N. (2011). RSEM: Accurate transcript quantification from RNA-seq data with or without a reference genome. *BMC Bioinformatics*, *12*(323), 1–16. doi: 10.1186/1471-2105-12-323

Lim, K. P., Chun, N. A. L., Gan, C. P., Teo, S. H., Rahman, Z. A. A., Abraham, M. T., Zain, R. B., Ponniah, S., & Cheong, S. C. (2014). Identification of immunogenic maged4b peptides for vaccine development in oral cancer immunotherapy. *Human Vaccines and Immunotherapeutics*, *10*(11), 3214–3223. doi: 10.4161/hv.29226

Lind, J. U., Yadid, M., Perkins, I., O'Connor, B. B., Eweje, F., Chantre, C. O., Hemphill, M. A., Yuan, H., … Parker, K. K. (2017). Cardiac microphysiological devices with flexible thin-film sensors for higher-throughput drug screening. *Lab on a Chip*, *17*(21), 3692–3703. doi: 10.1039/c7lc00740j

Lindsley, R. C., Gill, J. G., Kyba, M., Murphy, T. L., & Murphy, K. M. (2006). Canonical Wnt signaling is required for development of embryonic stem cell-derived mesoderm. *Development*, *133*(19), 3787–3796. doi: 10.1242/dev.02551

Lister, R., Pelizzola, M., Kida, Y. S., Hawkins, R. D., Nery, J. R., Hon, G., Antosiewicz-Bourget, J., Ogmalley, R., … Ecker, J. R. (2011). Hotspots of aberrant epigenomic reprogramming in human induced pluripotent stem cells. *Nature*, *471*(7336), 68–73. doi: 10.1038/nature09798

Liu, F., Xia, Z., Zhang, M., Ding, J., Feng, Y., Wu, J., Dong, Y., Gao, W., … Li, D. (2019). SMARCAD1 promotes pancreatic cancer cell growth and metastasis through Wnt/β-catenin-mediated EMT. *International Journal of Biological Sciences*, *15*(3), 636–646. doi: 10.7150/ijbs.29562

Long, Y., Wang, M., Gu, H., & Xie, X. (2015). Bromodeoxyuridine promotes full-chemical induction of mouse pluripotent stem cells. *Cell Research*, *25*(10), 1171–1174. doi: 10.1038/cr.2015.96

Lucarelli, P., Schilling, M., Kreutz, C., Vlasov, A., Boehm, M. E., Iwamoto, N., Steiert, B., Lattermann, S., … Klingmüller, U. (2018). Resolving the Combinatorial Complexity of Smad Protein Complex Formation and Its Link to Gene Expression. *Cell Systems*, *6*(1), 75–89. doi: 10.1016/j.cels.2017.11.010

Luz, M. a M., Marques, M. J., & Santo Neto, H. (2002). Impaired regeneration of dystrophin-deficient muscle fibers is caused by exhaustion of myogenic cells. *Brazilian Journal of Medical and Biological Research*, *35*(6), 691–695. doi: 10.1590/S0100-879X2002000600009

Lyons, G. E., Ontell, M., Cox, R., Sassoon, D., & Buckingham, M. (1990). The expression of myosin genes in developing skeletal muscle in the mouse embryo. *Journal of Cell Biology*, *111*(4), 1465–1476. doi: 10.1083/jcb.111.4.1465

Maffioletti, S. M., Sarcar, S., Henderson, A. B. H., Mannhardt, I., Pinton, L., Moyle, L. A., Steele-Stallard, H., Cappellari, O., … Tedesco, F. S. (2018). Three-Dimensional Human iPSC-Derived Artificial Skeletal Muscles Model Muscular Dystrophies and Enable Multilineage Tissue Engineering. *Cell Reports*, *23*(3), 899–908. doi: 10.1016/j.celrep.2018.03.091

Mandai, M., Watanabe, A., Kurimoto, Y., Hirami, Y., Morinaga, C., Daimon, T., Fujihara, M., Akimaru, H., … Takahashi, M. (2017). Autologous Induced Stem-Cell–Derived Retinal Cells for Macular Degeneration. *New England Journal of Medicine*, *376*(11), 1038–1046. doi: 10.1056/NEJMoa1608368

Marg, A., Escobar, H., Gloy, S., Kufeld, M., Zacher, J., Spuler, A., Birchmeier, C., Izsvak, Z., … Spuler, S. (2014). Human satellite cells have regenerative capacity and are genetically manipulable. *The Journal of Clinical Investigation*, *124*(10), 4257–4265. doi: 10.1172/JCI63992DS1

Marión, R. M., Strati, K., Li, H., Murga, M., Blanco, R., Ortega, S., Fernandez-Capetillo, O., Serrano, M., & Blasco, M. A. (2009). A p53-mediated DNA damage response limits reprogramming to ensure iPS cell genomic integrity. *Nature*, *460*(7259), 1149–1153. doi: 10.1038/nature08287

Martin, G. R. (1981). Isolation of a pluripotent cell line from early mouse embryos cultured in medium conditioned by teratocarcinoma stem cells. *Proceedings of the National Academy of Sciences of the United States of America*, *78*(12), 7634–7638. doi: 10.1073/pnas.78.12.7634

Mauro, A. (1961). Satellite Cell of Skeletal Muscle Fibers. *The Journal of Cell Biology*, *9*(2), 493–495. doi:

10.1083/jcb.9.2.493

Mayshar, Y., Ben-David, U., Lavon, N., Biancotti, J. C., Yakir, B., Clark, A. T., Plath, K., Lowry, W. E., & Benvenisty, N. (2010). Identification and classification of chromosomal aberrations in human induced pluripotent stem cells. *Cell Stem Cell*, *7*(4), 521–531. doi: 10.1016/j.stem.2010.07.017

Mendell, J. R., Kissel, J. T., Amato, A. A., King, W., Signore, L., Prior, T. W., Sahenk, Z., Benson, S., … Burghes, A. H. M. (1995). Myoblast transfer in the treatment of Duchenne's muscular dystrophy. *The New England Journal of Medicine*, *333*(13), 832–838. doi: 10.1056/NEJM199509283331303

Mendjan, S., Mascetti, V. L., Ortmann, D., Ortiz, M., Karjosukarso, D. W., Ng, Y., Moreau, T., & Pedersen, R. A. (2014). NANOG and CDX2 pattern distinct subtypes of human mesoderm during exit from pluripotency. *Cell Stem Cell*, *15*(3), 310–325. doi: 10.1016/j.stem.2014.06.006

Meng, J., Chun, S., Asfahani, R., Lochmüller, H., Muntoni, F., & Morgan, J. (2014). Human skeletal muscle-derived CD133+ Cells form functional satellite cells after intramuscular transplantation in immunodeficient host mice. *Molecular Therapy*, *22*(5), 1008–1017. doi: 10.1038/mt.2014.26

Mercuri, E., & Muntoni, F. (2013). Muscular dystrophies. *Lancet*, *381*, 845–860. doi: 10.1016/j.med.2019.04.003

Min, Y.-L., Bassel-Duby, R., & Olson, E. N. (2018). CRISPR Correction of Duchenne Muscular Dystrophy. *Annual Review of Medicine*, *70*(1), 239–255. doi: 10.1146/annurev-med-081117-010451

Minasi, M. G., Riminucci, M., De Angelis, L., Borello, U., Berarducci, B., Innocenzi, A., Caprioli, A., Sirabella, D., … Cossu, G. (2002). The meso-angioblast: a multipotent, self-renewing cell that originates from the dorsal aorta and differentiates into most mesodermal tissues. *Development*, *129*(11), 2773–2783. Retrieved from http://www.ncbi.nlm.nih.gov/pubmed/12015303

Montarras, D., Relaix, F., Zaffran, S., Buckingham, M., Cumano, A., Morgan, J., Colins, C., & Partridge, T. (2005). Developmental biology: Direct isolation of satellite cells for skeletal muscle regeneration. *Science*, *309*(5743), 2064–2067. doi: 10.1126/science.1114758

Montserrat, N., Nivet, E., Sancho-Martinez, I., Hishida, T., Kumar, S., Miquel, L., Cortina, C., Hishida, Y., … Izpisua Belmonte, J. C. (2013). Reprogramming of human fibroblasts to pluripotency with lineage specifiers. *Cell Stem Cell*, *13*(3), 341–350. doi: 10.1016/j.stem.2013.06.019

Müller, F.-J., Schuldt, B. M., Williams, R., Mason, D., Altun, G., Papapetrou, E. P., Danner, S., Goldmann, J. E., … Loring, J. F. (2011). A bioinformatic assay for pluripotency in human cells. *Nature Methods*, *8*(4), 315–317. doi: 10.1038/nmeth.1580

Murphy, M., & Kardon, G. (2011). Origin of vertebrate limb muscle: The role of progenitor and myoblast populations. In *Current Topics in Developmental Biology* (Vol. 96). doi: 10.1016/B978-0-12-385940-2.00001-2

Murry, C. E., & Keller, G. (2008). Differentiation of Embryonic Stem Cells to Clinically Relevant Populations: Lessons from Embryonic Development. *Cell*, *132*(4), 661–680. doi: 10.1016/j.cell.2008.02.008

Nakagawa, M., Koyanagi, M., Tanabe, K., Takahashi, K., Ichisaka, T., Aoi, T., Okita, K., Mochiduki, Y., … Yamanaka, S. (2008). Generation of induced pluripotent stem cells without Myc from mouse and

human fibroblasts. *Nature Biotechnology*, *26*(1), 101–106. doi: 10.1038/nbt1374

Nakanishi, M., Kurisaki, A., Hayashi, Y., Warashina, M., Ishiura, S., Kusuda-Furue, M., & Asashima, M. (2009). Directed induction of anterior and posterior primitive streak by Wnt from embryonic stem cells cultured in a chemically defined serum-free medium. *The FASEB Journal*, *23*(1), 114–122. doi: 10.1096/fj.08-111203

Negroni, E., Gidaro, T., Bigot, A., Butler-Browne, G., Mouly, V., & Trollet, C. (2015). Stem cells and muscle diseases: advances in cell therapy strategies. *Neuropathology and Applied Neurobiology*, *41*, 270–287. doi: 10.1111/nan.12198

Newman, A. M., & Cooper, J. B. (2010). Lab-specific gene expression signatures in pluripotent stem cells. *Cell Stem Cell*, *7*(2), 258–262. doi: 10.1016/j.stem.2010.06.016

Nishimura, K., Sano, M., Ohtaka, M., Furuta, B., Umemura, Y., Nakajima, Y., Ikehara, Y., Kobayashi, T., … Nakanishi, M. (2011). Development of Defective and Persistent Sendai Virus Vector. *Journal of Biological Chemistry*, *286*(6), 4760–4771. doi: 10.1074/jbc.m110.183780

Nishino, K., Toyoda, M., Yamazaki-Inoue, M., Fukawatase, Y., Chikazawa, E., Sakaguchi, H., Akutsu, H., & Umezawa, A. (2011). DNA Methylation Dynamics in Human Induced Pluripotent Stem Cells over Time. *PLoS Genetics*, *7*(5), 1–14. doi: 10.1371/journal.pgen.1002085

Nishizawa, M., Chonabayashi, K., Nomura, M., Tanaka, A., Nakamura, M., Inagaki, A., Nishikawa, M., Takei, I., … Yoshida, Y. (2016). Epigenetic Variation between Human Induced Pluripotent Stem Cell Lines Is an Indicator of Differentiation Capacity. *Cell Stem Cell*, *19*(3), 341–354. doi: 10.1016/j.stem.2016.06.019

Ohashi, F., Miyagawa, S., Yasuda, S., Miura, T., Kuroda, T., Itoh, M., Kawaji, H., Ito, E., … Sato, Y. (2019). CXCL4/PF4 is a predictive biomarker of cardiac differentiation potential of human induced pluripotent stem cells. *Scientific Reports*, *9*(1), 1–15. doi: 10.1038/s41598-019-40915-w

Ohi, Y., Qin, H., Hong, C., Blouin, L., Polo, J. M., Guo, T., Qi, Z., Downey, S. L., … Ramalho-Santos, M. (2011). Incomplete DNA methylation underlies a transcriptional memory of somatic cells in human iPS cells. *Nat Cell Biol*, *13*(5), 541–549. doi: 10.1038/ncb2239

Okano, H., Nakamura, M., Yoshida, K., Okada, Y., Tsuji, O., Nori, S., Ikeda, E., Yamanaka, S., & Miura, K. (2013). Steps toward safe cell therapy using induced pluripotent stem cells. *Circulation Research*, *112*(3), 523–533. doi: 10.1161/CIRCRESAHA.111.256149

Okita, K., Ichisaka, T., & Yamanaka, S. (2007). Generation of germline-competent induced pluripotent stem cells. *Nature*, *448*(7151), 313–317. doi: 10.1038/nature05934

Okita, K., Nakagawa, M., Hyenjong, H., Ichisaka, T., & Yamanaka, S. (2008). Generation of mouse induced pluripotent stem cells without viral vectors. *Science*, *322*, 949–953. doi: 10.1126/science.1164270

Olguín, H. C., & Pisconti, A. (2012). Marking the tempo for myogenesis: Pax7 and the regulation of muscle stem cell fate decisions. *Journal of Cellular and Molecular Medicine*, *16*(5), 1013–1025. doi: 10.1111/j.1582-4934.2011.01348.x

Oustanina, S., Hause, G., & Braun, T. (2004). Pax7 directs postnatal renewal and propagation of myogenic satellite cells but not their specification. *The EMBO Journal*, *23*(16), 3430–3439. doi:

10.1038/sj.emboj.7600346

Palmieri, B., & Tremblay, J. P. (2010). Myoblast transplantation: a possible surgical treatment for a severe pediatric disease. *Surgery Today*, *40*, 902–908. doi: 10.1007/s00595-009-4242-z

Panopoulos, A. D., Yanes, O., Ruiz, S., Kida, Y. S., Diep, D., Tautenhahn, R., Herrerías, A., Batchelder, E. M., … Belmonte, J. C. I. (2012). The metabolome of induced pluripotent stem cells reveals metabolic changes occurring in somatic cell reprogramming. *Cell Research*, *22*(1), 168–177. doi: 10.1038/cr.2011.177

Paulin, D., & Li, Z. (2004). Desmin: A major intermediate filament protein essential for the structural integrity and function of muscle. *Experimental Cell Research*, *301*(1), 1–7. doi: 10.1016/j.yexcr.2004.08.004

Peterson, S. E., & Loring, J. F. (2014). Genomic instability in pluripotent stem cells: Implications for clinical applications. *Journal of Biological Chemistry*, *289*(8), 4578–4584. doi: 10.1074/jbc.R113.516419

Phetfong, J., Supokawej, A., Wattanapanitch, M., Kheolamai, P., U-pratya, Y., & Issaragrisil, S. (2016). Cell type of origin influences iPSC generation and differentiation to cells of the hematoendothelial lineage. *Cell and Tissue Research*, *365*(1), 101–112. doi: 10.1007/s00441-016-2369-y

Philippi, S., Bigot, A., Marg, A., Vincent, M., Spuler, S., & Zacharias, U. (2012). Dysferlin-deficient immortalized human myoblasts and myotubes as a useful tool to study dysferlinopathy. *PLoS Currents*, *1*, 1–16. doi: 10.1371/currents.RRN1298

Plouhinec, J. L., Medina-Ruiz, S., Borday, C., Bernard, E., Vert, J. P., Eisen, M. B., Harland, R. M., & Monsoro-Burq, A. H. (2017). A molecular atlas of the developing ectoderm defines neural, neural crest, placode, and nonneural progenitor identity in vertebrates. In *PLoS Biology* (Vol. 15). doi: 10.1371/journal.pbio.2004045

Polo, J. M., Liu, S., Figueroa, M. E., Kulalert, W., Eminli, S., Tan, K. Y., Apostolou, E., Stadtfeld, M., … Hochedlinger, K. (2010). Cell type of origin influences the molecular and functional properties of mouse induced pluripotent stem cells. *Nature Biotechnology*, *28*(8), 848–855. doi: 10.1038/nbt.1667

Pourquié, O., Al Tanoury, Z., & Chal, J. (2018). The Long Road to Making Muscle In Vitro. *Current Topics in Developmental Biology*, *129*, 123–142. doi: 10.1016/bs.ctdb.2018.03.003

Qazi, T. H., Duda, G. N., Ort, M. J., Perka, C., Geissler, S., & Winkler, T. (2019). Cell therapy to improve regeneration of skeletal muscle injuries. *Journal of Cachexia, Sarcopenia and Muscle*, *49*, 1–16. doi: 10.1002/jcsm.12416

Quattrocelli, M., Giacomazzi, G., Broeckx, S. Y., Ceelen, L., Bolca, S., Spaas, J. H., & Sampaolesi, M. (2016). Equine-Induced Pluripotent Stem Cells Retain Lineage Commitment Toward Myogenic and Chondrogenic Fates. *Stem Cell Reports*, *6*(1), 55–63. doi: 10.1016/j.stemcr.2015.12.005

Quattrocelli, M., Palazzolo, G., Floris, G., Schöffski, P., Anastasia, L., Orlacchio, A., Vandendriessche, T., Chuah, M. K. L., … Sampaolesi, M. (2011). Intrinsic cell memory reinforces myogenic commitment of pericyte-derived iPSCs. *Journal of Pathology*, *223*(5), 593–603. doi: 10.1002/path.2845

Rao, L., Qian, Y., Khodabukus, A., Ribar, T., & Bursac, N. (2018). Engineering human pluripotent stem cells into a functional skeletal muscle tissue. *Nature Communications*, *9*(1), 1–12. doi: 10.1038/s41467-017-

02636-4

Redmer, T., Diecke, S., Grigoryan, T., Quiroga-Negreira, A., Birchmeier, W., & Besser, D. (2011). E-cadherin is crucial for embryonic stem cell pluripotency and can replace OCT4 during somatic cell reprogramming. *EMBO Reports*, *12*(7), 720–726. doi: 10.1038/embor.2011.88

Relaix, F., Rocancourt, D., Mansouri, A., & Buckingham, M. (2005). A Pax3/Pax7-dependent population of skeletal muscle progenitor cells. *Nature*, *435*(7044), 948–953. doi: 10.1038/nature03594

Relaix, F., & Zammit, P. S. (2012). Satellite cells are essential for skeletal muscle regeneration: the cell on the edge returns centre stage. *Development*, *139*(16), 2845–2856. doi: 10.1242/dev.069088

Reshef, R., Maroto, M., & Lassar, A. B. (1998). Regulation of dorsal somitic cell fates: BMPs and Noggin control the timing and pattern of myogenic regulator expression. *Genes and Development*, *12*(3), 290–303. doi: 10.1101/gad.12.3.290

Robertson, C., Tran, D. D., & George, S. C. (2013). Concise review: Maturation phases of human pluripotent stem cell-derived cardiomyocytes. *Stem Cells*, *31*(5), 829–837. doi: 10.1002/stem.1331

Rocheteau, P., Gayraud-Morel, B., Siegl-Cachedenier, I., Blasco, M. a., & Tajbakhsh, S. (2012). A subpopulation of adult skeletal muscle stem cells retains all template DNA strands after cell division. *Cell*, *148*(1), 112–125. doi: 10.1016/j.cell.2011.11.049

Rohwedel, J., Maltsev, V., Bober, E., Arnold, H. H., Hescheler, J., & Wobus, A. M. (1994). Muscle cell differentiation of embryonic stem cells reflects myogenesis in vivo: Developmentally regulated expression of myogenic determination genes and functional expression of ionic currents. *Developmental Biology*, Vol. 164, pp. 87–101. doi: 10.1006/dbio.1994.1182

Rouhani, F., Kumasaka, N., de Brito, M. C., Bradley, A., Vallier, L., & Gaffney, D. (2014). Genetic Background Drives Transcriptional Variation in Human Induced Pluripotent Stem Cells. *PLoS Genetics*, *10*(6), 1–11. doi: 10.1371/journal.pgen.1004432

Ruiz, S., Diep, D., Gore, A., Panopoulos, A. D., Montserrat, N., Plongthongkum, N., Kumar, S., Fung, H.-L., … Izpisua Belmonte, J. C. (2012). Identification of a specific reprogramming-associated epigenetic signature in human induced pluripotent stem cells. *Proceedings of the National Academy of Sciences*, *109*(40), 16196–16201. doi: 10.1073/pnas.1202352109

Sacco, A., Doyonnas, R., Kraft, P., Vitorovic, S., & Blau, H. M. (2008). Self-renewal and expansion of single transplanted muscle stem cells. *Nature*, *456*(7221), 502–506. doi: 10.1038/nature07384

Sambasivan, R., Yao, R., Kissenpfennig, A., Van Wittenberghe, L., Paldi, A., Gayraud-Morel, B., Guenou, H., Malissen, B., … Galy, A. (2011). Pax7-expressing satellite cells are indispensable for adult skeletal muscle regeneration. *Development*, *138*(17), 3647–3656. doi: 10.1242/dev.073601

Sampaolesi, M., Blot, S., D'Antona, G., Granger, N., Tonlorenzi, R., Innocenzi, A., Mognol, P., Thibaud, J. L., … Cossu, G. (2006). Mesoangioblast stem cells ameliorate muscle function in dystrophic dogs. *Nature*, *444*(7119), 574–579. doi: 10.1038/nature05282

Sampaziotis, F., De Brito, M. C., Madrigal, P., Bertero, A., Saeb-Parsy, K., Soares, F. A. C., Schrumpf, E., Melum, E., … Vallier, L. (2015). Cholangiocytes derived from human induced pluripotent stem cells for disease

modeling and drug validation. *Nature Biotechnology*, *33*(8), 845–852. doi: 10.1038/nbt.3275

Sanchez-Freire, V., Lee, A. S., Hu, S., Abilez, O. J., Liang, P., Lan, F., Huber, B. C., Ong, S. G., … Wu, J. C. (2014). Effect of human donor cell source on differentiation and function of cardiac induced pluripotent stem cells. *Journal of the American College of Cardiology*, *64*(5), 436–448. doi: 10.1016/j.jacc.2014.04.056

Sardo, V. Lo, Ferguson, W., Erikson, G. A., Topol, E. J., Baldwin, K. K., & Torkamani, A. (2016). Influence of donor age on induced pluripotent stem cells. *Nature Biotechnology*, *35*(1), 69–76. doi: 10.1038/nbt.3749

Sareen, D., Mehrnoosh, S., Ornelas, L., Winkler, M. A., Narwani, K., Sahabian, A., Funari, V. A., Tang, J., … Ljubimov, A. V. (2014). Differentiation of Human Limbal-Derived Induced Pluripotent Stem Cells Into Limbal-Like Epithelium. *Stem Cells Translational Medicine*, *3*, 1002–1012. doi: 10.5966/sctm.2014-0149

Schiaffino, S., & Reggiani, C. (2011). Fiber Types in Mammalian Skeletal Muscles. *Physiological Reviews*, *91*(4), 1447–1531. doi: 10.1152/physrev.00031.2010

Schiaffino, S., Rossi, A. C., Smerdu, V., Leinwand, L. A., & Reggiani, C. (2015). Developmental myosins: Expression patterns and functional significance. *Skeletal Muscle*, *5*(1), 1–14. doi: 10.1186/s13395-015-0046-6

Schmidt, M., Schüler, S. C., Hüttner, S. S., Eyss, B. Von, & Maltzahn, J. Von. (2019). Adult stem cells at work : regenerating skeletal muscle. *Cellular and Molecular Life Sciences*, *76*(13), 2559–2570. doi: 10.1007/s00018-019-03093-6

Schultz, E., Gibson, M. C., & Champion, T. (1978). Satellite cells are mitotically quiescent in mature mouse muscle: An EM and radioautographic study. *Journal of Experimental Zoology*, *206*(3), 451–456. doi: 10.1002/jez.1402060314

Seale, P., Sabourin, L. A., Girgis-Gabardo, A., Mansouri, A., Gruss, P., & Rudnicki, M. A. (2000). Pax7 is required for the specification of myogenic satellite cells. *Cell*, *102*, 777–786. doi: 10.1016/s0092-8674(00)00066-0

Shao, K., Koch, C., Gupta, M. K., Lin, Q., Lenz, M., Laufs, S., Denecke, B., Schmidt, M., … Wagner, W. (2013). Induced pluripotent mesenchymal stromal cell clones retain donor-derived differences in DNA methylation profiles. *Molecular Therapy : The Journal of the American Society of Gene Therapy*, *21*(1), 240–250. doi: 10.1038/mt.2012.207

Shea, K. L., Xiang, W., LaPorta, V. S., Licht, J. D., Keller, C., Basson, M. A., & Brack, A. S. (2010). Sprouty1 Regulates Reversible Quiescence of a Self-Renewing Adult Muscle Stem Cell Pool during Regeneration. *Cell Stem Cell*, *6*(2), 117–129. doi: 10.1016/j.stem.2009.12.015

Shelton, M., Metz, J., Liu, J., Carpenedo, R. L., Demers, S. P., Stanford, W. L., & Skerjanc, I. S. (2014). Derivation and expansion of PAX7-positive muscle progenitors from human and mouse embryonic stem cells. *Stem Cell Reports*, *3*(3), 516–529. doi: 10.1016/j.stemcr.2014.07.001

Shi, X., & Garry, D. J. (2006). Muscle stem cells in development, regeneration, and disease. *Genes and Development*, *20*(13), 1692–1708. doi: 10.1101/gad.1419406

Shiba, Y., Gomibuchi, T., Seto, T., Wada, Y., Ichimura, H., Tanaka, Y., Ogasawara, T., Okada, K., … Ikeda, U.

(2016). Allogeneic transplantation of iPS cell-derived cardiomyocytes regenerates primate hearts. *Nature*, *538*(7625), 388–391. doi: 10.1038/nature19815

Shimizu-Motohashi, Y., Komaki, H., Motohashi, N., Takeda, S., Yokota, T., & Aoki, Y. (2019). Restoring dystrophin expression in duchenne muscular dystrophy: Current status of therapeutic approaches. *Journal of Personalized Medicine*, *9*(1), 1–14. doi: 10.3390/jpm9010001

Shinin, V., Gayraud-Morel, B., Gomès, D., & Tajbakhsh, S. (2006). Asymmetric division and cosegregation of template DNA strands in adult muscle satellite cells. *Nature Cell Biology*, *8*(7), 677–687. doi: 10.1038/ncb1425

Skoglund, G., Lainé, J., Darabi, R., Fournier, E., Perlingeiro, R., & Tabti, N. (2014). Physiological and ultrastructural features of human induced pluripotent and embryonic stem cell-derived skeletal myocytes in vitro. *Proceedings of the …*, *111*(22), 8275–8280. doi: 10.1073/pnas.1322258111

Skuk, D., Goulet, M., Roy, B., Chapdelaine, P., Bouchard, J.-P., Roy, R., Dugré, F. J., Sylvain, M., … Tremblay, J. P. (2006). Dystrophin Expression in Muscles of Duchenne Muscular Dystrophy Patients After High-Density Injections of Normal Myogenic Cells. *Molecular Therapy*, *65*(4), 371–386. doi: 10.1097/01.jnen.0000218443.45782.81

Soleimani, V. D., Punch, V. G., Kawabe, Y. ichi, Jones, A. E., Palidwor, G. A., Porter, C. J., Cross, J. W., Carvajal, J. J., … Rudnicki, M. A. (2012). Transcriptional dominance of Pax7 in adult myogenesis is due to high-affinity recognition of homeodomain motifs. *Developmental Cell*, *22*(6), 1208–1220. doi: 10.1016/j.devcel.2012.03.014

Sommer, C. A., Christodoulou, C., Gianotti-Sommer, A., Shen, S. S., Sailaja, B. S., Hezroni, H., Spira, A., Meshorer, E., … Mostoslavsky, G. (2012). Residual Expression of Reprogramming Factors Affects the Transcriptional Program and Epigenetic Signatures of Induced Pluripotent Stem Cells. *PLoS ONE*, *7*(12), 1–10. doi: 10.1371/journal.pone.0051711

Soufi, A., Donahue, G., & Zaret, K. S. (2012). Facilitators and impediments of the pluripotency reprogramming factors' initial engagement with the genome. *Cell*, *151*(5), 994–1004. doi: 10.1016/j.cell.2012.09.045

Sousa-Victor, P., Gutarra, S., García-Prat, L., Rodriguez-Ubreva, J., Ortet, L., Ruiz-Bonilla, V., Jardí, M., Ballestar, E., … Muñoz-Cánoves, P. (2014). Geriatric muscle stem cells switch reversible quiescence into senescence. *Nature*, *506*(7488), 316–321. doi: 10.1038/nature13013

Stadtfeld, M., Apostolou, E., Akutsu, H., Fukuda, A., Follett, P., Natesan, S., Kono, T., Shioda, T., & Hochedlinger, K. (2010). Aberrant silencing of imprinted genes on chromosome 12qF1 in mouse induced pluripotent stem cells. *Nature*, *465*(7295), 175–181. doi: 10.1038/nature09017

Stadtfeld, M., Brennand, K., & Hochedlinger, K. (2008). Reprogramming of Pancreatic β Cells into Induced Pluripotent Stem Cells. *Current Biology*, *18*(12), 890–894. doi: 10.1016/j.cub.2008.05.010

Swartz, E. W., Baek, J., Pribadi, M., Wojta, K. J., Almeida, S., Karydas, A., Gao, F.-B., Miller, B. L., & Coppola, G. (2016). A Novel Protocol for Directed Differentiation of C9orf72-Associated Human Induced Pluripotent Stem Cells Into Contractile Skeletal Myotubes. *Stem Cells Translational Medicine*, *5*, 1–12.

doi: 10.5966/sctm.2015-0340

Tada, M., Takahama, Y., Abe, K., Nakatsuji, N., & Tada, T. (2001). Nuclear reprogramming of somatic cells by in vitro hybridization with ES cells. *Current Biology*, *11*(19), 1553–1558. doi: 10.1016/S0960-9822(01)00459-6

Takahashi, K., Tanabe, K., Ohnuki, M., Narita, M., Ichisaka, T., Tomoda, K., & Yamanaka, S. (2007). Induction of Pluripotent Stem Cells from Adult Human Fibroblasts by Defined Factors. *Cell*, *131*(5), 861–872. doi: 10.1016/j.cell.2007.11.019

Takahashi, K., Tanabe, K., Ohnuki, M., Narita, M., Sasaki, A., Yamamoto, M., Nakamura, M., Sutou, K., … Yamanaka, S. (2014). Induction of pluripotency in human somatic cells via a transient state resembling primitive streak-like mesendoderm. *Nature Communications*, *5*, 1–9. doi: 10.1038/ncomms4678

Takahashi, K., & Yamanaka, S. (2006). Induction of Pluripotent Stem Cells from Mouse Embryonic and Adult Fibroblast Cultures by Defined Factors. *Cell*, *126*(4), 663–676. doi: 10.1016/j.cell.2006.07.024

Takebe, T., Sekine, K., Enomura, M., Koike, H., Kimura, M., Ogaeri, T., Zhang, R. R., Ueno, Y., … Taniguchi, H. (2013). Vascularized and functional human liver from an iPSC-derived organ bud transplant. *Nature*, *499*(7459), 481–484. doi: 10.1038/nature12271

Tan, H.-K., Toh, C.-X. D., Ma, D., Yang, B., Liu, T. M., Lu, J., Wong, C.-W., Tan, T.-K., … Loh, Y.-H. (2014). Human Finger-Prick Induced Pluripotent Stem Cells Facilitate the Development of Stem Cell Banking. *Stem Cells Translational Medicine*, *3*(5), 586–598. doi: 10.5966/sctm.2013-0195

Tanabe, K., Nakamura, M., Narita, M., Takahashi, K., & Yamanaka, S. (2013). Maturation, not initiation, is the major roadblock during reprogramming toward pluripotency from human fibroblasts. *Proceedings of the National Academy of Sciences*, *110*(30), 12172–12179. doi: 10.1073/pnas.1310291110

Tanaka, A., Woltjen, K., Miyake, K., Hotta, A., Ikeya, M., Yamamoto, T., Nishino, T., Shoji, E., … Sakurai, H. (2013). Efficient and reproducible myogenic differentiation from human iPS cells: prospects for modeling Miyoshi Myopathy in vitro. *PloS One*, *8*(4), e61540. doi: 10.1371/journal.pone.0061540

Tedesco, F. S., Gerli, M. F. M., Perani, L., Benedetti, S., Ungaro, F., Cassano, M., Antonini, S., Tagliafico, E., … Cossu, G. (2012). Transplantation of genetically corrected human iPSC-derived progenitors in mice with limb-girdle muscular dystrophy. *Science Translational Medicine*, *4*(140), 1–13. doi: 10.1126/scitranslmed.3003541

Teichroeb, J. H., Betts, D. H., & Vaziri, H. (2011). Suppression of the imprinted gene NNAT and X-Chromosome gene activation in isogenic human iPS cells. *PLoS ONE*, *6*(10), 1–11. doi: 10.1371/journal.pone.0023436

Tonegawa, A., Funayama, N., Ueno, N., & Takahashi, Y. (1997). Mesodermal subdivision along the mediolateral axis in chicken controlled by different concentrations of BMP-4. *Development*, *124*(10), 1975–1984. Retrieved from http://www.ncbi.nlm.nih.gov/pubmed/9169844

Torrente, Y., Belicchi, M., Marchesi, C., D`Antona, G., Cogiamanian, F., Pisati, F., Gavina, M., Giordano, R., … Bresolin, N. (2007). Autologous transplantation of muscle-derived CD133+ stem cells in Duchenne

muscle patients. *Cell Transplantation*, *16*(6), 563–577. doi: 10.3727/000000007783465064

Torrente, Y., Belicchi, M., Sampaolesi, M., Pisati, F., Meregalli, M., D`Antona, G., Tonlorenzi, R., Porretti, L., … Bresolin, N. (2004). Human circulating AC133+ stem cells restore dystrophin expression and ameliorate function in dystrophic skeletal muscle. *Journal of Clinical Investigation*, *114*(2), 182–195. doi: 10.1172/jci20325

Trokovic, R., Weltner, J., Manninen, T., Mikkola, M., Lundin, K., Hämäläinen, R., Suomalainen, A., & Otonkoski, T. (2013). Small Molecule Inhibitors Promote Efficient Generation of Induced Pluripotent Stem Cells From Human Skeletal Myoblasts. *Stem Cells and Development*, *22*(1), 120730075754007. doi: 10.1089/scd.2012.0157

Trokovic, R., Weltner, J., Nishimura, K., Ohtaka, M., Nakanishi, M., Salomaa, V., Jalanko, A., Otonkoski, T., & Kyttälä, A. (2014). Advanced Feeder-Free Generation of Induced Pluripotent Stem Cells Directly From Blood Cells. *Stem Cells Translational Medicine*, *3*(12), 1402–1409. doi: 10.5966/sctm.2014-0113

Trounson, A., & DeWitt, N. D. (2016). Pluripotent stem cells progressing to the clinic. *Nature Reviews. Molecular Cell Biology*, *17*(3), 194–200. doi: 10.1038/nrm.2016.10

Turan, S., Farruggio, A. P., Srifa, W., Day, J. W., & Calos, M. P. (2016). Precise correction of disease mutations in induced pluripotent stem cells derived from patients with limb girdle muscular dystrophy. *Molecular Therapy*, *24*(4), 685–696. doi: 10.1038/mt.2016.40

Venuti, J. M., Morris, J. H., Vivian, J. L., Olson, E. N., & Klein, W. H. (1995). Myogenin is required for late but not early aspects of myogenesis during mouse development. *Journal of Cell Biology*, *128*(4), 563–576. doi: 10.1083/jcb.128.4.563

von Maltzahn, J., Jones, A. E., Parks, R. J., & Rudnicki, M. A. (2013). Pax7 is critical for the normal function of satellite cells in adult skeletal muscle. *Proceedings of the National Academy of Sciences*, *110*(41), 16474–16479. doi: 10.1073/pnas.1307680110

Vunjak-Novakovic, G., Bhatia, S., Chen, C., & Hirschi, K. (2013). HeLiVa platform: Integrated heart-liver-vascular systems for drug testing in human health and disease. *Stem Cell Research and Therapy*, *4*(58), 4–9. doi: 10.1186/scrt369

Waddington, C. H. (1957). *The Strategy of the Genes. A Discussion of Some Aspects ofTheoretical Biology*.

Wallace, G. Q., & McNally, E. M. (2009). Mechanisms of muscle degeneration, regeneration, and repair in the muscular dystrophies. *Annual Review of Physiology*, *71*, 37–57. doi: 10.1146/annurev.physiol.010908.163216

Warren, L., Manos, P. D., Ahfeldt, T., Loh, Y. H., Li, H., Lau, F., Ebina, W., Mandal, P. K., … Thorsten, M. (2010). Highly efficient reprogramming to pluripotency and directed differentiation of human cells with synthetic modified mRNA. *Cell Stem Cell*, *7*(5), 618–630. doi: 10.1016/j.stem.2010.08.012

Wernig, M., Meissner, A., Foreman, R., Brambrink, T., Ku, M., Hochedlinger, K., Bernstein, B. E., & Jaenisch, R. (2007). In vitro reprogramming of fibroblasts into a pluripotent ES-cell-like state. *Nature*, *448*(7151), 318–324. doi: 10.1038/nature05944

Wilmut, I., Schnieke, A. E., McWhir, J., Kind, A. J., & Campbell, K. H. S. (1997). Viable offspring derived from

fetal and adult mammalian cells. *Nature*, *385*(27), 810–813. doi: 10.1038/386200a0

Wosczyna, M. N., & Rando, T. A. (2018). A Muscle Stem Cell Support Group: Coordinated Cellular Responses in Muscle Regeneration. *Developmental Cell*, *46*(2), 135–143. doi: 10.1016/j.devcel.2018.06.018

Xi, H., Fujiwara, W., Gonzalez, K., Jan, M., Liebscher, S., Van Handel, B., Schenke-Layland, K., & Pyle, A. D. (2017). In Vivo Human Somitogenesis Guides Somite Development from hPSCs. *Cell Reports*, *18*(6), 1573–1585. doi: 10.1016/j.celrep.2017.01.040

Xiao, S., Lu, J., Sridhar, B., Cao, X., Yu, P., Zhao, T., Chen, C. C., McDee, D., … Zhong, S. (2017). SMARCAD1 Contributes to the Regulation of Naive Pluripotency by Interacting with Histone Citrullination. *Cell Reports*, *18*(13), 3117–3128. doi: 10.1016/j.celrep.2017.02.070

Xiaoti Xu, Wilschut, K. J. J. J., Kouklis, G., Tian, H., Hesse, R., Garland, C., Sbitany, H., Hansen, S., … Pomerantz, J. H. H. H. (2015). Human satellite cell transplantation and regeneration from diverse skeletal muscles. *Stem Cell Reports*, *5*(3), 419–434. doi: 10.1016/j.stemcr.2015.07.016

Yamada, G., Kioussi, C., Schubert, F. R., Eto, Y., Chowdhury, K., Pituello, F., & Gruss, P. (1994). Regulated Expression of Brachyury (T), NKX1.1 and PAX Genes in Embryoid Bodies. *Biochemical and Biophysical Research Communications*, *199*(2), 552–563. doi: 10.1006/bbrc.1994.1264

Yang, L., Soonpaa, M. H., Adler, E. D., Roepke, T. K., Kattman, S. J., Kennedy, M., Henckaerts, E., Bonham, K., … Keller, G. M. (2008). Human cardiovascular progenitor cells develop from a KDR+ embryonic-stem-cell-derived population. *Nature*, *453*(7194), 524–528. doi: 10.1038/nature06894

Ye, J., Ge, J., Zhang, X., Cheng, L., Zhang, Z., He, S., Wang, Y., Lin, H., … Deng, H. (2016). Pluripotent stem cells induced from mouse neural stem cells and small intestinal epithelial cells by small molecule compounds. *Cell Research*, *26*(1), 34–45. doi: 10.1038/cr.2015.142

Yin, H., Price, F., & Rudnicki, M. a. (2013). Satellite cells and the muscle stem cell niche. *Physiological Reviews*, *93*(1), 23–67. doi: 10.1152/physrev.00043.2011

Young, C. S., Hicks, M. R., Ermolova, N. V., Nakano, H., Jan, M., Younesi, S., Karumbayaram, S., Kumagai-Cresse, C., … Pyle, A. D. (2016). A Single CRISPR-Cas9 Deletion Strategy that Targets the Majority of DMD Patients Restores Dystrophin Function in hiPSC-Derived Muscle Cells. *Cell Stem Cell*, *18*, 1–8. doi: 10.1016/j.stem.2016.01.021

Yu, J., Vodyanik, M. A., Smuga-Otto, K., Antosiewicz-Bourget, J., Frane, J. L., Tian, S., Nie, J., Jonsdottir, G. A., … Thomson, J. A. (2007). Induced Pluripotent Stem Cell Lines Derived from Human Somatic Cells. *Science*, *318*(5858), 1917–1920. doi: 10.1126/science.1151526

Zammit, P. S., Golding, J. P., Nagata, Y., Hudon, V., Partridge, T. A., & Beauchamp, J. R. (2004). Muscle satellite cells adopt divergent fates: A mechanism for self-renewal? *Journal of Cell Biology*, *166*(3), 347–357. doi: 10.1083/jcb.200312007